Cranfield University

SCHOOL OF APPLIED SCIENCES

SAS Research Degree

PhD Thesis

Academic Year 2013-2014

Daniele Annicchiarico

Characterization of shrinkage effects in micro-injection moulding (µ-IM)

Supervisor: Dr. J. R. Alcock
October 2013

This thesis is submitted in partial fulfilment of the requirements for the degree of Philosophical Doctorate

i

To my father Giovanni

and my mother Maria Pompea

Abstract

This thesis characterizes the effects on shrinkage in microinjection moulding. The literature review considers four branches of investigation (material properties, processing parameters, mould design and specimen design). Two research gaps rise from the analysis of the literature review: the absence of a standardized methodology for measuring shrinkage of moulded parts at the micro-scale, and the absence of optimization stage that implements multiple quality criteria. Adequate research routes are set in order to address these gaps.

The conventional standard for determining shrinkage at the macro scale is adapted to the micro-scale and this bridges the first gap. The micro-mould replicates the same design of the standard, and a preliminary stage solves some mouldability problems: the implemented mould extended the mouldability range of processing parameters for improving the reliability of results. After the micro-mould validation, the study of shrinkage at the micro-scale considers the influence of five processing parameters: the mould and melt temperature, the holding time and pressure, then the injection pressure. The design of experiment approach identifies the critical parameters that affect moulding, post-moulding and total shrinkage in parallel to and normal to the flow direction within an interval of confidence of 95% for POM and 90% for 316L feedstock. Statistical tools analyse the results, and the trends of critical factors found confirmation in the literature. This methodology at the micro-scale can fill the first gap because it is on purpose designed for the micro-scale. Moreover, the binder of feedstock is a mixture of POM based polymers, and the use of a common platform permits to compare directly the two materials and highlight the influence of powder loading.

The optimization stage adopts desirability functions for achieving optimized values that simultaneously fulfil two requests: minimize shrinkage and maximize moulded part mass. The analysis of the literature review shows that few papers adopt multiple quality criteria approach as methodology for optimizing the results, and none consider jointly part mass and shrinkage. The optimized processing parameters allow moulding "optimized specimens", and results demonstrate that their total shrinkage and part mass achieve the requests. Even if the use of desirability functions produce results that

represents a compromise between the requests, the results show that overall shrinkage decreases and part mass increases. This approach demonstrates its reliability and bridges the second gap.

The last part of the thesis investigates the 316L feedstock behaviour for filling micro-features parallel to and normal to the flow oriented. The moulded features are investigated for studying the replication quality and the effect of the orientation of channels with dimension close to the feedstock lower mouldability value. These informations are available in the literature only for polymers, and the contribution of this part of thesis is to fill this gap by analysing a feedstock. The statistical approach permits to identify the critical factors that affect the feature replication quality. Optical investigations allow to identify the 316L feedstock lower mouldability value and to observe the influence of the orientation of features with dimensions near the lower limit.

Acknowledgements

Contents

CHAPTER 6 . RESULTS: STATISTICAL BASED OPTIMIZATION USING MULTIPLE QUALITY CRITERIA. POM CASE STUDY. 132

CHAPTER 7 . RESULTS: EVALUATION OF 316L FEEDSTOCK MOULDING SHRINKAGE 143

List of figures

xvi

List of tables

List of abbreviations

3DTMC	Three-dimensional thickness control method
A/R	Aspect ratio
ABS	Acrylonitrile Butadiene Styrene
AE	Acoustic emission analysis
Al_2O_3	Alumina
ASTM	American Society for Testing and Material
$CaCO_3$	Calcium carbonate
CAD	Computer-aided design
CAE	Computer-aided engineering
c_d	Channel dimension
CD	Compact disc
CEO	Change everything at once
CIM	Conventional injection moulding
co-PP	PP copolymer
COST	Change one setting at a time
DoE	Design of Experiment
DSC	Differential scanning calorimetry
DVT	Discontinuous thickness-variation
f_d	Feature dimension
FVF	Filled Volume fraction
GPS	General Purpose polystyrene

GRA	Grey relational analysis
HCPP	High crystalline PP
HDPE	High-density polyethylene
ICM	Injection compression moulding
iPP	Isotactic polypropylene
ISO	International Organization for Standardization
LDPE	Low-density polyethylene
LML	Lower mouldability limit
ME	Margin of error
MFI	Melt flow indices
MPI	Mould-flow Plastic Insight
MUCELL	Micro cellular injection moulding
MW	Microcrystalline wax
NA	Not available
PA	Polyamide
PC	Polycarbonate
PCA	Principal Component Analysis
PCM	Photo chemical machining
PET	Polyethylene terephthalate
PIM	Powder injection moulding
PMMA	Polymethylmethacrylate
POM	Polyoxymethylene
PP	Polypropylene
PS	Polystyrene
PSBR	Brome PS
PSE	Lenth's pseudo standard error
PVB	Polyvinyl butyral
PVT	Pressure-Volume-Temperature
RPSGA	Reduced Pareto Set Genetic Algorithm
RTM	Resin transferring moulding
S/N	Signal to noise ratio
SEM	Scanning Electron Microscopy

SU	Shrinkage uniformity
TMA	Thermo mechanical analysis
UV	Ultra violet
YSZ	Yttrium stabilized zirconium
μ-IM	Microinjection moulding
μ-PIM	Micro powder injection moulding

List of symbols

%	Magnitude
Av	Average
C	Critical factor
d	Cavity deep
d	Individual desirability
D	Overall desirability
L	Lower value in desirability function
Low	Lowest value
r_i	Desirability function weight
S	Slope
S_M	Moulding shrinkage
S_P	Post-moulding shrinkage
S_T	Total shrinkage
ţ	Quantile of t-distribution
T	Target value in desirability function
T_g	Glass-transition temperature
T_{melt}	Melt temperature
T_{mould}	Mould temperature
U	Upper value in desirability function
w	Cavity width
W	Part mass
y_i	Individual response
α	Alpha value
δ	Gap between melt front and feature edge

Publications

Edited versions of the chapters have been published, presented, submitted or will be submitted as follows:

Chapter 2: Review of factors that affect shrinkage of moulded part in injection moulding; Annicchiarico D., Alcock J.R. (2014); Materials and Manufacturing Processes; DOI: 10.1080/10426914.2014.880467

Chapter 5: A methodology for shrinkage measurement in micro-injection moulding; D.Annicchiarico, U.M. Attia, J.R. Alcock; Polymer Testing 32 (2013) 769-777.

A methodology for shrinkage measurement in micro-injection moulding; Annual DTC (Doctoral Training Centre) Conference, Cranfield University, 3 Dec 2012.

Chapter 6: Part mass and shrinkage in micro-injection moulding: statistical based optimization using multiple quality criteria; D.Annicchiarico, U.M. Attia, J.R. Alcock; Polymer Testing 32, (2013) 1079–1087.

Chapter 7: Shrinkage evaluation of a 316L moulding feedstock; D.Annicchiarico, U.M. Attia, J.R. Alcock; (Submitted).

Chapter 8: Processing optimisation in micro injection moulding using multiple quality criteria: 316L study. D. Annicchiarico, U.M. Attia, J.R. Alcock; (On writing).

Chapter 9: 316L feedstock feature reproduction at the micro-scale. D. Annicchiarico, U.M. Attia, J.R. Alcock; (On writing).

Chapter 1 . Introduction to micro-injection moulding

This chapter introduces the application field of the present thesis: the microinjection moulding (μ-IM). The comparison between μ-IM and conventional injection moulding (CIM) explain the greater number of processing parameters necessary at the micro-scale manufacturing. The structure of this thesis is reported at the end of the chapter.

1.1 General considerations of micro injection moulding

The area of application of this project was the microinjection moulding technique (μ-IM), where micro indicates that one or more dimensions of moulded parts are sub-millimetre in size [1]. Moulding of micro components from thermoplastic polymers has become a routinely used industrial production process. The development of micro moulding started more than 30 years ago. A lot of experience has been gathered in that time, and today micro moulding machines are commercially available.

Therefore, use of micro moulding in industry and the number of scientific institutes working in this field are expected to increase in the forthcoming years because the interest in micro system technology is growing as the miniaturization trend and micro devices applications.

Sparrow [2] predicted that micro devices would have a far-reaching influence within the next few years. Other analysts report the forecasting that the micro technology will be one of the main technologies of the 21st century [3]. Examples of application fields are aviation (micro air vehicles), biotechnology (reactor-separators), chemical process industry (substrate characterisation), and information technology (communication devices).

Three industrial sectors (see Figure 1-1) are strongly interested for every little improvement in microinjection moulding:

Medical. e.g. metallic micro-needles. Micro-needles can bypass the stratum corneum and macromolecular drugs can naturally diffuse into body using blood vessels. Drugs may be delivered via micro-hollow technology [4].

Bio-chemical. e.g. micro bioreactors for high-throughput screening system [5].

Energy. e.g. microcombustors with potential application in aerospace, electricity generation and heating [6].

The miniaturization was preferred in these fields because offers a better control, more precise measurements and more flexibility than the conventional scale.
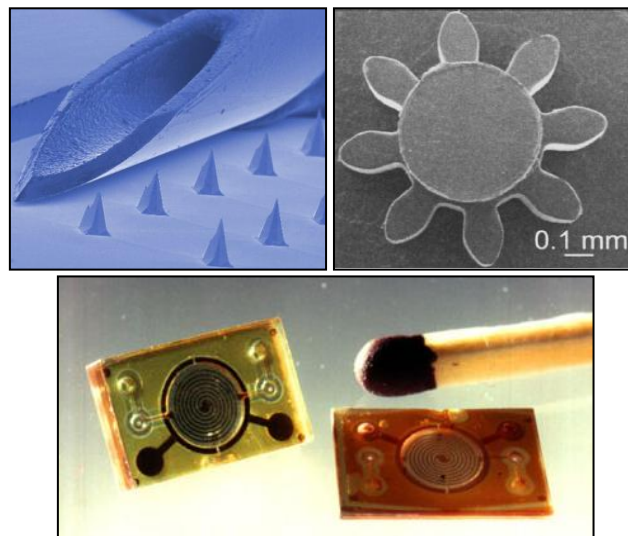
Figure 1-1. Examples of applications of μ-IM (clockwise): micro needles, micro gears, micro pumps.

1.2 Conventional injection moulding steps

The injection moulding process is a sequential operation that results in the transformation of plastic pellets into a moulded part. The material melted was injected under high pressure into the mould cavity for producing moulded parts [7].

Figure 1-2 depicts the main units of a typical injection-moulding machine: the clamping unit, the plasticizing unit and the drive unit. The clamping unit holds the mould: it is responsible to close, clamp and open the mould.
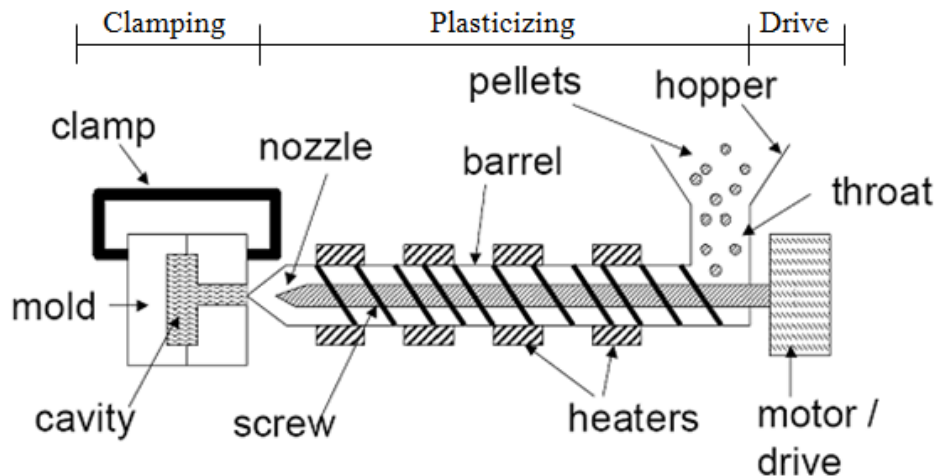
Figure 1-2. Injection moulding components [7].

The injection unit melts the plastic and injects it into the mould. The drive unit provides power to the plasticizing unit and clamping unit.

1.2.1 The injection moulding cycle

There are three main stages in the injection moulding cycle; stage 1, injection; stage 2, holding pressure and plasticizing; stage 3, ejection of the moulded part. When stage 3 was completed, the mould closes and the moulding cycle starts over again [7].

Stage 1. Injection of the plastic melts into the mould

The mould is closed and the nozzle of the extruder is pushed against the mould sprue. The screw, not rotating at this stage, injects the melted plastic into the mould.

Stage 2. Holding pressure and plastication

With the mould completely filled, the screw remains stationary for some time to hold the plastic in the mould under pressure (holding time). During the holding time, additional melt was injected into the mould to compensate the contraction due to cooling (shrinkage). Later, the gate (the narrow entrance into the cavity mould) freezes. At this point, the mould is isolated from the injection unit. As the melt cools and solidifies, the pressure should be high enough to avoid sink-marks, but low enough to allow easy removal of the parts.

During the plastication stage, a rotating screw pushes the material forward from the feed hopper through the barrel and towards the nozzle. When the gate freezes, the screw rotation is started (recovery). The rotation of the screw causes the plastic to be conveyed

forward. As the plastic moves forward, heat from the electric heater along the barrel starts to melt the plastic. At the discharge end of the screw, the plastic is completely melted. The melt that accumulates at the front of the screw pushes the screw backward. Thus, the screw rotates and moves backward at the same time.

The rotation of the screw stops when sufficient melt is accumulated in front of the screw. During screw recovery, the plastic in the mould is cooled, but typically, the cooling is not finished by the end of screw recovery. As a result, the screw will remain stationary for some period until cooling is completed (soak time). During this time, additional plastic will melt in the extruder from conductive heating.

Stage 3. Ejection

When the material in the mould has cooled sufficiently to retain its shape, the mould opens and the moulded part is ejected from the mould, then the mould closes and the cycle starts over again.

Figure 1-3 reports the different stages. The top bar shows the movement of the extruder screw, the middle bar shows the action going on inside the mould and the last bar indicates at what times the mould is open and closed. The major part of the injection moulding cycle is the cooling time required for the plastic in the mould to reduce to a temperature, which the part can be removed without significant distortion.
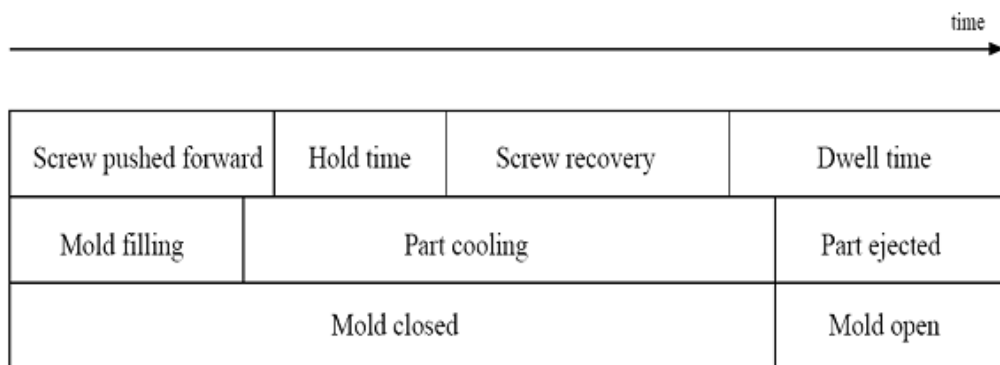
Figure 1-3. Injection moulding cycle time [7].

1.3 The micro-injection moulding machine

The main difference between the micro moulding machine and the CIM machines is that a small injection plunger of a few millimetres in diameter is used for melt injection and for control metering accuracy: the melt plastication and melt injection are separated

(Figure 1-4). Conventional moulding (CIM) machines have the screw-barrel system functions for both pellet plastication and melt injection. Moreover, in µ-IM, there are some extra parameters related to the control of plunger movement and melt storage settings. This makes process setup and optimization more difficult to perform compared with the CIM process [8].
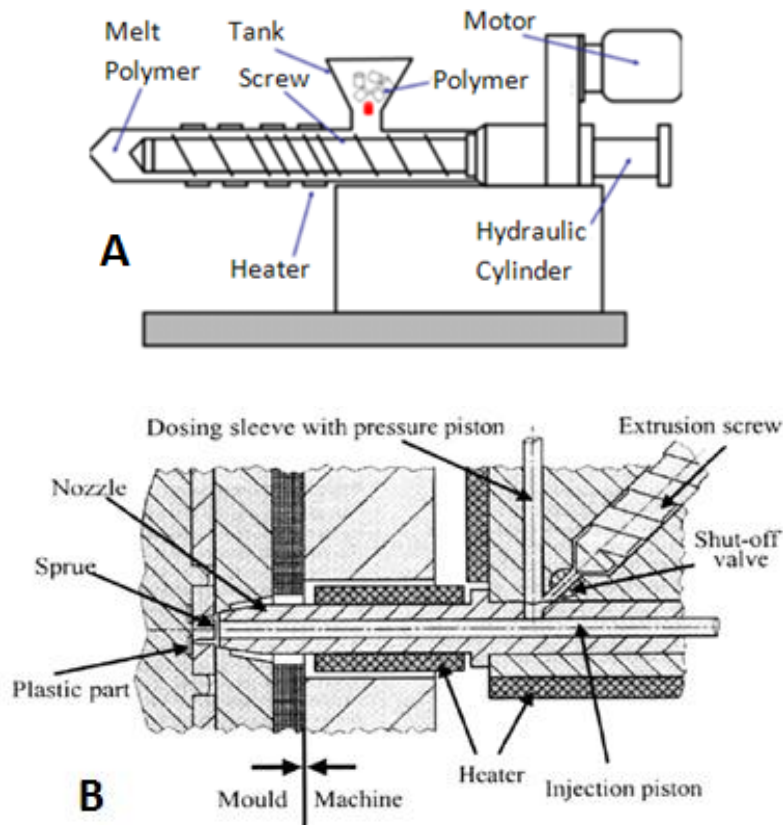
Figure 1-4. Design differences between CIM (A) and µ-IM (B) processing.

The µ-IM requests particular setting values also for the different material behaviour respect the conventional scale. Chapter 2 will report these aspects but for justifying this sentence, it is possible to report briefly the scale effect on material properties. Many publications indicate that the material (both pure polymer than feedstock) flows in the micro-scale in different way with respect to the macro-scale [9-11]. Mainly, the consequences related to the scale are:

- A micro-scale effect. When the external characteristic length (e.g. film thickness, channel depth) becomes comparable with the internal characteristic length (e.g. molecular dimension, polymer gyration radius) it is necessary to take into account

the long-range intermolecular forces and molecular packing effects. Experimental observation has shows that the molecules adjacent to the mould surface are pinned or oriented in the flow direction. A simplified scheme of a polymer is to thinks the chains connected by springs. When the channel's dimension become smaller, the number of springs across the gap decrease and the material appears to be more rigid [10].

- A collective molecular motion is a consequence of the micro-scale: all the molecular chains are involved in the motion. As result, a number of molecules greater than macro-scale are involved in injection stage [9].

- Layers of molecules. The feedstock inside the cavity mould forms a bonded layer with the wall. The velocity of the material, in these areas, it is zero. In this situation, only a bulk flow exists and the viscosity becomes "apparent" [9].

Experimental observations of liquids such as water, silicon oil, alcohol and polymer solutions in micro-channels with characteristic dimensions of tens of micrometers have shown that the viscosity close channel wall was 50-80% higher than the bulk viscosity of the fluid [11].

These rheological differences, caused by the miniaturization, make the processing parameters values higher than CIM. In addition, by considering that the sample weights are only a few grams, it is clear that a high metering accuracy is requested.

Further, the thermal properties in μ-IM (especially in micro powder injection moulding, μ-PIM) are differents from those in CIM. The thermal conductivity and heat capacity of powders are generally much higher than those of the binder components. Consequently, during solidification, the feedstock cools quickly. As a result, the control of injection temperature and mould wall temperature is much more important during μ-PIM process than CIM [12].

1.4 The micro powder injection moulding processing

The difference between μ-PIM (micro-powder injection moulding) and μ-IM is the different material injected, not the moulding process itself. The injection of pure polymer is referred as μ-IM and the moulded part is ready to be used. The injection of polymer mixed with powders (ceramic or metal) is known as μ-PIM, and the moulded

part need to be debinded (for removing the polymer) then sintered (for reaching the full powder density).

The μ-PIM processing typically consists of four steps illustrated in Figure 1-5:

- Initially, metal or ceramic powders are mixed with suitable organic binders to form the "feedstock". The binder forms a flow-vehicle between the metal powder particles, to get moulded parts of the desired shape. Binders are usually composed by a mix of polymers to support and maintain the shape of the components during processing;

- Additives, such as waxes and polymers with low molecular weight, are added in order to decrease the viscosity of the mixture and to provide a good binder powder interface;

- During moulding, the feedstock flow and fills a mould under heat and pressure to form a green part with the desired shape;

- The moulded part then undergoes a debinding step where the polymer is extracted (brown part), the next sintering stage permits to get full or almost full density [13].
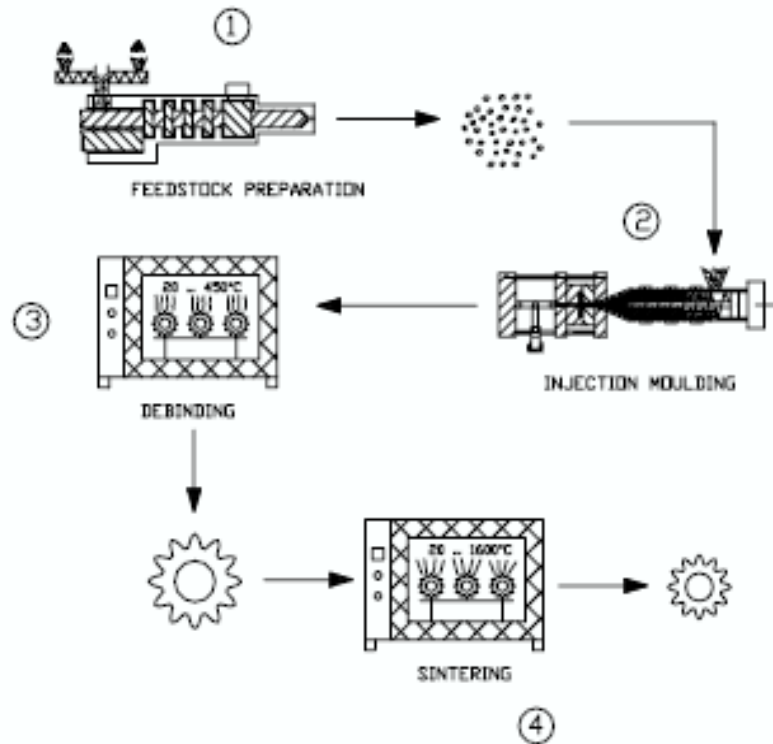
Figure 1-5. Steps of µ-PIM technique: 1) feedstock preparation; 2) injection moulding; 3) debinding; 4) sintering [13].

Even if debinded and sintered stages were not performed in this thesis, a brief description of these steps was reported below.

Debinding step

After the injection moulding step the specimen's composition is a mix of binder and metal powder, usually called "green part". During the debinding step, the major part of the binder is removed from the green parts, leaving a structure of metal powder (brown part). The most commonly used debinding procedures include thermal, solvent and catalytic [14].

The thermal debinding utilise a mechanism of thermal degradation: by successive dissociations, the polymer produces light molecules that can evaporate from the surface of moulded parts. The atmosphere under which thermal debinding is performed can affect the rate of binder removal, the density of final debinded part and carbon or oxygen content. Generally speaking, thermal debinding is not an efficient process, because a too high binder removal rate can generate cracks or shape

deformations caused by the excessive vapor pressure. For reducing these risks, low heating rates are used by increasing the time of this stage. On other side, the simplicity of this technique and the absence on chemical binder removal makes this approach still adopted. The main advantage of this technique is the possibility to switch from debinding to sintering only by increasing the temperature.

The solvent debinding is performed by diving the moulded part in a solvent (gas or liquid). The temperature during this debinding technique is typically around 50 and 60°C. The solvent (acetone, ethanol, heptanes or hexane) remove at least one binder component and produces open pores on the surface of moulded part. The reliability of solvent debinding is related to the geometry of moulded part (surface to volume ratio) because the solvent has to penetrate the part. Nowadays, the trend is to use water-soluble binders because of the simplicity to handle water based instead of organic based solvents. After debinding, parts are dried. Another type of solvent debinding is obtained by using supercritical fluid (CO_2), but the long processing time and high costs, makes this option not widely used.

Catalytic debinding is used for binders that decompose in smaller molecules in the presence of catalyst when exposed at adequate temperature. The feedstock used in the present thesis was a 316L metal powder mixed with polyoxymethylene polymer (POM): this binder could be removed by a catalytic procedure. The green part has to be placed in a gas furnace with a nitrogen atmosphere and few percent of gaseous nitric acid. Due to the catalyst, the reaction occurs at 110-140°C whereas it could only take place at temperatures of 200°C and over. In this acidic atmosphere the polyacetal was converted into its gaseous monomer, formaldehyde (see Figure 1-6). The debinding reaction takes place on the surface pores because the acid nitric gas cannot penetrate the binder. The binder removal progresses from the outside to the core at a velocity of 1-2 mm/h [15].
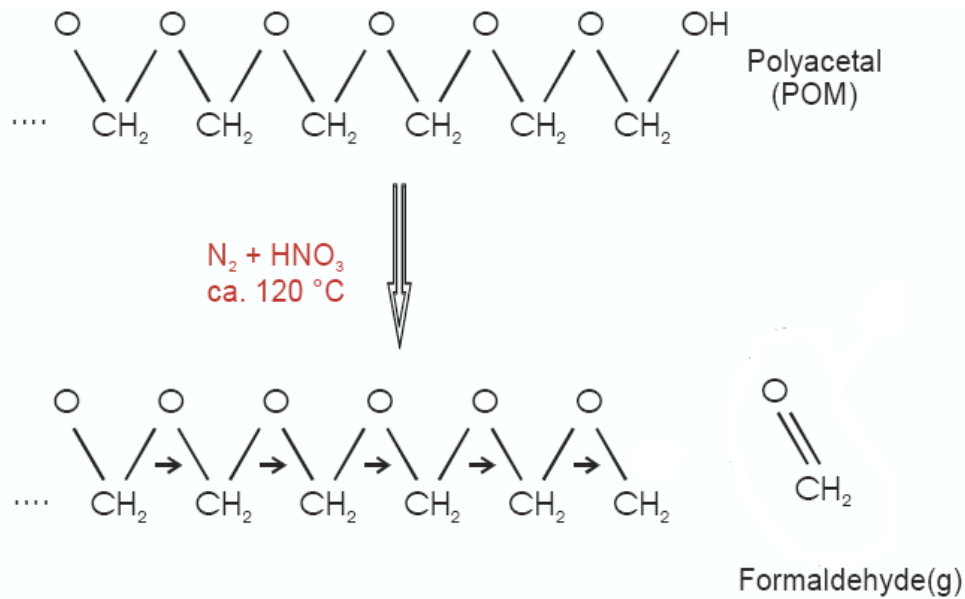
Figure 1-6. Schematic representation of the catalytic debinding step for POM.

After completion of polyacetal removal, there is a little amount (around 10%) of residual acid resistant binder component. This residual organic fraction will be removed during the sintering step [16].

Sintering step

After the debinding step, the remainder binder has to be removed by thermal degradation and the metal powder can be sintered to high densities of 95% and over. This thermal residual process can carried out either under vacuum or in a protective atmosphere, using a combination of nitrogen and hydrogen gases. Sintering temperatures are below the melting temperature of the metal or ceramic powder (70-90% of melting temperature). In this way the temperature in high enough for starting the crystallization process, but low enough for holding the particles unmelted. In this condition, the particles can crystallise into each other causing them to fuse together [14]. For 316L feedstock, the sintering temperature is around 1200-1300°C [15]. In this step, shrinkage can be as high as 20 percent.

1.5 The thesis structure

Figure 1-7 reports the thesis structure.

The chapter 2 reports the literature review, and its analysis contributed to identify a research gaps in μ-IM field. The methodology set for filling these gaps was described in chapter 3: this section reports the materials, the mould manufacturing, the metrology protocol and the statistical model adopted. Chapter 4 described the steps that were adopted for reaching the final micro-mould configuration and for solving some moulding problems. These procedures permitted to deal with real life approach and with the common problem solving used in injection moulding: the improved mould permitted to identify increased processing parameter ranges that explored all the material mouldability range. Chapter 5 and chapter 7 reports the numerical results related to the materials investigated (POM and 316L feedstock respectively). Following the statistical approach adopted for managing the results, a statistically based optimisation was applied to the experimental data. The analysis, adopted desirability functions for fulfilling multiple quality criteria requests. The results were reported in chapter 6 for POM and in chapter 8 for 316L feedstock. Chapter 9 investigate the 316L feedstock behaviour for filling micro-textures.

Each chapter concerning the experimental results (chapters from 5 to 9) was structured by reporting an introduction to the argument, the results and the discussion. An overall discussion and the conclusions were reported in chapter 10 and 11 respectively. Chapter 12 reports the future work.

Appendices A treated about trials for realizing micro-channel with width lower than 60 μm. Appendices B reports the micro-mould designs.
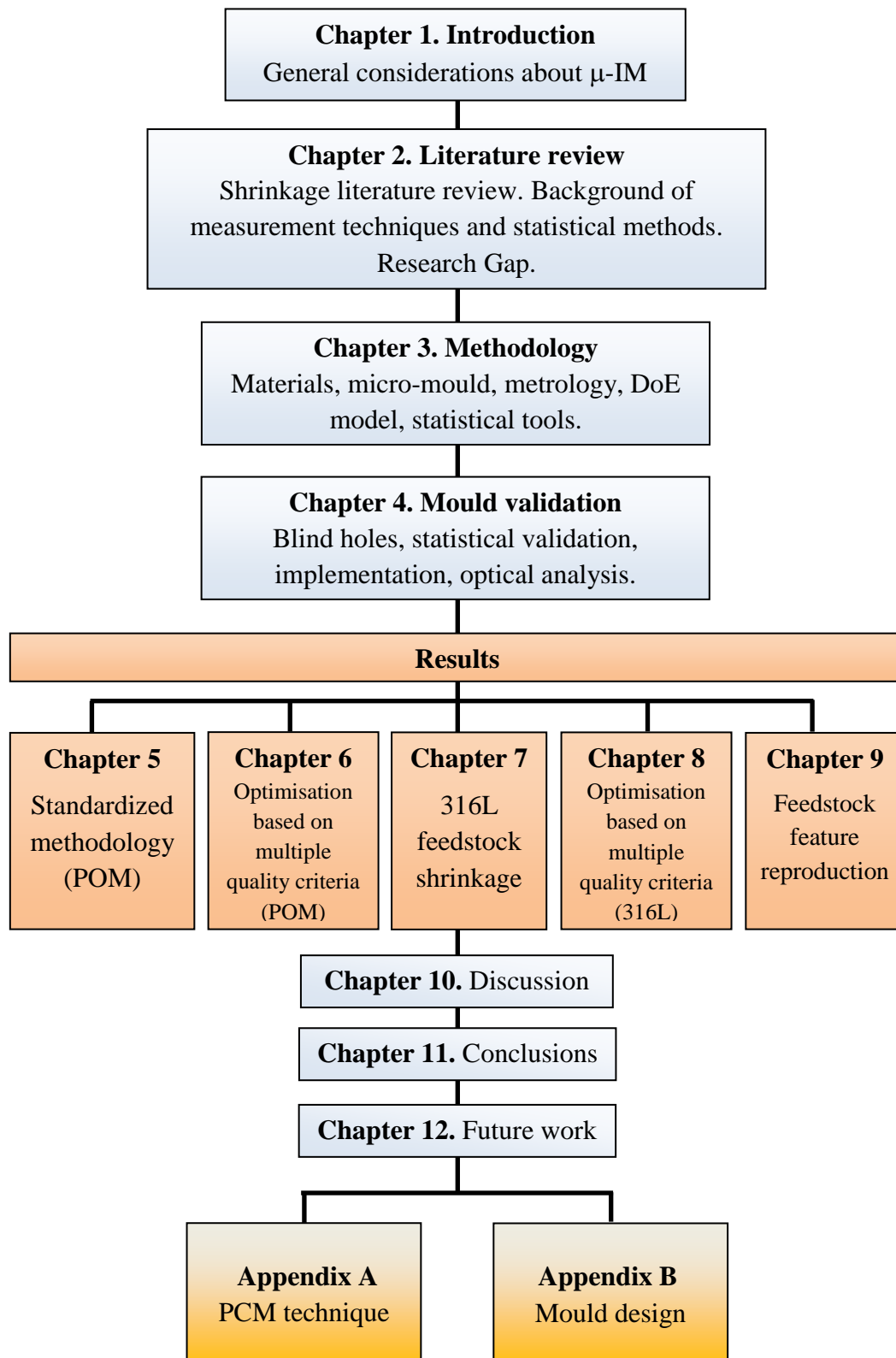
Figure 1-7. Thesis structure.

Chapter 2 . Literature review

This thesis adopted a systematically approach for determining the factors and for reducing the effects that shrinkage could generate. In this chapter was reported a literature review about shrinkage causes, and backgrounds about shrinkage measurement techniques and statistical approaches. The analysis of literature review identified the factors that affected shrinkage at macro and micro-scale and evidenced the absence of a standard suitable for the micro-scale. This fact, by considering the different material behaviour with respect to the conventional scale, was considered a gap. A further gap was identified in the absence of optimization stage that adopted simultaneously part mass and shrinkage results.

The end of this chapter lists the aim and the objectives of the thesis.

2.1 Structure of moulding shrinkage literature review

The literature review was focused about the processing parameters that affect shrinkage of moulded parts (both in macro than micro-scale) and considered only papers that experimentally validated the results. The definition normally accepted for moulding shrinkage was reported by Fischer in his "Handbook of moulded part shrinkage and warpage" [17]: "mould shrinkage (or in-mould shrinkage or moulded part shrinkage) usually refers to the difference between the linear dimension of the mould at room temperature and that of the moulded part at room temperature within forty-eight hours following ejection".

A start point on how to structure the literature review was the scheme reported by Stan et al. [18]: the authors organized different sources for depicting a diagram that considered factors that affect shrinkage and warpage (specimen and mould design, operator, environment, material properties, processing parameters, injection moulding machine and measurement). Experimental evidences [19] have shown that shrinkage and warpage were affected by different factors, even if warpage (defined as differential shrinkage) was generated by shrinkages. As consequence, a more focused structure

respect to the scheme reported by [18] was adopted and some sources of influence were considered negligible. In detail, the operator because a preliminary familiarization stages can identify the correct parameter range that will be statistically arranged; the factors due to the moulding machine because Battenfeld Microsystem 50 is a dedicated micro-injection machine and its great precision reduced the errors from inaccurate processing parameters control; the measurements because a dedicated metrology protocol was adopted; the environment because - despite was not possible to monitoring the room humidity - the Battenfeld permits to control the polymer temperature stored in a sealed hopper (set at 70°C) and this assure constant polymer conditions.

The result of these considerations was reported in Figure 2-1. The literature review was organized by considering branches connected to material properties (as crystallinity, morphology and PVT properties) and technical aspects. As technical aspects, were considered factors strictly connected to moulding process: processing parameters, mould design and specimen design. At the end of each branch, main conclusions were summarized and papers grouped in tables.
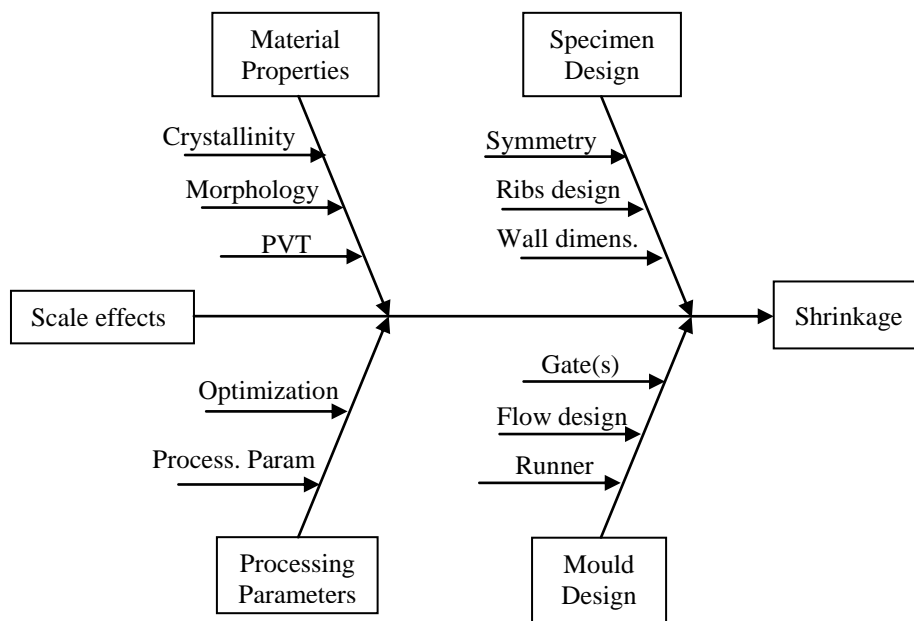
Figure 2-1. Factors considered in the literature review.

The diagram reported in Figure 2-1 starts with the indication of a scale effect because experimental evidences demonstrated that shrinkage was affected by the scale: for this reason, the scale effects were considered in the literature review.

2.2 Search methodology

The state of the art about shrinkage in injection moulding was approached by implementing SCOPUS, a bibliographic scientific database. A first research flow started by using the keywords "molding" AND "shrinkage", by limiting results to the last 10 years (2004-2013) in material science and engineering fields. Figure 2-2 reports the research flow adopted. The filter "composite" requested a dedicated screening because of the huge scientific works presented under this term.

4134	•Molding AND shrinkage
3707	•Material Science AND Engineering
2239	•Limited to 2004-13
1150	•AND NOT composites
1068	•AND NOT neural network
1021	•AND NOT clays
878	•AND NOT casting
496	•AND NOT thermal
487	•AND NOT cement
444	•AND NOT lithography
434	•AND NOT liquid crystal
428	•AND NOT thermoset
402	•AND NOT CAD
378	•AND NOT CAE
371	•AND NOT wafer
357	•AND NOT image
282	•AND NOT sintering
280	•AND NOT debinding
243	•AND NOT strength
	• Screening

Figure 2-2. SCOPUS results using "molding" AND "shrinkage" keywords.

Figure 2-3 reports the screening results. The analysed papers resulting from the first research flow were 50 papers with studies in the macro-scale and 24 papers with studies in the micro-scale.
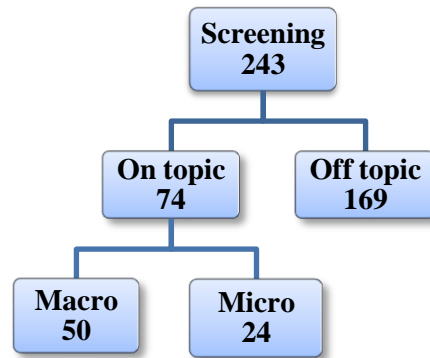
Figure 2-3. Papers considered from the screening "molding AND shrinkage".

The second literature research flow was performed considering the keyword "injection molding". The results were limited to the last 10 years (2004-2013) in material science and engineering fields. From the amount of these papers (10419) were selected the works that investigated 316L feedstock (302) and POM (137). Figure 2-4 reports the SCOPUS results.
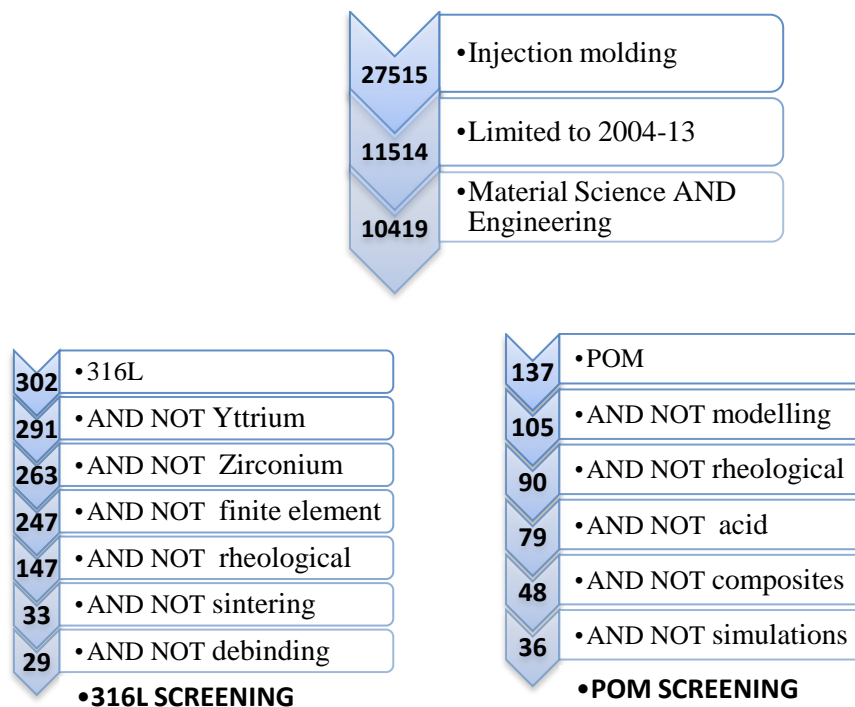
Figure 2-4. SCOPUS results using 316L feedstock and POM keywords.

Following the approach adopted previously, the papers were divided in "on topic" and "off topic". Figure 2-5 reports the results according to this division.
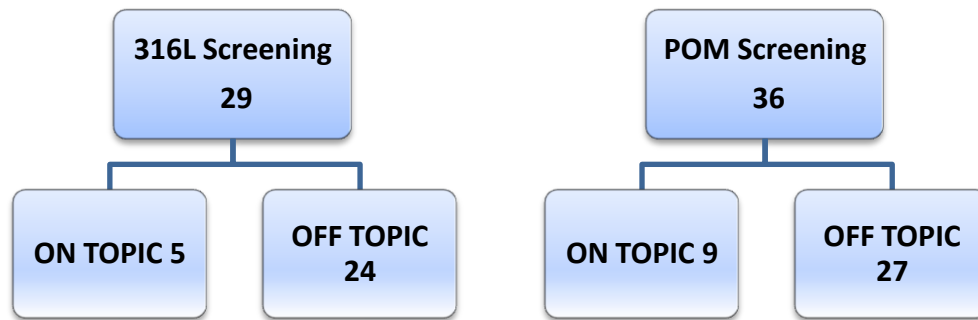
Figure 2-5. Screening results for 316L feedstock and POM keywords.

The final papers selected by adopting the paths reported in Figure 2-3 and Figure 2-5 cannot be considered as the full state of the art, because SCOPUS, even if a scientific database, cannot cover the entire knowledge in this field. For this reason, it was necessary to integrate the selected papers by considering also others sources available in the Web (Google Scholar, Web of Science, free online papers). The overall results were considered state of the art of shrinkage, and discussed in the present thesis for approaching shrinkage consequences.

Despite of the great importance of ceramic injection moulding, only few related papers appeared in the literature. This was because the greater part of papers that investigated shrinkage of ceramic parts, were focused about shrinkage resulted by debinding and sintering step and about rheology behaviour, instead of moulding shrinkage.

2.3 Exclusion statement

The research flow adopted filters that worked in the following way:
"composites" filter removed all the argument related to thermosetting resins and fibre reinforcements, "neural network" removed papers about modeling or predictions without experimental validations, "clays" removed papers about organoclays, "casting" removed papers that studied different technique respect injection moulding, "thermal" removed papers about thermal properties, "cement" removed papers that investigated different materials from thermoplastic polymers, "lithography" removed papers that argued about techniques different from injection molding, "liquid crystal" removed papers about birefringence properties or displays, "thermoset" removed papers about

17

thermoset materials, "CAD" and "CAE" removed papers about simulations without experimental validation, "wafer" removed papers about silica, "image" removed papers about non-destructive techniques, "sintering" and "debinding" removed papers concerned stages different from moulding, "strength" removed studies that investigated the mechanical properties of moulded materials.

In the research "injection molding" for 316L feedstock the filters worked in the following way:
"Yttrium" and "Zirconium" removed papers about materials different from thermoplastic, "finite element" removed papers about theoretical studies without experimental validation, "rheological" removed papers about pure viscosity characterization without connection with processing parameters, "sintering" and "debinding" removed papers about stages not considered in the present thesis.

In the research "injection molding" for POM, the filters worked in the following way:
"modeling" removed papers without experimental validations, "rheological" removed papers about viscosity studies, "acid" removed papers about organic or poly-lactic acids, "composites" removed papers about layered material and thermosetting resins, "simulations" removed papers about theoretical material behaviour.

2.4 Moulding shrinkage literature review

As reported in Figure 2-1, the literature investigated four branches at the macro and micro-scale: the material properties, the processing parameters, the mould and the specimen design influence.

2.4.1 Material property influences

Under the term "material properties" were considered aspects such as PVT behaviour, internal structure/morphology and material crystallinity. According to the literature reviewed, these properties affect moulding shrinkage and have to be considered.

2.4.1.1 Material properties at the macro-scale

PVT trend

The intrinsic cause for shrinkage of injection-moulded parts is the thermodynamic behaviour of the material, as reported in Figure 2-6. The PVT trend determined the

compressibility and thermal expansion of plastics as confirmed by studies [20; 21]. In detail, a different PVT behaviour between amorphous and crystalline materials was observed. In a melt condition, both classes have shown a linear dependency of the specific volume from the temperature. On the contrary, for the solid phase considerable differences were observed. Because of crystallization in semi-crystalline materials, the specific volume decreased exponentially (shrinkage was caused by these dimensional variations) with decreasing temperature, while amorphous materials still presented a linear dependency in the solid phase. This difference caused the greater shrinkage of crystalline thermoplastics respect the amorphous polymer. The curves labelled with the number from zero to 200 represents different polymer packing pressures [MPa]: the higher was the pressure, the lower was shrinkage.
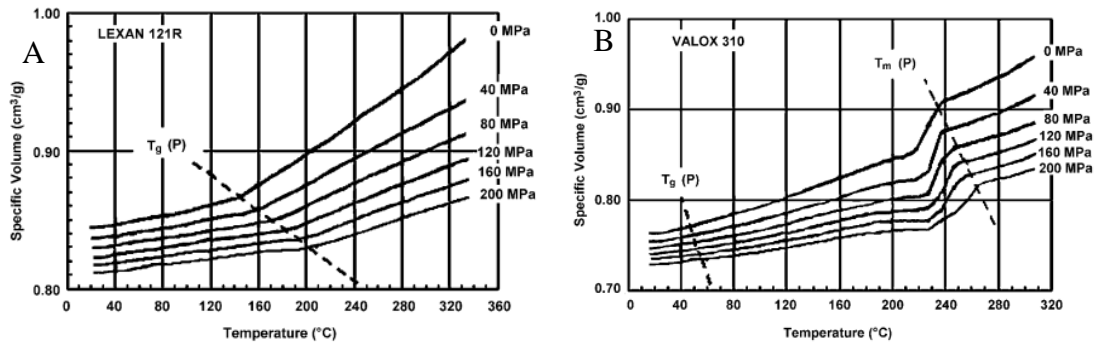
Figure 2-6. PVT diagram for an amorphous (A) and a crystalline (B) thermoplastic material [17] [Reprinted with permission from Elsevier editor].

Morphology contribution

Morphological aspects as the different density of the crystalline phase before and after the freezing [22] and the flow effect in terms of molecular orientation [23], can affect shrinkage. Investigations about molecular orientation shown that during the injection stage, the mould filling process can confer to polymer chains a predominant flow orientation because of the flow-induced crystallization. Moreover, in a mass of injected polymer melt, the molecular chains were naturally oriented along the flow direction. This ordered conformational state exhibits a higher (with respect to the randomly oriented configuration) free energy that drive the crystallization process [24].

Other authors confirmed the morphology contributions. During the injection stage the formation of frozen-layers in the melted polymer in contact with the mould surface were observed. The layers have shown an oriented molecule chain [25] and induced residual internal stresses that affect shrinkage [26]. The layered structure was located on the external area of moulded part, and the core-to-skin volume ratio has to be considered as factor that strongly affects shrinkage [27].

Crystallinity contribution

The dimensional stability of moulded parts was connected to crystallinity and experimental results evidenced that moulded part can potentially continue to shrink also days after the moulding stage [28]. Indeed, physically, the crystallization continues below the melting point and above the glass-transition temperature (T_g), and the more the material crystallize the more it shrinks. As demonstrated by [29] shrinkage starts inside the mould as soon as the polymer layer solidifies. It was also demonstrated that the crystallinity influenced the no-flow (sharp increase in viscosity value) and solidification conditions, the formation of frozen layer, the internal stresses and the in-mould shrinkage.

Summary

Material influences can affect shrinkage at the macro-scale. In details, the different PVT behaviour between amorphous and crystalline material polymers [20; 21] determines dimensional variations of moulded parts. Moreover, shrinkage can be determined also by different densities of crystalline phases [22], frozen-layers with flow-oriented molecules [23; 25] and residual internal stressed located in the layers [26]. The core-to-skin ratio affects shrinkage as well [27].

Drove by crystallinity, material can continue to shrink also day after be moulded [28]. Material starts to shrink inside the mould as the polymer touch the mould cavity wall [29].

Table 2-1 reports the papers about material properties that investigated shrinkage at the macro-scale.

	REF	MAT	PHENOM
PVT	[20; 21]	Amorf. – Cryst.	
Morphology	[22]	PP copolymer	Freezing
	[23]	PE	Molecular orientation
	[25]	PE	Oriented layers
	[26]	PP	Residual stresses
	[27]	PP	Core-to-skin ratio
Crystallinity	[28; 29]	iPP	Crystallinity

Table 2-1. Material properties influence at the macro-scale. MAT reports information about material and PHENOM is the phenomenon that caused shrinkage.

2.4.1.2 Material properties at the micro-scale

PVT trend

It is important to understand if the scale can affect material behaviour. An answer was provided by [11]: authors stated the different behaviour that polymeric material assumes when flows in micro channels respects macro geometry situation. The difference depends on size-dependent viscosity and wall slip phenomenon (as consequence of the great wall shear stress when filling micro-to-sub micro channels [11]). Results shown that in micro-scale, polymer flows differently respect macro-scale for the presence of intermolecular forces that occur due to the scale. Due to these influences, it result the necessity to improve the pressure of 20-30% in micro-scale respect the standard filling conditions.

However, despite this different behaviour, the PVT trend of material still follow the same conventional behaviour observed at the macro-scale: as the packing pressure increased, the shrinkage of semi-crystalline materials decreased with an exponential shape [30]. The author suggested that the shape of curves was determined by binder and his dominantly behaviour.

Polymer morphology contribution

Experimental results shown that semi-crystalline polymer shrinks more than amorphous polymers [31] and morphology was influenced by homogeneous dispersion of powder mixed with polymer [32]. The percentage of powder affected shrinkage, because the dimensional variations decreased by increasing the powder loading [33].

A relationship between binder microstructure and shrinkage was identified by [34], because a coarse flake binder structure leads to high shrinks during the transition from melt to solid state. The use of microcrystalline wax can confer a finer binder grain and a more isotropic (no preferred orientations) feedstock micro structure. These modifications resulted in a lower final shrinkage respect to coarse binder structure.

The relationship between polymer morphology and shrinkage involve different aspects of moulding processing not always simply to identify. Particle size, powder loading, but especially shear rate and polymer temperature can affect morphology and determine the feedstock viscosity [35] and the viscosity was directly related to shrinkage of moulded part as demonstrated by [36].

A study concerned the morphology differences between macro and micro-scale was carried out by [37]. By considering the crystallinity effects in the flow-direction of both macro and micro-parts of specimens moulded from isotactic polypropylene (iPP), evidences shown that the through-thickness morphology of micro-parts exhibited a similar ''skin–core'' type of structure to the macro-parts. However, in the micro-parts a large fraction of shear layer was present (highly oriented), whereas the macro-parts presented a large fraction of core layer (randomly oriented). The shear layer of micro-parts had a highly oriented 'shish-kebab' structure (Figure 2-7), with a pronounced orientation of iPP chains within lamellae. The authors calculated that the percentage thickness of the oriented region of the micro-parts (which included both the skin layer than the shear layer) was much greater than in the macro-parts (90% versus 15%). The complex combination of internal stress and cooling rate affect the crystallization kinetics (flow inducted phenomenon), and the shear layer results with higher degree of crystallinity respect the polymer core. As overall effect, also the degree of crystallinity was affected by scale-effects: in micro-scale, the degree of crystallinity was higher with respect to the macro-scale. These different degrees of orientation and crystallinity observed at the macro and micro-scale indicates that shrinkage data obtained at the macro-scale was unlikely to be directly extrapolatable to the micro-scale. Furthermore, they indicate the necessity of directionally dependent measures of shrinkage for micro-scale components, as the orientation is likely to produce anisotropy in the shrinkage behaviour.

The shish-kebab structure at the micro-scale was observed also by [38]. The crystallization was influenced by shear stress history, and the core area of moulded parts presented a spherulitic structure, with an increased density from the wall to the centre of moulded part.
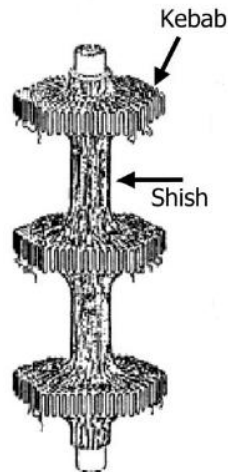
Figure 2-7. Shish-kebab structure [Reprinted with permission of author] [39].

Crystallinity contribution

Studies demonstrated that the scale influenced the crystallinity (in terms of crystal size, degree, ratios) and this affects shrinkage also. As stated by [40] during the analysis of semi-crystalline polymer (HDPE), crystallinity was influenced by processing parameters and by the scale: an increased crystal dimension and crystallinity degree was observed at the micro-scale with respect to macro-scale.

Again, processing parameters influenced micro morphology and crystallinity as demonstrated by [41]. Final results evidenced that processing parameters affected the thickness and the molecular orientation in the skin layer: these factors contributed also to improve the mechanical properties in micro more than in macro-parts, since the skin layer represented a larger fraction of the overall thickness.

Summary

By summarizing the information about material influence at the micro-scale, it was possible to say that, concerning PVT trend, also at the micro-scale amorphous and crystalline materials continue to exhibit different behaviour [30].

Considering morphology, conclusions confirm that at the micro-scale semi-crystalline materials shrinks more than amorphous [31] and differences can be determined by powder loading [33] and degree of powder dispersion [32]. The grain structure was determined by the binder but can be tuned (from coarse to fine) by mixing suitable waxes: these adds influenced final shrinkage [34]. Dimensional variations were connected to viscosity [36] and affected by processing parameters [35] that can determine final crystallinity [40].

However, at the micro-scale, a higher percentage of oriented layers were observed with respect to macro-scale [41], and this higher fraction at the micro with respect to the macro-scale promotes higher shrinkage [37].

Table 2-2 reports the works concerning the material properties that affect shrinkage at the micro-scale.

	REF	MAT	PHENOM.
PVT	[30]	Amorf. – Cryst.	
	[11]	PS	Different flow behaviour
Morphology	[31; 33]	ZnO+PP HDPE,PS,ABS	Shrinkage
	[32]	Al$_2$O$_3$+PP	Powder dispersion
	[34]	HDPE+MW	Binder structure
	[35]	316L feedst.	Viscosity
	[36]	316L feedst.	Viscosity vs. shrinkage
	[37]	iPP	Scale influence
	[38]	PE	Shish-kebab
Crystallinity	[40]	HDPE	Scale influence
	[41]	HDPE, POM, PC	Layers molecular oriented

Table 2-2. Material properties that affect shrinkage at the micro-scale. PHENOM concerned the physical phenomenon associated to shrinkage, and MAT the polymer investigated.

2.4.2 Processing parameter influences

The greatest number of works about shrinkage were focused on the study of processing parameter influence mainly for two reasons: firstly, for being effective the determination of material property aspects that affect shrinkage have to be followed by many trials for modifying these aspects (e.g. to change the crystallinity degree, to tailor the correct feedstock/polymer to be injected), and this takes time by requesting specific

competences; secondly, by using the statistical approaches nowadays available it is possible to identify the critical processing parameters with an high degree of precision and reduce shrinkage by optimizing the factors. Indeed, to deal with injection moulding (but more generally with every engineering process) requests to manage with a great number of parameters, and only by adopting a methodic approach to shrinkage phenomenon was possible to determine what factors can be considered critical. The use of statistical approaches (design of experiment or Taguchi methods, just to mention the most common) is an effectual way to operate, and every parameter identified as critical, often, was the result of statistical treatments of data.

Many authors, also considering the great range of feedstock/polymer suitable for every application, preferred the second approach.

2.4.2.1 Processing parameters at the macro-scale

When injected material fills completely the mould, the screw remains stationary for some time to keep the plastic in the mould under pressure (holding time). During the holding stage, an additional material is injected into the cavity mould for compensating the shrinkage caused by cooling effects [7]: this sentence condenses the concept that the most part of injection moulding parameters can potentially produce effects in terms of shrinkage. Holding parameters, amount of materials, injection, cooling stage, temperatures: all these factors were investigated for identifying their influence on shrinkage.

The parameters that critically affect shrinkage were organized by naming the factors, then by reporting the research results.

Cooling time

Cooling time is the elapsed time required the melt to reach its Vicat softening temperature [42]. It is also commonly defined as the time from the end of packing stage toward ejection.

This parameter affected shrinkage according to [43] and was considered the second critical parameter after the holding pressure by [44]. By using a hybrid optimization method that combined Taguchi methods, grey relational analysis and PCA, [45] investigated shrinkage of moulded gear: results shown that this factor was the third

critical parameter after melt temperature and packing pressure. As stated by [46] and [47], an increase of cooling time decreases shrinkage. This trend it was likely due to an higher probability of molecules to attain a more favorable configuration during increased time of cooling. The criticity of cooling time in terms of shrinkage was confirmed also by considering techniques lightly different from injection moulding as MUCELL (microcellular injection moulding) [48].

Packing (or holding) time

Packing time was defined as the time necessary for filling the mould cavity as full as possible without causing undue stress on the molds or causing flash on the finished parts [42]. The packing time is strictly connected to the gate freeze time, because after gate freezing an additional time does not produce further effects. Besides it is important to set a suitable packing time during injection moulding stages, because if the packing pressure is released before complete gate freezing (e.g. too short packing time), melt could flow back from the cavity mould (backflow) by determining lacks of material in final specimen [29].

Different approaches (numerical simulation [49], Taguchi methods [50-52] coupled with hybrid optimization [45], DoE [48; 53; 54]) and consequent experimental validations, identified the packing time as a critical factor. According to [55] this factor resulted critical for amorphous (ABS) but not for semi-crystalline polymer (PP). By analysing polymer wax, [56] confirmed the critical influence in terms of shrinkage. Also by considering ceramic based feedstock (tungsten mixed with polymer wax [57]), this parameter confirmed to critically affect shrinkage. About trend, to increase this parameter leads to decrease shrinkage (parallel to the flow direction [47]). Authors [58] confirmed that to increase this parameter leads to decrease shrinkage.

By using strain gauges, [29] measured the transient shrinkage history of an iPP rectangular slab as a function of the holding pressure, and confirmed that shrinkage decreased by increasing the packing time.

Packing (or holding) pressure

Once the majority of the plastic (95%) has been injected using injection pressure, the injection machine shift to apply the packing (or holding) pressure. This pressure (lower

than injection pressure) permitted the final filling of the mold by packing the molecules together. Holding pressure was applied until the gate freezes: once that happened, the pressure has no more effect on the molecules on the other side of the gate. If holding pressure was decreased before the gate freezes, the inversion of pressure gradients causes a dramatic decrease of pressure evolution inside the cavity mould [29] and the material in the cavity can be sucked back out of the cavity ("backflow" phenomenon).

A not properly set packing pressure value can cause shrinkage according to [59].

Studies that adopted Taguchi approaches [19; 45; 50; 60; 61] or different methods [44; 48; 53; 54; 62-65] identified this parameter as strongly critical. Shrinkage starts as soon as melted polymer fills the cavity mould, and was critically affected by holding pressure [29; 66].

By analysing semi-crystalline material (PP) [55; 67-70], PP filled with $CaCO_3$ [71], ceramic feedstock as Zr [72] (in combined effect with mould temperature) or W [57], authors found that packing pressure was the most influential factor (above different parameters considered).

Evidences shown that packing pressure can produce directional responses in terms of shrinkage: by improving holding pressure, transversal shrinkage of ceramic moulded parts was decreased [73]. Regardless the flow direction, similar results was reported by the authors [58; 74; 75], that confirmed how high holding pressure leads to lower shrinkage. Considering a square specimen geometry of an amorphous polymer (ABS), this parameter affected shrinkage both in longitudinal (first in ranking order) that transversal (second in ranking order) direction [76]. As general trend seems that to increase this parameter, promote the decrease of shrinkage [77-79] and a re-orientation of melt molecules [67].

A contrary result was presented by [80]. The authors focused their researches on the reduction of injection moulding cycle time by using cooling water containing activated carbon pellets. Under this particular condition, it was demonstrated that cycle time and shrinkage can be efficiently reduced by a low packing pressure.

This parameter can be considered an important factor that affects shrinkage because of many conclusions and studies. Is not negligible the property to influence directional

shrinkage response even by rearranging molecular chains. Generally, to improve this parameter leads to decrease shrinkage, except the particular conditions tested by [80].

Melt temperature

Melt temperature was defined as the temperature at which the polymer changes from solid to liquid state, that is became fluid and can be injected in the mould.

Many authors [61; 69; 81-83] adopted Taguchi methods for determining the influence of this parameter: results demonstrated that melt temperature critically affect shrinkage. Moreover melt temperature affect both longitudinal than transversal shrinkage [76].

Same conclusions were assessed even by considering different materials as semi-crystalline (HDPE [49; 84], PS [69; 85], PP [44; 47; 55; 68]), polymer wax [56], amorphous (ABS [55], PVC [51], PC/ABS [75]) or ceramic based feedstock (W [57], Si_3N_4 [86]).

An interesting effect of melt temperature was reported by [85] that described the relationship between melt temperature and melt flow within the cavity cross through the gate. Outcomes shown that this parameter influenced the amount of material inside the cavity mould as well, and consequently shrinkage because under a more pronounced amount of melt flow, the area near the gate can receive much material for compensating part shrinkage. However, [85] did not identify a clear trend in terms of shrinkage effects.

Mould temperature

Mould temperature was defined as the temperature of mould surface in contact with melt.

Authors [61; 83] investigated this parameter by using Taguchi methods: results have shown that mould temperature can be considered a critical factor. Same result was confirmed by adopting different statistical approaches as the grey-fuzzy logic analysis [62]. Often works that identified mould temperature as critical parameter, coupled this result with melt temperature: in these cases authors talk generally of "temperatures".

This parameter was identified as critical by considering amorphous (PS and PC [64], PMMA [60]) semi-crystalline polymers (PP [64], Nylon 46 [50], HDPE [84]), or ceramic feedstock (Zr [72], coupled with holding pressure).

The confirmation of the importance of this factor was reported by [76], which proved that mould temperature affected shrinkage both in transversal than longitudinal direction. About the trend, according to [58; 77; 87] high mould temperature increases shrinkage, even if other authors identified an opposite trend [61; 64; 84]: both were confirmed by [75] (study about PC/ABS cellular cover) that identified a decrease of shrinkage between 60-70°C, and an increase between 70-80°C.

Injection pressure

Injection pressure was defined as the pressure on the face of the injection screw when melt material was injected into the mould [42].

By adopting a new methodology based on RPSGAe (Reduced Pareto Set Genetic Algorithm with Elitism technique), [78] shown that shrinkage decreased when injection pressure increased. Similar conclusions were stated by [46], that investigated a semi-crystalline polymer (HDPE) mixed with ceramic powder ($CaCO_3$), by [57] (W material) and by [87] with different materials. This parameter has shown a directional influence in terms of shrinkage, because affected transversal shrinkage in reinforced PET specimens [88], and longitudinal shrinkage in co-PP [47].

However, all the authors identified the same trend, which is to increase the injection pressure leads to decrease shrinkage.

Injection speed (or velocity)

The injection speed was defined as the speed which the polymer was injected into the cavity mould, determined by the screw movement on forward during melt injection.

The influence of this parameter was evaluated in papers that considered shrinkage longitudinal to, and transversal to, the flow direction: this parameter was the fourth factor affected shrinkage in transversal direction, and the second factor that critically affected longitudinal shrinkage [76]. Authors [47; 58; 74] shown that high values of this parameter leads to high shrinkage in parallel to but not in normal to the flow direction.

A reduction of transversal shrinkage by increasing the velocity speed was confirmed by [73] during the analysis of ceramic feedstock.

Further considerations

In the papers that considered the influence of processing parameters in terms of moulding shrinkage at the macro-scale, it was possible to collect also general indications about different aspects: e.g. compression factors [85; 89; 90], appropriate mould design [91-94] and suitable processing conditions [61; 93; 95; 96] can reduce and compensate shrinkage.

Some papers identified differences between parallel to and normal to the flow shrinkage. According to [97], the packing pressure, the injection velocity and melt and mould temperature affect shrinkage parallel to the flow; whilst melt and mould temperature, packing pressure and injection velocity affect shrinkage normal to the flow. According to [47] (by analysing co-PP and co-PP mixed respectively with $CaCO_3$, SiO_2 and PSBR), the processing parameters affected shrinkage in the length but not in the width and thick. According to [88], transversal shrinkage was affected by injection pressure. According to [98] shrinkage along length was affected by mould temperature, injection pressure, screw rotation speed, mould temperature-injection pressure interaction and mould temperature-screw rotation speed interaction; while along the width direction shrinkage was affected by mould temperature, injection pressure, screw rotation speed, mould temperature-screw rotation interaction. The authors [99] considered PP specimens, and longitudinal shrinkage was between 2 and 4 times more (on the average) that shrinkage in transversal direction. The authors [76] stated that transversal shrinkage was critically affected by melt temperature, packing pressure, mould temperature and injection velocity; longitudinal shrinkage was affected by packing pressure, injection velocity, melt temperature and mould temperature.

Concerning the trends, high injection velocity leads high shrinkage in parallel to but not in normal to the flow direction [74]; to increase holding pressure leads to decrease shrinkage [64; 73; 74; 78; 79]; an increase of pressure during the holding phase induce a molecular re-orientation in the melt [67]; high packing pressure and mould temperature leads to reduce shrinkage [60]. General trend seems to indicate that high processing parameter values, except for the injection velocity, causes shrinkage decrease.

At last, also the moulding technique affects the shrinkage. Considering the micro-cellular injection moulding process (Mucell), this technique reduce shrinkage with respect to conventional injection moulding [100; 101], and the supercritical fluid content adopted during injection stage was identified as critical factor [53]. In Mucell processing, holding time, holding pressure and mould temperature affect shrinkage [48].

Table 2-3 reports the papers about processing parameter that affects shrinkage at the macro-scale. The paper marked with the asterisk referred to works that reported the interval of confidence of the statistical analysis (95%).

The arrows indicate whether a factor increasing causes an increase (↑) or a decrease (↓) in shrinkage.

PAR	REF	MAT	APPROACH	GEOMETRY	Shrink. resp.
Cooling t	[43]	POM		Plate with holes	
	[44]	PP	Taguchi	Convex shell	
	[45]*	PP	Hybrid method	Gear	
	[46]	CaCO$_3$+HDPE		Square plate	↓
	[48]	PP	DoE	Box	
	[47]	co-PP		ASTM D955	↓
Packing (holding) t	[57]	W + PW		Stand. tensile, cylinder	↓
	[56]	PS+PW		Gas turbine blade	
	[49]	HDPE	Taguchi	Shell geometry	
	[52]*	PC/ABS	Taguchi	Thin shell part	
	[45]*	PP	Hybrid method	Gear	
	[55]*	ABS	Taguchi	Rectangular specimen	
	[29]	iPP	Strain gages	Rectangular geometry	
	[51]*	PVC	Taguchi	Conical specimen	
	[50]	Nylon 4,6	Taguchi	Gear	↓
	[54]	PP	DoE	Box	
	[58]				↓
	[47]	co-PP		ASTM D955	↓
	[53]*	PP	DoE	Box	
	[48]	PP	DoE	Box	
Packing (holding) P	[72]	Zr + vinyl acet.	ANOVA	Parallelepiped shape	↓
	[57]	W + PW		Stand. tensile, cylinder	↓
	[58]				↓
	[75]*	PC/ABS	Taguchi	Cellular cover	↓
	[19]	PP	Taguchi	Box	↓
	[45]*	PP	Hybrid method	Gear	
	[61]	PC/ABS	Taguchi	Thin wall	
	[60]	PMMA	Taguchi	Rectangular cavity	↓
	[44]	PP	Taguchi	Convex shell	
	[65]	Nylon, TVP	DoE	Rectangular plate	↓
	[64]	PC, PS, PP		Tubular fittings	↓
	[54]	PP	DoE	Box	
	[48]	PP	DoE	Box	
	[53]*	PP	DoE	Box	
	[63]	PP	Taguchi	Rectangular geom.	
	[62]	PC/ABS	Grey-fuzzy logic	Thin-shell	
	[66]	PS, HDPE, PVC	On-line technique	Tensile bar	
	[70]	95% PP+5% clay	Taguchi		
	[69]*	PP, PS	Taguchi	Rectangular specimen	
	[55]*	PP	Taguchi	Rectangular specimen	
	[68]	PP	Model. and exp. valid.	Rectangular bars	↓
	[67]	PP		Rectangular plates	↓
	[71]*	PP+CaCO$_3$	Taguchi	Square specimen	
	[80]	TP polyolefin			
	[73]	LDPE + Al$_2$O$_3$		T shape specimen	↓ (n)
	[74]*	PP	DoE	Plate with constant and variable thick	↓
	[76]*	ABS	ANOVA	Square geometry	↓ (p) ↓ (n)
	[79]	PP		Plate and tubular	↓
	[78]	PS	RPSGAe	Rectangular geometry	↓
	[77]				↓

	Ref	Material	Method	Geometry	Influence
	[50]	Nylon 4,6	Taguchi	Gear	↓
	[29]	iPP	Strain gages	Rectangular geometry	
Melt T	[57]	W + PW		Stand. tensile, cylinder	↓
	[56]	PS+PW			
	[58]				↑
	[75]*	PC/ABS	Taguchi	Cellular cover	↓
	[84]	HDPE	Art. neural network	Cable clamps	↑
	[86]	Si_3N_4 + PP	Box-Behnken	Micro channels	↑
	[61]	PC/ABS	Taguchi	Thin wall	↓
	[51]*	PVC	Taguchi	Conical specimen	
	[83]	316L	Taguchi		
	[82]	PP	Taguchi	Circular shape specimen	
	[81]	PP	Taguchi	Box	↓
	[69]*	PS	Taguchi	Rectangular specimen	
	[76]*	ABS	ANOVA	Square geometry	↑ (n)
	[49]	HDPE	Taguchi	Shell geometry	
	[85]	PS	Taguchi	Rectangular specimen	↓
	[55]*	ABS, PP	Taguchi	Rectangular specimen	
	[47]	co-PP		ASTM D955	↓
	[44]	PP	Taguchi	Convex shell	
	[68]	PP	Model. and exp. valid.	Rectangular bar	↓
Mould T	[61]	PC/ABS	Taguchi	Thin wall	↓
	[72]	Zr + vinyl acet.	ANOVA	Parallelepiped shape	↑
	[58]				↑
	[64]	PC, PS, PP		Tubular fittings	↓
	[87]	PMMA, Nylon 6/6, Acetal, PP, LDPE			↑
	[83]	316L	Taguchi		
	[84]	HDPE	Art. neural network	Cable clamps	↓
	[62]	PC/ABS	Grey-fuzzy logic	Thin-shell	
	[76]*	ABS	ANOVA	Square geometry	
	[75]*	PC/ABS	Taguchi	Cellular cover	
	[77]				↑
	[60]	PMMA	Taguchi	Rectangular cavity	↓
	[50]	Nylon 4,6	Taguchi	Gear	↓
Injection P	[57]	W + PW		Stand. tensile, cylinder	↓
	[78]	PS	RPSGAe	Rectangular geometry	↓
	[87]	PMMA, Nylon 6/6, Acetal, PP, LDPE			↓
	[47]	co-PP		ASTM D955	↓
	[88]	PET		Box and plate shapes	↓ (n)
	[46]	$CaCO_3$+HDPE		Square plate	↓
Injection speed	[73]	LDPE + Al_2O_3		T shape specimen	↓ (n)
	[76]*	ABS	ANOVA	Square geometry	↓ (p)
	[74]*	PP	DoE	Plate with constant and variable thickness	↑ (p)
	[58]				↑↓
	[47]	co-PP		ASTM D955	↓

Table 2-3. Processing parameters influence on shrinkage at the macro-scale.

2.4.2.2 Processing parameters at the micro-scale

Compared to the macro-scale, in the micro-scale authors investigated also the replication quality. This aspect was connected to shrinkage and often the two concepts overlap, because a lack of precision in replication quality was determined by final dimensional variations due to un-controlled or under-estimated material shrinkage. These conclusions were confirmed by [102], which focused their researches on the replication quality of micro-channels moulded by µ-IM: final results shown that shrinkage phenomenon was the main reason for lack of replication quality. Moreover, as resulted by [103], the replication quality was mathematically defined with similar formula adopted for shrinkage measurement, but with opposite interpretation because an high replication quality is advisable.

The definitions of processing parameters were reported only if not already reported in the previous section.

Injection Pressure

Specimens moulded with high values of temperatures and pressures exhibited low crystallinity and better feature replications [104].

By adopting Taguchi methods, [105] investigated the influence of processing parameters in POM micro-rods moulded part: injection pressure was identified as shrinkage critical factor.

The critical influence of this parameter was confirmed also by [106]. The authors considered ceramic based feedstock (SiO_2, TiO_2 and ZnO powders mixed with PP binder in different percentages of 10-20-30 vol. %). Results identified the injection pressure as factor that, by increasing the powder loading, can decrease shrinkage.

Mould temperature

This parameter was considered critical according to [107-109] studies. The authors [31] investigated amorphous (GPS and ABS) and a semi-crystalline polymer (HDPE), by studying shrinkage both longitudinal to than transversal to the flow direction. The mould temperature is a critical parameter both for GPS than ABS, and affect shrinkage along the flow direction (the first in ranking order for both the polymers) and

transversal to the flow direction (ranked as the second and the first parameter respectively). Shrinkage of semi-crystalline polymer was affected by mould temperature both in longitudinal to (the third in ranking order) than transversal to (the second in ranking order) the flow direction.

By considering semi-crystalline (POM [105; 110; 111], HDPE and PP [104], HCPP and PC [112; 113], PP and PA [110] or PA mixed with 316L [114]) amorphous polymers (PMMA [104; 112; 115], PS [104; 112], COC [116], ABS [117]) or ceramic feedstock (Zr [118]), results identified the mould temperature as a critical parameter affecting shrinkage at the micro-scale. Also, authors [111; 119; 120] determined that by increasing this parameter, leads to increase the replication quality. Same trend was determined by [121] even considering a different material (316L feedstock).

An indirect confirmation of critical influence of mould temperature in terms of shrinkage, was reported by [106]. An analysis of ceramic based feedstocks (SiO_2, TiO_2 and ZnO in different percentages of 10-20-30 vol.%), confirmed that an increasing of mould temperature permitted to increase the powder percentage to be injected, and the increased powder loading permitted to decrease shrinkage as demonstrated by [13; 122].

A result in contrast about the trends indicated above, was reported by [123] that evidences how high mould temperature enhanced shrinkage and sink mark of micro-moulded sheet cavities.

Melt temperature

In the study conducted by [31], the authors investigated the influence of five parameters in terms of shrinkage both longitudinal to than transversal to the flow direction, by moulding amorphous (GPS and ABS) and semi-crystalline polymers (HDPE). The melt temperature resulted a critical parameter for GPS but not for ABS. Melt temperature affect GPS shrinkage along the flow direction (the second in ranking order) and transversal to the flow direction (ranked as the first factor). Shrinkage of HDPE was affected by melt temperature both in longitudinal to (the fourth in ranking order) than transversal to (the third in ranking order) the flow direction.

Other authors gave only general indications. In details, this parameter affected shrinkage in semi-crystalline (POM [119], HDPE [104], HCPP [113], PC [112; 113], PP [104]) amorphous (PMMA [104; 109; 112], PS [104; 112]) or cyclic olefin polymers [116].

About the trend, [121] determined that high melt temperature enhanced complete filling of 316L feedstock micro-features. Even if these authors did not investigate shrinkage, the measurements of micro-array shown that final dimensions replicated the cavity mould design: it is likely that melt temperature critically affect shrinkage too, and high values permits to reduce dimensional variations. Also [115] concluded that the replication of PMMA micro-channels array increased with high melt temperature values.

Holding time

The holding time critically affected shrinkage according to [109]. A combined effect of holding time and mould temperature was identified as critical by [119].

In the study conducted by [31], the authors investigated the influence of five parameters in terms of shrinkage both longitudinal to than transversal to the flow direction, by moulding amorphous (GPS and ABS) and semi-crystalline polymers (HDPE). Holding time affect GPS shrinkage transversal to the flow direction, then ABS and HDPE shrinkage both transversal to than longitudinal to the flow direction.

Packing (or holding) pressure

It is likely that this parameter contribute to reduce shrinkage because determine the overpressure inside the cavity mould at the end of injection stage. In μ-IM, the packing pressure can help the filling of micro-cavities in the mould insert to be filled with the polymer more than by applying a higher injection pressure. The holding pressure was considered critical parameter that affects shrinkage by [109; 124].

About the material, this parameter affected shrinkage of semi-crystalline (POM [8; 119], PE[31], HCPP [113], PC [112; 113], PP [104]) amorphous (PMMA [112; 115] or PS [112]) and 316L feedstock [121].

About trend, to increase this factor leads to decrease shrinkage (both in parallel to than normal to the flow direction), as confirmed by [117] by considering ABS square moulded parts.

Filling time

Injection moulded aspheric lenses were investigated by [109]. The author investigated six parameters, and filling time is the fourth critical factors affecting shrinkage.

Cooling time

The cooling time is a critical factor that affects shrinkage according to [109].

Barrel temperature

According to indications reported in [125], the melt temperature was controlled by the barrel temperatures, screw speed, injection speed and back pressure. Because of the jackets around the barrel can regulate the point at which the material will start to plasticize, authors considered the barrel temperature as factor to be investigated.

This parameter can affect the replication quality as confirmed by [111].

Injection velocity (or speed)

According to the conclusions of authors [111; 115], the injection speed affect shrinkage, and by considering semi-crystalline (PC [112]), amorphous material (PS and PMMA [112], ABS [117]), or ceramic based feedstock (Zr [118]) results confirmed this result. The authors [118] stated that to increase this parameter reduce shrinkage of moulded parts.

Metering size

The amount of material injected in the mould (expressed in mm^3) was defined as metering size. The author [8] studied this parameter and its effects during the mould of micro gears realised with a semi-crystalline polymer (POM). The statistical treatments of results shown that metering size critically affect shrinkage.

Filling flow (or filling flow rate)

The flow rate was defined as the volume of polymer that fills the cavity per second (expressed in $cm^3 \ s^{-1}$). Authors [126] demonstrated that the filling of the molten

polymer was enhanced by applying a high flow rate, and this parameter was essential to achieve the good replication quality. Considered the connection between replication quality and shrinkage, filling flow affects shrinkage as well.

Further considerations

Also in the papers that considered the influence of processing parameters in terms of shrinkage at the micro-scale, it was possible to get general indications about other aspects.

An improvement in terms of replication quality (connected to shrinkage) can be obtained by improving mould temperature according to different studies [113; 120; 121], by improving melt temperature and cavity pressure [113], or by an increasing of mould temperature, melt temperature, injection velocity and packing pressure [112].

As general trend, injection pressure decreased when temperature parameters (melt and mould) increased. According to [123] the increased mould temperature enhanced shrinkage, while the increased pressures parameters reduced shrinkage.

Table 2-4 summarize the papers about processing parameters that affect shrinkage and replication quality at the micro-scale. The paper marked with the asterisk referred to works that reported the interval of confidence of the statistical analysis (95%). The arrows indicate whether a factor increasing causes an increase (↑) or a decrease (↓) in shrinkage or replication quality.

PAR	REF	MAT	METHODOLOGY	GEOMETRY	Shrink. (S) / replic. quality (RQ)
Injection P	[104]	HDPE, PP (Crys) PMMA, PS (Am)	Dimens. analysis, rough., feature replic., X-ray	Micro and nano features	$S_{Crys} > S_{Am}$ S ↓
	[105]	POM	Taguchi	Micro-rods	
	[106]	SiO$_2$, TiO$_2$ and ZnO + PP		Square specimen	S ↓
Mould T	[31]	HDPE (Crys.) ABS, PS (Am.)	Taguchi	Rectangular bar	$S_{Crys} > S_{Am}$ S ↑ / S ↓
	[104]	HDPE, PP (Crys.) PMMA, PS (Am.)	Dimens. analysis, rough., feature replic., X-ray	Micro and nano features	$S_{Crys} > S_{Am}$ RQ ↑
	[109]	PMMA	Taguchi	Optical lenses	
	[105]	POM	Taguchi	Micro-rods	
	[117]	ABS	Response Surface	Square specimen	S ↓
	[108]	POM+10-20% GRF	DoE		
	[111]	PP (Crys.) POM (Crys.) ABS (Am.)	Dimens. analysis	Micro-features	RQ ↑ / RQ ↑ (pin geom.)
	[121]	316L+LDPE	Dimens. analysis	Micro pins array	RQ ↑
	[106]	SiO$_2$, TiO$_2$ and ZnO + PP		Square specimen	S ↓
	[123]	PP		Sheet cavity	S ↑
	[115]	PMMA	Dimens. analysis	Micro-channels	RQ ↑
	[120]	HDPE, PP (Crys.) PMMA, PS (Am.)	Dimens. analysis	Micro-features	$S_{Crys} > S_{Am}$ RQ ↑
	[110]	PP, PA, POM	Taguchi	Micro-gear	
	[119]*	POM	DoE	Square plate	S ↓
	[114]	316L+PA		Micro pillars array	
	[116]*	COC	ANOVA	Diffraction gratings	RQ ↑
	[118]	ZrO$_2$		Cylinder	
	[107]	PP	Taguchi	MAV wing structure	
	[113]	HCPP, PC	Dimens. analysis	Micro-structures	RQ ↑
	[112]	PS, PMMA, PC	Dimens. analysis	Micro-channels	RQ ↑
Melt T	[31]	PE (Crys.) ABS (Am.) PS (Am.)	Taguchi	Rectangular bar	$S_{Crys} > S_{Am}$ S ↑ / S ↓ / S ↓
	[104]	HDPE, PP (Crys.) PMMA, PS (Am.)	Dimens. analysis, roughness, feature replications, X-ray	Micro and nano features	$S_{Crys} > S_{Am}$ RQ ↑
	[109]	PMMA	Taguchi	Optical lenses	
	[121]	316L+LDPE	Dimens. analysis	Micro pins array	RQ ↑
	[115]	PMMA	Dimens. analysis	Micro-channels	RQ ↑
	[113]	HCPP, PC	Dimens. analysis	Micro-structures	RQ ↑
	[119]*	POM	DoE	Square plate	S ↓
	[116]*	COC	ANOVA	Diffraction gratings	RQ ↑
	[112]	PS, PMMA, PC	Dimens. analysis	Micro-channels	RQ ↑
Packing (holding) t	[31]	PE (Crys.) ABS (Am.) PS (Am.)	Taguchi	Rectangular bar	$S_{Crys} > S_{Am}$ S ↑ / S ↓ / S ↓(n)
	[119]*	POM	DoE	Square plate	S ↓
	[109]	PMMA	Taguchi	Optical lenses	
	[109]	PMMA	Taguchi	Optical lenses	
	[117]	ABS	Response Surface	Square specimen	S ↓

Parameter	Ref.	Material	Analysis	Specimen	Results
Packing (holding) P	[104]	HDPE, PP (Crys.) PMMA, PS (Am.)	Dimens. analysis, roughness, feature replications, X-ray	Micro and nano features	$S_{Crys} > S_{Am}$ RQ ↑
	[113]	HCPP, PC	Dimens. analysis	Micro-structures	RQ ↑
	[124]	POM, LCP	DoE	Dog bone specimen	
	[119]*	POM	DoE	Square plate	S ↓
	[8]	POM	DoE	Micro-gears	
	[121]	316L+LDPE	Dimens. analysis	Micro pins array	
	[112]	PS, PMMA, PC	Dimens. analysis	Micro-channels	RQ ↑
	[115]	PMMA	Dimens. analysis	Micro-channels	RQ ↑
	[31]	PE (Crys.) ABS (Am.) PS (Am.)	Taguchi	Rectangular bar	S ↑ $S_{Crys} > S_{Am}$ S ↓ S ↓ (n)
Filling t	[109]	PMMA	Taguchi	Optical lenses	
Cooling t	[109]	PMMA	Taguchi	Optical lenses	
Barrel T	[111]	PP, POM (Crys.) ABS (Am.)	Dimens. analysis	Micro-features	RQ ↑
Injection speed	[111]	PP, POM (Crys.) ABS (Am.)	Dimens. analysis	Micro-features	RQ ↑
	[115]	PMMA	Dimens. analysis	Micro-channels	RQ ↑
	[117]	ABS	Response Surface	Square specimen	
	[118]	Zr		Cylinder	↓
	[112]	PS, PMMA, PC	Dimens. analysis	Micro-channels	RQ ↑
Metering size	[8]	POM	DoE	Micro-gears	
Filling rate	[126]	Cyclic olefin	Taguchi	Micro-features	RQ ↑

Table 2-4. Processing parameters that influence shrinkage and replication quality at the micro-scale.

2.4.3 Design influences

Mould and specimen design aspects can affect shrinkage as well. As resulted by papers reviewed, at the macro-scale both aspects were considered, whilst at the micro-scale authors investigated mainly the specimen optimization.

2.4.3.1 Design solutions at the macro-scale

Specimen design

According to authors [58; 77] the thin-walled parts shrinks less that thicker part. Particular geometries, as ribs, were investigated by [91] for designing an optical CD pickup: a correct rib design, a suitable thickness and a correct gate position permitted to reduce shrinkage. Besides, to increase rib thickness leads to decrease the warpage as

well. Similar conclusions resulted also from [18] that stated how the specimen wall thickness, its border radius and ribs geometries affect shrinkage.

Even if sintering was not considered in the present thesis it is interesting to report that, according to [127] results, geometrical parameters affect the shrinkage also during this stage, i.e. thickness shrinkage decreases as the aspect ratio of width/thickness increase.

A general confirmation of the connection between geometry of moulded parts and dimensional stability (shrinkage and warpage) resulted from [128] even if the authors did not provide further details.

By considering the specimen shape, authors [129] manufactured a four-cavity injection mould with convex, concave, square and fan-shaped parts. Final results shown that the convex and concave parts shrank towards its geometry centre; shrinkage of outer diameter of fan-shaped part it was bigger that inner diameter and the angle of the fan-shaped parts become bigger than its original value.

Mould design

According to [130] high runner length produced higher shrinkage. The authors investigated rectangular PP bars, and experimental results evidenced that the heat losses occurred in longer runner affect shrinkage.

Concerning the mould elements, [94] identified the running size as critical parameter. Moreover, [93] stated that an improved gate design reduced shrinkage. Similar conclusions was reported by [92] about position gate. According to [18], mould characteristics (i.e. best gate position, runner diameter, smoothest flow path) have to be optimized for reducing shrinkage.

A not well designed mould can lead to asymmetrical mould temperature conditions caused by unbalanced heat transfer between the two mould sides: these conditions enhanced shrinkage and warpage [131]. For minimizing these effects, the authors built a numerical analysis model of discontinuous-thickness-variation (DTV). Theoretical results were validated experimentally and demonstrated that both shrinkage than warpage increased by varying the ratio depth/thickness in mould cavity. The difference of mould temperature between the mould core and cavity side contributed to warpage

and shrinkage. Also the cooling channel shape affects the thermal efficiency of the mould, and consequently shrinkage as well [132].

Another factor that can affect shrinkage is the mould material [133]. By using a metal (Al) or an epoxy moulds, the mould temperature profile varied: as resulted, shrinkage varied because of the different heat mould distribution.

Summary

Summarizing, the papers that investigated the effect of design at the macro-scale have shown that wall thickness [77], wall aspect ratio [127], ribs or border radius [18] affect shrinkage. It was verified a connection between specimen geometry and shrinkage [128; 129]. Regarding the mould design, gate position and runner diameter [18], and the balanced heat distribution inside the mould [131] affect shrinkage as well. Table 2-5 depicts the results.

2.4.3.2 Design solutions at the micro-scale
Specimen design

Specimen design can affect shrinkage at the micro-scale. The presence of holes decreased the packing pressure effect in the zone behind the hole, and as consequence shrinkage in these areas increased [38]. The base of rib geometries showed an increased shrinkage respect the upper part because this area was the last to solidify [134].

Ribs with different geometries (triangular, trapezoidal and rectangular section) and layout angle respect to the flow direction (0°, 45°, 90°) were considered for determining their influence in terms of shrinkage and warpage by [135]. Conclusions demonstrated that triangular and rectangular rib-cross section (45°, 90°) reduced dimensional variation of amorphous (PC/ABS) and semi-crystalline (PA66) polymers; while trapezoidal rib-cross section geometry (45°, 90°) was the most suitable geometry for minimizing dimensional variations in POM polymer.

It was observed that larger shrinkage occurred in the thin and narrow part of the specimen because of frozen layer, while on the contrary the thick specimen part shown smaller shrinkage because of the more easy molten filling [32].

Table 2-5 summarize the design factors that affect shrinkage. The paper marked with the asterisk referred to works that reported the interval of confidence of the statistical analysis (95%). The arrows indicate whether a factor increasing causes an increase (↑) or a decrease (↓) in shrinkage.

SCALE		REF	MAT	METHOD	FACTOR	Factor effect in shrinkage
Micro	Specimen	[32]	Al_2O_3	Dimens. analysis	Thickness	↑(behind the holes) ↑(rib base)
		[38]	PE	Dimens. analysis	Holes	
		[134]	POM	Dimens. analysis	Ribs	
		[135]*	PC/ABS, POM, PA66	Taguchi	Ribs	
Macro	Mould	[94]*	PC/ABS	Taguchi	Runner size	↑
		[93]	ABS	3D Thick. Contr. Meth.	Gate design	
		[92]	PS		Gate design	
		[132]	ABS, PP		Cooling runner	
		[18]			Gate, runner, wall thick.	
		[131]	ABS	Disc. Thick. Var.	Heat distribution	
		[133]	Mould mat. affect shrink.		Mould temp. profile	
	Specimen	[91]		C-Mould; exp.val	Wall thick, ribs	
		[77]			Thickness	↑
		[58]				↑
		[127]	316L		Aspect ratio	↓
		[128]	PC, HDPE	Dimens. analysis	Box Geometry	
		[129]	PP	Dimens. analysis	Concavity, convexity	
		[18]			Ribs	

Table 2-5. Design influence.

2.5 Literature review outcomes

The literature reviewed permitted to identify the critical factors that influence shrinkage and their response followed by a factor increasing. Table 2-6 summarise the results.

Branches	Factors	Scale	Phenomenon or parameters observed
Material properties	Crystallinity	Macro	Crystallinity.
		Micro	Scale influence, oriented molecular layers, shish kebab.
	Morphology	Macro	Freezing, molecular orientation, oriented layers, residual stresses, core-to-skin ratio.
		Micro	Shrinkage, powder dispersion, binder structure, viscosity.
	PVT	Macro	Differences between amorphous and semi-crystal polymers.
		Micro	Different flow behaviour, Differences between amorphous and semi-crystal polymers.
Processing	Processing parameters	Macro	Cooling time, packing pressure, packing time, melt temperature, mould temperature, injection pressure, injection speed.
		Micro	Injection pressure, mould temperature, melt temperature, packing time, packing pressure, filling time, cooling time, injection speed, metering size, barrel temperature.
Design	Mould	Macro	Runner size, gate design, cooling runner, wall thickness, heat distribution, mould temperature profile
		Micro	-
	Specimen	Macro	Wall thickness, ribs, A/R, geometry, concav-convex.
		Micro	Holes, ribs, thickness.

Table 2-6. Critical factors that affect moulding shrinkage.

Table 2-7 grouped the factors that affected shrinkage within the interval of confidence (95%).

Branches	Sub-branches	Scale	Critical factors within the interval of confidence
Processing	Processing parameters	Macro	Cooling time, packing pressure, packing time, melt temperature, mould temperature, injection speed.
		Micro	Mould temperature, melt temperature, packing time, packing pressure.
Design	Mould	Macro	Runner size.
	Specimen	Micro	Ribs.

Table 2-7. Factors that shown critical influence within the interval of confidence of 95%.

2.5.1 Material properties

As resulted from Table 2-7, no material aspects critically affect shrinkage within an interval of confidence. Despite of this, evidences have shown that material properties can drive shrinkage behaviour. The apparent contradiction it is likely to derive from the

chemical point of view adopted in these studies. Indeed the works that analyzed the material influence were conducted by considering polymer chains, morphology structure, crystallinity or rheology and this leads to identify trends rather than factor values because based on aspects not simply controllable: as result, the researches that considered these aspects have connected qualitatively the factors with shrinkage but did not quantify their influence. This did not mean that the results reported in Table 2-6 were wrong but only that was not possible to quantify the statistical influence of those factors on shrinkage.

Crystallinity

It was demonstrated that the crystallinity influenced the formation of frozen layer, the internal stresses and the in-mould shrinkage. By comparing the structure at micro and macro-scale, differences in terms of dimensions of polymer crystal and crystallinity degree (both increased in micro-scale) were observed.

Morphology

It was demonstrated that the scale did not affect the structure of moulded parts but the ratio between the oriented external layers (skin) and the randomly oriented molecules (core): at the micro-scale, a higher presence of oriented layers respect macro-scale was observed. The oriented layers have shown a flow-induced crystallization with a highly oriented 'shish-kebab' structure, and this leads to different shrinkage by comparing macro or micro-scale.

PVT

The PVT graph identified the origin of shrinkage as caused by thermodynamic behaviours. Semi-crystalline polymers differ from amorphous: because of crystallization of solid phase, the specific volume of semi-crystalline materials decreases exponentially (shrinkage was caused by these dimensional variations) with decreasing temperature while amorphous materials present a linear dependency in the solid phase. This difference was the reason for the greater shrinkage of crystalline thermoplastics respect the amorphous polymer. However, the same trend was observed both in macro than micro-scale.

2.5.2 Processing parameters

The processing parameters that affect shrinkage were summarized in Table 2-8.

Processing parameters			S	RQ
	Macro	Cooling time	↓	
		Packing pressure	↓	
		Packing time	↓	
		Melt temperature	↓	
		Mould temperature	↑↓	
		Injection pressure	↓	
		Injection speed	↑↓	
	Micro	Injection pressure	↓	-
		Mould temperature	↑↓	↑
		Melt temperature	↓	↑
		Packing time	↑↓	-
		Packing pressure	↓	↑
		Filling time	-	-
		Cooling time	-	-
		Injection speed	↓	↑
		Metering size	-	-
		Barrel temperature	-	↑

Table 2-8. Shrinkage response (S) and replication quality (RQ) trend followed by a factor increasing; – represent a trend not reported.

Despite of the greater part of works adopted a statistical methodology, not all the papers reported the interval of confidence value. Table 2-9 reports the critical factors by considering an interval of confidence of 95%. The arrows represent the greater part of trend reported in papers, and indicate whether a factor increasing causes an increase (↑) or decrease (↓) in shrinkage or replication quality. The double arrows (↑↓) indicate the balanced presence of both responses and the impossibility to identify a clear trend.

In μ-IM, the presence of extra parameters (e.g. plunger control and melt barrel storage settings) makes the process and the optimization more difficult to optimize respect CIM: this explain the higher number of critical factors as resulted in Table 2-8.

Processing parameters			S	RQ
	Macro	Cooling time	↓	
		Packing pressure	↓	
		Packing time	↓	
		Melt temperature	↓	
		Mould temperature	↑↓	
		Injection speed	↑↓	
	Micro	Mould temperature	↑↓	↑
		Melt temperature	↓	↑
		Packing time	↑↓	-
		Packing pressure	↓	↑

Table 2-9. Critical processing parameters within the interval of confidence of 95%; – represent a trend not reported.

The situation of processing parameters differs from that resulted for the material property. This was likely due to the engineering point of view adopted during the study of processing parameter influence. Indeed, in contrast to the chemical, the engineering approach conducted studies based on statistical models, by setting the factors and by recording the relative outcomes. Under these conditions, every result was identified within a defined interval of certainty and it was possible to determine and quantify each parameter influence.

Macro

At the macro-scale, general trend indicate that shrinkage decreases by increasing the critical factors. Temperature and packing (holding) related parameters shown to be topic parameters that determined shrinkage. Cooling time and injection speed was held other critical parameters.

Micro

The results reported in Table 2-9 shown a greater presence of double arrows (↑↓) in micro with respect to macro-scale. This is likely due to the statistical noise at the micro-scale that makes difficult to identify a clear trend of critical factors that affect shrinkage [136]. For simplifying the study of factor effects in such scale, authors also considered the replication quality (inversely related to shrinkage): results shown that the replication quality is increased by increasing the factor settings.

Also at the micro-scale, temperature and packing related parameters demonstrated to be critical factors that affect the final shrinkage.

2.5.3 Design

Results seem to indicate that authors adopted a different design approach for reducing shrinkage: at the micro-scale, solutions were rather focused on specimen optimization, whilst at the macro-scale also mould design optimization was considered.

Macro

Within the interval of confidence, as resulted from Table 2-7, the runner diameter critically affects shrinkage respectively at the macro-scale. This factor affected the heat exchange inside the cavity mould.

Micro

Within the interval of confidence, the shape of ribs (triangular, rectangular and semi circular) critically affect shrinkage at the micro-scale. The ribs considered in the paper, presents the same area and length: under this condition, the shape affects shrinkage.

2.6 Other theoretical background

Other aspects were considered for approaching efficiently shrinkage phenomenon. In detail, it was necessary to have an outlook about techniques for measuring shrinkage, standards and books that treated about shrinkage, previous works about standardized approaches and statistical models usually adopted.

2.6.1 Background of techniques for measuring micro shrinkage

In the literature were reported different methods for measuring shrinkage at the micro-scale: optical, laser beam based by interferometry, volumetric, mechanical or rheometrical. Not all these methods presented a good accuracy, and often the decision about the use of one rather than another was connected to the available equipment.

Table 2-10 reports the main methods for measuring dimensions in micro-scale or micro-parts and − if indicated in the paper − the accuracy.

Method	Equipment	Accuracy
Optical	Colour digital camera [137]	30-40 pixel/cm
	Low power beam (λ=632nm) [138]	± 1μm
	Triangulation by laser (λ=650nm) [139]	NR
	Microscopy [140]	NR
	AFM [141]	NR
	Moiré interferometry [142]	NR
	SEM [143]	NR
	Laser Confocal meter [144]	NR
Mechanical	Linear expansion [145]	NR
	Piezoelectric material [146]	NR
	Linear expansion [147]	NR
Others	Rheometry, TMA (film), Pycnometry [148]	0.003% (Pycn)
	Mercury dilatometer [149]	NR
	TMA (cylinder specimen) [150]	NR

Table 2-10. Methods for determining dimensions at the micro-scale.

As reported in Table 2-10, few papers indicate the accuracy. In any case, some considerations can be made. Even if not reported, mechanical techniques seem to have the poorest accuracy because they often consist simply in a linear measurement with a calliper. Only in the case of piezoelectric use, the accuracy is high, but the authors [146] used this method for a polymer film measurement. The accuracy of optical methods it depends on the wavelength used, and regarding the other methods, only data about pycnometry was reported. For this thesis, was adopted an optical method: details were reported in the methodology chapter.

Table 2-11 reports the standards and books consulted for the present thesis that argued about shrinkage measurement procedures.

Standards and books consulted (focused on mechanical tests)
ASTM D955-89 [151]
ISO 294-4 [152]
ISO 294-3 [153]
Saechtling H. [154]
Davis J.R. [155]
UNIPLAST Society [156]

Table 2-11. Standards and books consulted.

2.6.1.1 Standardized methodologies adopted for determining moulding shrinkage in previous works

To date, only one author has adopted an international standard to the micro-scale [31]. This was a continuation of work at the macro-scale [157]. For the micro-scale study, the authors determined the amount of shrinkage parallel to and normal to the flow direction in three commercial polymers: acrylonitrile butadiene styrene (ABS), polystyrene (PS) and high-density polyethylene (HDPE) [31]. The mould and the specimen followed the standard macro-scale reference ASTM D955-89 [151], which is a rectangular bar of length to width ratio of 10:1. Despite the standard recommend to use a square geometry for measuring shrinkage normal to the flow direction, authors adopted the rectangular geometry. This specimen was reduced in scale by a factor of approximately 25, for final dimensions of 5 mm x 0.5 mm x 0.125 mm.

2.6.2 Background of statistical methods: DoE or Taguchi?

The present thesis adopted a statistical method for managing the experimental results derived for shrinkage determination. Nowadays, there are two approaches normally used for dealing with these problems: the DoE approach and the Taguchi methods.

Both methods were based on the classical fractional designs developed by Sir Ronald A. Fisher in the 1920's [158] but at the same time they cannot be considered equivalent. This paragraph analysed the relative strengths and weaknesses of each approach, by giving the reason of the final method adopted. Generally speaking, both the techniques can be thought as tools for optimising some process which has controllable inputs (processing parameters) and measurable outputs (generally quality or productivity oriented). Typical aims might be to maximise or minimise some output.

The use of statistical methods it is necessary for the correct study of factors that affect the output. The study could be performed using two different strategies. A first strategy [159] could adopt the COST (Change One Setting at a Time) approach by changing one factor at time and study the output effect. Unfortunately this does not usually works because this approach is not able to identify the interactions between factors. A more suitable strategy consists to adopt the CEO (Change Everything at Once) approach and both DoE than Taguchi uses this last method.

2.6.2.1 Design of Experiments: how does it works

DoE theory starts with the assumption that all inputs might be interact with all other inputs [160]. There are no previous hypotheses or knowledge about factor independences. This powerful statement costs in terms of a great number of experimental runs. Indeed, if the processing is characterised by three factors, each with two possible levels, it is necessary to perform eight tests (2^3). By considering the actual complex manufacturing process, and the number of factors, it is simple to see how the number of tests can quickly become huge.

This is not completely true, because not all DoE approaches looks at all possible interactions: if all the possible interactions were considered, they was called "full factorial" DoE. By considering a fraction ("fractional factorial" DoE) it is possible to eliminate some interactions and to decrease the amount of total runs, but the model is still based on the idea of full modeling. The decreasing of number tests is paid with

lower precision (by assuming that the results are still correct in a reasonable interval of confidence) and aliasing effect. There is a big literature that explains DoE and aliasing effect. For the purpose of present thesis, was used the statistical handbook website [161]. The aliasing (or confounding) effect means that for some combinations is not possible to estimate correctly the effects. Also, they cannot be estimated separately from one another and are likely to be confused [162]. This phenomenon occurs when the fractional factorial design was adopted, because not all the runs were investigated and the amounts of data were not sufficient to determine the correct cause-effect for each result.

Aliasing is a critical aspect for Taguchi designs too, and it is very difficult to find any published information on the alias structures for this method [163]. These designs are often very low in resolution and therefore give very misleading results on specific effects.

The DoE was originally applied for agricultural applications and was designed under the strong condition that the results have to be get it right the first time. This leads to another characteristic of the DoE approach: not only are all interactions studied, but they are all studied at the same time in one big round of tests.

These considerations were used for assessing the strengths and the weaknesses of the DoE approach. The strength is that it is possible to investigate all possible interactions between inputs at the same time without any previous knowledge of how the process works, and this is very useful when it is necessary to predict results without previous information. The weakness is that there is no way to use of any a priori process knowledge that we might happen to have and there is no way to make the experiment more efficient by thinking about how the inputs really do interact.

2.6.2.2 Example of DoE application

In the paper of Zhao J. et al [8], the authors applied the DoE for studying the effect of processing parameters in μ-IM. The aim of this work was to investigate the processing parameter influence in terms of quality part (part mass and metering accuracy). In their study, the authors investigated five processing parameters with two levels (injection speed, melt temperature, mould temperature, metering size and hold pressure time). The

51

half two-level fractional factorial design was used for studying the process. The authors recognized that the fractional model cannot completely explore the wide region of processing combination, but the identified trend can indicate the direction for further experimentation.

As results, the statistical treatment identified a strong interaction between the metering size and the holding pressure; the optimized processing parameters were experimentally validated.

2.6.2.3 Taguchi methods: how does it works

If DoE came directly from the world of statistics and agricultural science, Taguchi methods [160] came from the world of design engineering. Taguchi methods start with the assumption that the processing under examination is an engineering system or some manufacturing process. As consequence the relationships between the processing factors are, or was, known. This is a completely different situation respect the "blind knowledge" of DoE. The additional knowledge was used for making the experiment more efficient and more focused into interactions that were known.

Experiments based on Taguchi methods, are focused on process robustness [164]. An important distinction in Taguchi methods was that the factors were divided in "under control" and "out of control", or in Taguchi terms in "control factors" and "noise factors" respectively. Often, if not early studied, a preliminary stage try to identify control factors and noise factors. It is usual to identify as noise factors external factors as humidity, operator influence, vibrations.

On the contrary of full factorial DoE approach, the Taguchi will test a very small subset of all possible combinations. The choices of the used combinations have to be studied and adopted, and also for the Taguchi there is a huge literature for giving indications in that direction. A simple layout of Taguchi was reported in Table 2-12.

Taguchi arrays	No. factors	No. levels	No. runs	Equivalent runs in DoE
L4	3	2	4	8
L8	7	2	8	128
L12	11	2	12	2048
L16	15	2	15	32768
L27	13	3	27	1594323

Table 2-12. Taguchi experimental layouts.

In Table 2-12, the L4 array, for example, is an experimental layout designed for three control factors, each at two levels. A full factorial DoE of all combinations of these factors would require eight tests (2^3). The Taguchi L4 layout indicates that using a subset of four of these eight tests, the main effects can be determined.

Another major difference between DoE and Taguchi is the use of the noise factors. In a traditional DoE, each combination of inputs is tested once. In a Taguchi test, each combination which is tested several times even if each of these replications is different because a different levels of noise factors were used. This permits to determine not only which combinations of inputs give the requested level of output, but which gives the most repeatable ones. Taguchi calls this quality robustness, or insensitivity to noise.

On the contrary from DoE (full factorial version), Taguchi recommends a final confirming experiment because a small fraction of all possible input combinations was investigated. Indeed, the statistical result could identify an un-tested combination of input decisions as "optimal", and for this reason it is always necessary to confirm the results from Taguchi. Table 2-13 summarizes the differences between DoE and Taguchi.

	DoE	Taguchi
Objectives	Gather scientific knowledge about factor and their interactions.	Obtain reproducible results and robust products.
Process knowledge	DoE assumes no understanding of the fundamental mechanisms governing the process we are investigating.	Taguchi assumes we have a certain understanding of the process and the interactions that are likely to exist between inputs.
Combinations	DoE tests all combinations of	Taguchi tests a small fraction of

		all possible combinations, but in a manner that allows us to calculate the affects of all inputs on the output.
of inputs tested	input levels, or some symmetrical subset (fractional design).	
Noise factors	DoE traditionally ignores noise factors, although they could be added to the experimental plan.	Taguchi makes use of Noise Factors to test robustness of the system and find optimal inputs.
Understanding of variability	DoE ignores variability in the process; it assumes a deterministic nature to the system, and finds combinations of input variables that maximize or minimize output, as the case may be.	Taguchi assumes a stochastic nature to the system; it looks at both the levels of output and the variability of the output; it lets us select levels of input variables to maximize or minimize output or to minimize variability of output (i.e., maximize robustness).
Confirming experiment	DoE requires no confirming experiment (only for the full factorial model). In effect, the confirming experiment was taken care of in the original experimental plan.	Taguchi recommends a confirming experiment just to make sure, since the winning set of inputs was probably not part of the original experimental plan.

Table 2-13. Differences between DoE and Taguchi.

2.6.2.4 Example of Taguchi application

Bong-Kee Lee et al. [126] used the Taguchi L_{18}. In their study, the authors optimized 3 processing parameters (packing pressure, filling flow rate and mould temperature) of 3 levels. The aim of the Taguchi approach was to make a product or process less variable when confronted with variations over which little or no control (environment humidity, random events) was possible. The result of a manufacturing process was considered much more robust how much more it was able to maintain high level of quality by varying of these uncontrolled events (noise). The authors applied this model for studying the level of replication of flow-through micro filters. The signal to noise ratio (S/N) was calculated (it is not explained in which way) from the average of the filled volume fraction (FVF) of the mould cavities. As result, this paper indicated the most sensitive processing parameters that affect the replication quality.

2.6.2.5 Statistical model adopted in the present thesis

The present thesis set a standardized methodology for studying moulding shrinkage at the micro-scale. Despite of the influence of processing parameters that affect shrinkage were often investigated, no standardized procedure was proposed. As consequence, is unknown if previous results could be confirmed under the new situation.

The manufacturing process permits to control the feedstock humidity, and remove the operator influence. The processing starts after the temperatures were balanced, and the moulded part was measured after uninterrupted number of cycles. Under these hypotheses, at this stage, it was possible to consider the noises as not influent.

It is likely that combined effects can affect the final results but on other side, there is the request to minimise the runs (often the resources in the industrial word are limited). The fractional factorial approach seems to be a suitable statistical model to be adopted.

Summarizing, it is possible to adopt the same point of view used by [8] for explaining the reason to adopt DoE instead of Taguchi methods. It is clear that a fractional model can give limited results, but considering the absence of standard at the micro-scale and the consequent lack of knowledge about previous interaction in terms of shrinkage under a standardized methodology, the identified trend can indicate the direction for further works.

2.7 Summary

The shrinkage literature review reported in this chapter evidenced that temperature related parameters, packing parameters, injection speed and cooling time affect shrinkage at the macro-scale, whilst temperature and packing related factors effect shrinkage at the micro-scale. Considering design aspects, running size at macro and ribs design at micro-scale influence critically shrinkage. Within the interval of confidence, no material properties influenced shrinkage, but it is likely that this was the consequence of the chemical point of view adopted by authors.

The considerations about theoretical backgrounds contributed to identify an optical methodology as the more suitable for measuring shrinkage at the micro-scale. Comparison between statistical approaches leads to consider the design of experiment approach the more suitable to be adopted in the present thesis.

2.8 Thesis aim

For operating effectively with μ-IM technique, is necessary to investigate all aspects that may cause errors in the final product. Shrinkage affects every injection-moulded part, regardless to the scale, and has to be minimized for realizing outcomes that respect the specimen design. This request is more urgent at the micro-scale, by considering the high precision requested by miniaturized parts compared to conventional moulded specimens. For example in optical applications (diffraction gratings [116], optical lens [165]), a discrepancy of few microns it might produce a moulded part not suitable for the application. Moreover, shrinkage can generate voids, sink marks and warpage [166; 167]. Therefore, to operate in micro-scale is ineffectiveness without precision and respect of design, and to investigate about causes of micro-shrinkage is important for reaching the precision that micro-scale request. For this reason, the aim of this thesis is to investigate the effects of shrinkage in microinjection moulding. Under this aim, two research gaps were identified.

The first came directly from the literature review analysis. Despite the importance of shrinkage control and reduction, the literature reviewed has shown the absence of a standardized and accepted reference adopted for measuring the shrinkage of moulded parts in micro-scale because every authors considered own specimen design. In the only previous work that adopted a standard for determining shrinkage at the micro-scale, the authors [31] implemented a rectangular geometry for investigating shrinkage. However, the adopted standard recommended a square specimen when shrinkage normal to the flow is to be measured. Moreover, the literature demonstrated that the material behaviour was affected by the scale and is not possible to extend the macro results in the micro applications. All these considerations lead to the necessity to set a methodology for measuring shrinkage of moulded parts at the micro-scale. It was chosen to investigate the injection stage because, as stated by [168], this stage is the most important because many potential defects (weld line, binder separation, jetting flow, short shot) occur during injection.

The second gap was identified by considering the methodologies of the optimization process adopted from authors and reported in papers: it was observed that optimizations were not performed by using multiple quality approach but only by implementing single

target at time (e.g. respect of measures, parameter reduction). This was considered as an aspect that can be improved, because is possible to conduct optimizations by using multiple requests, as will be shown in chapters 6 and 8.

Summarizing, the objectives of the present thesis are:

i. Set a standardised methodology suitable for the micro-scale (gap);

ii. Statistically detect the critical processing parameters with the proposed methodology;

iii. Characterize shrinkage in micro-injection moulding with the proposed methodology;

iv. Identify and validate with a multiple quality criteria approach the combination of optimised processing parameters that permits to minimise moulding shrinkage and maximize part mass (gap).

On the surface of the micro-mould will be manufactured micro-features. The analysis of the micro-channels will permit:

v. To define the low mouldability of the feedstock and to determine the influence of orientation;

vi. To identify critical factors that affect feedstock feature reproduction along the z-axis.

Chapter 3 . Methodology

The previous chapter evidenced the absence of standardized procedure for measuring shrinkage at the micro-scale. By starting from the more similar standard available for measuring shrinkage (ISO 294-3) a procedure suitable for the scale was proposed: the methodology implemented the entire standard except the dimensions adapted to the scale. Shrinkage measurements implemented, unchanged, all of ISO 294-4. By following the standards, a micro-mould was manufactured and the steps reported in this chapter. The materials adopted were two commercial polymers normally used in μ-IM and μ-PIM. The metrology was performed by using an optical method. This technique, if on the one hand can efficiently conduct measurements at the micro-scale, on the other side requests high precision for identifying the real specimen profile: examples of artefact situations were reported. The statistical methodology was discussed from the familiarization step to the final optimisation stage with the multiple quality criteria approach. The Pareto chart, the main effects and the interaction plot were used for studying the critical factors that affect shrinkage. All the statistical approach was performed using the program Minitab 16 [162].

3.1 The materials

Two materials normally used in μ-IM and μ-PIM were investigated: the pure polymer Polyoxymethylene BASF Ultraform® W2320 003 [15] and the feedstock Catamold® 316LS BASF [15]. These materials were depicted in Figure 3-1.

These commercial materials were chosen because this thesis was focused on parameters optimization rather than to tailor a suitable feedstock. Others authors [13; 169-171] preferred to investigate shrinkage by mixing selected binders and powders for controlling and estimating the influence of size particle, percentage, kind of polymer.

Figure 3-1. 316L feedstock (A) and POM (B) pellets.

3.1.1 The polyoxymethylene (POM)

The pure polymer moulded was the POM (melting point 166°C, tensile strength at room temperature 65MPa, linear thermal expansion coef. 0.6E-4 mm mm^{-1} C^{-1}). This semi-crystalline polymer was chosen because it was expected to display different behaviour in parallel to respect normal to the flow direction: the behaviour it was less likely to see in amorphous material [172; 173]. The different behaviour displayed between transversal and longitudinal direction was confirmed by numerical data reported on MatWeb site [174]: the material shown different shrinkage considering two perpendicular directions, with longitudinal to the flow higher that transversal to the flow shrinkage. To display different values should permits to evaluate simply the moulding shrinkage and the optimisation effects.

As demonstrated in the literature review, material crystallinity can determine shrinkage, and POM presents an anisotropic lattice structure [175]: the crystal constants are $a = 4.77$ Å, $b = 7.65$ Å, $c = 3.56$ Å (Figure 3-2).
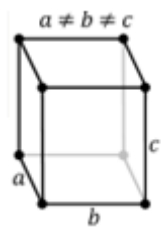
Figure 3-2. POM lattice.

The POM crystals can arrange in a helicoidal structure as reported in Figure 3-3 [176; 177], and to form a shish-kebab structures. The authors [178], reports other indications about POM dimensions: with X-ray techniques, the authors identified the POM as a lamellar structure, formed by chain folded crystals with a spacing of $\approx$ 18nm. Nano fibres of POM realized with spinning techniques have shown a diameter of $\approx$ 1μm [179].
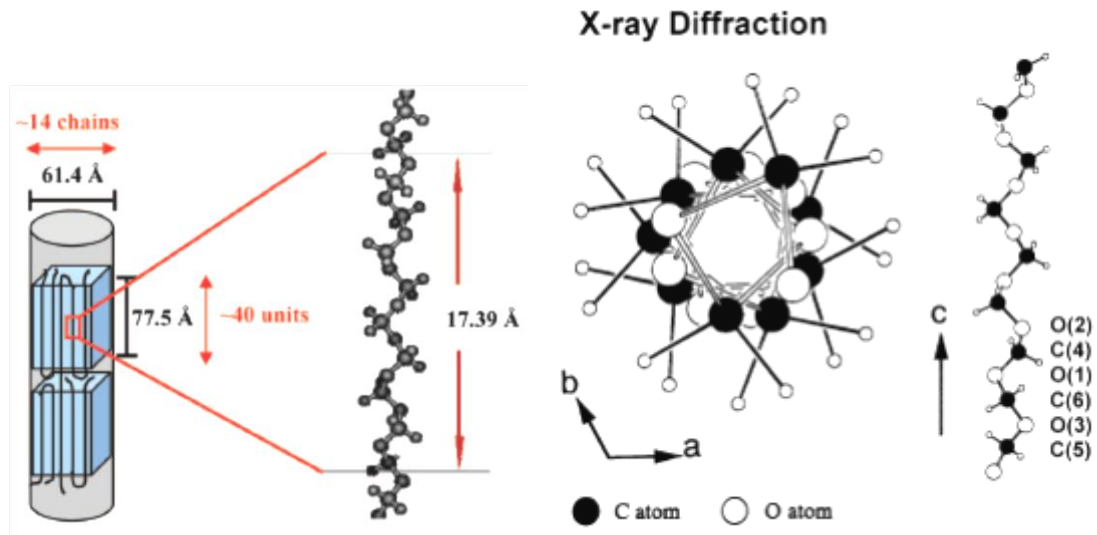
Figure 3-3. POM helicoidal chain [176] and X-ray structure [177].

3.1.2 The 316L feedstock

The 316L feedstock (sintered part characteristics: density $\geq 7.9 g/cm^3$; yield strength $\geq$180 MPa; ultimate tensile strength $\geq$ 510 MPa; elongation $\geq$ 50 %; hardness 120 HV10) consists in ready-to-mould granules for the production of sintered components in an austenitic stainless steel type 316L realized by microinjection moulding machines for thermoplastic polymers. The metal is in powder form with a D_{50}=4-5 μm. The parameter D_{50} is the Mass Median particle Diameter (MMD): physically it means that for the mass median, one-half of mass of all particles is contributed by particles with a size smaller than the mass median size, and one-half by particles larger than the mass median size [180].
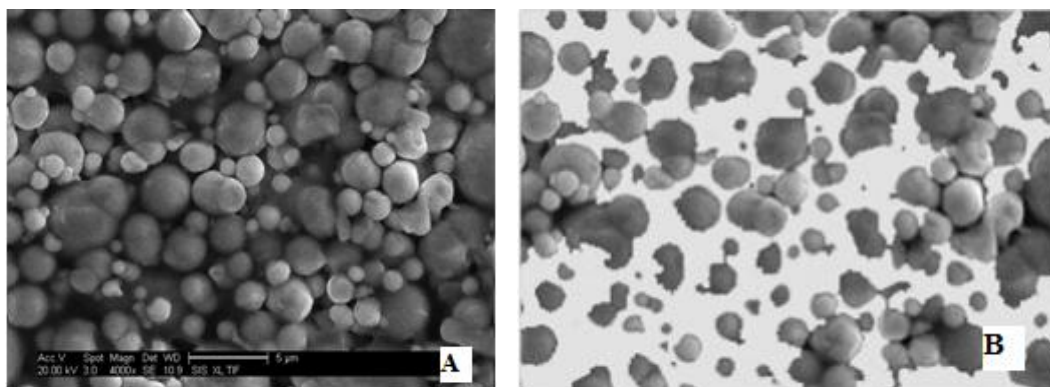
Figure 3-4. The feedstock after injection moulding (A) and the same image (modified with free software ImageJ) with the binder coloured in white (B).

The moulded feedstock (Figure 3-4) is formed for the 40% by the volume by a mixture of polymers (binder). For confidential reasons, was not possible to obtain information about the exact binder composition, except that is a mixture of POM based polymers. Figure 3-5 reports the metal powder composition acquired with the EDAX SEM analysis.

Element	Weight%	Atomic%
C	26.15	53.52
O	12.73	19.56
Si	0.21	0.19
Cr	8.02	3.79
Fe	46.42	20.43
Ni	5.27	2.21
Mo	1.19	0.30
Totals	100.00	
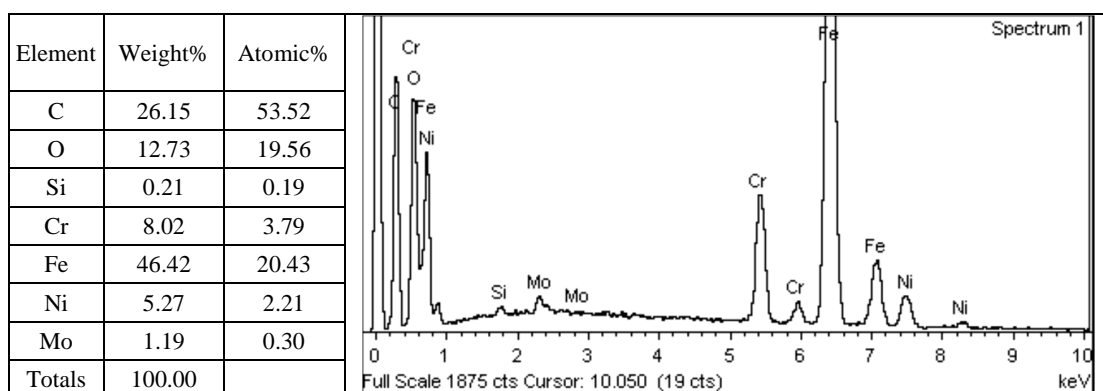
Figure 3-5. Chemical composition of the powder steel.

This feedstock was chosen because the presence of POM as binder makes possible to study the influence of powder loading (316L metal powder) by direct comparison.

3.2 Mould design

The mould was manufactured by implementing the same design reported in ISO 294-3 [153] except the dimensions adapted to the micro-scale. This design was normally used for measuring shrinkage in conventional injection moulding. The original mould dimensions reported in [153] were approximately 180mm x 72mm, and the square

61

specimen dimensions were 60÷62mm x 60÷62mm x 2.0÷2.1mm. They were reduced by a factor of six for being suitable for the micro-scale. Figure 3-6 depicts a no-shrinkage specimen; the volume of the part is around 156 mm^3.
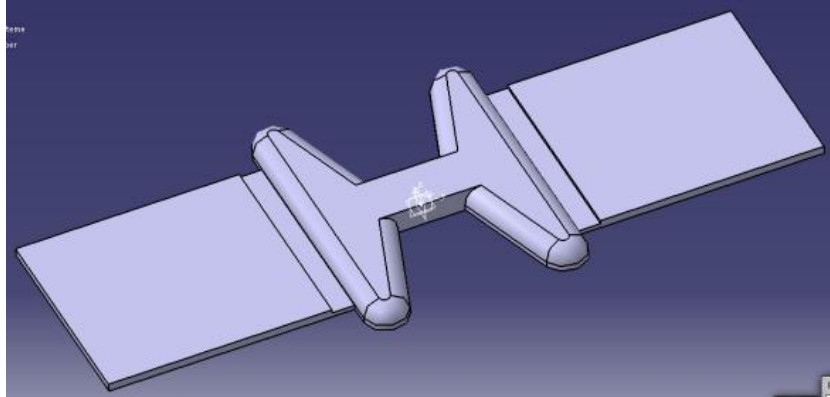
Figure 3-6. The specimen design.

The micro-mould maintained the same triangular gate runner of the standard. The gate has shown a width bigger compared to the specimen for generating a uniform velocity in the melt front that should fill the cavity without turbulences in the injected material. The request of a uniform melt front for filling the cavity mould is an important condition especially by injecting a feedstock, because Karatas et al. [181] demonstrated that a not uniform melt flow could generate a not homogeneous powder distribution with particles accumulation. Similar triangular gate was used by Yao et al. [11] for modelling the polymer filling process in micro channels and by Règnier et al. [140] for determining the orthotropic (different properties along different orthogonal directions) shrinkage in conventional moulding. Different gate can create not uniform melt front, as demonstrated by Su et al. [182]: the elliptical melt front generated by the edge gate does not permits the uniform molecular orientation because the front velocity was not constant. Figure 3-7 reports the micro-mould design.
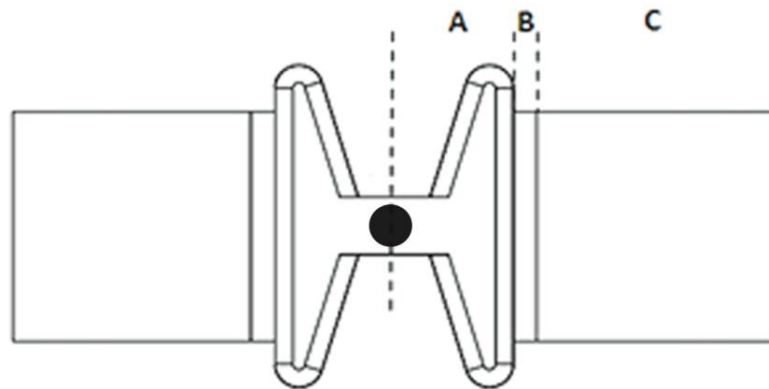
Figure 3-7. Different parts of mould: the runner (A), the rectangular gate (B), the square specimen (C). The black point represents the mould sprue.

More details of micro-mould design were reported in Appendix B. Eight 1 mm thick ejector pins symmetrical positioned were used in the micro-mould design to reduce the likelihood of bending due to the thin specimen on ejection.

Micro-features manufacturing

Micro-features oriented on parallel to and normal to the flow direction were manufactured by micro-milling technique: Figure 3-8 reports their design. These micro-channels were studied for investigating the feedstock replication quality along the z-axis (perpendicular to the flow direction). The analysis of the littlest channel (60 μm) should determine the connection between feature orientation and low mouldability limit.

Tests were performed for manufacturing micro-channels with lateral dimension lower than 60 μm using the PCM technique: the results of these tests were reported in Appendix A.
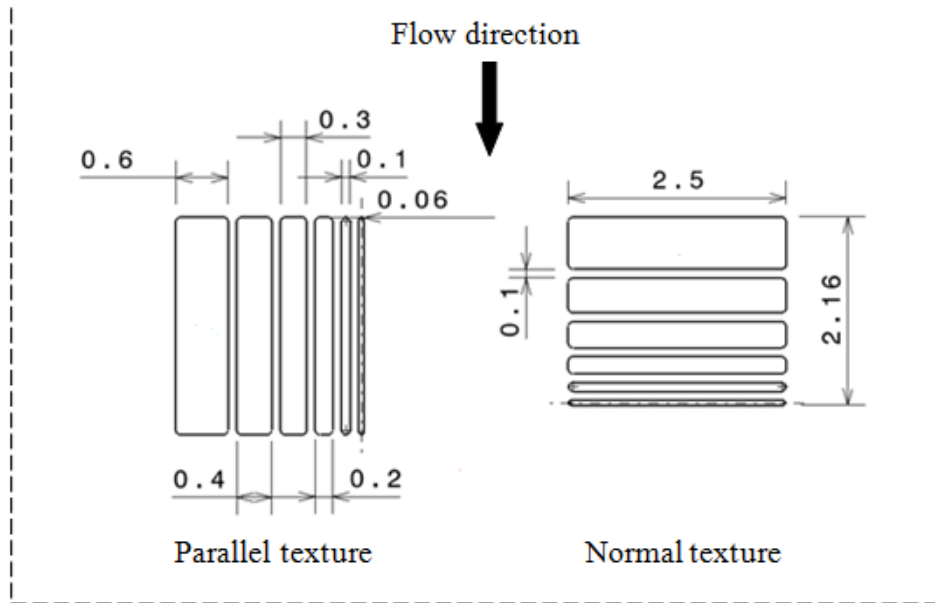
Figure 3-8. Texture dimensions in millimeters.

The position of micro-features was reported in Figure 3-9, the results in chapter 9 and their design in Appendix B.
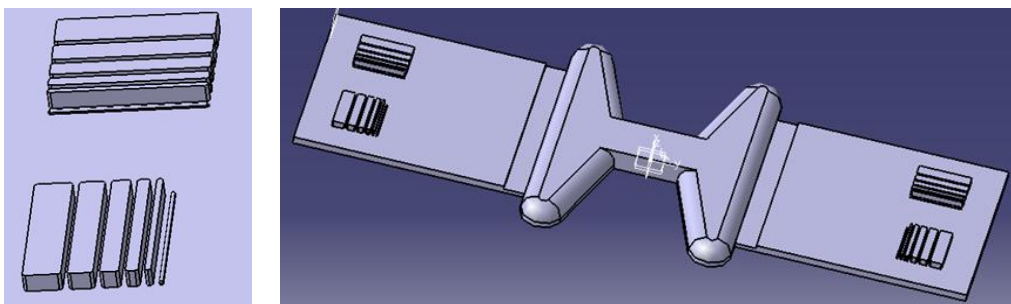
Figure 3-9. The specimen with the micro-features.

The features exhibits differents aspect ratio (A/R=height/lateral dimension) as depicted in Figure 3-10: 0.5, 0.75, 1, 1.5, and 3 (referred respectively to channels with breadth of 600μm, 400μm, 300μm, 200μm and 100μm). The smallest channel (60 μm) has an A/R=1.
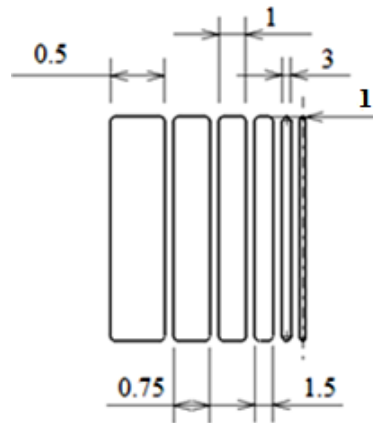
Figure 3-10. Aspect ratio of micro features.

3.2.1 Mould manufacturing

The mould manufacturing was realized by using the KERN Evo for ultra precision machining (Figure 3-11). The design of the 5-axis system permitted the high accuracy of this kind of precision machine: this positioning system ensured a workpiece precision of one micron, with a surface quality of 0.1 μm. The tool HLS 2003-020 was used for manufacturing the mould, with a diameter of 300 μm, effective length of 2 mm and a flute length of 0.4 mm.

About the micro-features, the channels with breadth from 100 to 600 μm were manufactured with a micro drill of 100 μm of diameter while the channel with breadth of 60 μm was realized with a ball nose tool with 60 μm of diameter.

The rotational speed was approximately 30,000 rpm and the feed rate was of 45 mm min^{-1}. An oil/air coolant was used.

Figure 3-11. KERN Evo micro precision machine.

After micromachining, the final dimensions of the single square cavity were length= 9.987±0.001 mm, breadth= 9.980±0.001 mm, height=0.349±0.001 mm. These values were used as reference for calculating shrinkage.

At the end of mould manufacturing, the micro-mould was tested with 316L feedstock for controlling the absence of errors realized during the design step. The validation steps were reported in chapter 4.

3.3 Micro moulding injection machine

A Battenfeld Microsystem® 50 (Figure 3-12) all-electric moulding machine was used in the present study.

Figure 3-12. The Battenfeld Microsystem 50 micro moulding machine.

As stated in the introduction, the μ-IM technique requests particular injection machine that presents different injection design respect the conventional equipment. The Battenfeld 50 injection system is composed of a screw plastication barrel, a plunger injection system and a control of melt dosage barrel as shown in Figure 3-13.
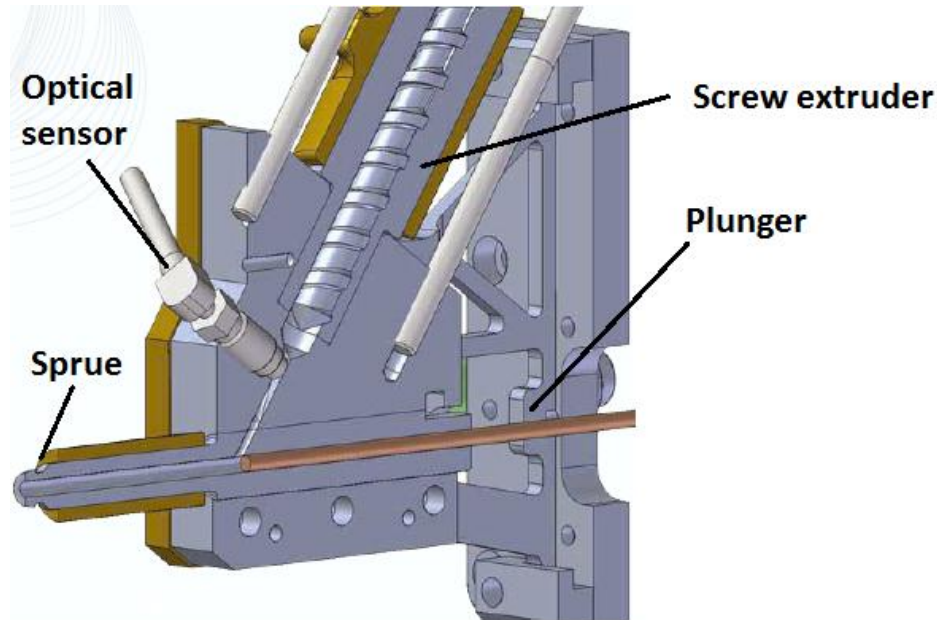
Figure 3-13. Injection unit of Battenfeld Microsystem 50 [183].

By using the screw plastication extruder, a small diameter plunger/needle can be used for melt injection to achieve precise measurable strokes to control melt accuracy. The plasticizing screw of the moulding machine has a diameter of 14 mm, and a 5 mm diameter dose barrel is employed for storage of polymer melt. The 5 mm diameter plunger allows shot weights ranging from 25 milligrams to 1 gram. The machine maximum clamping force, injection speed, and theoretical injection volume are 50 kN, 760 mm/s, and 1.1 cm^3, respectively. During the moulding process, plastic pellets are plasticized by the fixed extruder screw and fed into the metering chamber. In the metering chamber, an optical sensor monitored the amount of melt in the chamber against the pre-set volume. After the set volume has been achieved, the plunger in the dosage barrel delivers the shot volume to the injection barrel. The injection plunger then pushes the melt into the mould. Once the plunger injection movement was completed, a holding pressure was applied to the melt with a slight forward movement (maximum 1 mm) of the injection plunger.

3.4 Specimen measurements technique

For measuring shrinkage, it was used optical measurement equipment: the TESA Visio 300. The precision of the TESA instrument is ±1μm. Figure 3-14 depicts the operating principles.
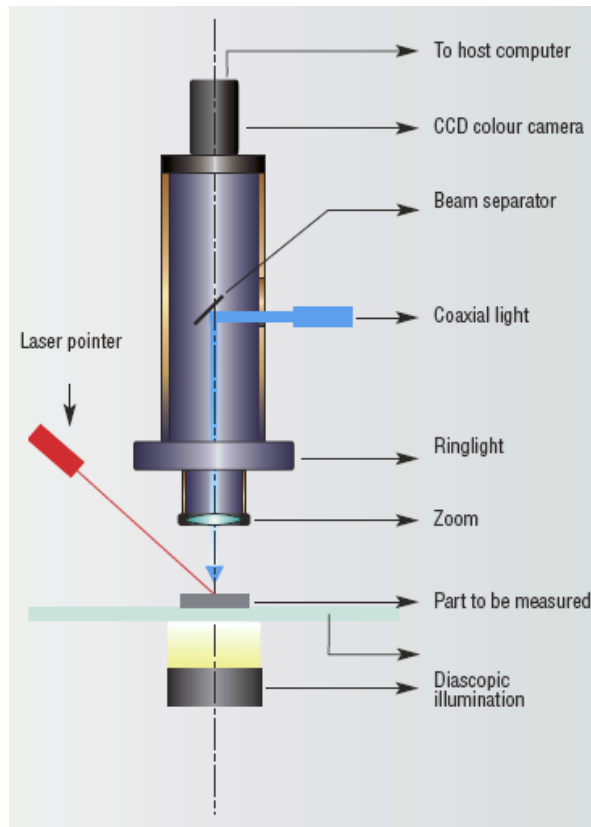
Figure 3-14. Operating principle of TESA Visio 300 [184].

The technology of this equipment consists in an optical system integrated by a camera with zoom lenses. The analysis of the image it was possible by using lights with three different orientations:

• Diascopic illumination located under the glass plate; make it possible to evidence the sample's profile;

• Ringlight for a detailed visualisation of the upper surface of the sample;

• Coaxial light to view inside a blind hole or a cavity if the sample has one.

As starting a plane, a line and a point on the specimen have to be identified. These elements were used as reference during all the measurement stage.

For measuring the specimens, the protocol illustrated in Figure 3-15 was adopted. The measurements were conducted using always the same square specimen of two (c) reported in Figure 3-7. As the corner close to the gate was always present, this was chosen as the zero point. The specimen it was moved 5 mm to point 1. A line position was measured. The specimen was moved in flow direction until the opposite edge was reached. A second line position was measured (2). The specimen was moved back by 5 mm and then moved cross direction until the edge was found. A line position was measured (4). Specimen was moved in the opposite direction to the other edge. A final line position was measured (5). The same equipment and procedure was used to measure the mould cavity.
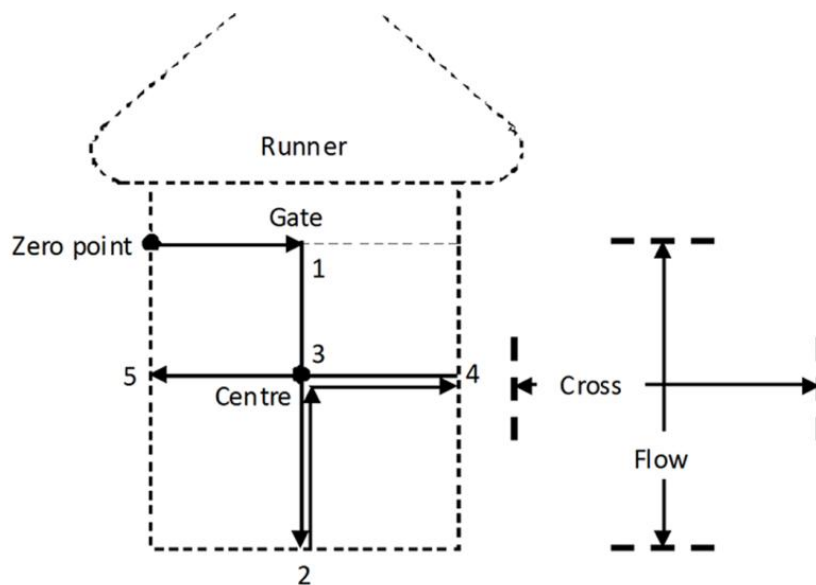
Figure 3-15. Measurement protocol adopted.

The distances can be measured between two points or two lines: it was preferred this last option because more reliable and precise. In optimal condition, i.e. a well-defined border without flashes, the TESA system set up around 100 point/mm for creating the line. The distance between the two lines was the result of the average distance.

Often, the operating conditions were far from the optimal conditions for the presence of flashes or incomplete filling, and that makes difficult to identify the border profile. In these cases, the numbers of points effectively used for draw the line were less than 100 for millimetres, and often the points were spread in an area rather than aligned. By

varying the light or the magnitude solved these problems. Common situations were summarised below.
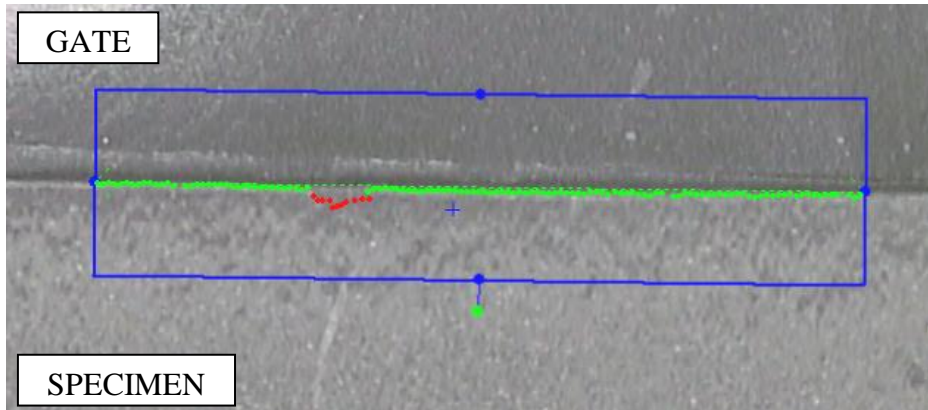
Figure 3-16. Example of line definition.

Figure 3-16 depicts a common situation during TESA operation: areas of different colours disturbed the correct line identification. The optical system identified the problem as red points not considered during the measuring step. For reducing these areas it was increased the ringlight brightness. An example of well-defined border was depicted in Figure 3-17.
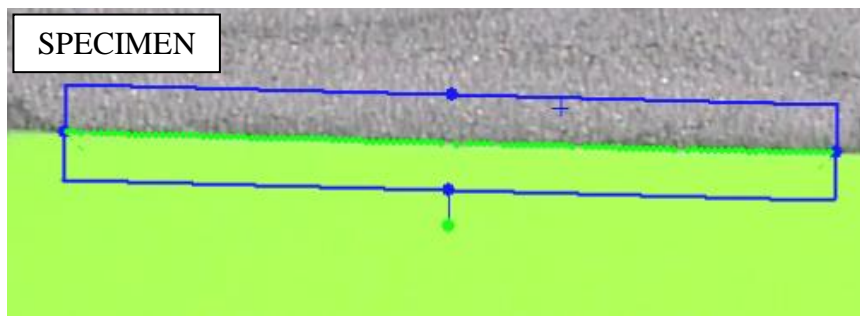
Figure 3-17. Well-defined border.

Sometimes, the detection of the border was not so easy: the situations reported in Figure 3-18 were solved by changing the light condition and magnification value.

70
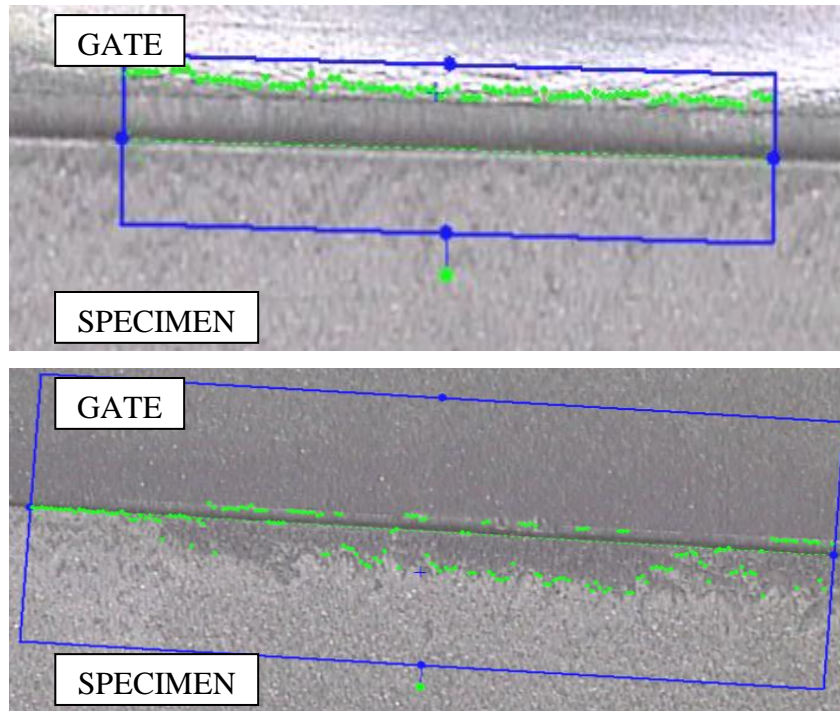
Figure 3-18. Spread out spots.

The flashes on the external borders can be confused with the real profile, as in Figure 3-19. The operator experience and the knowledge of the specimen profile helps to identify the line proposed from the TESA acquisition system as not correct. The situations reported in Figure 3-19 can be solved by changing the area of measurement (if the new was still located in the middle area of the specimen), or by improving the magnification for reducing the contrast of specimen flashes/end.
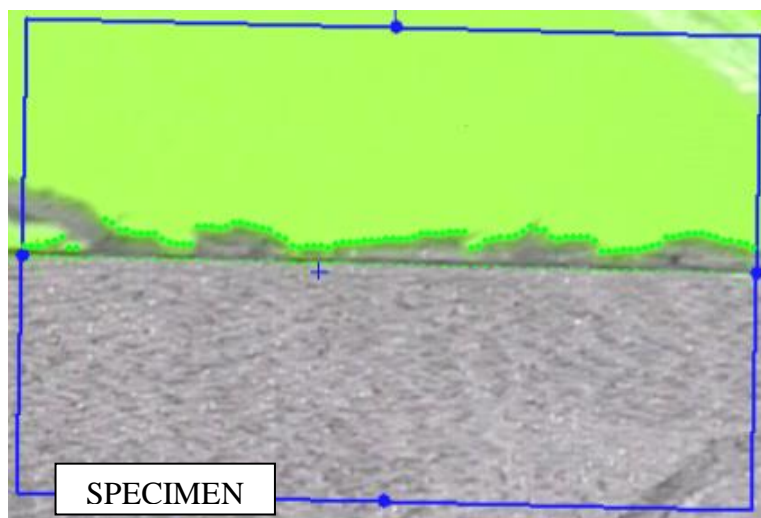
Figure 3-19. Wrong profile individuation.

In the presence of little flashes, as reported in the Figure 3-20, the TESA software suggests an auto correction.
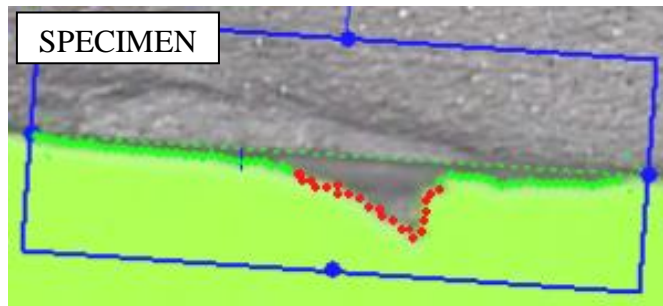
Figure 3-20. Result of auto correction.

The line identified in Figure 3-20 was rejected, because the solution suggested by TESA system (the green points) not corresponding to real profile as reported in Figure 3-21 (accepted) and the rejected area (red points) was relevant respect the proposed line.
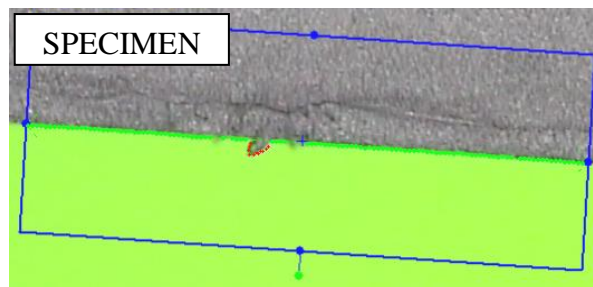
Figure 3-21. Profile correction accepted.

Concerning the study of micro-textures reported in Chapter 9, the TESA Visio 300 was equipped with the littlest touch probe available (ball nose diameter of 1 mm), and this determined that the only channel measurable was the feature with breadth of 600 μm. The height of μ-feature was determined by adopting the protocol depicted in Figure 3-22: the specimen surface was used as reference plane (Ref), and then the feature height was measured on the middle (2) and on the ends (1-3).
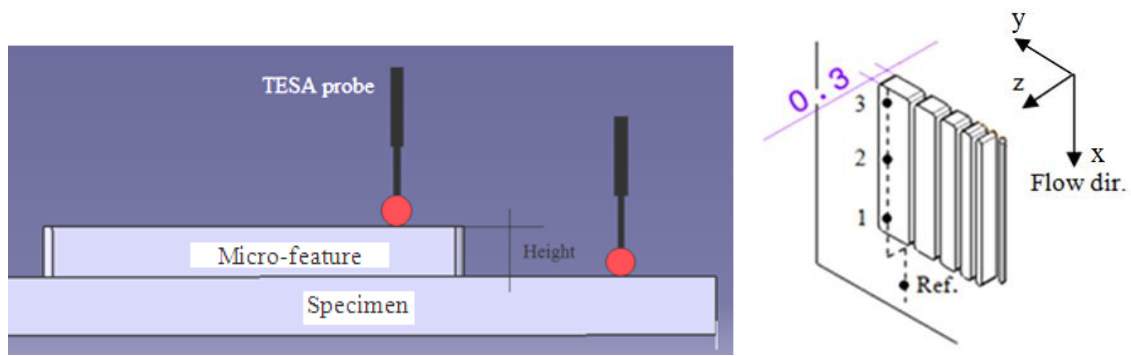
Figure 3-22. Measurement protocol adopted (probe tip not in scale).

3.5 DoE: model choice

The efficiency and the productivity are topic objectives in productive field. As consequence, every problem solving approach need to be quickly and precise. In injection moulding industry, even the development time have to be shortness. For obtaining the maximum quality of a new product, is not a good idea change only one variable at a time (paragraph 2.6.2) for the high number of tests that his approach request and for the impossibility to detect combined effects. The statistical approach allows determining the critical processing parameters with a low number of tests. The term critical mean a parameter that strongly affects the result of the processing analysed within an interval of confidence. In industrial fields, this approach was named "Design of Experiment" (DoE). DoE consists in a controlled variation of the input parameters in order to study the output corresponding variation. For each run, were measured the output results. The aim of these operations was to optimize, to characterise or to improve the quality of the output product [185]. DoE was traditionally divided in 3 different steps:

- **Step 1: Screening.** Screening was used at the beginning of the experimental procedure to explore the factors and identify their range.
- **Step 2: Optimization.** The objective was to predict the response values for all possible combinations of factors and to identify an optimal experimental point that fulfils specific requests.
- **Step 3: Robustness testing.** The third objective was the robustness testing. Small fluctuations in the factor levels (noise) permits to study the sensitivity of the responses.

73

The injection moulding processing was considered low noise affected, because the external conditions (e.g. humidity, vibrations) were believed constant during the moulding stage. These conditions determined the choice to conduct experiments without replications (defined as repetitions of the entire experiment or a portion of it, under more than one condition [164]) for identifying factors only connected to processing parameters: as consequence no data about fluctuations were available, and step 3 (robustness) was not performed.

The half fractional factorial design was implemented in the present thesis. The term "fractional" indicate that was used a statistically significant percentage of all the possible tests. This statistical approach, which start from the full experimental test number (5 processing factors with 2 possible levels that makes 32 total runs), adopted 16 experimental tests (half fractional design) with a final resolution of V. Whit this resolution the statistical treatment will not exhibit alias between the main effects, two or three factors interactions, but two-factor interactions are confounded with three-factor interactions [161; 164]. The matrix of the statistical model by considering 5 two-level factors was reported in Table 3-1.

A	B	C	D	E
+	−	+	−	+
+	−	−	+	+
+	+	−	−	+
+	−	−	−	−
+	+	+	−	−
−	−	+	−	−
+	−	+	+	−
−	+	+	−	+
−	+	−	+	+
−	−	+	+	+
+	+	−	+	−
+	+	+	+	+
−	+	−	−	−
−	+	+	+	−
−	−	−	−	+
−	+	−	+	−

Table 3-1. Matrix of fractional factorial design. The sign + indicates the high value of processing parameter and − indicates the low value.

3.5.1 Step 1: Screening

Resulting from the literature reviewed, the μ-IM presents different parameters that critically affect moulding shrinkage. Table 3-2 reports five critical factors that were chosen for shrinkage investigation. As resulted from literature reviewed, these parameters were not independent each other's: it was expected that the parameters influence would be highlighted during the statistical study. Preliminary experimental tests were conducted for determining the initial value parameters, and a short guideline during the familiarization stage was reported in Table 3-2. After different test cycles, the initial values were identified and reported in Table 3-3.

Factors	Guideline of range selection
Holding time	A lower hold time allowed material to expand out of cavity mould, a higher time was considered non-productive because the feedstock solidified in a shorter time.
Holding pressure	Have to keep the feedstock pressed inside the cavity mould at the end of the injection cycle. The value was lower than injection pressure.
Injection pressure	As first references were used the values reported in 316L feedstock and POM datasheet.
Mould temperature	A too lower value made difficult the injection step (shear too high), a too higher value made the time processing long for waiting for the feedstock solidification.
Melt temperature	The degradation temperature of our binder was 200°C. It was chosen a temperature lower that this upper limit, but not too low for avoiding too high viscosity.

Table 3-2. Guidelines of parameter values selection.

The processing parameters values reported in Table 3-3, referred to the values identified after the improvement of mould configuration (blind holes with ejection pins). The steps occurred for reaching the acceptable mould configurations were reported in chapter 4.

	POM			316L feedstock		
Factors	Initial Values	Value +	Value –	Initial Values	Value +	Value –
Injection press [bar]	850	900	800	900	930	870
Holding press [bar]	500	550	450	250	300	200
Melt temp [°C]	195	200	190	194	198	190
Mould temp [°C]	100	115	85	135	140	130
Holding time [s]	3	4	2	3	4	2

Table 3-3. The values investigated values for POM and 316L feedstock.

Each of the processing parameter values listed in Table 3-3 were the result of a preliminary screening (familiarization stage) performed for identifying the high and low values. The initial values for each parameter were selected, such that the higher (+) value was obtained by increasing from an initial setting until the presence of flash start to be notable. The lower value (–) was obtained by decreasing the parameter value until notable defects started to appear (for example, incomplete filling or low edge definition). Table 3-4 reports the processing parameters held constant during the moulding.

	POM	316L feed.
Cooling time [s]	17	15
Metering volume [mm^3]	210	185
Injection speed [mm s^{-1}]	250	300

Table 3-4. Processing parameters kept constant.

The difference in terms of metering volume (total amount of material injected) between POM and 316L feedstock, is likely to be the consequence of their different viscosities. Indeed, as demonstrated by [167], polymer viscosity – by making the cavity filling more or less easier – can affect the metering size.

Different factors respect those reported in Table 3-2 were adopted for investigating the replication quality of feedstock-moulded parts (Chapter 9). More in detail, the injection pressure was substituted by the injection speed. The new factor was chosen according to works reported in the literature review, because the injection speed affected the

replication quality in microinjection moulding as well. The injection speed was considered also by Vasco et al. [134] (that investigated the POM mouldability of ribs with different aspect ratio), by Zhang et al. [186] and by Park et al. [187] (that investigated PET moulded parts with high aspect ratio). Besides, hesitation effect is the consequence of a flow sequence fast-slow-fast [188], and this could suggest a relationship with the speed.

The statistical model implemented in this chapter was the half-fractional factorial matrix reported in Table 3-1. The processing parameter values, identified after a familiarization stage, were reported in Table 3-5. Table 3-4 reports the parameters kept constant.

Processing Parameters	Initial Values	Value +	Value −
Injection speed [mm s^{-1}]	200	250	150
Holding pressure [bar]	300	400	200
Melt temperature [°C]	195	198	192
Mould temperature [°C]	135	140	130
Holding time [s]	3.5	5	2

Table 3-5. Processing parameters adopted for investigating the 316L feedstock micro-features.

3.5.2 Step 2: Optimization

The screening stage has identified the range of factors. After specimen manufacture and sample measurements for evaluating shrinkage, the next step was the optimization. The aim was the prediction of the response values for all possible factors combinations within the experimental region (and within the confidence interval) for identifying the experimental values that permits to achieve the requests. By treating several responses at the same time, it is usually difficult to identify a single experimental point at which the goals for all responses were fulfilled, and therefore the result often reflects a compromise between partially conflicting goals.

The experimental results were examined in terms on factor effects. With the term "effect" was meant the change in response when the process parameters changed from the low (−) to the high (+) value (Table 3-3). In the two-level factorial design, the average main effect can be calculated as the average response at the high value level minus the average response at the low value level [8]. A positive consequence of the

experimental observations conducted in a paired comparisons, was the possibility to study the interaction between the process parameters: this result was impossible to obtain by changing one factor at a time as already mentioned. If an interaction exists between two processing parameters A and B, the effect of "high A" and "low B" will give a different result from the combination "low A" and "high B". As conclusion, the behaviour of the parameter A was considered as not linear, and it depends on the level of parameter B, and vice versa.

3.5.2.1 Statistical tools

The statistical study was performed by using the statistical program Minitab 16 [162]. The identification of critical parameters and their effects was performed using statistical tools normally adopted in DoE [162; 164]: the Pareto chart, the main effect plot, the interaction plot. Desirability functions were implemented during the optimization stage.

3.5.2.2 Pareto chart

The Pareto chart is a bar chart that graphically ranks the criticity of factors from largest to smallest. This representation helps to determine the magnitude and the importance of the processing parameters and to prioritise the problems. The chart displays the absolute value of the effects and draws a reference line (red line) on the chart. The value of the reference line was calculated as reported in Equation 1.

Equation 1 $$ME = \mathfrak{t} * PSE$$

ME is the margin of error (alias reference line), and $\mathfrak{t}$ is the $(1 - \alpha / 2)$ quantile of a t-distribution with degrees of freedom equal to the (number of effects/3). For 5 factors and for $\alpha=0.05$, $\mathfrak{t}=2.571$; for $\alpha=0.10$, $\mathfrak{t}=2.015$.

Minitab adopted Lenth's pseudo standard error (PSE) for evaluating ME. The PSE was based on the concept of sparse effects, which assumes the variation in the smallest effects was due to random error. Lenth's method [189] computes the PSE in the following steps:

1. Calculates the absolute value of the effects
2. Calculates S, which is $1.5 *$ median of the effects in step 1
3. Calculates the median of the effects that are less than $2.5 * S$

4. Calculates PSE, which is 1.5 ∗ the median calculated in step 3

Alpha (α) is the maximum acceptable level of risk expressed as a probability ranging between zero and one. Usually, the smaller the α value, the less the probability to incorrectly reject the null hypothesis (the null hypothesis is usually a hypothesis of "no difference"). For each processing parameter analysed in terms of shrinkage effects there are two hypotheses: the alternative hypothesis H_1 (the factor is statistically influent for shrinkage) and the null hypothesis H_0 (the factor is not statistically influent). The processing parameter was evaluated according to the Lenth's method. If this method produces a value lower or equal to alpha value, then the factor analysed was statistically significant and the null hypothesis was rejected. On the contrary, if the Lenth's method produces a value higher than alpha value was not possible to claim the statistical significance of the factor and the null hypothesis has to be accepted. An example of Pareto Chart was depicted in Figure 3-23.
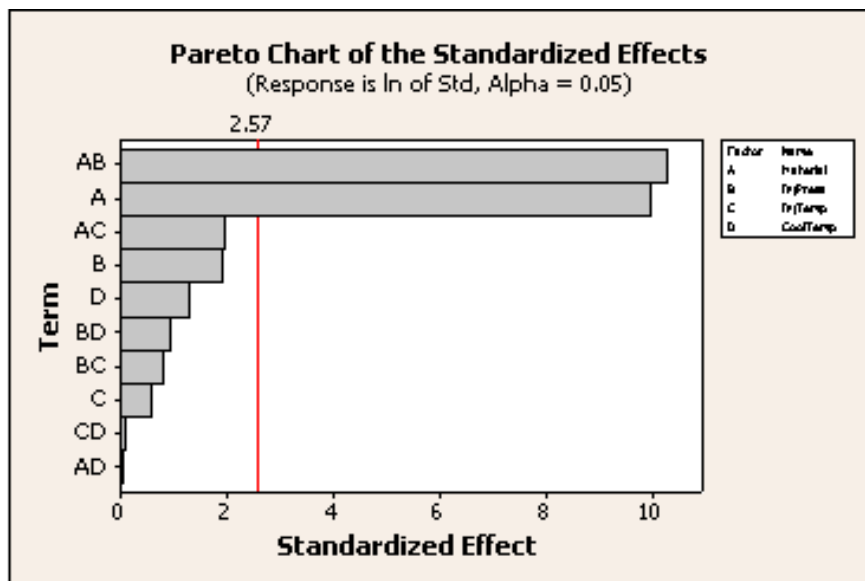
Figure 3-23. Example of Pareto chart [162].

According to example reported in Figure 3-23, two significant effects cross the reference line (α): one single effect (A) and one combined effect (AB). The largest effect was the combined (AB) because it extends the farthest.

3.5.2.3 Main effects plot

The main effect graph helps to visualize the effect of the factors on the response and to compare the relative strength of the effects. Minitab 16 plots the response for each factor by connecting the points for each factor. The average of all the data was represented as an horizontal line (reference). If the line represented on the main effect graph was horizontal (parallel to the reference line), there was no main effect present and the response does not change depending on the factor level. If the line was not horizontal, there may be a main effect present and the response mean change depending on the factor level. The greater the slope of the line, the stronger the effect. An example of main effect graph was reported in Figure 3-24.
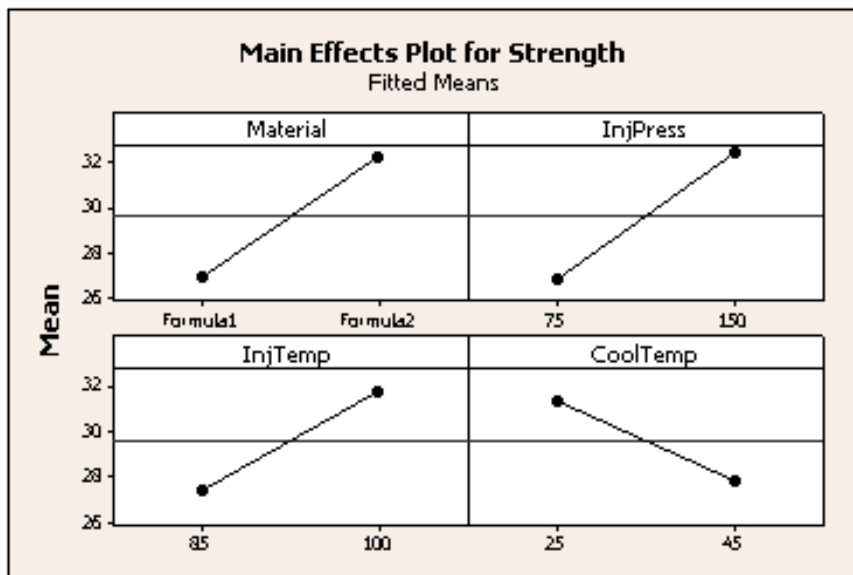
Figure 3-24. Example of main effect plot [162].

The main effects plot reported in Figure 3-24 give us the following information: formula 2 produced stronger effect than formula 1; high injection pressure produced stronger effect than low injection pressure; high injection temperature produced stronger effect than low injection temperature, then low cooling temperature produced stronger effect than high cooling temperature. The average of all the data (also named overall mean) is about 29.6 and was plotted across each panel: this was the horizontal line reported in Figure 3-24.

3.5.2.4 Interaction plot

The main effects plot can give information only about the magnitude and slope of a single processing parameter. Sometimes the critical factor can be determined by a combination of two single factors. In that chase, when the effect of a one factor depends on the level of the other factor, instead of the main effects plot was necessary to consider the interaction plot.

An example of this type of statistical plot was reported in Figure 3-25. The example represents two different supplements (1 and 2) with four different percentages of whey (0%, 10%, 20% and 30%). Parallel lines indicate no interaction. The greater the difference in slope between the lines, the higher the degree of interaction. However, the interaction plot does not tell if the interaction is statistically significant, because this information was furnished only by the Pareto chart. The plot reported in Figure 3-25 indicates an antagonistic interaction (the lines cross each other) between the supplement and the whey content. The supplement with the highest quality level depends on the whey content: supplement 1 was better when the whey content was 0 and 10%, while supplement 2 was better when the whey content was 20 and 30%.
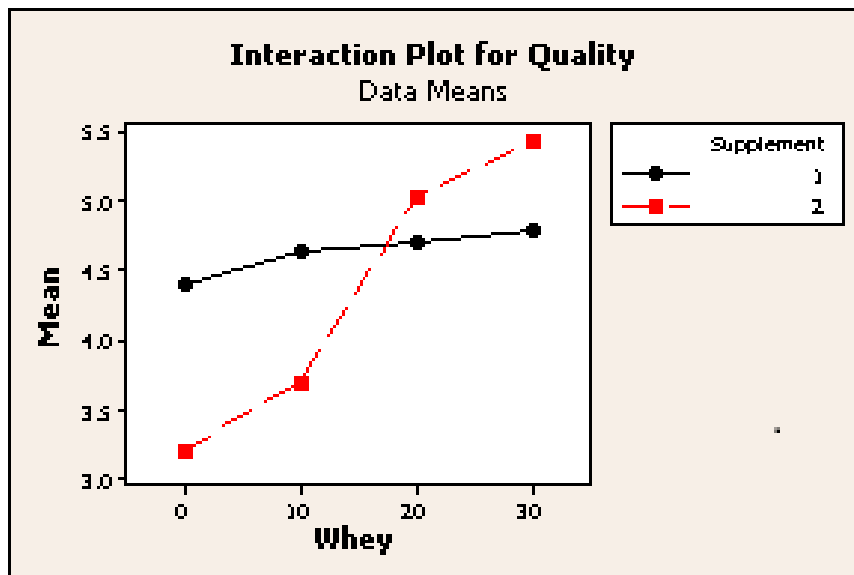
Figure 3-25. Example of interaction plot [162].

3.5.2.5 Desirability functions

The optimization stage operates using desirability functions. Desirability functions were used to predict a combination of processing parameters that fulfilled the requests

81

(maximisation, minimisation or target). Each response y_i was individually converted into a desirability function d_i that translates each effect between 0 (the effect of our process were out of target and unacceptable) and 1 (the effects were relevant to our target value or range). The individuals d_i were combined in the overall desirability, D, where D= $(d_1 \times d_2 \times d_m)^{1/m}$ and m was the number of responses: also D has a range between 0 and 1, and have to be maximized; the values 0 and 1 has the same meaning of those reported for d_i. The mathematical functions were set for our requests: it depends on if the aim was to maximise (d_1), minimise (d_2) or obtain the target value (d_3) of analysed results (shrinkage, as example). The individual functions for meeting these requirements were represented in Equation 2, Equation 3, and Equation 4 respectively [161].

Equation 2
$$d_1 = \begin{cases} 0 & y < L \\ \left(\frac{y-L}{T-L}\right)^r & L \leq y \leq T \\ 1 & y > T \end{cases}$$

Equation 3
$$d_2 = \begin{cases} 1 & y < T \\ \left(\frac{y-U}{T-U}\right)^r & T \leq y \leq U \\ 0 & y > U \end{cases}$$

Equation 4
$$d_3 = \begin{cases} 0 & y < L \\ \left(\frac{y-L}{T-L}\right)^{r1} & L \leq y \leq T \\ \left(\frac{y-U}{T-U}\right)^{r2} & T \leq y \leq U \\ 0 & y > U \end{cases}$$

U and L are the upper and lower limits, y is the response, T is the target and r-values are the function weight (linear or non-linear), which in this case are all set to be equal to one. The function weight will determine the shape of the desirability functions: for weight equal to one the shape will be a line, for different values the curve will show a concavity or convexity. Desirability functions cannot indicates optimized parameters values outside the lower and high factors level.

3.6 Shrinkage measurement

Whilst ISO 294-3 [153] was implemented for designing the mould, ISO 294-4 [152] was implemented for measuring moulded specimens. This standard is currently adopted for converting dimensional variations of moulded parts in shrinkage values in material datasheets (Novodur®, Makrolon®, APEC® from Bayer, Hostaform® from Ticona, Campus® from Grilon BS just to name a few example), in technical publications [154-156], is used as a reference in handbook about shrinkage in microscale [17; 154] and adopted by internationals societies [155; 156]. Table 3-6 reports the mathematical formulas adopted.

Moulding Shrinkage	$S_{Mp} = 100 \ \frac{l_c - l_1}{l_c}$; $S_{Mn} = 100 \ \frac{b_c - b_1}{b_c}$
Post-moulding Shrinkage	$S_{Pp} = 100 \ \frac{l_1 - l_2}{l_1}$; $S_{Pn} = 100 \ \frac{b_1 - b_2}{b_1}$
Total Shrinkage	$S_{Tp} = 100 \ \frac{l_c - l_2}{l_c}$; $S_{Tn} = 100 \ \frac{b_c - b_2}{b_c}$

Table 3-6. Mathematical formulas for measuring shrinkage. Subscripts p and n are respectively parallel and normal measurement to flow direction; c is related to mould cavity centre; 1 and 2 referred to 1 hour and 24 hour measurements [152].

Shrinkage it was expressed as percentage number related to the cavity mould dimension depicted in Figure 3-26.
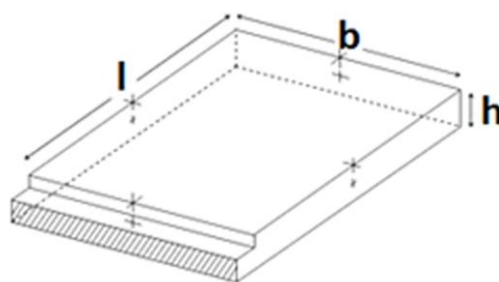
Figure 3-26. Cavity mould directions.

The parameters reported in Table 3-6 were defined as follows:

S_M (moulding shrinkage) is the difference in dimensions between a dry test specimen after 1 hour and the mould cavity in which it was moulded;

S_P (post-moulding shrinkage) is the difference in dimensions of moulded test specimen after 1 hour and 24 hours;

S_T (total shrinkage) is the difference in dimensions between a test specimen after 24 hours and the mould cavity in which it was moulded.

Using the optical equipment and the metrology protocol adopted, the formulas reported in Table 3-6 were implemented for determining shrinkage.

3.7 Summary

This chapter drawn the path of methodologies implemented in this thesis. The adoption of ISO 294-3 adapted to the scale was proposed as methodology for dealing with the absence of standardized methodology for measuring shrinkage at the micro-scale. A micro-mould was manufactured by using micro-milling technique, optical equipment was used for measuring specimen dimensions according to ISO 294-4 procedures, DoE approach was chosen for statistical treatment of data and two polymers normally used in μ-IM was examined.

Chapter 4 . Mould validation

The micro mould manufactured by adapting at the micro-scale the design of standard, has to be tested before to proceed to validate the methodology proposed for measuring shrinkage in such scale.

It was necessary to perform this kind of validation for two reasons. Firstly, is usual for a mould to present issues after the mould manufacturing stage and the solution of these aspects occur only by testing the mould: this approach represents a usual problem solving approach in injection moulding, and it could be interesting to apply the same procedure at the micro-scale. Moreover, the mould implementation is considered an important part of this thesis because further knowledge could be achieved during this stage. Secondly, the validation stage can be the occasion for testing and for practicing with DoE, by observing how any choice performed by the operator can affect statistical parameter as the desirability functions. In other words, it is likely that the decision to conduct shrinkage characterization under not perfect moulding conditions affects the response of statistic parameters. Similarly, the solution of moulding problems should be reflected in a variation of statistical parameter values. The literature review does not report information about the connection between moulding problems and response in terms of statistical parameters, probably because before to use the statistical approaches the mould has to work continuously without problems. In such case, the specimens were statistically investigated just to see this relationship.

The chapter described all the steps, from the first familiarization stage and statistical results to the solution adopted for solving mouldability problems and subsequent validation. At the end of these stages, the micro-mould implemented was used for shrinkage investigation.

The validation stage used the 316L feedstock, because considered a material more difficult to be injected with respect to the pure polymer (i.e. feedstock exhibit higher viscosity compared to pure polymer). During this stage, the troubleshooting of mouldability issues leads to identify a range of processing parameters that explore a

broad spectrum of material behaviour and an optical evaluation will compare the specimen before and after the moulding implementation.

4.1 Mould validation

After manufacturing, the mould was tested for controlling the absence of errors (e.g. poor mould design, wrong pins length) made during the design step.

As first result, the mould did not present serious issues as wrong length of pins or problems during clamping. The only difficulty encountered was the attachment of the specimen to the wrong mould half upon opening the mould, as it was attached to the fixed mould half rather than the mobile mould half. This aspect was considered not negligible because for removing the specimen it was necessary to interrupt the cycle of injection, with unlikely effects on the mould temperature. As first solution, the mould design was implemented with the manufacture of two blind holes on the mobile side, as showed in Figure 4-1.
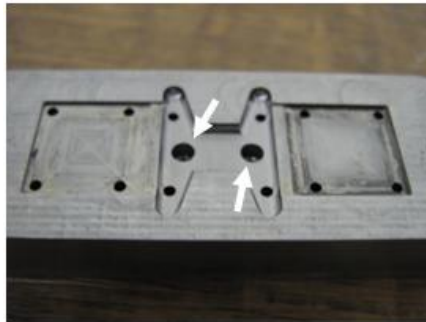
Figure 4-1. The blind holes manufactured into the mould runner.

The profile of the blind holes was reported in Figure 4-2. The conical shape permitted a little volumetric expansion of the material, sufficient to remove the specimen from the fixed mould half.
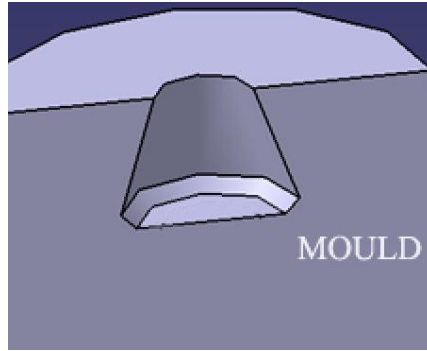
Figure 4-2. Section of blind holes profile.

Figure 4-3 depicts the 316L feedstock specimen moulded with the blind holes.
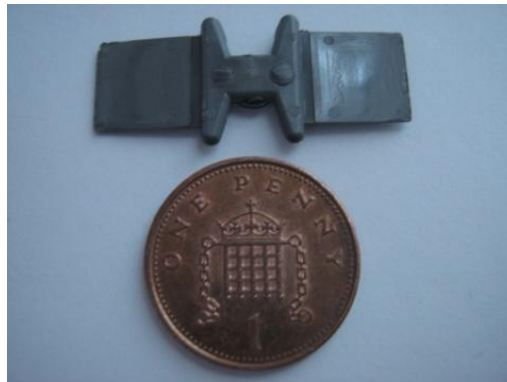
Figure 4-3. 316L feedstock moulded specimen with blind holes in the runner.

The specimens moulded using the micro-mould modified with the blind hole was investigated using DoE approach for studying shrinkage.

4.2 Specimen shrinkage results

Table 4-1 reports the five processing parameters chosen as factors to be investigated in the present thesis. Preliminary test runs identified the initial values and their range: these values were arranged using the fractional factorial matrix reported in Table 3-1.

	316L feeds. (Blind holes)		
Processing Parameters	Initial Values	Value +	Value −
Injection press [bar]	900	930	870
Holding press [bar]	400	450	350
Melt temp [°C]	195	198	192
Mould temp [°C]	110	115	105
Holding time [s]	2	3	1

Table 4-1. 316L feedstock processing parameter values.

Table 4-2 reports the combination of processing parameters and shrinkage values. The specimens' dimensions were measured according to the procedure reported in paragraph 3.4 Specimen measurements technique, and the conversion from measure to shrinkage followed the method described in paragraph 3.6 Shrinkage measurement.

Run	Hold time [s]	Hold Press. [bar]	Inj. Press. [bar]	Mould Temp. [°C]	Melt Temp. [°C]
1	3	450	930	115	198
2	1	450	930	115	192
3	3	350	930	105	198
4	1	350	870	115	192
5	3	350	870	105	192
6	1	450	930	105	198
7	1	350	870	105	198
8	1	350	930	115	198
9	3	350	870	115	198
10	1	450	870	105	192
11	1	450	870	115	198
12	3	350	930	115	192
13	3	450	870	105	198
14	3	450	870	115	192
15	1	350	930	105	192
16	3	450	930	105	192

316L feedstock shrinkage results [%] (mould with blind holes)						
Run	S_{Mp}	S_{Mn}	S_{Pp}	S_{Pn}	S_{Tp}	S_{Tn}
1	2.962±0.004	3.735±0.022	-2.238±0.004	-3.461±0.009	0.790±0.004	0.403±0.003
2	2.795±0.009	2.338±0.013	-1.425±0.017	-2.025±0.018	1.409±0.001	0.360±0.001
3	2.441±0.010	1.687±0.010	-0.826±0.018	-0.951±0.017	1.635±0.010	0.752±0.008
4	3.289±0.015	2.781±0.011	-2.072±0.022	-2.432±0.015	1.286±0.005	0.416±0.003

5	3.125±0.007	3.776±0.022	-1.939±0.011	-3.349±0.032	1.246±0.003	0.553±0.006
6	2.228±0.005	1.342±0.008	-0.998±0.008	-0.871±0.012	1.252±0.003	0.483±0.002
7	2.806±0.019	1.985±0.012	-1.884±0.028	-1.616±0.017	0.975±0.003	0.401±0.005
8	3.382±0.005	3.035±0.004	-1.831±0.008	-1.703±0.008	1.613±0.003	1.383±0.006
9	2.695±0.020	2.346±0.006	-1.371±0.029	-1.888±0.008	1.360±0.003	0.502±0.001
10	1.231±0.003	0.530±0.004	-0.060±0.005	-0.006±0.008	1.172±0.003	0.524±0.006
11	2.678±0.005	2.267±0.001	-1.781±0.007	-1.969±0.002	0.944±0.001	0.342±0.001
12	2.802±0.011	1.644±0.012	-1.734±0.015	-1.196±0.017	1.116±0.001	0.468±0.001
13	1.098±0.007	0.422±0.001	0.043±0.010	0.011±0.003	1.140±0.001	0.433±0.002
14	1.284±0.002	0.302±0.001	-1.167±0.003	0.046±0.002	1.119±0.001	0.348±0.001
15	1.412±0.003	0.374±0.001	-0.196±0.005	0.016±0.002	1.219±0.003	0.390±0.002
16	1.384±0.005	0.378±0.001	-0.050±0.008	0.118±0.002	1.335±0.004	0.495±0.001

Table 4-2. Results of 316L feedstock shrinkage measurements (mould with blind holes) expressed as mean value ± standard deviation.

Each shrinkage value resulted from the measurement of five specimens theoretically moulded for a number of uninterrupted cycles after each new set of process parameters. The term "theoretically" was used because at this stage, even with the manufacture of blind holes in the runner, was not possible to operate in cycling mode: the mould continued to present mouldability problems that makes the injection processing not continuous. The combinations of processing parameter that gave issues were identified in Table 4-2 with grey and black cells: the grey cells identified a discontinuous cycling that requested occasional operator's assistance, the black cells identified a processing that requested continues operator's assistance. It was possible to identify the combination high melt-high mould temperature as the combination that gave more serious mouldability problems (black cells).

4.2.1 Post moulding shrinkage trend

Even under mouldability problems, results of specimens reported in Table 4-2 were analyzed. The first analysis of data has shown unexpected feedstock behaviour. Moulding and total shrinkage trend confirmed the general material progression: the specimen dimensions were smaller than cavity mould [17; 31]. The post-moulding shrinkage shown some negatives values, where minus sign represented a specimen expansion respect the dimensions 1 hour after moulded. It could be useful a simple representation of this trend, as depicted in Figure 4-4 that represented the dimension (not shrinkage) of a specimen (the 12th) that shown a partially measure recover after 1, 24 and 36 hours in parallel to and normal to the flow direction.
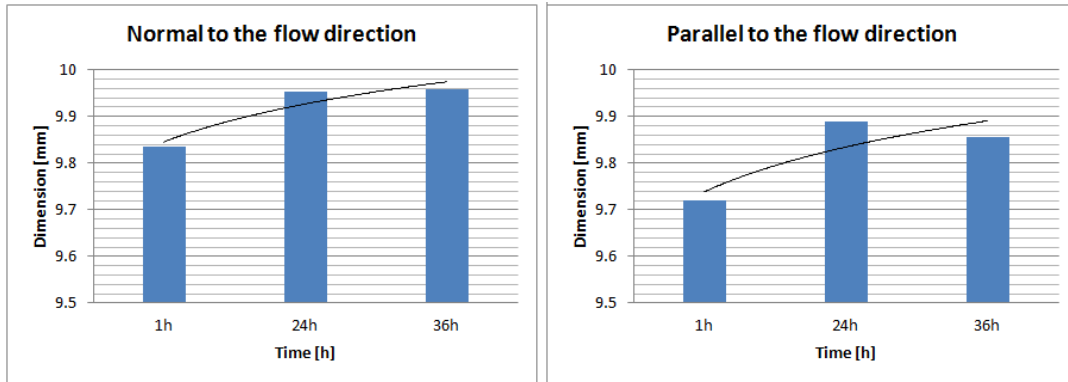
Figure 4-4. Dimensions of specimen 12 compared to the cavity mould.

The specimen tends to the cavity mould dimensions (length=9.987±0.001 mm, breadth=9.980±0.001 mm) but shrinkage prevents the complete recovery. Investigations that are more accurate were realized by using strain gages on a second specimen (randomly chosen as the 12nd). The strain gages were oriented parallel to and normal to the flow direction (Figure 4-5).
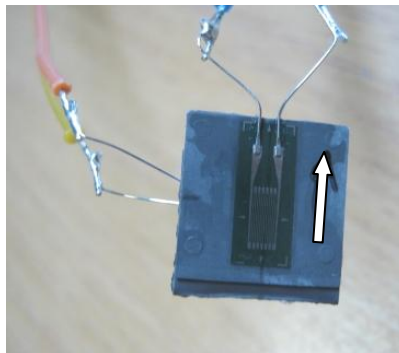
Figure 4-5. Strain gage in parallel to the (front) and normal to (rear) the flow direction (represented by the arrow).

Figure 4-6 depicts the trends of strain in parallel to the flow (A) and normal to the flow (B) direction monitored for 72 hours: both shown similar drift.
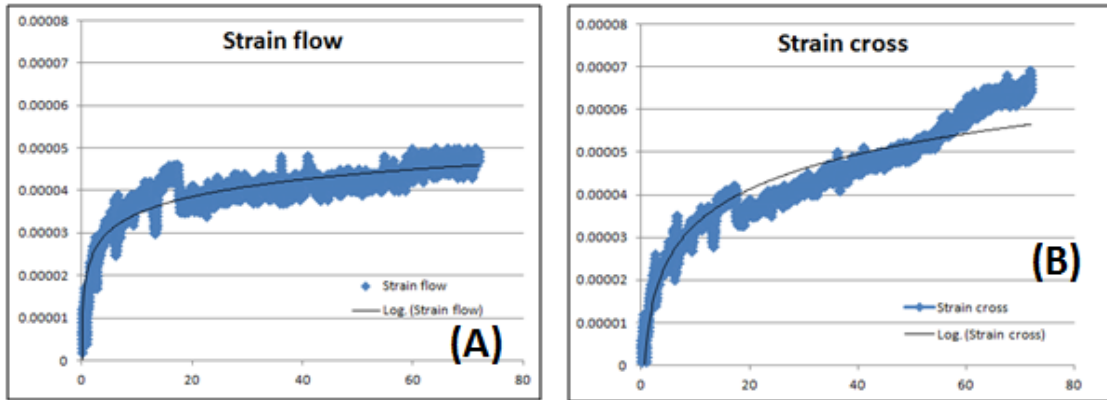
Figure 4-6. Strain trend during 72 hours (x-axes) in parallel to (A) and normal to (B) the flow direction for 316L feedstock specimen.

The strain gage results confirmed the trend reported in Figure 4-4. The y-axis of Figure 4-6 represents the strain gage clock instead of shrinkage because the aim of the graph it was only to depict a trend.

By considering a pure polymer, this post-moulding trend did not find explanation in the literature because evidences [28] reports that after moulding, polymers (especially semi-crystalline materials) can continue to shrink (not to expand as evidenced in Figure 4-4) at room temperature. Shrinkage can occur even in the cold because the opportunity for crystallization exists in a temperature window below the melting point of the polymer and above the glass-transition temperature (T_g). Processes like injection molding involve rapid cooling of the polymer as it was injected in the mould. This rapid reduction in temperature is needed to solidify the material so that the part can assume its intended shape. However, as long as the polymer remains at a temperature above its glass transition there will be sufficient mobility at a molecular level to allow the crystal structure to develop, and only once the temperature drops below this point no more crystals can form. The T_g of acetal (the POM used as binder in 316L feedstock) is around -80°C, room temperature is 100° C above the T_g of acetal: so as the moulded parts can shrink also after moulding because they had enough freedom at a molecular level to continue crystallizing. However, by considering a feedstock material (polyester based concrete), [190] confirmed shrinkage trend similar to Figure 4-6. Besides high amount of additives inside the concrete can decrease shrinkage.

91

The 316L feedstock post moulding shrinkage behaviour is based on a mechanism that should be further investigated. It is likely that the high powder percentage (60 vol. %) could play a role, but for detecting this aspect is necessary to perform a tomography test. As first hypothesis, the mechanical stress conferred to metal powder, highly compressed during the moulding stage, could be supposed to play a role.

4.3 Results of critical factors study

Despite the combination of processing parameters reported in Table 4-3 did not produce a continuous processing cycle, a statistical study of results was performed for investigating the effects of discontinuous moulding cycle on statistical outcomes and for testing the DoE. The alpha factor (α) was set equal to 0.05: this means that the chance to find an effect that does not really exist was the 5%.

The processing factors were labelled as follow: holding time (A), holding pressure (B), injection pressure (C), mould temperature (D) and melt temperature (E). Combinations of two of these factors were indicated with the proper letters.

4.3.1 Moulding shrinkage (S$_M$)

Moulding shrinkage in parallel to the flow direction

Figure 4-7 depicts the Pareto chart of critical parameters that affect moulding shrinkage in parallel to the flow direction. The statistical analysis did not identify any critical factor.
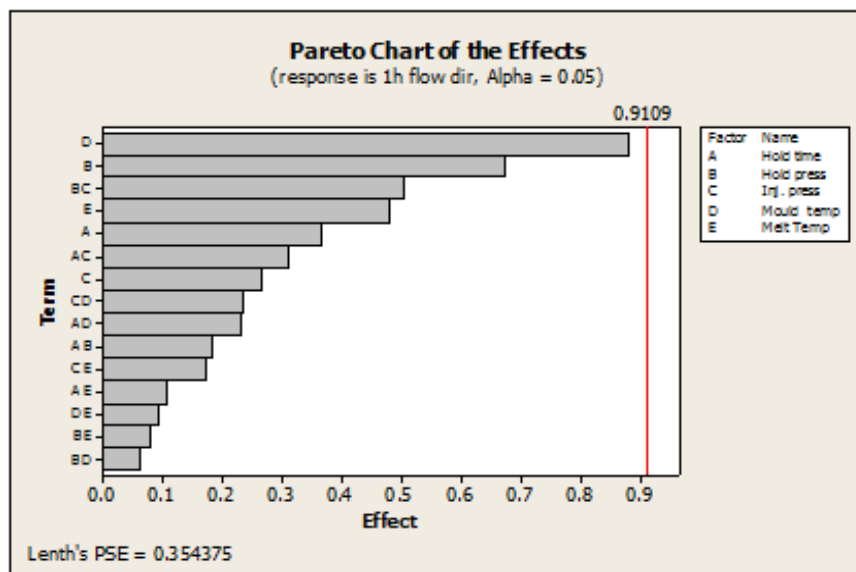
Figure 4-7. Pareto chart of processing parameters effects for moulding shrinkage in parallel to the flow direction.

Moulding shrinkage in normal to the flow direction

Figure 4-8 depicts the Pareto chart of critical parameters that affect moulding shrinkage in normal to the flow direction. The statistical results did not identify any critical factor.
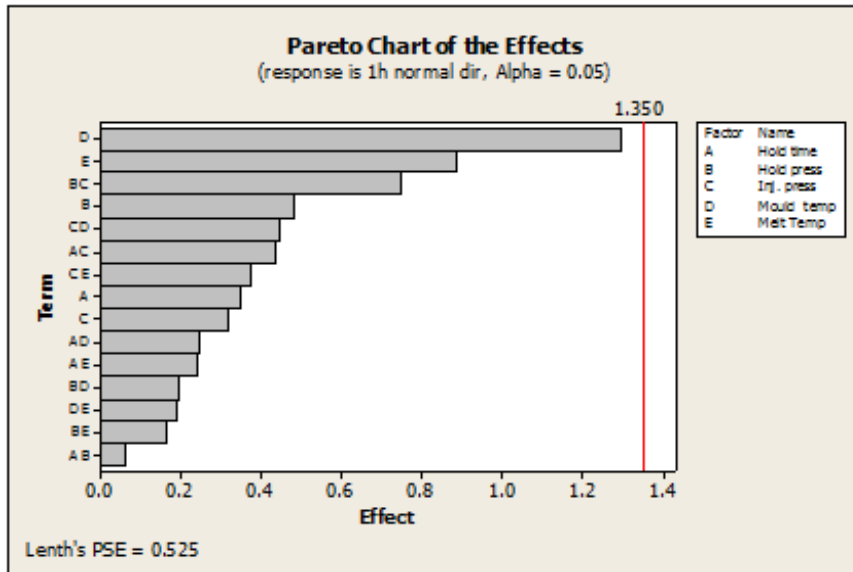
Figure 4-8. Pareto chart of processing parameters effects for moulding shrinkage in normal to the flow direction.

4.3.2 Post moulding shrinkage (S_P)

24 hours after the injection moulding stage, the post moulding shrinkage was measured. The specimens used in this step and the storage methods (at room temperature) were the same of the previous test.

Post moulding shrinkage in parallel to the flow direction
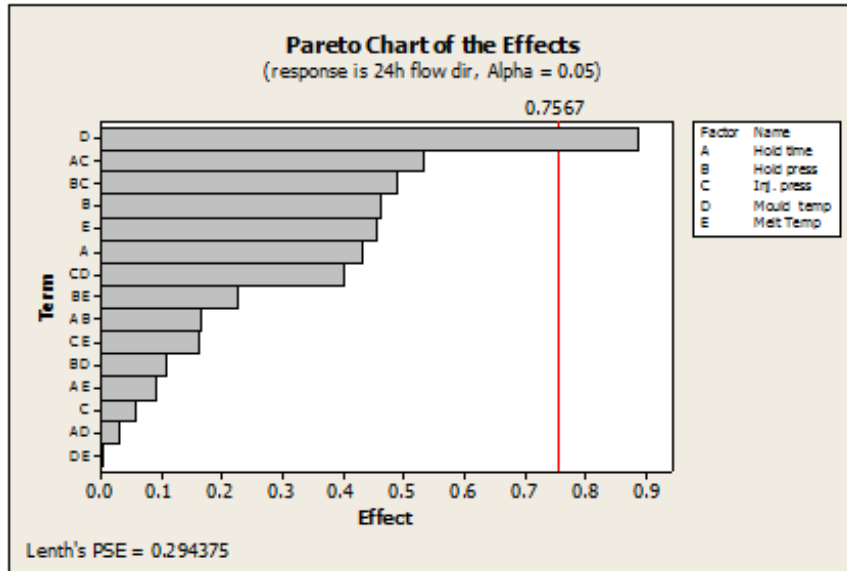
Figure 4-9. Pareto chart of processing parameters effects for post-moulding shrinkage in parallel to the flow direction.

The Pareto chart depicted in Figure 4-9 reports the effect of processing parameter after 24 hours in parallel to the flow direction. The mould temperature (D) was identified as critical parameter and affected the post-moulding shrinkage within the interval of confidence considered.

Figure 4-10 reports the main effect plot of the critical factor identified by Pareto chart. Results have shown that by increasing the mould temperature, the mean value of post-moulding shrinkage decreases.
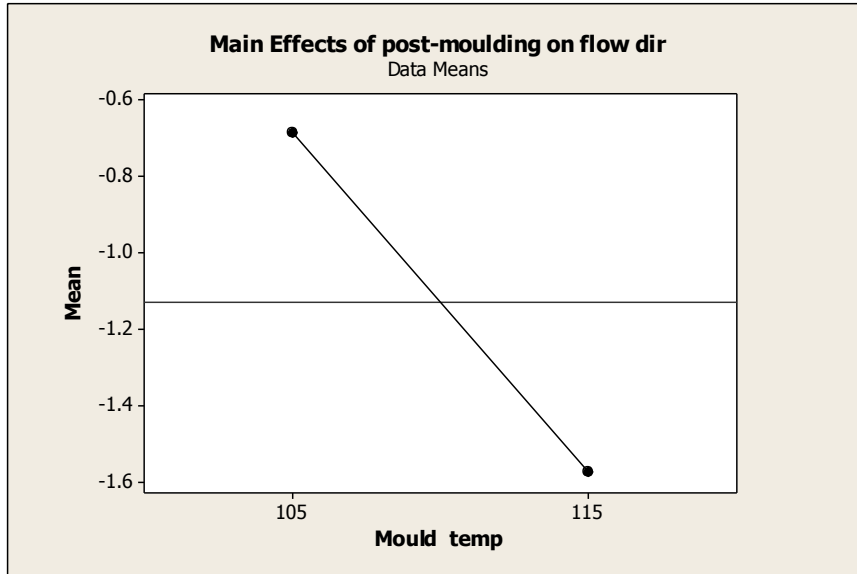
Figure 4-10. Main effect plot of mould temperature vs. post-moulding shrinkage in parallel to the flow direction.

Post moulding shrinkage in normal to the flow direction
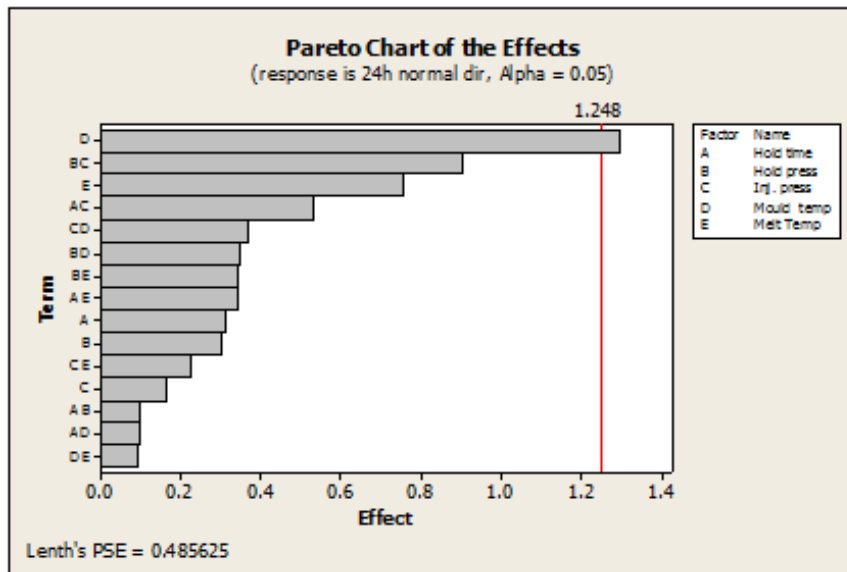
Figure 4-11. Pareto chart of processing parameters effects for post-moulding shrinkage in normal to the flow direction.

Figure 4-11 represents the Pareto chart of post-moulding shrinkage in normal to the flow direction. The mould temperature was identified as critical factor.

Figure 4-12 reports the main effect plot of mould temperature: by increasing this parameter, the mean value of post-moulding shrinkage decreases.
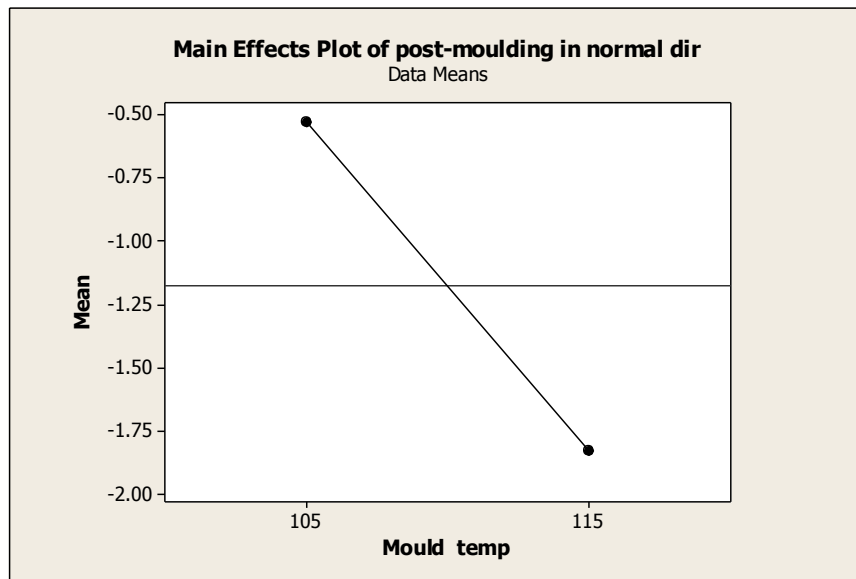
Figure 4-12. Main effect plot of mould temperature vs. post-moulding shrinkage in normal to the flow direction.

4.3.3 Total shrinkage (S_T)

Total shrinkage was expressed as the percentage difference between specimen dimension 24 hours after moulding and the cavity mould dimension. As predicted by the literature, the final dimensions resulted smaller than cavity mould.

Total shrinkage in parallel to the flow direction
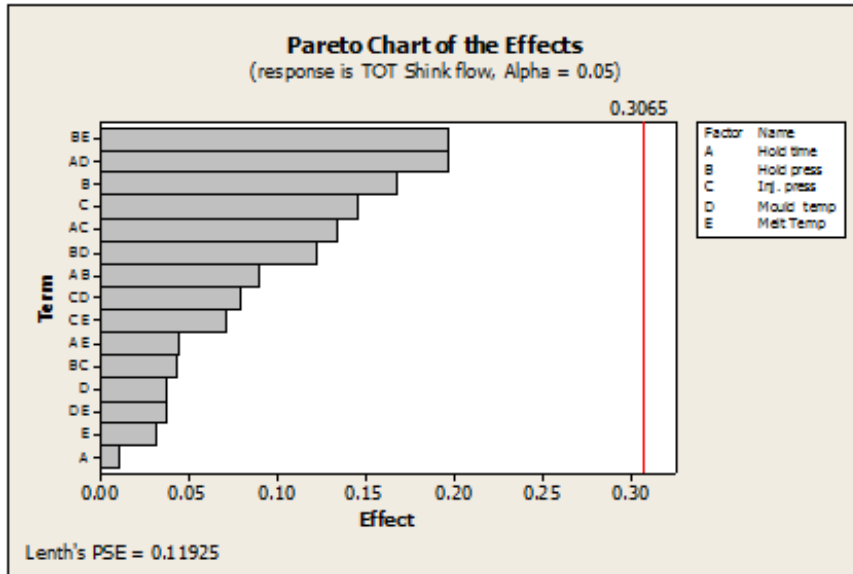
Figure 4-13. Pareto chart of total shrinkage in parallel to the flow direction.

Figure 4-13 represents the effect of process parameters in terms of total shrinkage: no critical parameters were identified.

Total shrinkage in normal to the flow direction
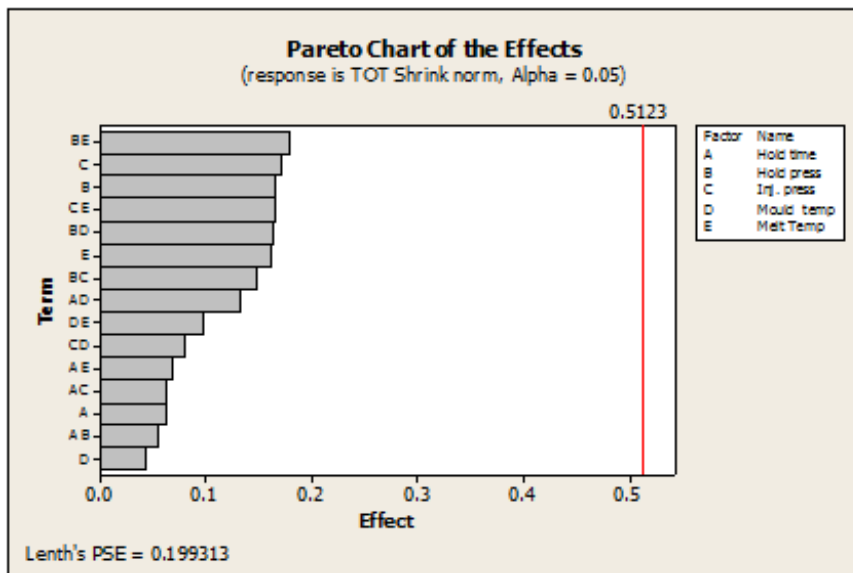
Figure 4-14. Pareto chart of total shrinkage in normal to the flow direction.

According to Figure 4-14 results, no critical parameters affect total shrinkage in normal to the flow direction.

4.4 Parameter optimization

The statistical analysis of critical factors identified the mould temperature as critical parameter that affect post-moulding shrinkage both parallel to than normal to the flow direction. No others critical factors were identified as parameters that affect shrinkage.

The optimization stage was performed, and parameters that minimize shrinkage were identified. This phase adopted desirability functions (D), ranged between 0 and 1.

Optimal D 0.78078	High Cur Low	Hold tim 3.0 [3.0] 1.0	Hold pre 450.0 [450.0] 350.0	Inj. pre 930.0 [914.6098] 870.0	Mould t 115.0 [115.0] 105.0	Melt Tem 198.0 [198.0] 192.0
Composite Desirability 0.78078						
TOT Shin Minimum y = 0.7989 d = 0.60962						
TOT Shri Minimum y = 0.350 d = 1.0000						
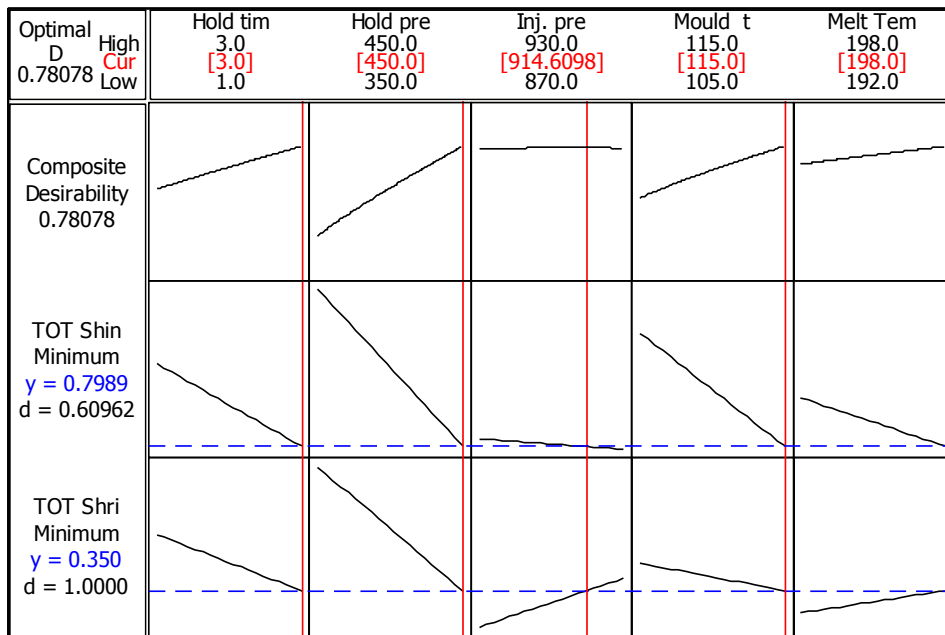
Figure 4-15. Optimized parameter values; mould with blind holes.

The optimization stages were performed using all the total shrinkage values reported on Table 4-2: for both (parallel and normal) the optimization was performed by using the minimization mode, with target value equal to 0.35% and maximum (upper) value equal to 1.5% (Figure 4-16). The value of 0.35% was chosen because some total shrinkage in normal to the flow direction present values close to this limit, even if the values of total shrinkage in parallel direction are clearly higher. These conditions are quite severe, and the low desirability value evidenced the difficulty to achieve these targets. On the contrary, the maximum value of 1.5% should be more easily to achieve by considering that the greater part of total shrinkage presents values lower than this limit.
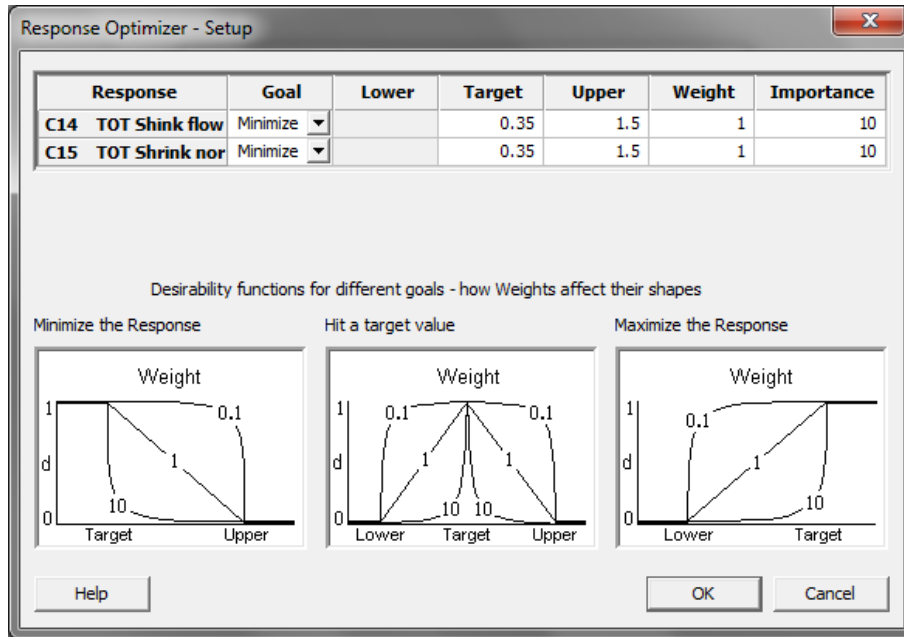
Figure 4-16. Response optimizer setting; mould with blind holes.

The first row of Figure 4-15 reports the shape of the composite desirability function: this parameter combines the individual desirabilities into an average for highlight the relative importance of the responses. The second row is related to the S_{Tp} (total shrinkage in parallel to the flow direction). The last row represents the S_{Tn} (total shrinkage in normal to the flow direction). Considering that the aim was to minimize shrinkage, the statistical optimization was set in "minimized mode". At the end of optimization stage, optimum processing parameters were those that could reduce the shrinkage with likelihood equal to desirability value: these values were reported in the bracket square on top of Figure 4-15. Concerning the optimized temperature values, they were identified in a mould temperature equal to 115°C and melt temperature equal to 198°C. By comparing these temperature values with those reported in Table 4-2, it is possible to observe that the combination high mould-high melt temperatures makes the moulding stage difficult to be realized in continuous cycling (black and grey cells). For this reason the results have to be re-considered. Moreover, overall desirability value was 0.78, while the aim is to operate under overall value equal to 1.

A second optimization stage was performed using the same numerical data reported in Table 4-2 but without considering the rows with the black cells (related to the worse mouldability conditions, with continue operator's assistance) on the left side: the aim of

this stage was simply to detect how the desirability value changes by removing some runs. By removing the black cell results, the optimization stage analysed only the combinations of processing parameters that were able to make the mouldability processing continuous (even if the grey cells gave some mouldability problems as well). Optimization stage adopted the same response optimizer setting reported in Figure 4-16. Figure 4-17 reports the optimized processing parameters under these conditions.
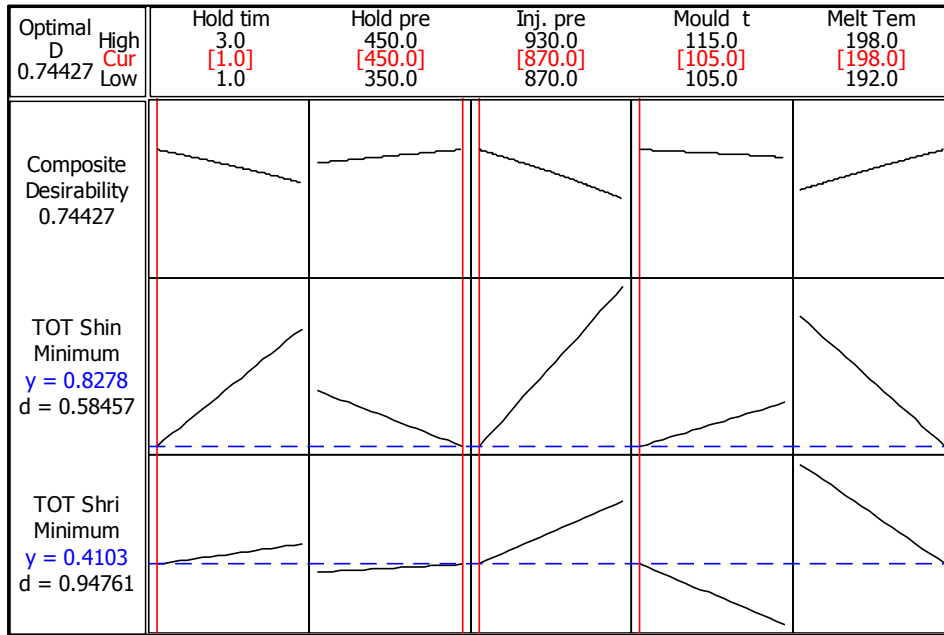
Figure 4-17. Optimized processing parameters calculated without black cells data.

The results of the optimized parameters under these conditions were reported on top of Figure 4-17. The overall desirability value dropped from 0.78 (with all the experimental results considered) to 0.74 (with the rows with black cells not considered): conclusion was that to remove two processing combinations, has produced a worse optimization.

A specimen was moulded with the optimized parameters reported on top of Figure 4-17: the total shrinkage was reduced respect to Table 4-2 results. Table 4-3 reports the numerical data.

S_{Mp} [%]	S_{Mn} [%]	S_{Pp} [%]	S_{Pn} [%]	S_{Tp} [%]	S_{Tn} [%]
0.771±0.007	0.835±0.022	-0.087±0.014	-0.287±0.012	0.698±0.014	0.549±0.009

Table 4-3. Shrinkage values for 316L feedstock (mould with blind holes).

However, it was possible to obtain a lower difference between shrinkage in parallel to, and normal to, the flow direction: shrinkage seems to be more symmetric in both directions respect to Table 4-2 results.

For improving the overall desirability and consider all the processing parameter combinations, the best solution was to realize a further mould improvement by inserting two ejection pins in the blind holes. This configuration permitted to increase the mould temperature and solved the ejection problems, even if it was necessary to perform a new familiarization stage with new shrinkage measurements and new optimization stage. The results chapter describe the steps next to the pin insertions. Indeed, this last modification demonstrated to be suitable for improving the mouldability ranges and for solving the ejection problems and it was considered as final mould configuration.

4.5 Optical investigations

The effect of pin insertion inside the blind holes can be highlighted by considering the optical investigation of moulded parts before and after the mould improvement. An optical analysis of moulded specimens reported in Table 4-2 was conducted by considering the gate and border area depicted in Figure 4-18.
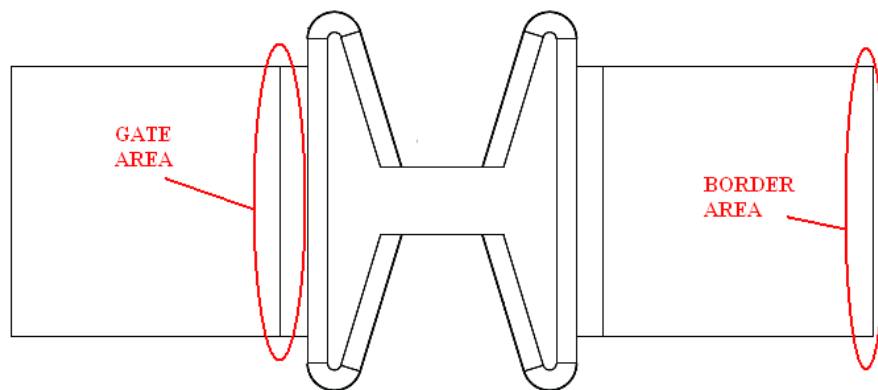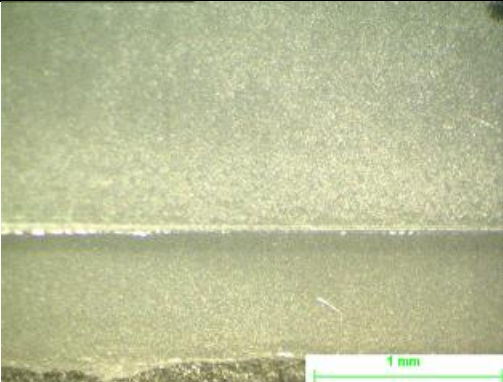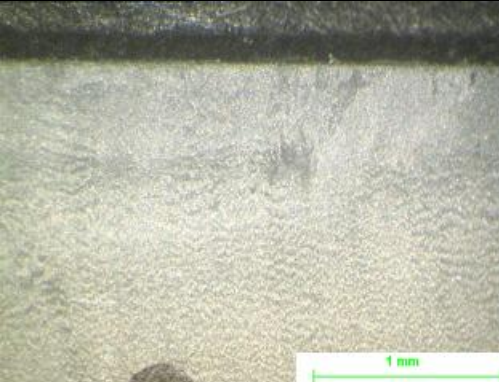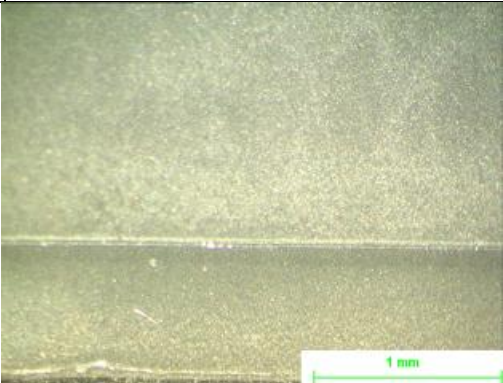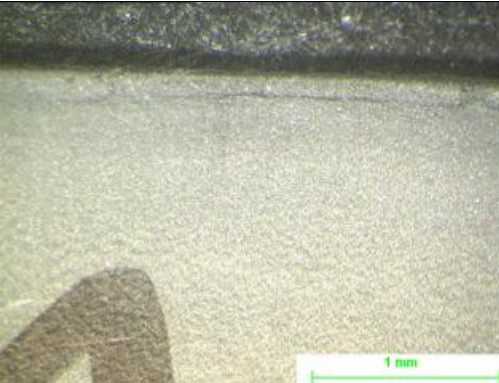
Figure 4-18. Areas observed with the optical microscope.

4.5.1 Specimen moulded with micro-mould with blind holes

Figure 4-19 reports the optical investigation results and consequent comment of the part represented (mould with blind holes).

Gate area	Border area
1	
Well defined	Well defined
2	
Flow trace	Delaminations
3	
Flow trace	Delaminations
4	
Well defined	Delaminations

5	Flow trace	Flow junction
6	Well defined	Well defined
7	Well defined	Delaminations
8	Well defined	Well defined

9		
	Well defined	Delaminations
10		
	Flow trace	Delaminations
11		
	Well defined	Well defined
12		
	Well defined	Delaminations

13	Flow trace	Delaminations
14	Well defined	Delaminations
15	Flow trace	Delaminations
16	Flow trace	Delaminations
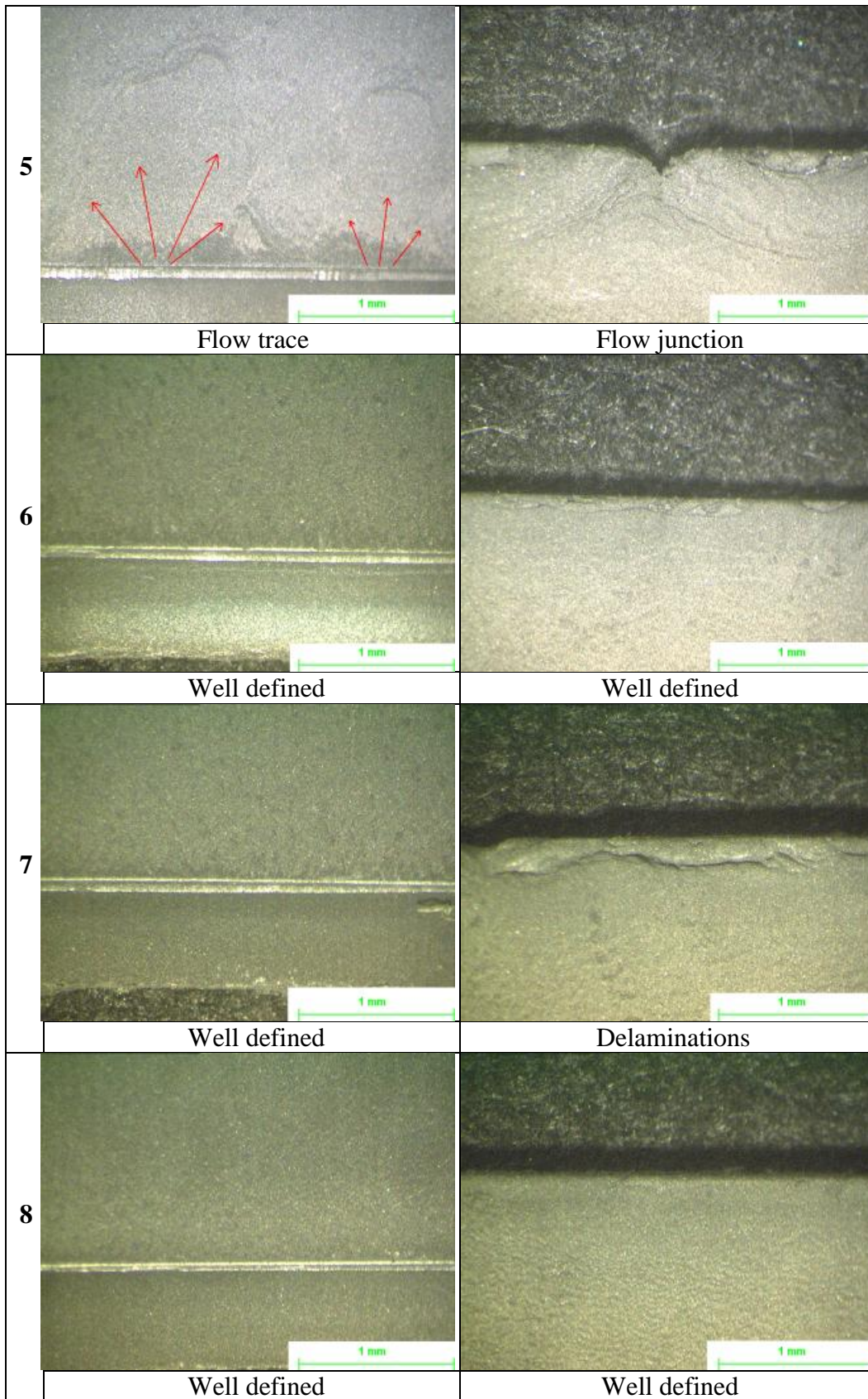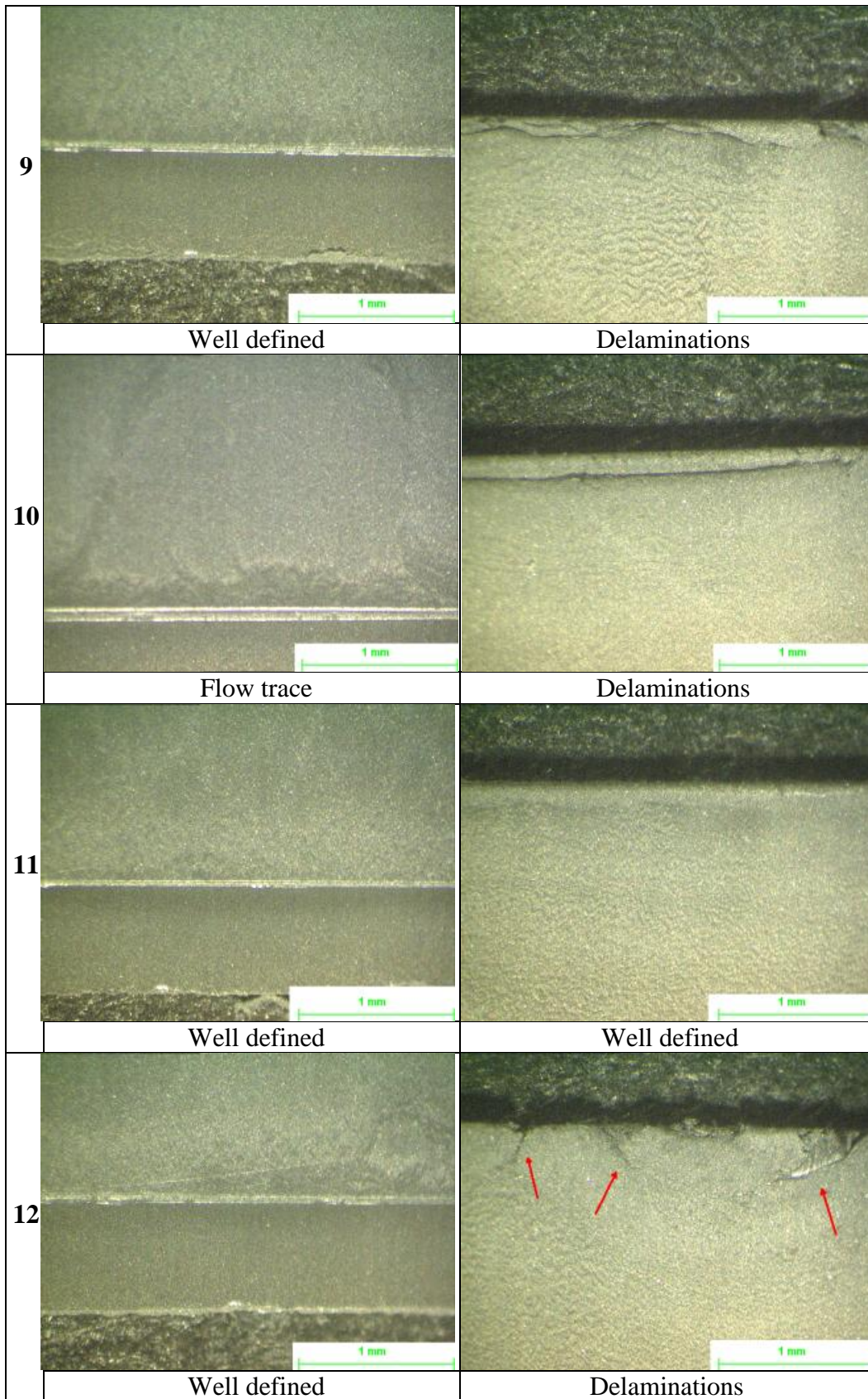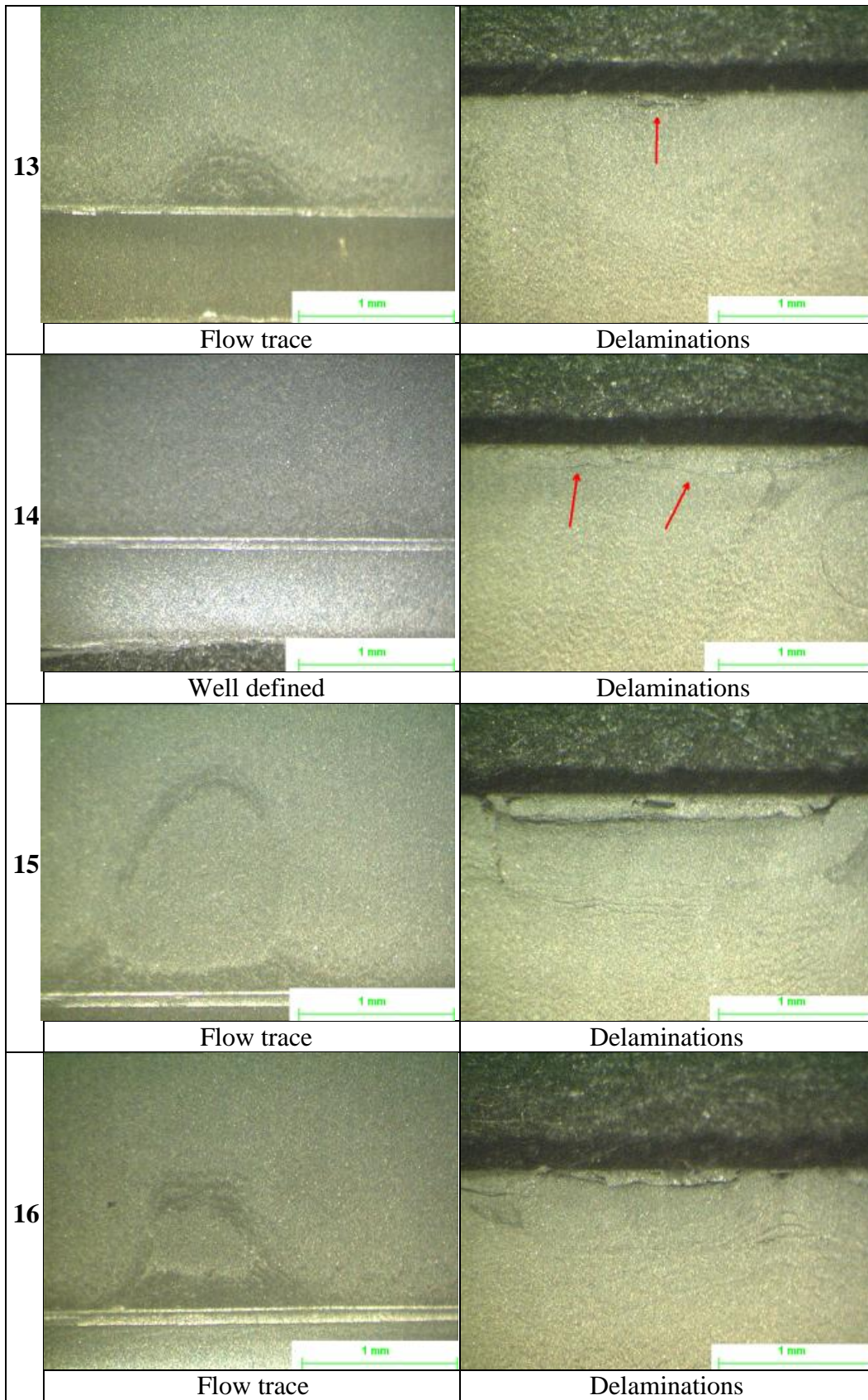
Figure 4-19. Optical analysis of gate and edge areas.

The analysis of flow lines could be used to diagnose filling dynamics, as suggested by Bociaga et al. [191]. The specimens 2, 3, 5, 8, 13, 15, 16 in the gate area shown record grooves (or ripples) phenomenon caused, usually, by low processing parameters values (temperature parameters and injection speed) or high melt cooling rate. Experimental studies were realized for determining the effect of "flow lines", and results have shown that the lines were the outcome of repeated melt advance and cooling: Figure 4-20 depicts this mechanism.
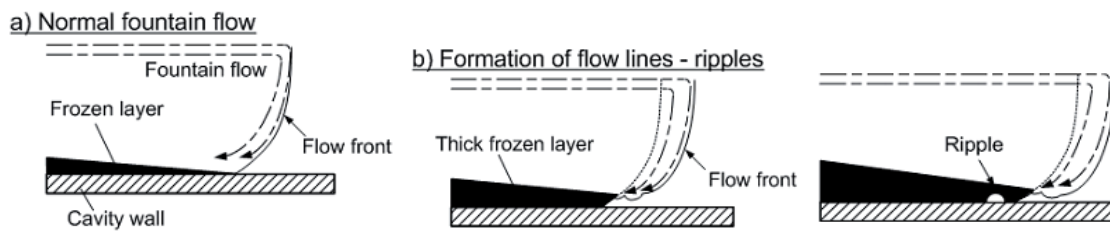
Figure 4-20. Generation of flow lines [192].

The melt freezes on a cavity wall, but the interior part of the melt stream moves forward. Due to the fountain flow, the melt is pushed towards the cavity wall. If the frozen layer is too thick (because of low mould temperature and flow velocity), the flow front has too much time to solidify and is deformed. As the result, the ripple on the wall was created [192].

Specimen 5 shown flow junction lines in the border area. Usually junction lines occur when the melt meet some obstacle along the flow path [191].
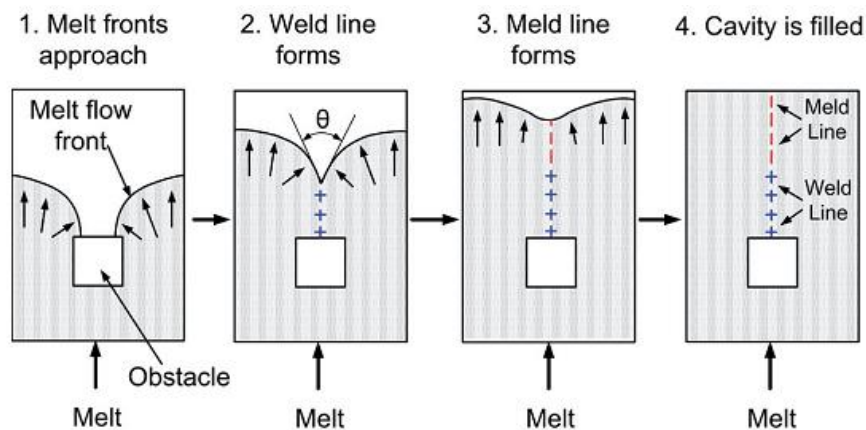
Figure 4-21. Weld lines created from an obstacle [191].

The picture of specimen 5 border area depicts weld lines created by the meeting of two melt fronts that flow from the opposite directions (situation 2 of Figure 4-21).

It is likely that the steel powder forms local agglomerations inside the melt flow, as investigated by Karatas et al. [181], and this could constitute an obstacle. The mechanism for the creation of powder aggregates inside the feedstock flow was well represented by Thornagel [193] (Figure 4-22).
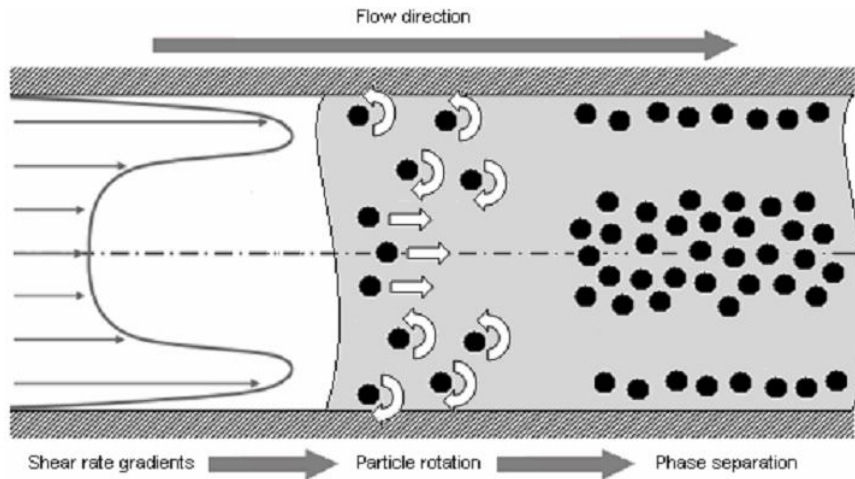
Figure 4-22. Flow pattern of PIM feedstock across the channel [193].

The flow profile, has shown a local shear stress gradients that cause powder-binder separation: this gradient forces the powder particles to leave areas of high gradients for filling the areas of low gradient and produce the powder concentration, as depicted in Figure 4-23.
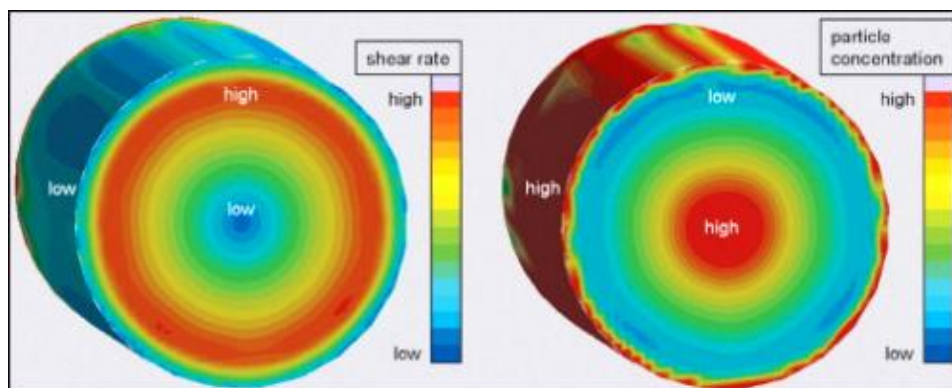
Figure 4-23. Modelling of powder-binder separation [193].

The powder concentration becomes a lump that can create two feedstock fronts and to reproduce the situation reported in Figure 4-21.

By using the free software ImageJ [194], it was possible to estimate the angle formed by the two flow fronts, as depicted in Figure 4-24.
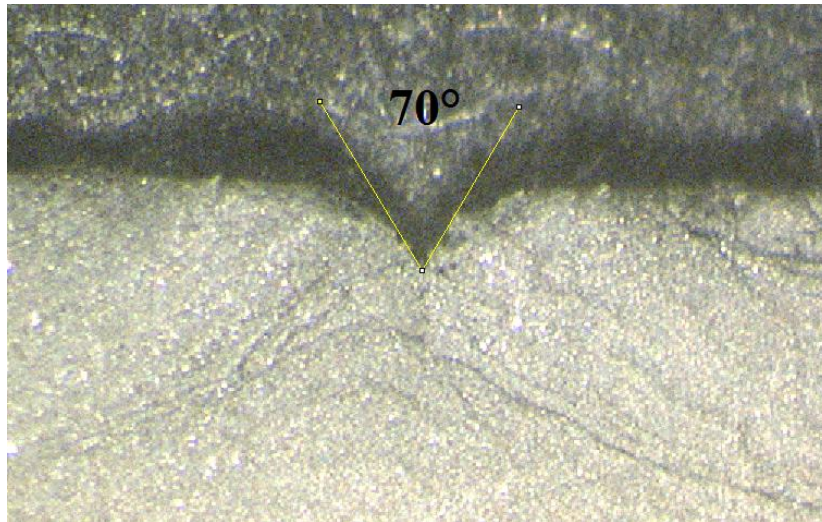
Figure 4-24. Angle value formed by the junction of two melts fronts in specimen 5.

The specimen numbers 2, 3, 4, 7, 9, 10, 12, 13, 14, 15 and 16 on the border area presented delaminations (separation of layers in the moulded part that can be peeled off) [195]. They results from insufficient layer bonding due to low homogeneities in the melt flow and high shear stresses.

Different specimens shown flow patters (1, 4, 9, 10, 12 and 14) in the area behind the border, likely due to not optimized cooling and holding parameters [191].

The better surface definition was about specimens 1, 6, 8 and 11; but the specimens 1, 8 and 11 were moulded with the processing combinations that gave problems and were not suitable for a cycled injection processing.

The process parameters for manufacturing the specimen 6 have the closer values of ours optimized parameters, except the injection pressure value: 930 bars instead of 870 bars. This specimen shows well-defined edges and no flow sign on the surface.

The optical analysis of specimen moulded with optimized values was reported in Figure 4-25, shown a well edge definition and the absence of the jetting flows: his was evidence that the optimized parameters improved also the quality surface.
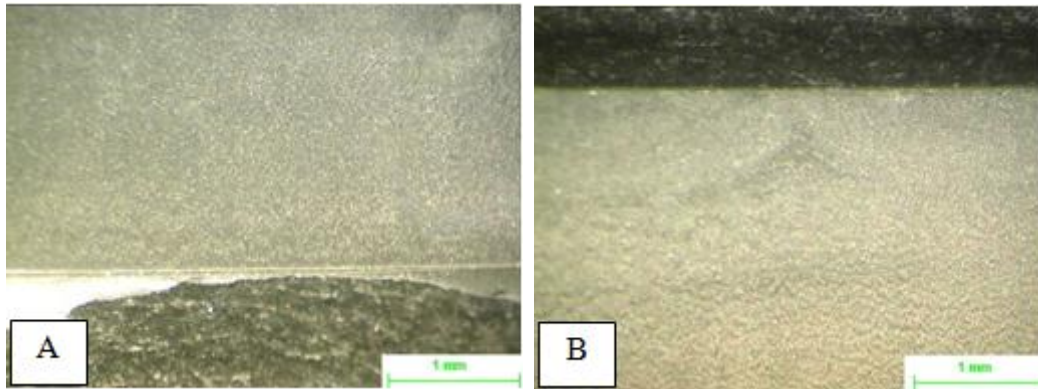
Figure 4-25. Optical view of the gate (A) and border (B) of specimen moulded with optimized parameters (mould with blind holes).

4.5.2 Specimens moulded with mould with pins inside blind holes

The statistical study of the specimens moulded with the improved mould was analysed in the thesis. In the present paragraph, optical analysis was realized for discussing the effect of increased temperature range and for showing that all the mouldability range of 316L feedstock was explored. The pictures reported in Figure 4-26 represents the border area of the specimen moulded with the micro-mould improved by insertion of pins inside the blind holes, by using the combination of processing parameters reported in Table 3-3 (316L feedstock values). Figure 4-26 depicts only the border area because the gate area was fully filled for all specimens without visible flow patterns.

Border area of 316L feedstock	
(1) Completely filled, flashes	**(2)** Completely filled, flashes

(3) Partially filled

(4) Completely filled, flashes

(5) Partially filled

(6) Partially filled, flow junction

(7) Partially filled

(8) Completely filled

(9) Completely filled, flashes	**(10)** Partially filled
(11) Completely filled, flashes	**(12)** Completely filled
(13) Partially filled	**(14)** Completely filled

111

| (15) Partially filled | (16) Partially filled |

Figure 4-26. Optical analysis of specimens moulded with pins inside blind holes. Scale of specimens 10, 13, 15 and 16 it is 4 mm; the scale for others pictures it is 2 mm.

A great difference with respect to the specimens moulded with mould in configuration "blind holes" (depicted in Figure 4-19) was the extreme variability in terms of specimen quality. The insertion of pins inside the blind holes permitted to increase the temperature range and to explore all the mouldability range of 316L feedstock: in this way, results of optimization stage will be more reliable. Indeed Figure 4-26 shown a high specimen variability (from partially to fully filled, with or without flashes), and a strong processing parameter influence (on the contrary of specimens moulded in configuration "blind holes" that maintained their shape although flow patters). Moreover, the most important thing, all specimens were moulded in cycling mode without operator's assistance.

4.6 Summary

During the mould validation, some problems of mouldability were evidenced. However, shrinkage data were statistically treated for investigating the effects of discontinuous moulding cycle on statistical outcomes. An improvement of mould configuration was proposed by manufacturing two ejection pins in the runner: the insertion of pins solved the mouldability problems and permitted a continue injection cycling. The optical analysis of specimens moulded with the two different mould configurations shown that the increased temperature values permitted to explore all the mouldability feedstock range: this will assure a greater reliability of optimized values.

Chapter 5 . Results: standardized methodology for measuring shrinkage in μ-IM. POM case study.

The validated mould can be now used for moulding specimens and measuring their shrinkage. The POM was used as injected polymer at this stage: the familiarization identified the range of processing parameters, and DoE treatment analyzed the experimental results: critical factors were determined. The conversion of dimensional variations in shrinkage values was performed by using the ISO 294-4. The critical parameters were discussed and compared with the small amount of prior data available in the literature.

5.1 Research contribution

In the only previous work that adopted a standard for micro shrinkage measurements, a rectangular mould was used for measuring shrinkage both parallel to and cross-flow [31]. However, the ASTM D955-89 standard recommends a square specimen when cross-flow shrinkage is to be measured. Therefore, the approach taken here will to implement all of ISO 294-3 square mould design except the dimensions. Such a design would also comply with the square mould design from ASTM D955-89.

The triangular gate designed in ISO 294-3, should create a uniform melt flow without turbulence to allow a wide polymer front for filling the cavity mould, and does not exhibit melt fracture. This contrasts with prior work in which an edge gate was used [31].

5.2 Designing a micro-scale shrinkage test

Table 5-1 reports the processing parameters analysed for POM, and Table 5-2 their combination values affectively tested using the half-fractional factorial model. The processing parameters were the results of familiarization stage conducted with the implemented mould (ejection pins inside the blind holes).

Process Parameters	Initial Values	Value +	Value -
Injection press [bar]	850	900	800
Holding press [bar]	500	550	450
Melt temp [°C]	195	200	190
Mould temp [°C]	100	115	85
Holding time [s]	3	4	2

Table 5-1. POM processing parameter values.

	Combination of processing parameters investigated					Half Fractional Factorial matrix				
Run	Hold time [s]	Hold press [bar]	Inj. press [bar]	Mould temp [°C]	Melt temp [°C]	Hold time	Hold press	Inj. press	Mould temp	Melt temp
1	2	450	900	85	190	+	-	+	-	+
2	4	450	900	85	200	+	-	-	+	+
3	4	550	800	85	200	+	+	-	-	+
4	4	550	900	85	190	+	-	-	-	-
5	2	550	800	115	190	+	+	+	-	-
6	2	550	900	85	200	-	-	+	-	-
7	2	550	800	85	190	+	-	+	+	-
8	4	450	900	115	190	-	+	+	-	+
9	2	450	800	85	200	-	+	-	+	+
10	4	450	800	85	190	-	-	+	+	+
11	2	450	900	115	200	+	+	-	+	-
12	4	550	800	115	190	+	+	+	+	+
13	2	550	900	115	190	-	+	-	-	-
14	4	450	800	115	200	-	+	+	+	-
15	4	550	900	115	200	-	-	-	-	+
16	2	550	800	115	200	-	+	-	+	-

Table 5-2. Matrix of half-fractional factorial design and processing values investigated.

5.3 POM shrinkage measurements

Table 5-3 shows the effect of each process parameter combination in terms of moulding (S_M), post moulding (S_P) and total (S_T) shrinkage. Shrinkage values are given in percentages and are quoted for the parallel to (p) and normal to (n) the flow direction for times of 1 and 24 hours post moulding.

Run	S_{Mp} [%]	S_{Mn} [%]	S_{Pp} [%]	S_{Pn} [%]	S_{Tp} [%]	S_{Tn} [%]
1	6.910±0.014	2.731±0.022	0.793±0.022	0.068±0.031	7.649±0.008	2.797±0.007
2	6.566±0.002	3.335±0.008	0.104±0.004	-0.440±0.012	6.664±0.001	2.909±0.001
3	5.067±0.005	3.227±0.008	0.043±0.008	-0.349±0.011	5.108±0.004	2.890±0.001
4	5.977±0.008	2.862±0.003	0.122±0.015	-0.061±0.004	6.092±0.009	2.802±0.002
5	3.809±0.002	3.178±0.001	0.081±0.004	0.040±0.001	3.887±0.002	3.217±0.001
6	4.676±0.010	2.932±0.004	0.310±0.016	-0.010±0.006	4.972±0.009	2.923±0.001
7	6.783±0.010	2.825±0.001	-0.009±0.015	-0.005±0.002	6.775±0.007	2.820±0.001
8	3.722±0.001	3.228±0.002	0.007±0.002	0.026±0.002	3.728±0.001	3.253±0.001
9	6.989±0.004	2.838±0.001	-0.022±0.007	0.566±0.009	6.968±0.004	3.388±0.009
10	7.948±0.010	2.824±0.001	0.007±0.017	-0.489±0.008	7.954±0.010	2.350±0.008
11	3.660±0.001	3.177±0.001	0.010±0.001	-0.083±0.002	3.670±0.001	3.096±0.001
12	3.600±0.001	3.170±0.001	0.086±0.001	-0.016±0.001	3.683±0.001	3.155±0.001
13	3.640±0.001	3.199±0.001	-0.011±0.001	-0.023±0.001	3.629±0.001	3.177±0.001
14	3.616±0.001	3.268±0.001	0.024±0.001	0.030±0.002	3.640±0.001	3.297±0.002
15	3.437±0.001	3.134±0.001	-0.065±0.002	0.469±0.003	3.373±0.001	3.603±0.004
16	3.662±0.002	3.116±0.001	-0.029±0.004	-0.089±0.001	3.633±0.002	3.030±0.001

Table 5-3. POM shrinkage results expressed as mean value ± standard deviation.

For making Table 5-3 more clear, the numerical results were reported as graph of POM shrinkage parallel to (Figure 5-1) and normal to (Figure 5-2) the flow direction. Each graph reports only the moulding (S_M) and the total (S_T) shrinkage, not the post-moulding (S_P) shrinkage: this because S_M and S_T are calculated with respect to the mould dimensions, while S_P is the shrinkage between 1 and 24 hours. Besides, the standard deviations were not reported by considering their low values.
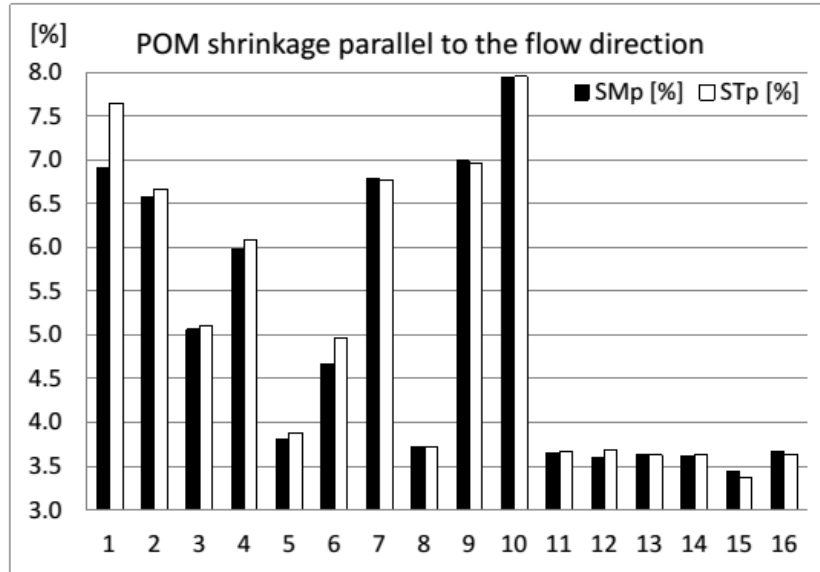
Figure 5-1. POM shrinkage parallel to the flow direction.
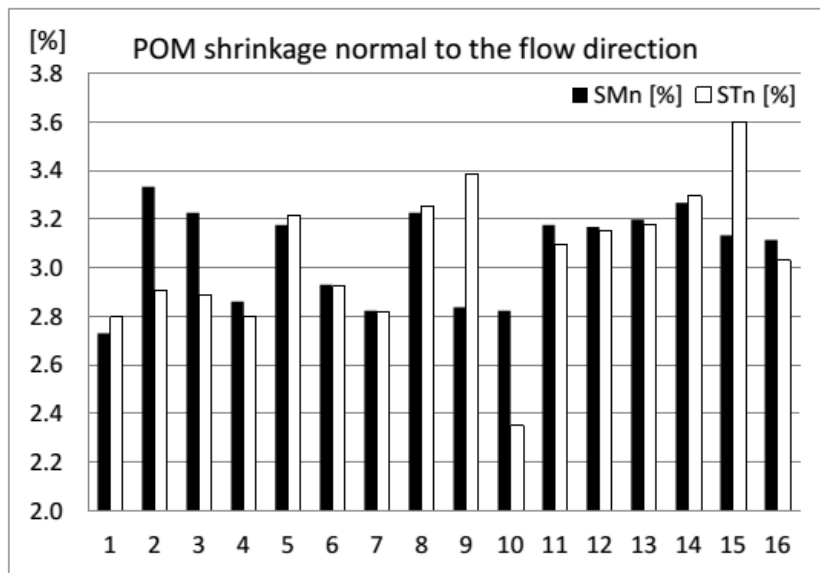
Figure 5-2. POM shrinkage normal to the flow direction.

5.3.1 POM moulding shrinkage in parallel to the flow direction

The Pareto chart depicted in Figure 5-3 represents the critical factor that affect moulding shrinkage in parallel to the flow direction. It shows the magnitude and the effect of single or combined process parameters, along with a reference line indicating statistical significance. For this work an alpha value of 0.05 was adopted i.e. the confidence limit was 95%. The processing parameters were labelled as A (hold time), B (hold pressure), C (injection pressure), D (mould temperature) and E (melt temperature).

The combined influences of two of these parameters were described using two of the above letters.

Pareto analysis of moulding shrinkage in parallel to the flow direction has shown that the mould temperature is the only critically significant parameter (under the confidence interval considered).
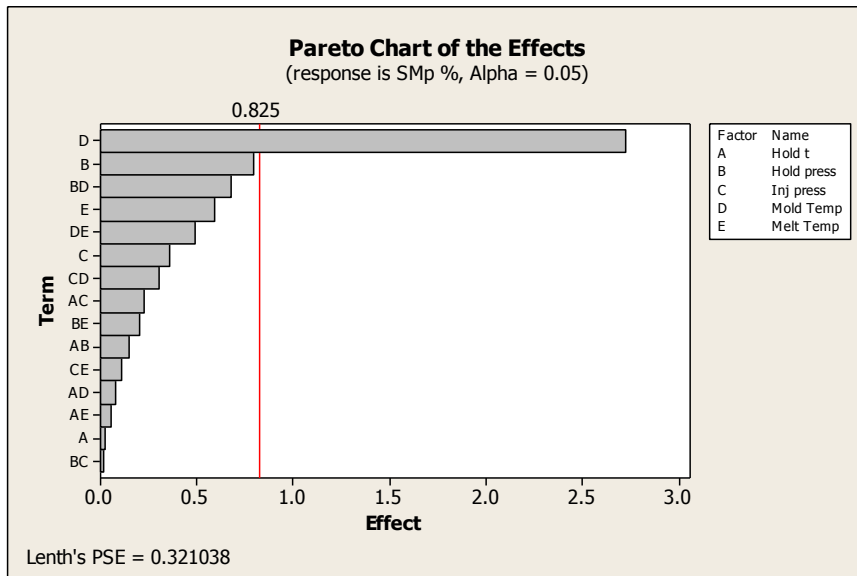
Figure 5-3. Pareto chart of POM mould shrinkage in parallel to the flow direction.

Figure 5-4 reports the main effect plot for the factor identified by Pareto chart as critical (the mould temperature) for moulding shrinkage in parallel to the flow direction. Each main effect chart analyse the single processing parameters, the slope of the line representing the magnitude and direction of the effect on the response. Vertical axes represent the means of the response variable for each factor level. An increasing of mould temperature leads to decrease mould shrinkage S_{Mp}.
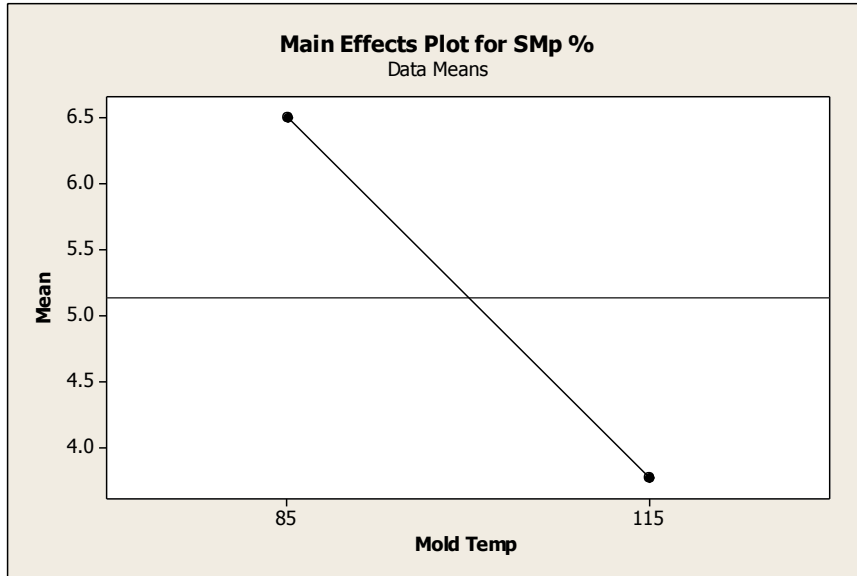
Figure 5-4. Main effects of POM mould shrinkage in parallel to the flow direction.

5.3.2 POM moulding shrinkage in normal to the flow direction

Figure 5-5 represents the Pareto chart of mould shrinkage in normal to the flow direction. As for the mould shrinkage in parallel to the flow direction, the mould temperature was the only statistically significant factor.
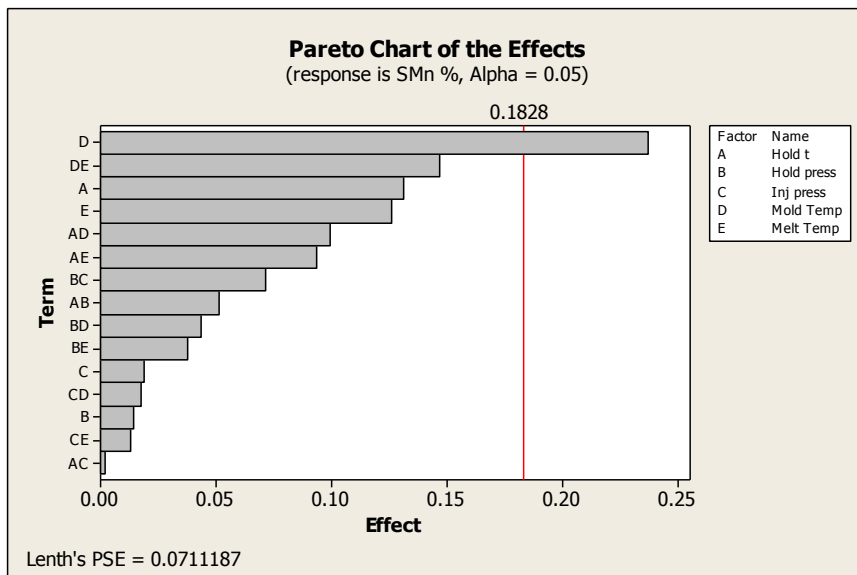
Figure 5-5. Pareto chart of POM mould shrinkage in normal to the flow direction.

Figure 5-6 reports the main effect for the critical factor identified from Pareto chart. The slope is the opposite respect the mould shrinkage in parallel to the flow direction case: higher mould temperature value leads to increase shrinkage.
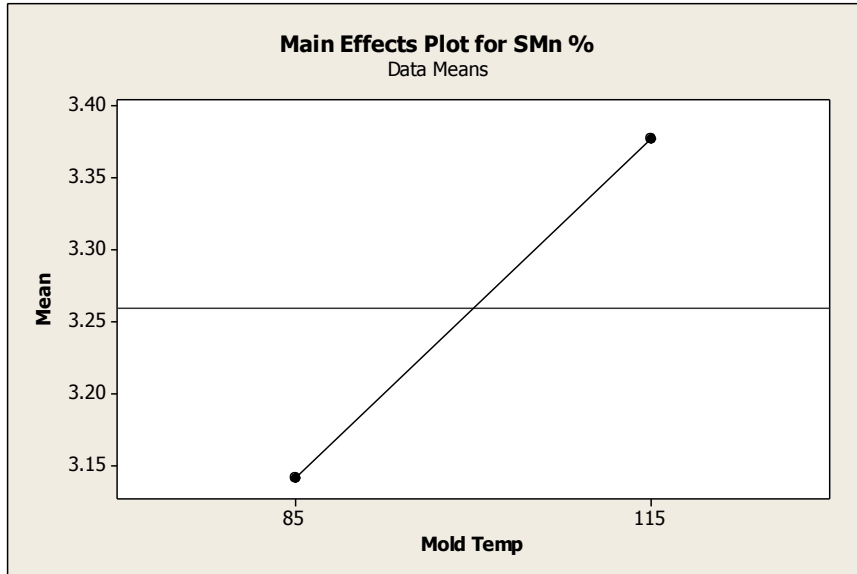
Figure 5-6. Main effects of POM mould shrinkage in normal to the flow direction.

5.3.3 POM post moulding shrinkage in parallel to the flow direction

The Pareto chart in Figure 5-7 shows post mould shrinkage parallel to the flow direction: no statistically significant effects were detected.
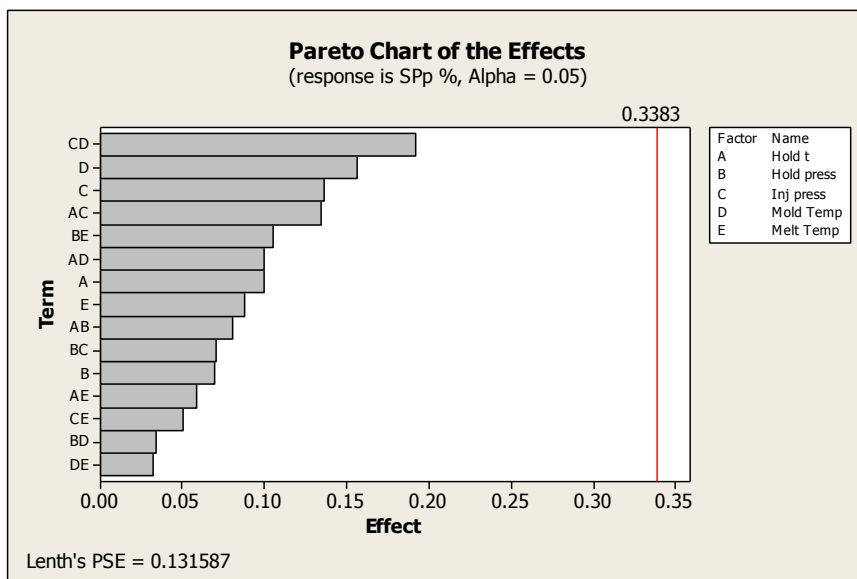
Figure 5-7. Pareto chart of POM post mould shrinkage in parallel to the flow direction.

5.3.4 POM post moulding shrinkage in normal to the flow direction

Figure 5-8 reports the Pareto chart of post moulding shrinkage in cross direction. The combined effect of hold time and mould temperature has a statistically significant effect on shrinkage.
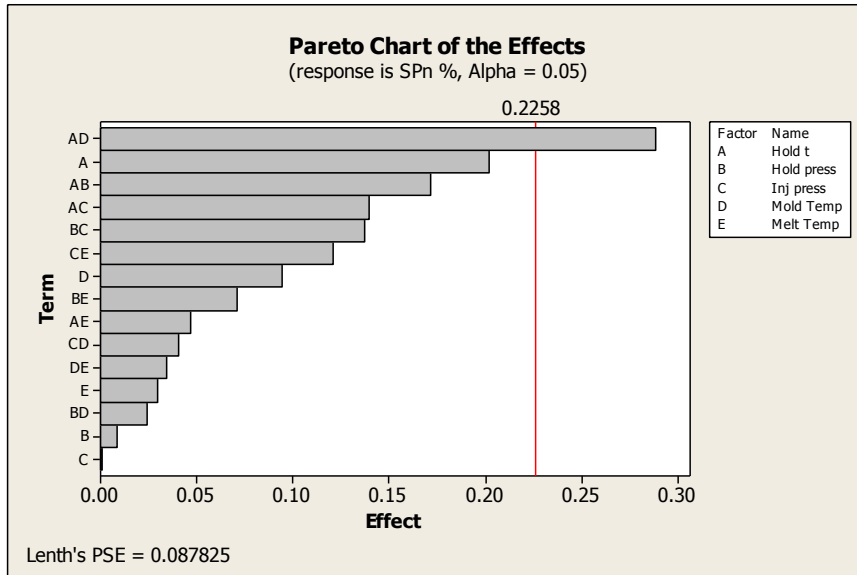
Figure 5-8. Pareto chart of POM post mould shrinkage in normal to the flow direction.

Figure 5-9 shows the corresponding interaction plot. The boxes show the change of post moulding shrinkage in normal to the flow direction (S_{Pn}) respect this interaction. The top right box plots the mean shrinkage as a function of mould temperature; the bottom left box plots the mean shrinkage as a function of hold time.

Considering mould temperature (top right), post moulding shrinkage in normal to the flow direction S_{Pn} moving from the low (85°C) to the high (115°C) temperature increase when hold time is high (4 s) and decrease when it is low (2 s). Considering hold time (bottom left) moving from the low (2 s) to the high (4 s) time, S_{Pn} increase when mould temperature is high (115°C) and decrease when it is low (85°C).
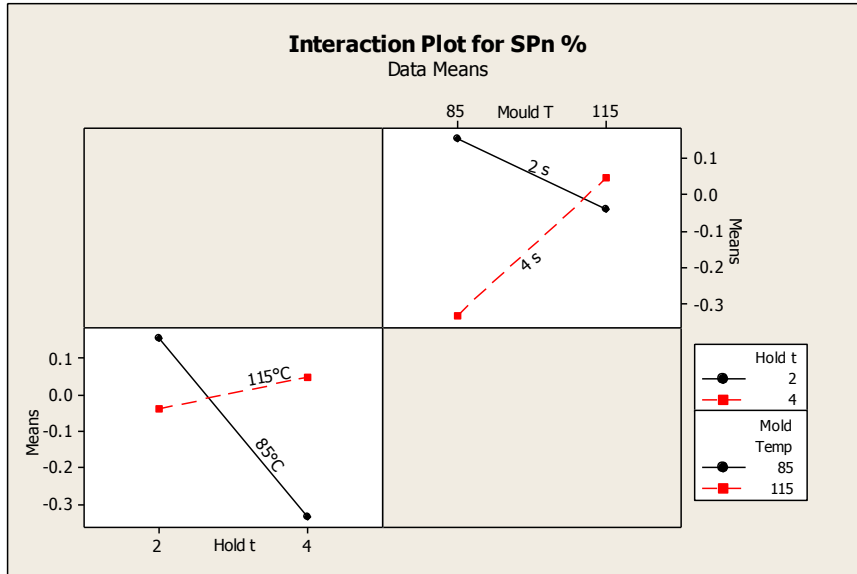
Figure 5-9. Interaction plot between holding time and mould temperature for post moulding shrinkage in normal to the flow direction.

5.3.5 POM total shrinkage in parallel to the flow direction

Figure 5-10 reports the Pareto chart in flow direction of total shrinkage. Three factors had statistically significant effects on shrinkage: the mould temperature, hold pressure and melt temperature. In addition, two combinations of factors had statistically significants: hold pressure with mould temperature and mould temperature with melt temperature.
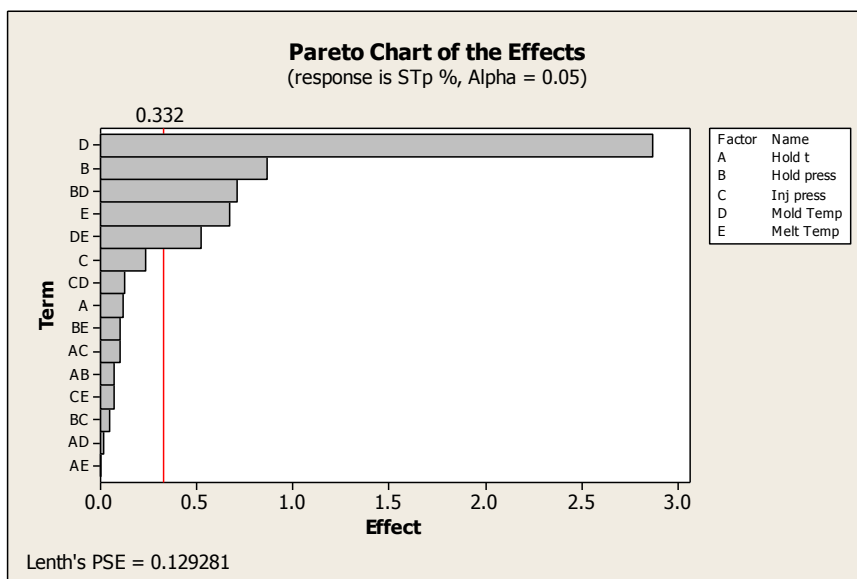
Figure 5-10. Pareto chart of total shrinkage in parallel to the flow direction.

Figure 5-11, shows the corresponding main effects plot, and the slope of mould temperature, holding pressure and melt temperature. The analysis of the direction permits to say that an increasing of all these factors leads to a decreasing of shrinkage.
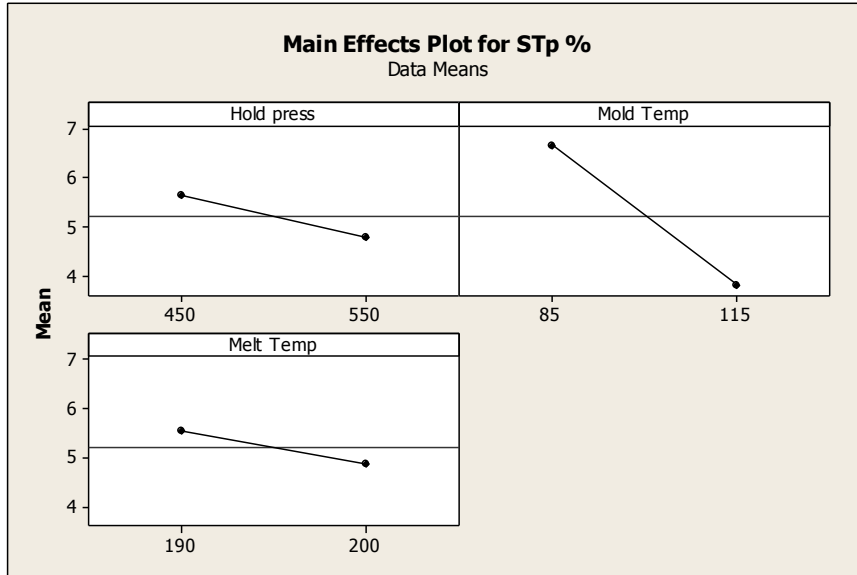
Figure 5-11. Main effect of total shrinkage in parallel to the flow direction.

The plot of Figure 5-12 represents the interaction between holding pressure and mould temperature. The boxes show the change of total shrinkage, in parallel to the flow direction S_{Tp}, with both mould temperature and hold pressure. The top right box plots the mean shrinkage as a function of mould temperature; the bottom left box plots shrinkage as a function of hold pressure.

Considering mould temperature (top right), the decrease of total shrinkage in parallel to the flow direction S_{Tp} moving from the low (85°C) to the high (115°C) temperature is larger when hold pressure is low (450 bar) than when it is high (550 bar). Considering hold pressure (bottom left), the decrease of S_{Tp} moving from the low (450 bar) to the high (550 bar) pressure is larger when mould temperature is low (85°C) than when it is high (115°C).
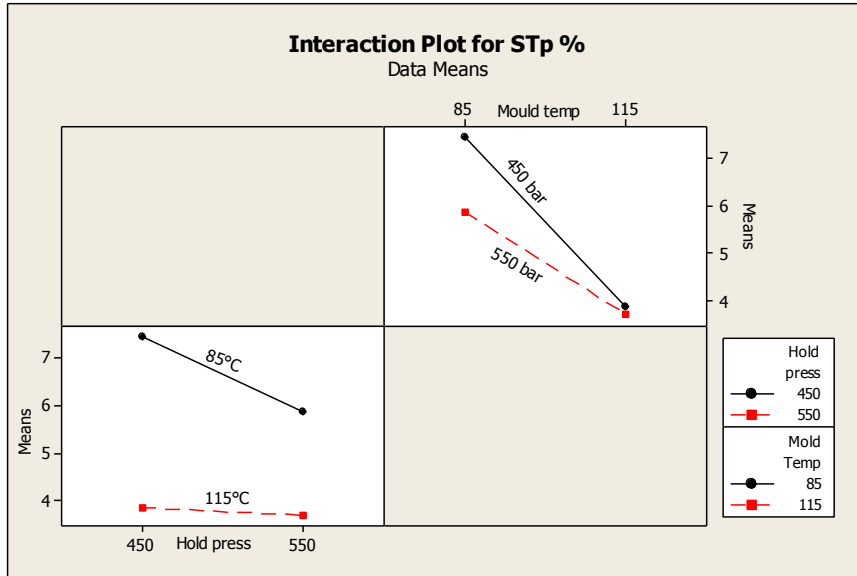
Figure 5-12. Interaction plot between holding pressure and mould temperature for total shrinkage in parallel to the flow direction.

Figure 5-13 represents the interaction between melt and mould temperatures. The boxes show the change of total shrinkage, in parallel to the flow direction S_{Tp}, with both mould temperature and melt temperature. The top right box plots shrinkage as a function of melt temperature, the bottom left box plots shrinkage as a function of mould temperature.

Considering mould temperature (top right box), the decrease of total shrinkage in parallel to the flow direction S_{Tp} as we move from the low (85°C) to the high (115°C) temperature is larger when melt temperature is low (190°C) than when it is high (200°C). Considering melt temperature (bottom left box), the decrease of S_{Tp} moving from the low (190°C) to the high (200°C) temperature is larger when mould temperature is low (85°C) than when is high (115°C).
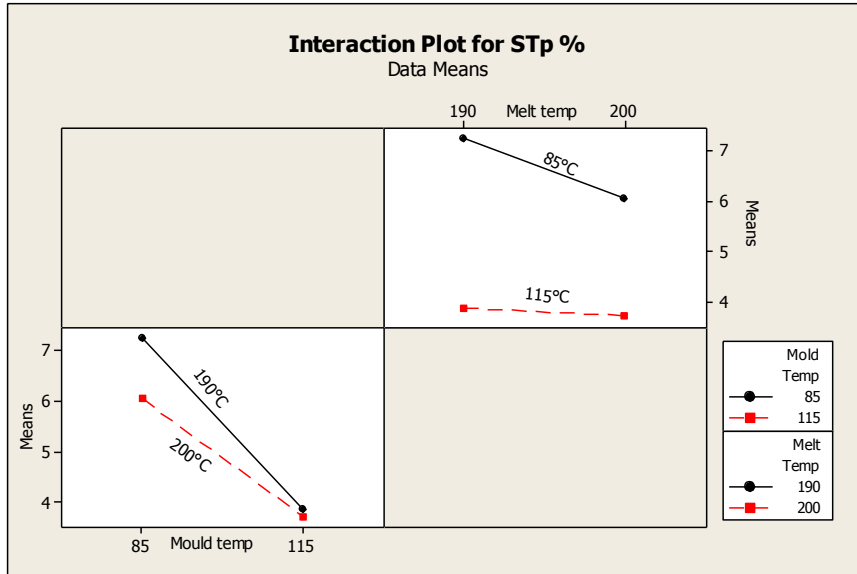
Figure 5-13. Interaction plot between melt and mould temperature, for total shrinkage in parallel to the flow direction.

5.3.6 POM total shrinkage in normal to the flow direction

In contrast to the total shrinkage on parallel to the flow direction, the total shrinkage in normal to the flow direction did not show any statistically significant effects, as reported in Figure 5-14.
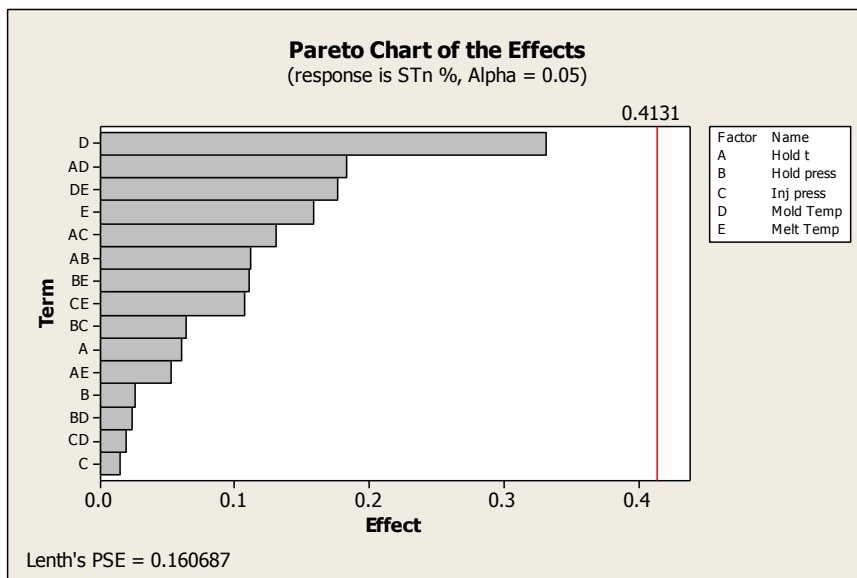
Figure 5-14. Pareto chart of total shrinkage in normal to the flow direction.

5.3.7 Optical investigation of POM specimens

Figure 5-15 reports the border area of the moulded specimens. The circle and the line reproduced the position of the ejection pin and the border of the sample moulded with the optimized parameters (Figure 6-5). By comparing these markers with the specimen profiles, it was possible to estimate the effect of processing parameter combinations in terms of filling percentage. Moulded parts were optically investigated for being sure that the combination of processing parameters investigated a mouldability range wide enough for identifying the optimized factor values that minimize shrinkage (as will be demonstrated in chapter 6).

Specimen 1
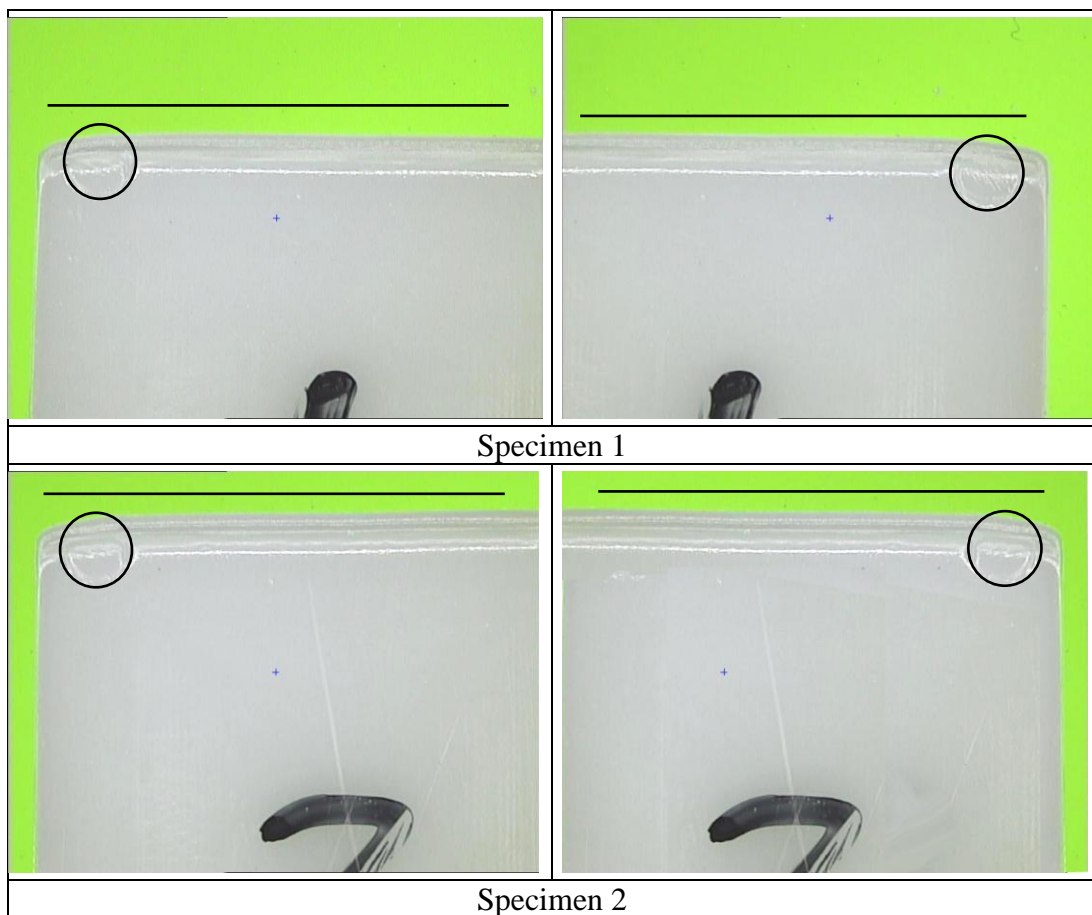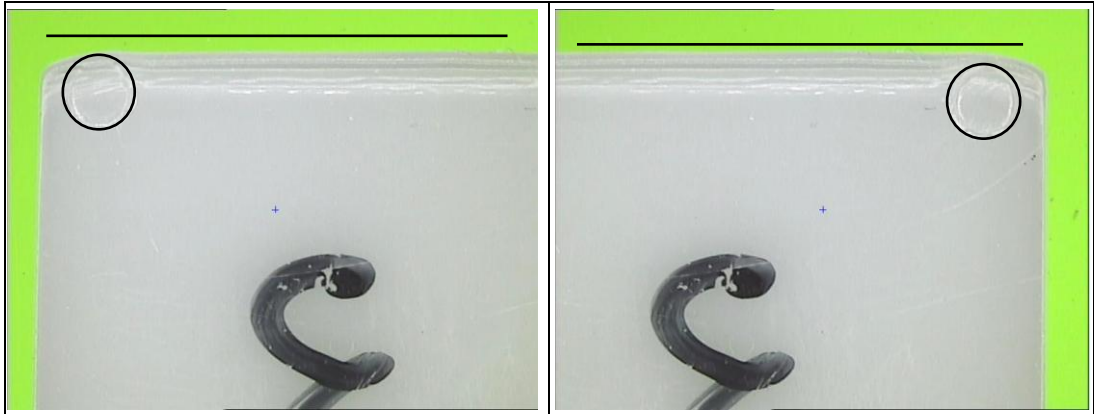
Specimen 2
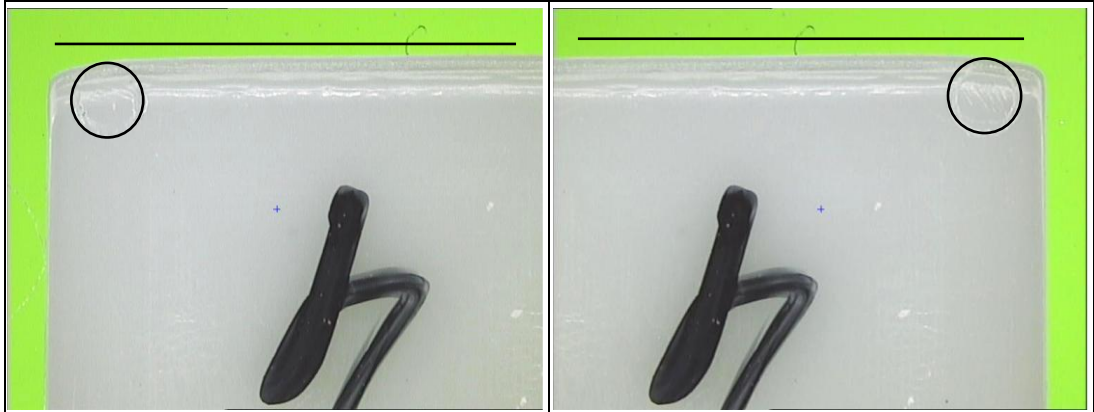
Specimen 3

Specimen 4

Specimen 5

126
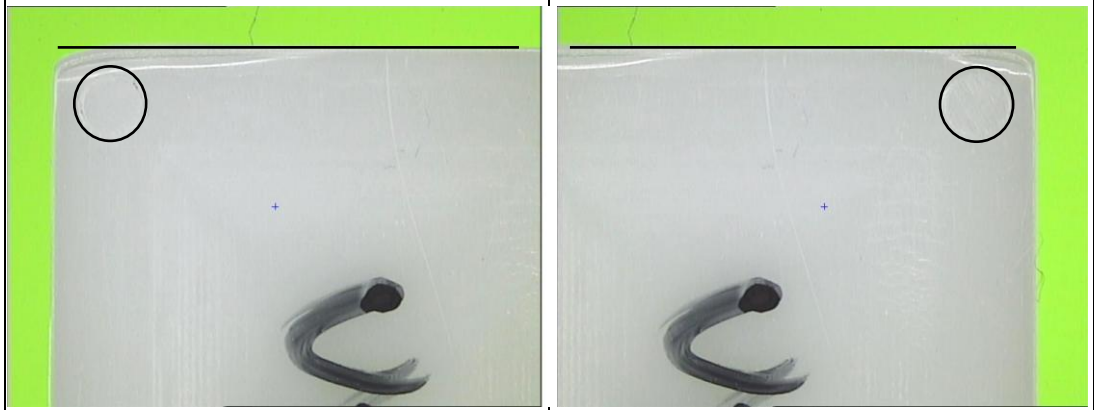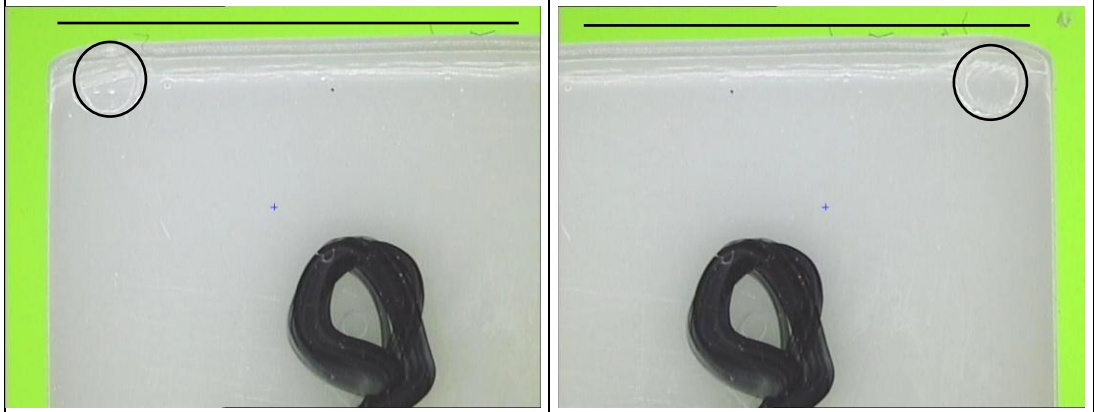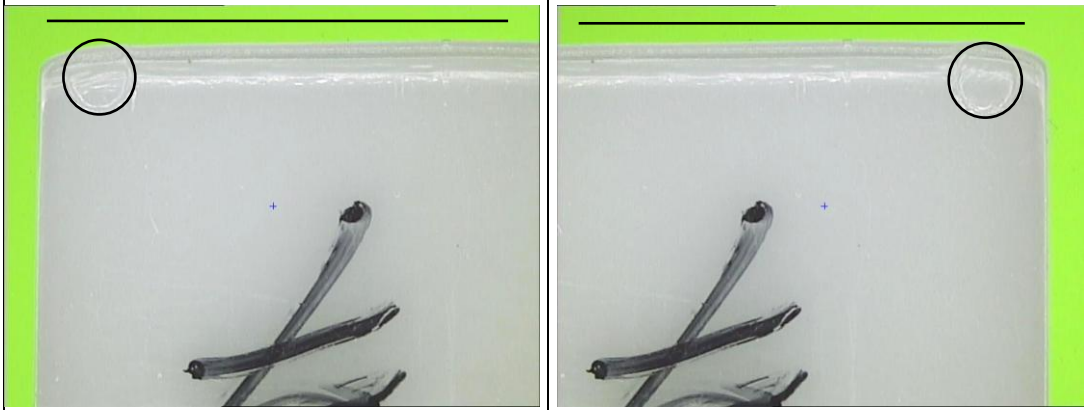
Specimen 6
Specimen 7
Specimen 8
Specimen 9
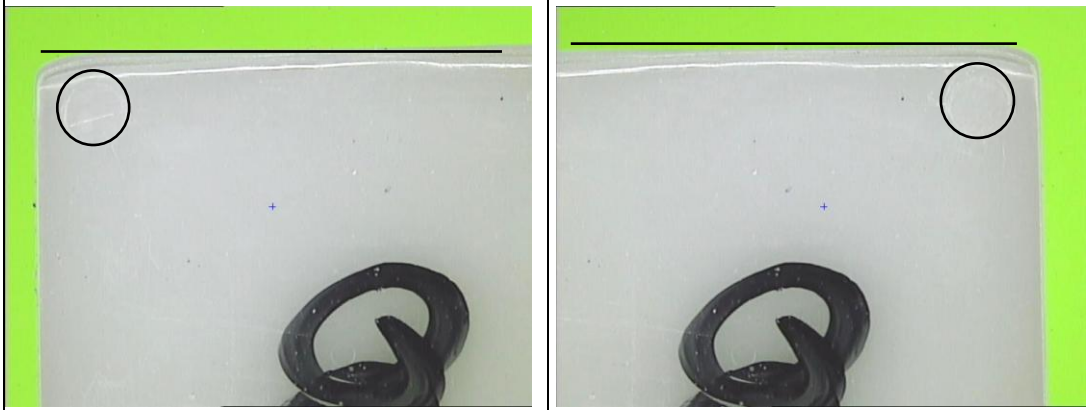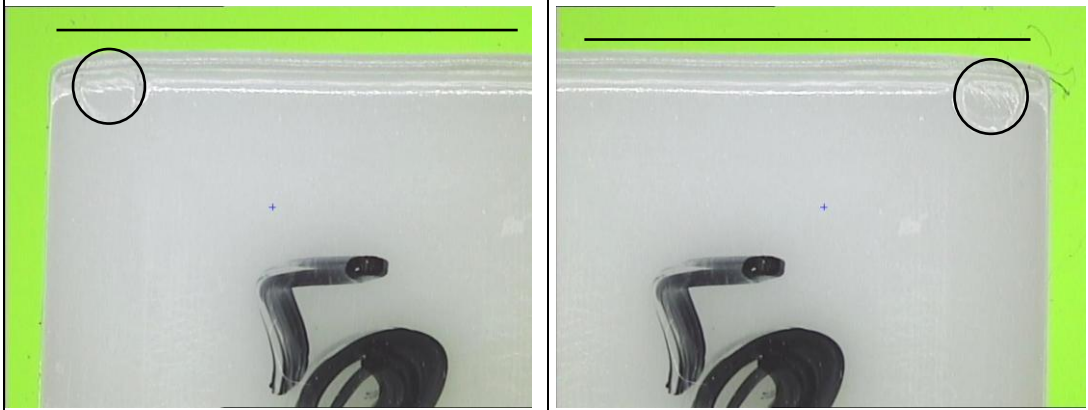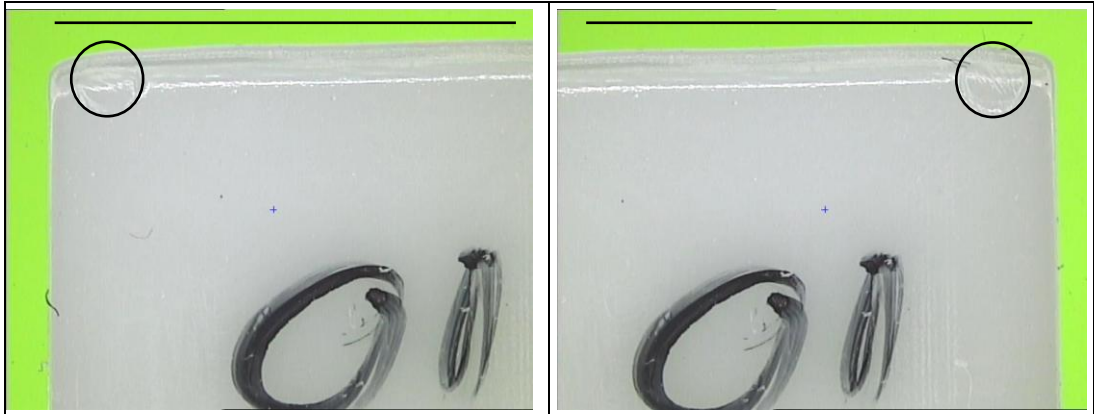
Specimen 10
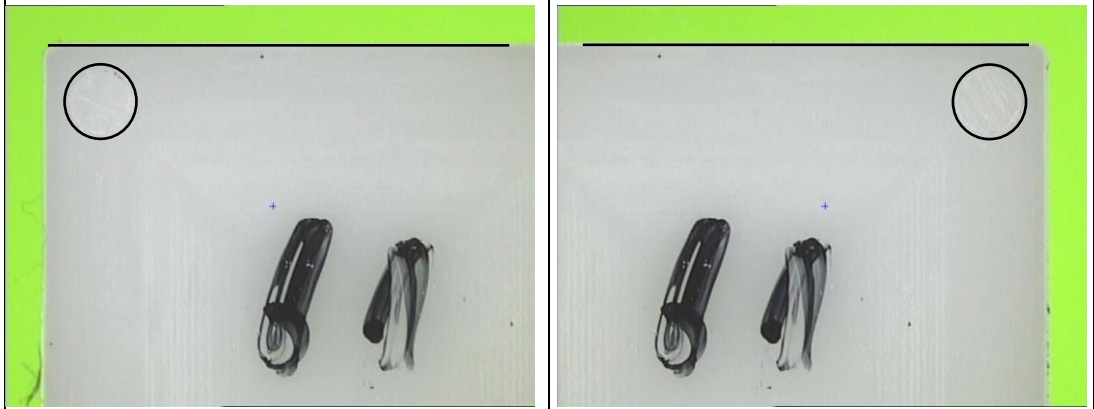
Specimen 11
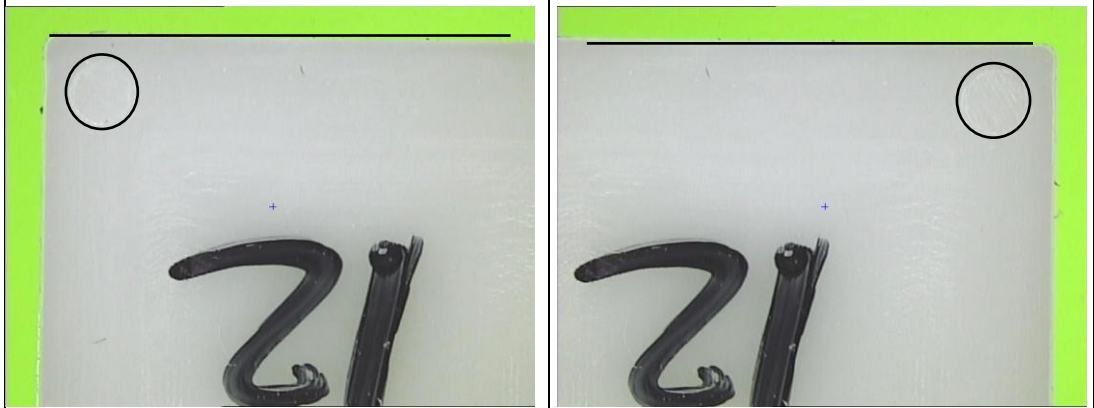
Specimen 12
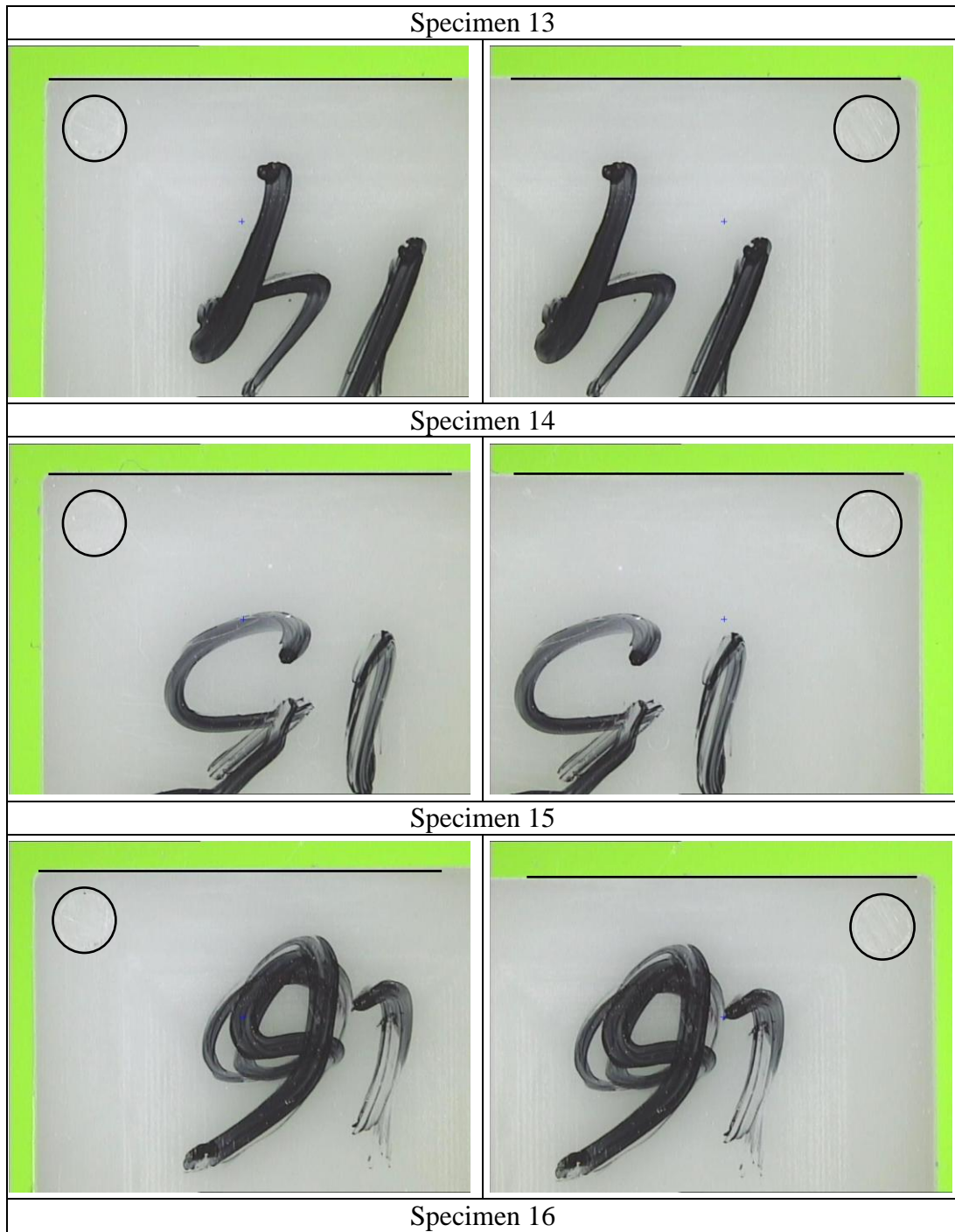
Figure 5-15. Optical investigation of POM samples. The circle and the line replicated the ejection pin and the border position of optimized specimen.

Results of optical analysis shown that shape of moulded parts varied from specimens partially to fully filled: a mouldability range sufficient for approaching to shrinkage optimization was investigated.

5.4 Discussion

Table 5-4 grouped the factors that have a statistically significant effect on shrinkage for POM.

POM shrinkage results		
S_{Mp}	Mould temperature	↓
S_{Mn}	Mould temperature	↑
S_{Pn}	Holding time & mould temperature	−
S_{Tp}	Mould temperature	↓
	Holding pressure	↓
	Mould temperature & holding pressure	↓
	Melt temperature	↓
	Melt temperature & mould temperature	↓

Table 5-4. DoE results of the effect of processing factors for POM polymer. The arrows indicate whether a factor increasing causes an increase (↑) or decrease (↓) in shrinkage. (−) indicates no clear trend.

The results reported in Table 5-4 shown that data obtained from the micro-mould can detect statistically significant factors by discriminating between the parallel to, and normal to, the flow shrinkage.

It is notable from Table 5-4 the strong influence of temperature parameters on shrinkage. POM is a crystalline polymer, and the temperature parameters (mould and melt temperature) are known to drive the crystal growth (rate of crystallization) by controlling the transition from melt to solid state [196].

The same statistical significant influence of temperature parameters (melt and mould) was seen in the only prior work in this area, which indicated that higher temperature parameters enhanced shrinkage both parallel and normal to the flow [31]. However, the authors did not state whether they were reporting S_M or S_T values, so their work cannot be directly compared with the trends shown in Table 5-4.

The method strength was to adapt a macro standard at the micro-scale. The experimental results shown that the critical parameters detected in such a scale were the same factors that affect shrinkage in micro-scale. Except for factors that affected post-moulding shrinkage along normal to the flow direction, each trend of critical parameters

was identified. A general increasing of factor values leads to shrinkage decreasing; mould temperature shown opposite behaviour for moulding shrinkage along normal direction.

5.5 Summary

The methodology proposed it was suitable for detecting micro shrinkage because the method appears capable to discriminate between cross and parallel shrinkage on the micro-scale: the data presented in Table 5-4 indicates that it can because it shows different trend in flow and cross shrinkages.

Moreover, a comparison of the results obtained with prior data was made. At the micro-scale, this method has advanced over prior work because improved the mould design: the mould used in [31] was inadequate to examine shrinkage normal to flow direction. After comparison of the statistical results reported in the present paper with flow [31], the agreement with prior data was good, but a finer-level of statistically significant results was obtained as the methodology produced data on effects both parallel and normal to the flow for mould shrinkage, post-mould shrinkage and total shrinkage. The methodology successfully proposed was published.

Chapter 6 . Results: statistical based optimization using multiple quality criteria. POM case study.

This chapter investigated the feasibility to adopt multiple quality criteria for optimizing POM shrinkage. By considering the optimization stages from the literature review, the absence of this approach was noticed. Few papers adopted this approach and simultaneous requests of part mass maximization and shrinkage minimization was never observed. Aim of this chapter was to bridge this gap.

Desirability functions were implemented for achieving the requests. Results were validated and confirmed the fulfillment of the objectives.

6.1 Optimising multiple quality criteria using desirability functions

Injection moulding literature indicates the important role of part mass in shrinkage, where shrinkage is reduced when part mass is maximized (without overfilling behaviour such as flash) [17]. However, it is difficult to use part mass as a factor in an experiment, as it is not a variable that can be easily controlled independently (unlike, for example, mould temperature). It may also be affected by the same factors that influence shrinkage.

In a previous study conducted by Zhao et al., metering size was used as a factor (and part mass as a response) [8]. However, two issues act to reduce the usefulness of metering size as a factor. Firstly, its accuracy. The metering size accuracy of a dedicated micro-moulder (Battenfeld 50) - as used here - has been estimated elsewhere in the literature at 20 mm^3 [8]. Secondly, the variation of metering size volume with polymer temperature [30].

Also Ong et al. [197] analysed micro parts using DoE methodology. Result evidenced the mould temperature as the most significant factor affecting the part mass. A general

trend has shown that maximum cavity filling resulted from an increasing of mould temperature, injection rate and injection pressure.

In order to use part mass data to attempt to optimise shrinkage, an optimization based on multiple quality criteria method was proposed, i.e. it attempts to optimise for both the minimum total shrinkage and the maximum part mass, because of the known effect of one factor on the other. To the author's knowledge, no works that requested simultaneously part mass maximization and shrinkage minimization are known and the present method could bridge this gap. Shrinkage was measured according to the proposed procedure reported in the previous chapter [119].

About the use of desirability functions, similar procedure was used also by Attia et al. [198]: contribution respect [198] was the standardised mould used and the different material injected (a semi-crystalline instead of amorphous polymer).

An optimisation of total shrinkage would be particularly hard to achieve for polymers that show anisotropic shrinkage behaviour, as the POM adopted in the present thesis [197].

6.2 Results

6.2.1 POM shrinkage results

The methodology proposed in Chapter 5 provided the total shrinkage values (S_T), on flow (p) and cross (n) direction. Table 6-1 reports the lowest (Low) and the average (Av) values of POM total shrinkage as obtained from previous measurements. The average reported on Table 6-1 was calculated by considering all the data reported in the column of total shrinkage.

$S_{Tp\,Low}$ [%]	$S_{Tp\,Av}$ [%]	$S_{Tn\,Low}$ [%]	$S_{Tn\,Av}$ [%]
3.63±0.01	5.09±1.66	2.35±0.01	3.03±0.26

Table 6-1. POM lowest and average total shrinkage values according to Table 5-3 results.

The chapter 5 already reported and commented the critical factors that affect total shrinkage. They were mould temperature, hold pressure and melt temperature; in

addition, two combinations of factors had statistically significants: hold pressure with mould temperature and mould temperature with melt temperature.

6.2.2 POM part mass results

Using the same statistical tools previously adopted, part mass was analysed. Figure 6-1 and Figure 6-2 represents the Pareto chart and the main effects for POM part mass. The Pareto chart in Figure 6-1 shows that in terms of part mass, the statistically significant processing parameters were the mould temperature, the hold pressure and the melt temperature.
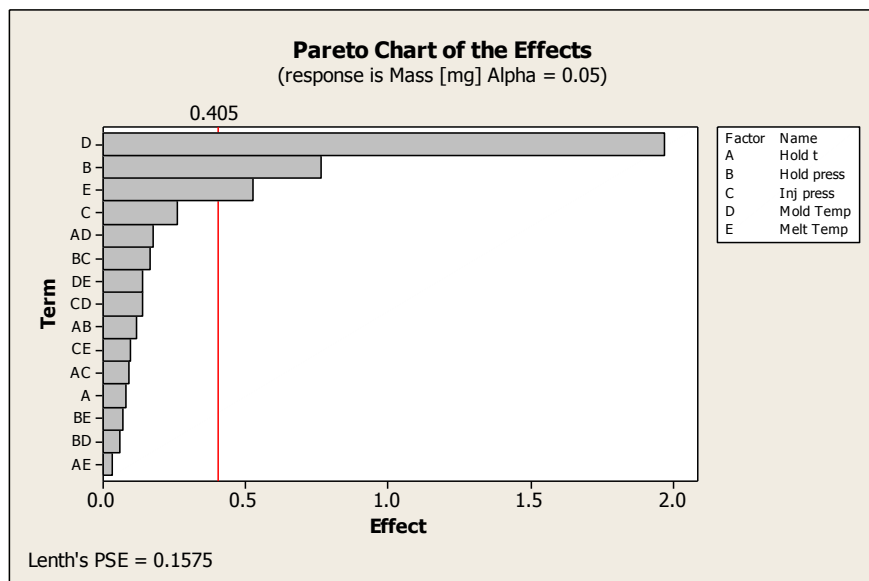
Figure 6-1. Pareto chart of POM part mass.

The main effect plot, shown in Figure 6-2, reports how changing each process parameter between the low and high values affect the actual magnitude of the specimen mass. The slopes of the three significant parameters identified from the Pareto chart are all positive in the main effect plot, which means that part mass was directly related to each of the three parameters.
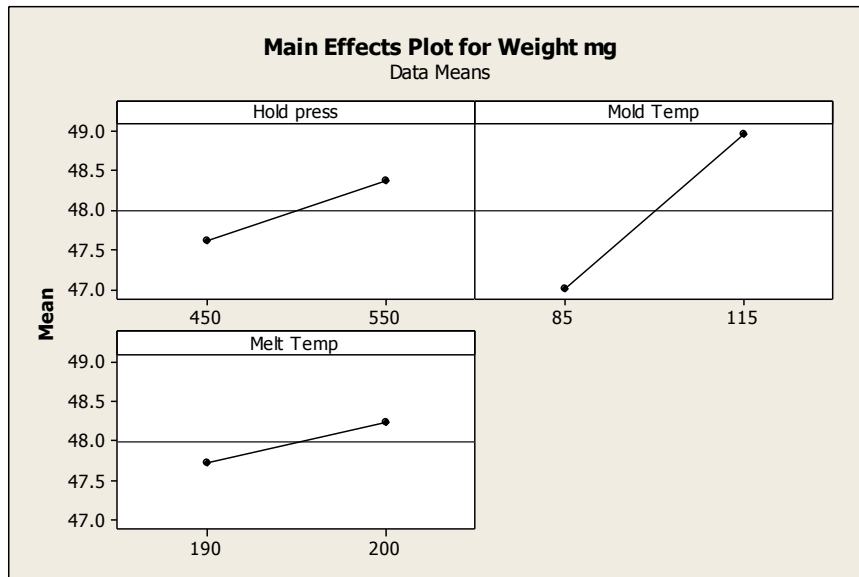
Figure 6-2. Main effect plot of POM part mass.

6.3 Optimisation step

The overall analysis of critical factors were summarised in Table 6-2.

	Parallel to the flow	Normal to the flow
S_T	Mould temp Hold press Mould temp and hold press Melt temp Mould temp and melt temp	None
W	Mould temp, hold press, melt temp	

Table 6-2. Critical processing parameters.

Table 6-3 reports the values of part mass (W) and total shrinkages (S_T). All the data reported in Table 6-3 are the average of measurements conducted using five moulded specimens, chosen after a number of uninterrupted cycles of injection machine after each new set of process parameters. This was done to reach stable operation conditions such that random errors are minimised and, hence, optimisation results are more reliable. The part mass values shown in Table 6-3 include both the specimen and the attached gate masses. This has been done because to cut the gate from the specimen could cause profile damage that affect shrinkage measurements. The gate mass was estimated to contribute to about 1% of total part mass (0.51 ± 0.03 mg gate mass).

Run	W [mg]	S_{Tp} [%]	S_{Tn} [%]
1	46.73±0.39	7.649±0.008	2.797±0.007
2	46.98±0.23	6.664±0.001	2.909±0.001
3	47.64±0.33	5.108±0.004	2.890±0.001
4	47.50±0.52	6.092±0.009	2.802±0.002
5	48.19±0.44	3.887±0.002	3.217±0.001
6	47.60±0.38	4.972±0.009	2.923±0.001
7	46.93±0.31	6.775±0.007	2.820±0.001
8	48.23±0.12	3.728±0.001	3.253±0.001
9	46.57±0.18	6.968±0.004	3.388±0.009
10	46.09±0.44	7.954±0.010	2.350±0.008
11	49.32±0.13	3.670±0.001	3.096±0.001
12	48.99±0.03	3.683±0.001	3.155±0.001
13	49.15±0.08	3.629±0.001	3.177±0.001
14	48.73±0.19	3.640±0.001	3.297±0.002
15	49.42±0.06	3.373±0.001	3.603±0.004
16	49.73±0.12	3.633±0.002	3.030±0.001

Table 6-3. Part mass (W) and total shrinkage (S_T) on flow (p) and cross (n) direction.

As explained in the paragraph 3.5.2.5 Desirability functions, the optimization according to multiple quality criteria will be performed using the Equation 2 for maximising the part mass and the Equation 3 for minimising shrinkage. The values used as upper and lower limit during the optimization stage were selected according to the results reported in Table 6-3: for the part mass a target value of 49.5 mg (lower limit 48 mg) was set, and for shrinkages (both parallel to, and normal to, the flow direction) the target value was 3.5% (upper limit 4%). Part mass target value was 49.5 mg because closer to the higher part mass value (specimen of 16th run). Shrinkage target was the medium-low value between the specimens with low S_T. Figure 6-3 reports the screenshot of Minitab 16 used in this stage and the set values. As stated the requests during the optimization stage were to minimise the shrinkage and maximise the part mass.

The results of the optimization stage can be considered achievable the more the individual desirability function d_i and overall desirability D values resulted close to 1.
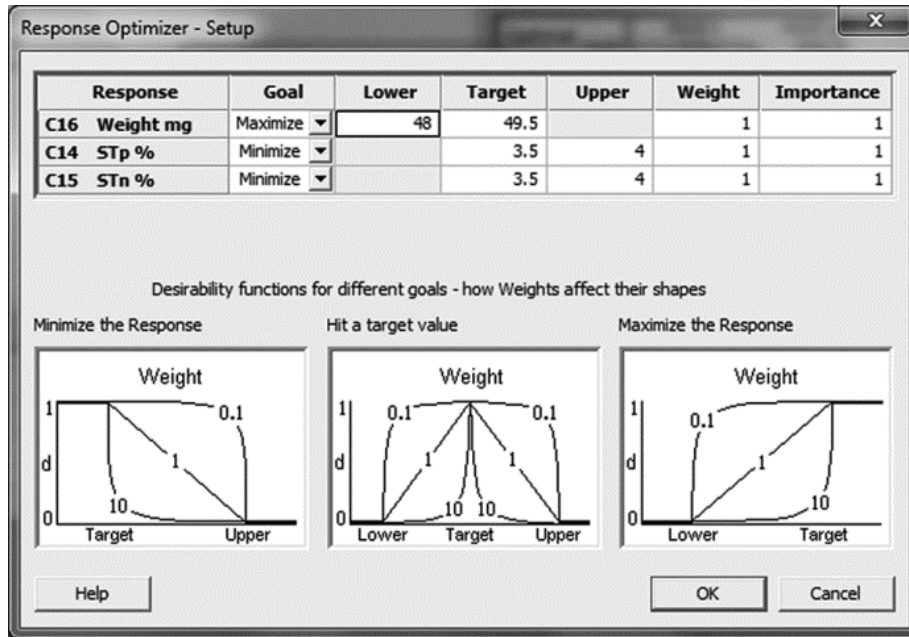
Figure 6-3. POM optimization stage.

Figure 6-4 depicts the outcome of Minitab during this stage. The letter d is the single desirability function, while D is the overall desirability function; letter y is the individual response, the optimized parameters were reported in bracket.
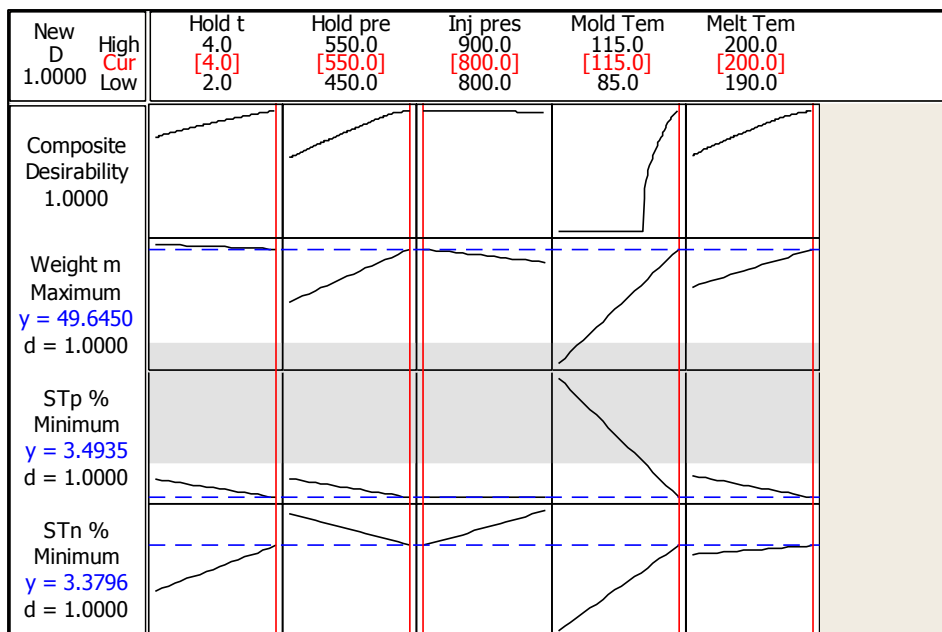
Figure 6-4. POM's optimized parameters.

Table 6-4 reports the final optimised results.

Hold t [s]	Hold P [bar]	Inj. P [bar]	Mould T [°C]	Melt T [°C]	S_{Tp} [%]	S_{Tn} [%]	W [mg]
4	550	800	115	200	3.352±0.001	3.298±0.004	49.42±0.08

Table 6-4. Optimized parameters with total shrinkage and part mass results.

Figure 6-5 depicts the border of optimized parameter. The circle and the line referred to ejection pin and specimen border and were used in Figure 5-15 for comparing the effect of the different processing parameter combinations in terms of filling percentage.
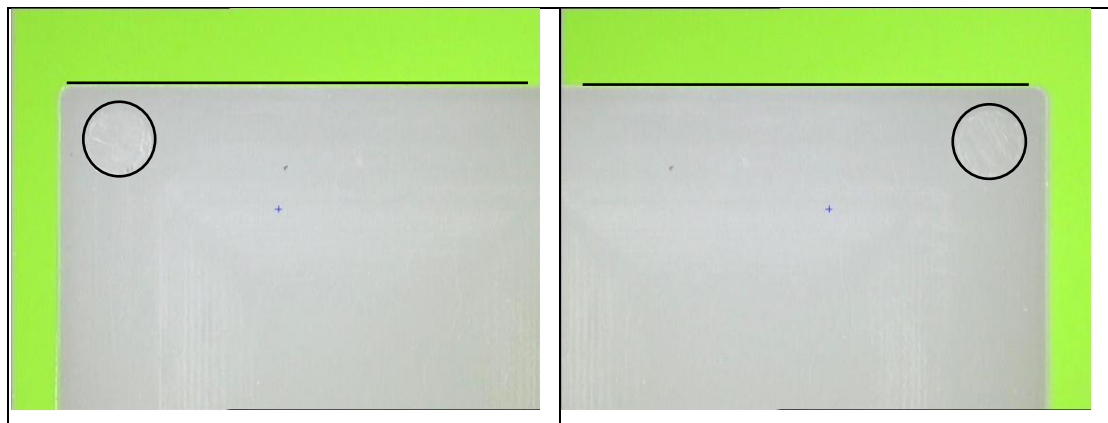
Figure 6-5. Optical investigation of optimized POM specimen.

Results can be compared with those reported in Table 6-1. Table 6-5 summarise the optimised values in terms of percentage with respect to the average part mass and total shrinkage and respect the best results before the optimization.

POM		$S_{Tp\ Opt}$ [%] (3.35)	$S_{Tn\ Opt}$ [%] (3.30)	W_{Opt} [mg] (49.42)
$S_{Tp\ Av}$ [%]	(5.09)	-34%		
$S_{Tn\ Av}$ [%]	(3.03)		+9.2%	
W_{Av} [mg]	(47.98)			+3%
$S_{Tp\ Low}$ [%] (15th run)	(3.37)	-0.1%		
$S_{Tn\ Low}$ [%] (10th run)	(2.35)		+40%	
W_{High} [mg] (16th run)	(49.73)			-0.1%

Table 6-5. POM optimization stage effect.

During the manufacturing stage, the filling percentage of specimen varied: some combinations resulted in fully filled samples, whilst other processing combinations resulted in partially filled specimens. Figure 6-6 reports the mass distribution of the

specimens relative to different process parameters. The x-axis shows the weight of the specimens moulded with the runs from 1 to 16 as reported in Table 6-3. The run number 17 referred about the specimen moulded with the optimised processing parameters of Table 6-4. The y-axis shows the resulting specimen mass expressed in milligrams. In Figure 6-6, the white bars indicate mass values for specimens moulded with processing parameter combinations that include low mould temperature (85°C), while the grey bars refer to mass values resulting from processing parameter combinations involving high mould temperature (115°C).
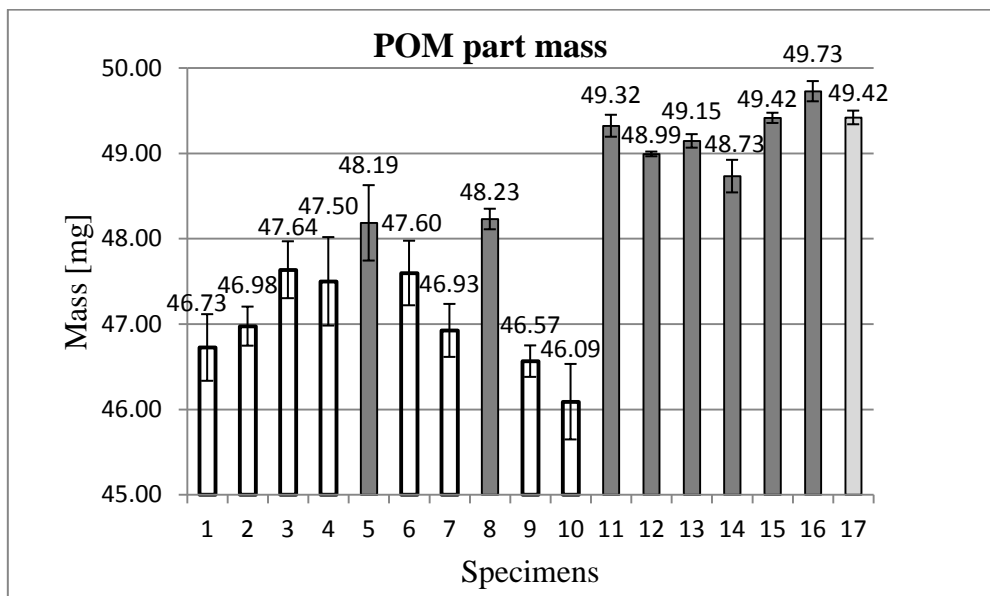
Figure 6-6. POM part mass distribution.

6.4 Discussion

The critical factors that affect the total shrinkage and the part mass were summarized in Table 6-2. The analysis of shrinkage critical factors reported in Table 6-2 shown that the temperatures (mould and melt), the hold pressure and their combination resulted critical factors for the total shrinkage in parallel to the flow direction. In addition, the same processing parameters resulted critical for the part mass. About the part mass, our conclusions agrees with Ong et al. [197] that identified the mould temperature as a critical factor for the cavity filling. In terms of metering accuracy, Zhao [8] conclusions shown that also the holding pressure has critical influence. Thesis results confirmed both authors and evidenced the importance of the temperature parameters as consequence of the POM crystallinity that tends to form an anisotropic structure [175].

The crystallinity was considered a parameter strongly affected by temperature. Considering that the transition from fuse to solid take place in cavity mould, this explain the importance of mould temperature as well.

Table 6-4 reports the optimised parameters values referred to total shrinkage and part mass values. As reported in paragraph 3.5.2.5 Desirability functions, optimization stage cannot indicate optimized parameters outside the lower and high levels of the factors (Table 5-1). A comparison of optimised values with the range reported in Table 5-1 shown the absence of values between the + and − intervals. This could be explained considering the optimisation stage setting and the compromise related to multiple quality criteria requests.

The optimisation stage was performed with the individual desirability function d_i and the overall desirability D equal to 1. Table 6-5 reports the lower and the average shrinkage values. The reported shrinkages on flow direction (S_{Tp}) is higher than that on cross direction (S_{Tn}): this was caused by POM anisotropic structure and by the normal injection effect that stretch the polymer chains long the injection direction more than cross directions. As consequence of this stretching, at the end of manufacturing process the polymer tends to recover the original dimensions on flow more than on cross direction. The anisotropic behaviour of POM was confirmed by the indication reported on MatWeb site [174] for pure POM polymer. Also Velarde et al. [199] highlighted the same trend for HDPE: their cross shrinkage differs from the flow shrinkage and the general behaviour is anisotropic. To set the same shrinkage values for both the directions (3.5% as reported in Figure 6-3) for reducing this anisotropy was a strong condition. The cross shrinkage has to be increased from an average value of 3.02% to 3.5%, while the decrease on flow direction is from an average value of 5.09% to 3.5%. Also the limit set for the part mass is quite strong: was set a target value equal to 49.5 mg and only one specimen presents a part mass higher (49.73 mg, 16th run of Table 6-3). To work in such limit conditions caused to have no final optimised parameters between the + and − interval.

Moreover, the statistical results by applying multiple quality criteria (to minimize shrinkage whilst maximize part mass) shown the same trend. According to main effect plots both shrinkage minimizations than part mass maximization were achieved by

maximizing processing parameter values: this explain why optimized parameters (except injection pressure) referred to the maximum values.

About the range values explored, during the familiarisation stage the specimen appearance ranged from completely to partially filled, hence the experimentation window can be considered suitable for the purposes of the present study.

The effect of the optimisation using multiple quality criteria was estimated by considering the Table 6-5. A comparison between the numerical results after the optimisation with those before the optimisation (both average and low values), shown that shrinkage in parallel to the flow direction was reduced (-34% with respect to the average value, -0.1% with respect to the best shrinkage value). Shrinkage reduction in parallel to the flow direction seems to be balanced by a slight increase in shrinkage in normal to the flow direction (+9.2% with respect to the average value, +40% with respect to the best shrinkage value). The optimised part mass shown a +3% change with respect to the average part mass and -0.1% change with respect the best (highest) part mass value. Such a reduction in part mass with respect the best target value does not produce negative effects in terms of incomplete filling or low edge definition.

Figure 6-6 confirmed the critical influence of mould temperature (critical factor for shrinkage and part mass): the relatively short white bars indicate mass values for specimens moulded with process-parameter combinations that include low mould temperature (85°C). The relatively long grey bars refer to mass values resulting from process-parameter combinations involving high mould temperature (115°C). The 17th bar was the weight of the optimised specimen. The optimization stage were performed simultaneously by minimising the shrinkage and maximising the part mass. Both these criteria are not in contrast each other, because to maximise the part mass permits to reduce the shrinkage [17], even if the final results have to balance the two requests. Despite of this, the specimen moulded with the optimised parameter (the 17th column depicted in Figure 6-6) didn't show higher weight but lower shrinkage in both direction, because the optimisation using multiple quality criteria made a compromise between the set requests of minimise the shrinkage and maximise the weight.

6.5 Summary

The adoption of multiple quality criteria during the optimization stage permitted to minimize total shrinkage whilst part mass was maximized. The optimal condition that permitted to fulfill both the requests was determined by using the desirability function. The temperatures (mould and melt) and the hold pressure were identified as critical factors for shrinkage and part mass. Results have shown that multiple quality optimization approach can be efficiently adopted because both requests were fulfilled. The methodology presented in this chapter was published.

Chapter 7 . Results: evaluation of 316L feedstock moulding shrinkage

Experimental evidences have shown that feedstock performance was controlled by the "backbone" polymer [200]. It might be concluded that, if the shrinkage behaviour of the pure polymer was known, then the feedstock based on that polymer could exhibit shrinkage behaviour predictable from the polymer itself. Purpose of this chapter was to investigate this trend for a μ-PIM moulded part. This analysis was performed by processing the feedstock and by comparing the results with pure polymer for seeing whether the shrinkage behaviour was the same or not.

The pure polymer results (POM) were reported in the chapter 5, and were not replicated here. The first part of this chapter was focused on the study of 316L feedstock shrinkage, following the same scheme adopted for POM in chapter 5. The influence of powder loading and the comparisons between 316L feedstock and POM were reported in the discussion at the end of this chapter.

7.1 Methodology

The investigation of 316L feedstock shrinkage was conducted by using the same micro-mould adopted for the POM shrinkage study. The familiarization stage identified the range of processing parameter values (Table 7-1), and the half-fractional factorial matrix (Table 3-1) was implemented from DoE. Similarly to chapter 5, the range of processing parameters was selected, such that the higher (+) value was obtained by increasing from an initial setting until the presence of flash start was notable and the lower value (-) was obtained by decreasing the parameter value until notable defects started to appear (for example, incomplete filling or low edge definition).

Processing Parameters	Initial Values	Value +	Value −
Injection pressure [bar]	900	930	870
Holding pressure [bar]	250	300	200
Melt temperature [°C]	194	198	190
Mould temperature [°C]	135	140	130
Holding time [s]	3	4	2

Table 7-1. 316L feedstock processing parameter values.

Table 7-2 reports the processing parameter combinations and the statistical matrix investigated for 316L feedstock shrinkage study.

	Processing parameters randomly ordered					Half-Fractional Factorial matrix				
Run	Hold t [s]	Hold P [bar]	Inj. P [bar]	Mould T [°C]	Melt T [°C]	Hold time	Hold press	Inj. press	Mould temp	Melt temp
1	4	300	930	140	198	+	-	+	-	+
2	2	300	930	140	190	+	-	-	+	+
3	4	200	930	130	198	+	+	-	-	+
4	2	300	870	140	190	+	-	-	-	-
5	4	200	870	130	190	+	+	+	-	-
6	2	300	930	130	198	-	-	+	-	-
7	2	200	870	130	198	+	-	+	+	-
8	2	200	930	140	198	-	+	+	-	+
9	4	200	870	140	198	-	+	-	+	+
10	2	300	870	130	190	-	-	+	+	+
11	2	300	870	140	198	+	+	-	+	-
12	4	200	930	140	190	+	+	+	+	+
13	4	300	870	130	198	-	+	-	-	-
14	4	300	870	140	190	-	+	+	+	-
15	2	200	930	130	190	-	-	-	-	+
16	4	300	930	130	190	-	+	-	+	-

Table 7-2. Matrix of half-fractional factorial model and 316L feedstock processing combination investigated.

7.2 316L feedstock shrinkage measurements

Every runs were performed for an uninterrupted number of cycles, and then five specimens were measured. Table 7-3 reports the 316L feedstock shrinkage values.

Run	S_{Mp} [%]	S_{Mn} [%]	S_{Pp} [%]	S_{Pn} [%]	S_{Tp} [%]	S_{Tn} [%]
1	0.651±0.002	0.447±0.003	-0.136±0.005	0.119±0.005	0.515±0.004	0.566±0.003
2	0.806±0.002	0.621±0.002	-0.095±0.005	-0.237±0.004	0.712±0.005	0.385±0.003

3	0.834±0.007	0.699±0.006	0.789±0.019	0.325±0.020	1.616±0.018	1.022±0.017
4	0.758±0.005	0.603±0.002	-0.128±0.008	-0.083±0.004	0.631±0.004	0.521±0.003
5	0.843±0.002	0.586±0.001	-0.252±0.004	-0.484±0.004	0.598±0.003	0.104±0.003
6	0.726±0.002	0.684±0.003	0.126±0.004	-0.328±0.004	0.851±0.003	0.358±0.002
7	0.686±0.003	0.374±0.002	0.010±0.006	0.573±0.006	0.696±0.003	0.945±0.005
8	0.842±0.001	0.497±0.002	-0.128±0.001	0.192±0.002	0.715±0.001	0.688±0.001
9	0.656±0.001	0.524±0.001	0.084±0.003	-0.053±0.004	0.740±0.002	0.471±0.003
10	0.771±0.001	0.560±0.003	0.192±0.003	0.144±0.005	0.961±0.003	0.702±0.003
11	0.879±0.003	0.583±0.002	-0.097±0.005	-0.007±0.003	0.783±0.002	0.575±0.002
12	1.052±0.003	0.383±0.004	-0.028±0.005	0.362±0.005	1.024±0.001	0.743±0.002
13	0.599±0.002	0.690±0.001	0.535±0.007	0.037±0.004	1.130±0.006	0.727±0.003
14	0.961±0.003	0.542±0.001	-0.084±0.008	0.006±0.003	0.877±0.007	0.548±0.003
15	0.800±0.004	0.344±0.001	0.031±0.006	0.331±0.006	0.830±0.002	0.674±0.006
16	1.289±0.004	0.493±0.003	-0.100±0.007	-0.088±0.005	1.191±0.005	0.406±0.002

Table 7-3. 316L feedstock shrinkage results expressed as mean value ± standard deviation.

For making Table 7-3 more clear, the numerical results were reported as graph of 316L feedstock shrinkage parallel to (Figure 7-1) and normal to (Figure 7-2) the flow direction. Each graph reports only the moulding (S_M) and the total (S_T) shrinkage, not the post-moulding (S_P) shrinkage: this because S_M and S_T are calculated with respect to the mould dimensions, while S_P is the shrinkage between 1 and 24 hours. Besides, the standard deviations were not reported by considering their low values.
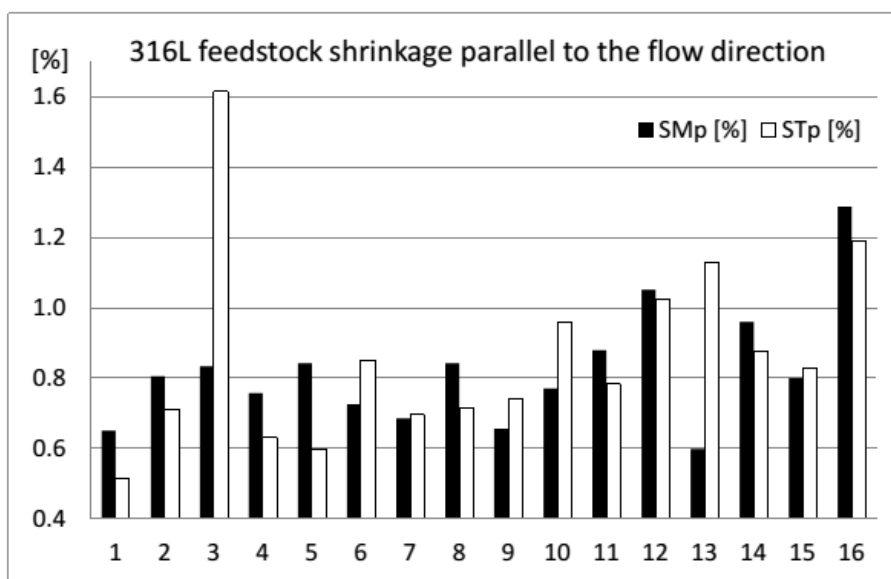
Figure 7-1. 316L feedstock shrinkage parallel to the flow direction.
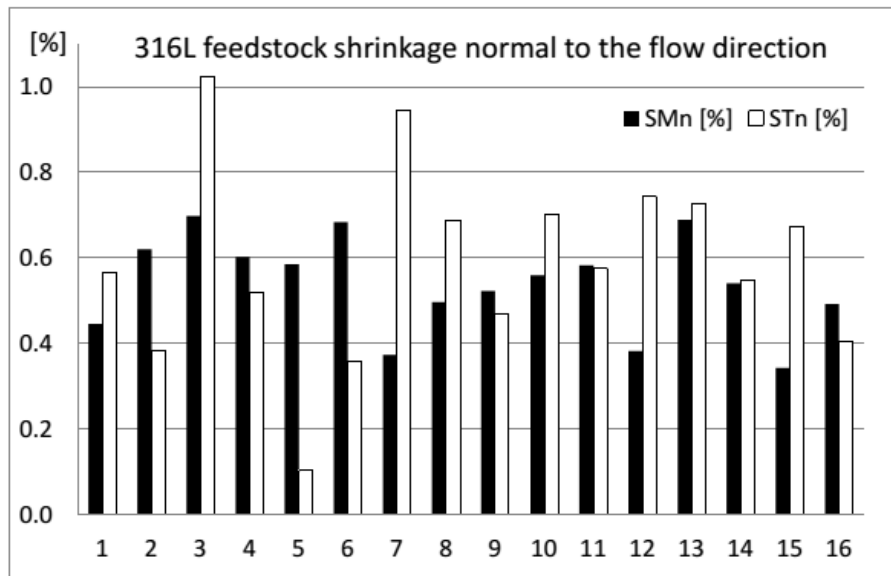
Figure 7-2. 316L feedstock shrinkage normal to the flow direction.

7.2.1 316L feedstock moulding shrinkage in parallel to the flow direction

The statistical study of 316L feedstock shrinkage was conducted by using a different alpha value (0.1 instead of 0.05) respect POM studies. The reason of this different value was reported in the discussion.

The Pareto chart depicted in Figure 7-3 represents the moulding shrinkage in parallel to the flow direction (S_{Mp}). As reported in Figure 7-3, each processing parameter was represented by a letter. If the significant effect is associated with a combination of more than one parameter, relevant letters are groups together. The processing parameters were labelled as A (hold time), B (hold pressure), C (injection pressure), D (mould temperature) and E (melt temperature). Pareto's results shown that there was not critical factors that affect the moulding shrinkage in parallel to the flow direction within the 90% confidence level.
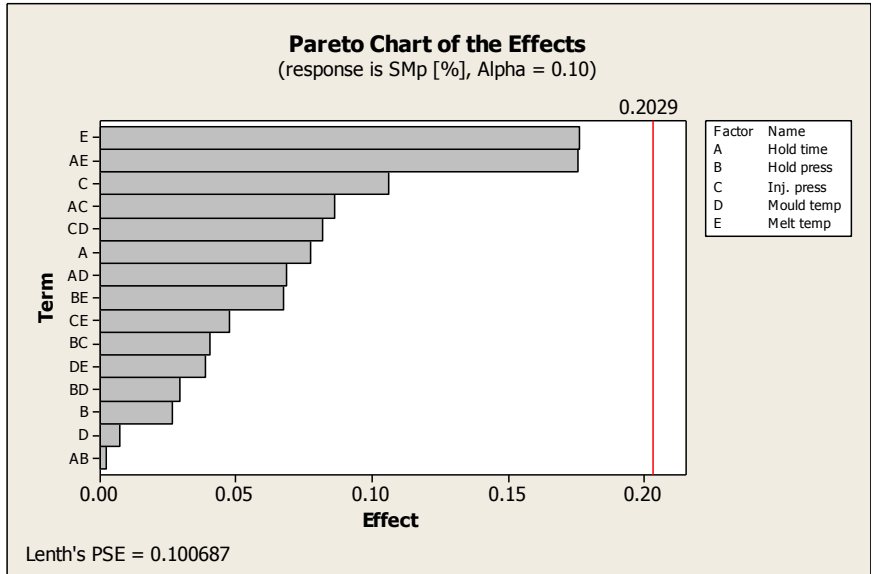
Figure 7-3. Pareto Chart of 316L feedstock moulding shrinkage in parallel to the flow direction.

7.2.2 316L feedstock moulding shrinkage in normal to the flow direction

Figure 7-4 represents the Pareto chart of moulding shrinkage in normal to the flow direction: no statistically significant factors were detected within the 90% confidence level.

147
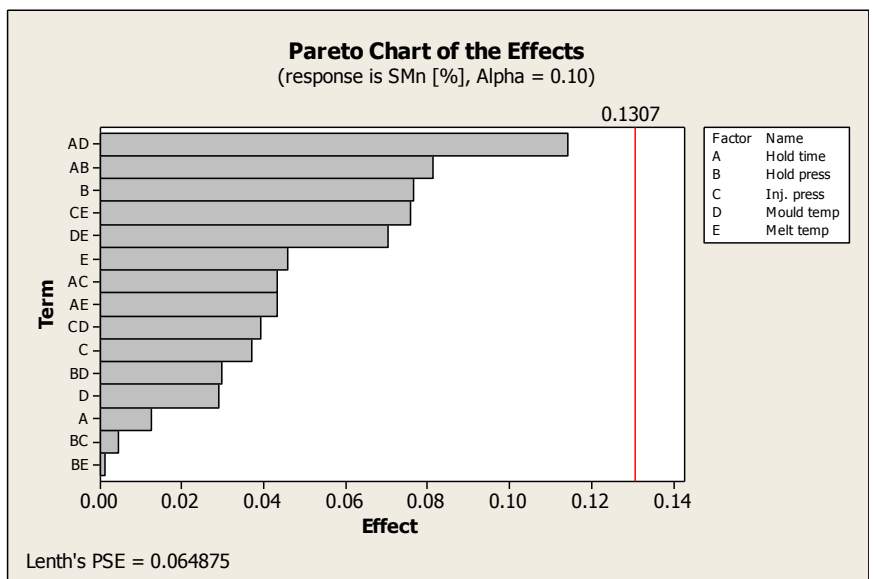
Figure 7-4. Pareto Chart of 316L feedstock moulding shrinkage in normal to the flow direction.

7.2.3 316L feedstock post moulding shrinkage in parallel to the flow direction

Figure 7-5 depicts the Pareto chart for post-moulding shrinkage in parallel to the flow direction: the mould temperature was identified as a critical parameter.
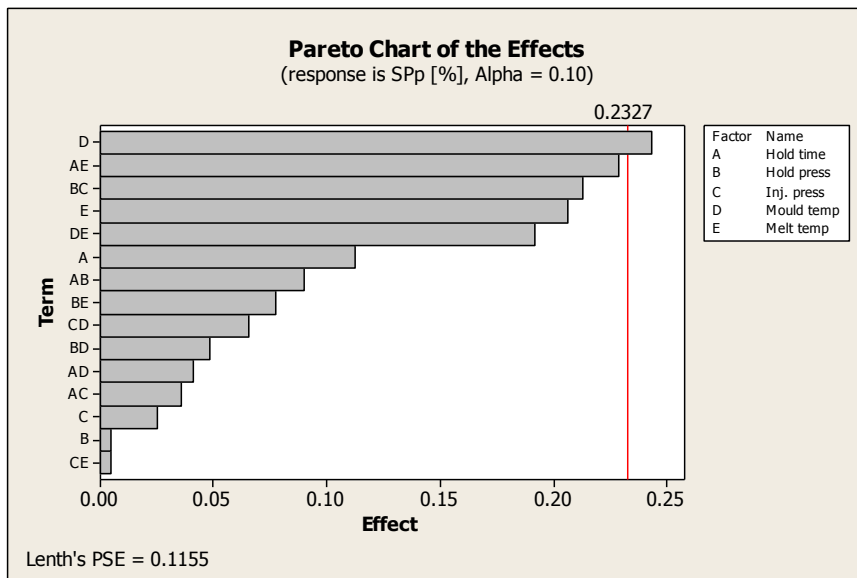
Figure 7-5. Pareto Chart of 316L feedstock post mould shrinkage in parallel to the flow direction.

Figure 7-6 reports the main effect plot: the slope of the critical factor shows that the S_{Pp} decreases when the mould temperature increases.
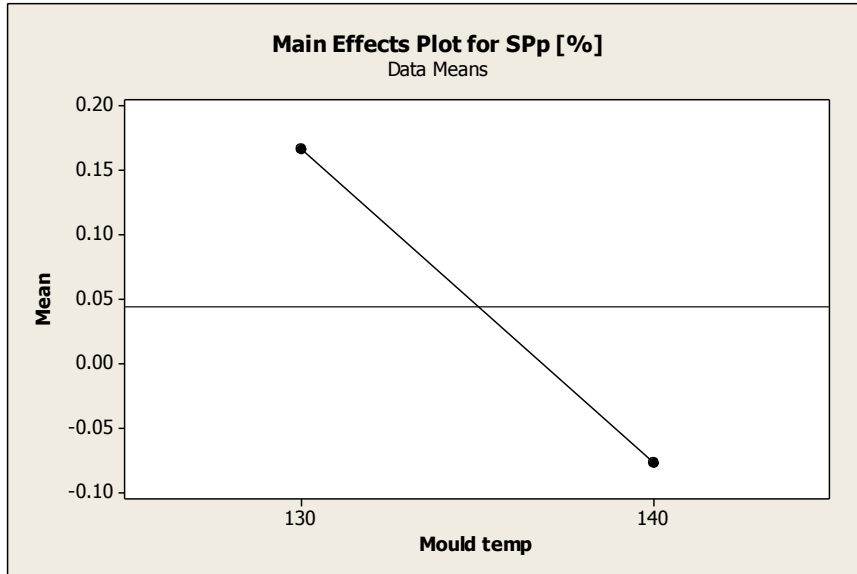
Figure 7-6. Main effect of 316L feedstock post moulding shrinkage in parallel to the flow direction.

7.2.4 316L feedstock post moulding shrinkage in normal to the flow direction

Figure 7-7 reports the Pareto chart of post moulding shrinkage in normal to the flow direction: no critical factors were detected within the 90% of confidence level.
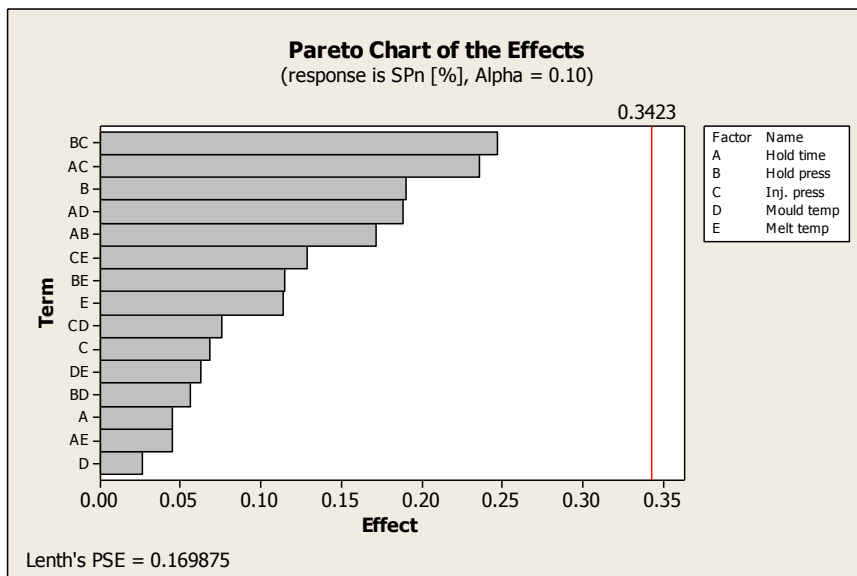
Figure 7-7. Pareto chart of 316L feedstock post moulding shrinkage in normal to the flow direction.

7.2.5 316L feedstock total shrinkage in parallel to the flow direction

Figure 7-8 reports the Pareto chart for the total shrinkage in parallel to the flow direction: no critical processing factors were detected within the 90% confidence level.
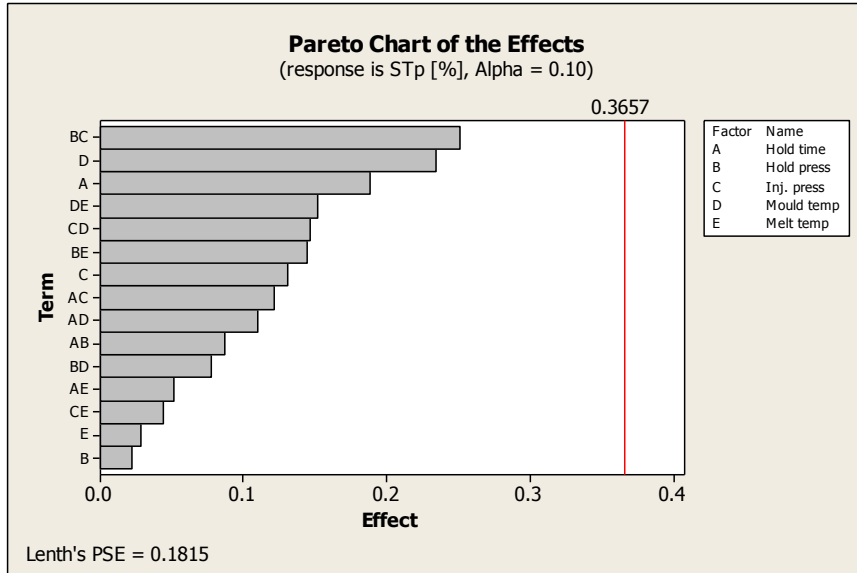
Figure 7-8. Pareto chart of 316L feedstock total shrinkage in parallel to the flow direction.

7.2.6 316L feedstock total shrinkage in normal to the flow direction

The total shrinkage in normal to the flow direction was critically affected by the combination of holding pressure and injection pressure, as reported in Figure 7-9.
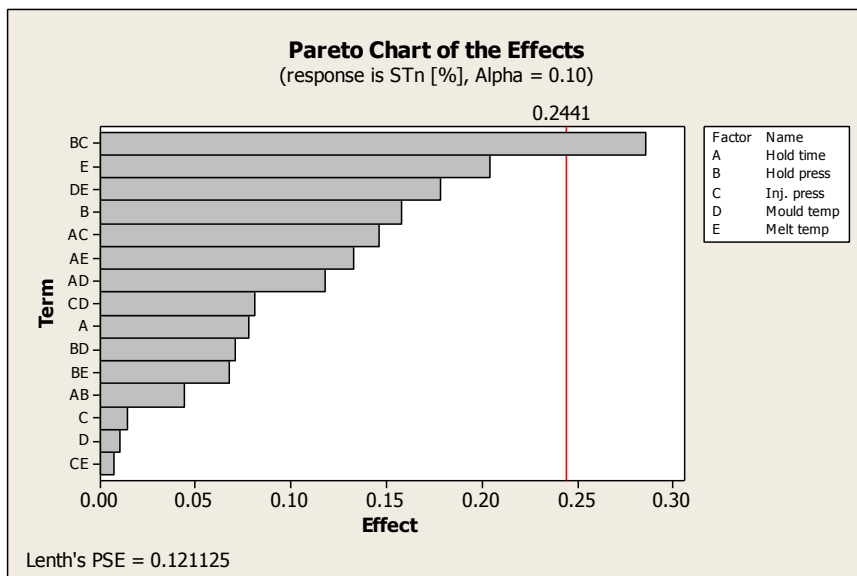
Figure 7-9. Pareto chart of 316L feedstock total shrinkage in normal to the flow direction.

Figure 7-10 represents the interaction between injection pressure and holding pressure (labelled as BC in Figure 7-9). The boxes show the changing of total shrinkage, in normal to the flow direction S_{Tn}. The top right box plots shrinkage as a function of injection pressure, the bottom left box plots shrinkage as a function of hold pressure.

Considering injection pressure (top right) moving from the low pressure (870 bar) to the high pressure (930 bar), shrinkage improves with the low hold pressure value (200 bar) and decreases with the high hold pressure value (300 bar). Considering hold pressure (bottom left) moving from the low pressure (200 bar) to the high pressure (300 bar), shrinkage improves with the low injection pressure value (870 bar) and decreases with the high injection pressure value (930 bar).
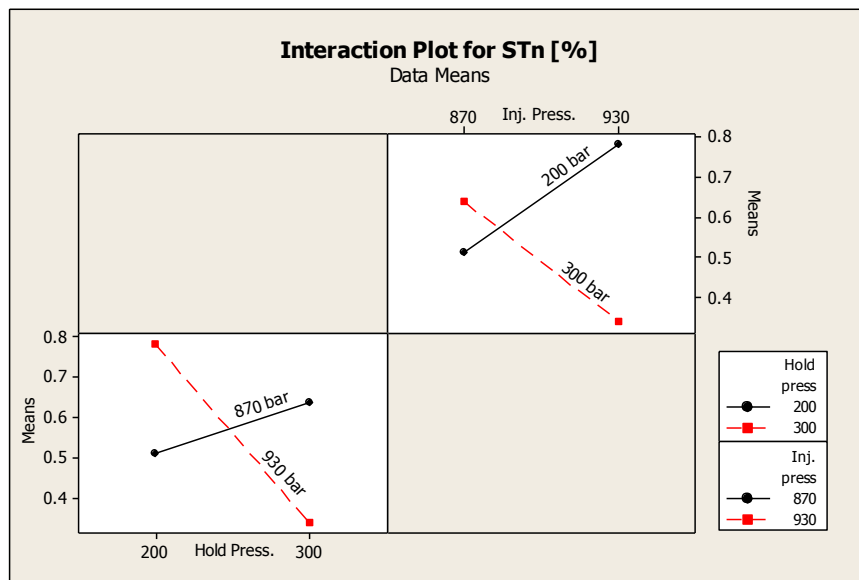
Figure 7-10. Interaction plot of 316L feedstock for total shrinkage in normal to the flow direction.

7.3 Discussion

This discussion is divided into three parts: (a) factors affecting 316L feedstock shrinkage; (b) a comparison between 316L feedstock and pure polymer behavior; (c) potential mechanisms behind critical factors.

7.3.1 316L feedstock shrinkage

Table 7-4 reports the critical factors that affect 316L feedstock moulding shrinkage.

316L feedstock		
S_{Pp}	Mould temperature	↓
S_{Tn}	Holding and injection pressure	↓

Table 7-4. 316L feedstock shrinkage critical factors. The arrow indicates that a factor increasing causes a decrease (↓) in shrinkage.

The statistical study identified the mould temperature a critical parameter for post-moulding shrinkage in parallel to the flow direction. The combination of hold pressure and injection pressure was identified as interaction that affected total shrinkage in normal to the flow direction. The trends reported in Table 7-4, showed that an increase in the values of critical factors leads to decrease shrinkage of moulded part.

Same trends and critical factors were identified by Fu et al. [114], which recommends high factor settings for improving the cavity filling. About the parameters, mould temperature was considered critical by Tay et al. [121]; injection pressure and mould temperature were identified as critical by Huang et al. [106]. Unfortunately, these papers did not report the interval of confidence.

7.3.2 Comparison between 316L feedstock and pure polymer moulding shrinkage

Table 7-5 compares average of 316L feedstock shrinkage value as resulted from Table 7-3 and POM shrinkage average values as resulted from Table 5-3. POM shrinkage is about five times more in parallel to the flow and six times more in normal to the flow with respect to 316L feedstock shrinkage. There is little prior work in the literature to compare this result against, though high powder loading has been shown to lead to lower shrinkage at the micro-scale [106] (though without any estimate of statistical significance). The results reported in Table 7-5 confirm this conclusion: POM shrinkage is about five times more in parallel to the flow and six times more in normal to the flow with respect to 316L feedstock.

	$S_{Tp\ AV}$ [%]	$S_{Tn\ AV}$ [%]
POM	5.089±1.658	3.026±0.266
316L feed.	0.867±0.274	0.590±0.227

Table 7-5. Total shrinkage (S_T) average values between POM and 316L feedstock in parallel to (p) and normal to (n) the flow direction.

For the polymer, the total shrinkage parallel is 68% greater than normal to the flow; for the feedstock, it is 47%. A spherical powder shape is thought to influence shrinkage as it makes the feedstock more isotropic (no preferred molecular orientations) with respect to crystalline POM [201]. This may be the underlying mechanism here.

7.3.3 Mechanism behind the critical factors

Table 7-6 summarize the 316L feedstock and POM critical factors.

	316L feedstock			POM		
				Mould T	↓	S_{Mp}
				Mould T	↑	S_{Mn}
S_{Pp}	Mould T	↓				
				Hold t - mould T	–	S_{Pn}
				Mould T	↓	
				Hold P	↓	
				Mould T - hold P	↓	S_{Tp}
				Melt T	↓	
				Mould T - melt T	↓	
S_{Tn}	Hold P - Injection P	↓				

Table 7-6. DoE results of 316L feedstock and POM critical factors. The arrows indicate whether a factor increasing causes an increase (↑) or a decrease (↓) in shrinkage, (–) indicates no clear trend.

As resulted in Table 7-6, 316L feedstock presents a lower number of critical factors with respect to POM, and this is likely due to a overlap of two aspects.

The first aspect is connected to the high powder loading: high power loading leads to low shrinkage, hence low "signal" value.

As a second effect, the noise due to the scale and uncontrollable process conditions (e.g. the external environment temperature) makes difficult to estimate the critical factors because of the low feedstock shrinkage (signal values) [136]. Indeed,

noise can be considered constant during the tests, but S/N ratio is lower compared to binder and this affect significance by adding uncertainty to the results: as outcome, influential parameters did not exceed the confidence threshold [202]. This did not mean that no parameters were significant, but it means that confidence was lowered due to uncertainty. Considering the specific 316L feedstock results, this requested to increase the alpha value from 0.05 to 0.1 (consequently, the confidence threshold decreased from 95 to 90%). A higher alpha value means to be more likely to reject a true null hypothesis, but it means also be more likely to detect real critical factors affecting the shrinkage.

The differences in terms of critical factors were discussed below.

The mould temperature is present as critical factor both for 316L feedstock (S_{Pp}) than for POM polymer (S_{Mp}, S_{Mn}, S_{Tp}) in Table 7-6. The critical influence of this parameter has been previously shown in several studies, for pure polymers [111; 117] and for feedstocks [106; 121]. The trend of this factor is also confirmed by the literature: an increase of mould temperature leads to shrinkage decrease.

The holding pressure factor is present both in 316L feedstock (S_{Tn}, with injection pressure) and in POM (S_{Pn}, with mould temperature). The presence of this parameter was confirmed by works that investigated pure polymers (POM [8; 119]) and feedstock [121] as well. Similarly to the trend reported in the present chapter, literature results evidenced that high holding values leads to reduce shrinkage.

In Table 7-6, the injection pressure is present only for 316L feedstock (S_{Tn}, with holding pressure). This result contrasts with the literature, because works have shown that injection pressure affected polymers [104; 105] and feedstock [106] shrinkage as well. However, the presence of injection pressure as a critical parameter for 316L feedstock and not for POM, it might be connected to the feedstock powder loading. Works has shown that to increase powder-loading leads to increase feedstock viscosity [203], and the viscosity affects injection pressure [204]. The relationship between viscosity and injection pressure is not simply predictable due to pseudo-plastic feedstock behaviour and temperature influences [170].

The 316L feedstock did not show as critical parameters neither holding time nor melt temperature (both present in POM). The absence of holding time for feedstock was

confirmed by the literature, because the holding time emerged to be critical only for pure polymers [31; 109] and no works reported the critical influence of this parameter for feedstock. The absence of melt temperature is not simply explainable, because is an important parameter both for feedstock [121] than for pure polymers [31]. However the presence of melt temperature as critical parameter for feedstock was observed only in one works above nine (Table 2-4), and a combined effect with melt temperature is a second ranking effect for feedstock S_{Pp} (Figure 7-5).

Summarizing the results reported above, it is possible to say that the presences of mould temperature and hold pressure for both and the hold time only for polymer were confirmed by the literature results. On the contrary to literature indications, results has shown that injection pressure is not critical for POM and melt temperature is not critical for feedstock. Regarding injection pressure, it is likely that the powder loading caused the criticity of this parameter in feedstock and not in polymer. Regarding melt temperature, further studies have to be performed even if in the literature only one work above nine identified this parameter as critical for feedstock.

These considerations were grouped in Table 7-7. The critical factors were compared with trends available in the literature.

	316L feedstock	POM	Literature
Mould temperature	Yes	Yes	Both
Hold pressure	Yes	Yes	Both
Injection pressure	Yes	No	Both
Hold time	No	Yes	Only pure polymers
Melt temperature	No	Yes	Both

Table 7-7. Comparison between pure polymer and feedstock critical factors. "Yes" indicate the presence; "No" the absence of critical factor. The third column reports whether factor affects are reported in the literature.

7.4 Summary

The influences of five processing parameters (injection and hold pressure, holding time, melt and mould temperature) in terms of shrinkage for 316L moulding feedstock were investigated.

The statistical treatment identified the critical factors that affected feedstock shrinkage: the mould temperature for post-moulding shrinkage in parallel to the flow direction, and

the combination hold pressure-injection pressure for total shrinkage in normal to the flow direction.

The results were discussed by considering different aspects: factors affecting 316L feedstock shrinkage, a comparison between 316L feedstock and pure polymer shrinkage values and a discussion by comparing each critical factor in pure polymer and feedstock.

By considering feedstock and pure polymer, the comparison between shrinkage values in the parallel to and normal to the flow direction presented similar percentage results and trends, even if feedstock shrinkage values were lower with respect to pure polymer as consequence of powder loading. The comparison of critical factors in some case presented different situations with respect to the literature review, i.e. the absence of melt temperature between the feedstock critical factors

Chapter 8 . Results: statistical based optimization using multiple quality criteria. 316L feedstock case study.

In the present chapter, the optimization by using multiple quality criteria, already described in chapter 6 and by [205], was applied on 316L feedstock. Similarly to the procedure applied to POM, the optimization required shrinkage minimization and part mass maximization simultaneously. By using different material (316L feedstock instead of POM), it is likely to produce different results. Considered the results already acquired, shrinkage numerical results were just summarized whilst the 316L feedstock part mass study was fully described.

8.1 Results

As explained in paragraph 7.3.3, the statistical study about 316L feedstock adopted an α value equal to 0.10. This statistically means that the possibility of finding an effect that does not really exist was 10%. Same α value was used for part mass characterization.

Table 8-1 reports total shrinkages values of 316L feedstock (S_T) in parallel to (p) and normal to (n) the flow direction (as resulted from Table 7-3) and the part mass (W) values. Part mass included both the specimen than the attached gate weight, because to divide the gate from the specimen caused profile damage that affected shrinkage measurements. Gate mass was estimated to contribute to about 1.5% of total part mass (3.10±0.03 mg gate mass).

Run	W [mg]	S_{Tp} [%]	S_{Tn} [%]
1	214.99±0.47	0.515±0.004	0.566±0.003
2	215.37±0.91	0.712±0.005	0.385±0.003
3	199.82±4.35	1.616±0.018	1.022±0.017
4	212.24±0.84	0.631±0.004	0.521±0.003
5	191.56±3.19	0.598±0.003	0.104±0.003

6	203.50±2.62	0.851±0.003	0.358±0.002
7	201.75±4.10	0.696±0.003	0.945±0.005
8	212.91±0.58	0.715±0.001	0.688±0.001
9	213.92±0.54	0.740±0.002	0.471±0.003
10	184.81±3.73	0.961±0.003	0.702±0.003
11	214.34±0.60	0.783±0.002	0.575±0.002
12	211.03±0.43	1.024±0.001	0.743±0.002
13	194.83±1.36	1.130±0.006	0.727±0.003
14	212.06±0.44	0.877±0.007	0.548±0.003
15	186.51±6.31	0.830±0.002	0.674±0.006
16	182.51±1.96	1.191±0.005	0.406±0.002

Table 8-1. 316L feedstock specimen mass results (W) with total shrinkage (S_T) parallel to (p) and normal to (n), the flow direction.

8.1.1 316L feedstock shrinkage results

Table 8-2 reports the 316L feedstock lowest (Low) and the average (Av) values for total shrinkage (S_T), on parallel to (p), and normal to (n), the flow direction. The average reported on Table 8-2 was calculated by considering all the data reported in the column of total shrinkage.

$S_{Tp\ Low}$ [%]	$S_{Tp\ Av}$ [%]	$S_{Tn\ Low}$ [%]	$S_{Tn\ Av}$ [%]
0.515±0.004	0.867±0.274	0.104±0.003	0.590±0.227

Table 8-2. 316L feedstock lowest and average S_T values.

According to statistical results reported in chapter 7, 316L feedstock total shrinkage normal to the flow direction was critically affected by the interaction between holding pressure and injection pressure (Figure 7-9). The total shrinkage in parallel to the flow direction did not present critical factors (Figure 7-8).

8.1.2 316L feedstock part mass results

Using the same statistical tools used for total shrinkage, the critical factors that affect 316L feedstock part mass were analysed. The processing parameters were labelled as A (hold time), B (hold pressure), C (injection pressure), D (mould temperature) and E (melt temperature).

Figure 8-1 represents the Pareto chart of the 316L feedstock part mass. Two single factors had statistically significant effects on part mass: the mould temperature D and the melt temperature E. In addition, one combination of factor had statistically significance: mould temperature with melt temperature DE.
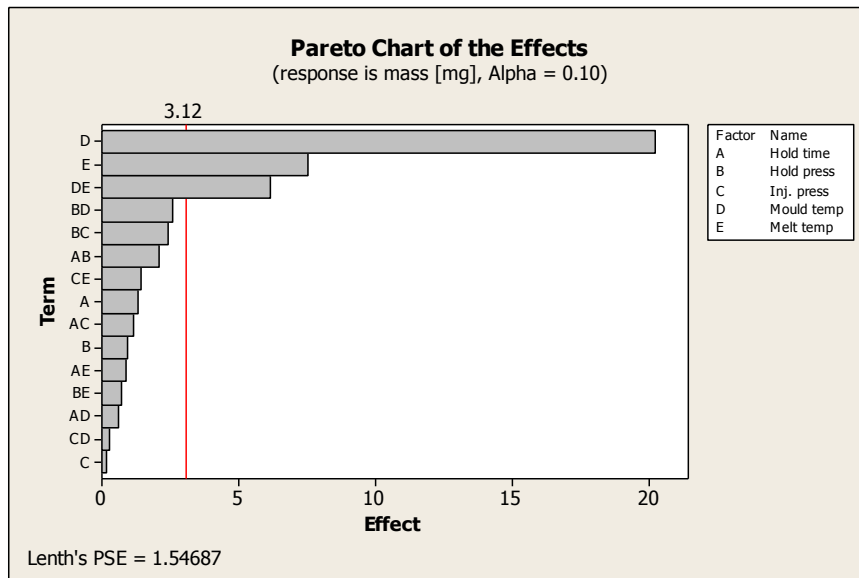
Figure 8-1. Pareto chart of 316L feedstock part mass.

Figure 8-2 represents the main effects chart of the 316L feedstock part mass critical factors. The main effects plot reports how changing each process parameter between the low and high values affects the actual magnitude of specimen mass. The slopes of the two significant parameters (mould temperature and melt temperature) identified from the Pareto chart, are all positive in the main effects chart, which means that an increase in specimen mass is directly related to each of the two parameters.
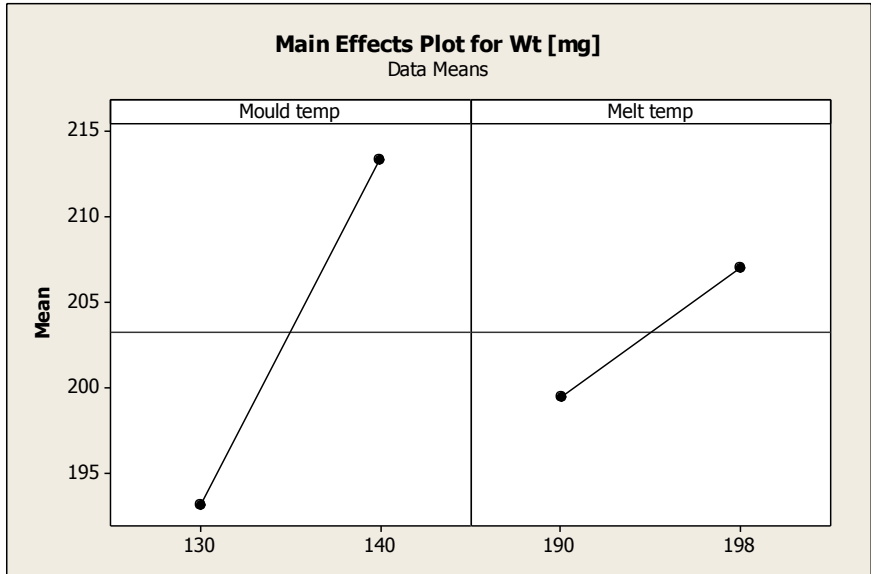
Figure 8-2. Main effect plot of critical 316L feedstock part mass factors.

Figure 8-3 represent the interaction between melt and mould temperatures (labelled as DE in Figure 8-1). The boxes show the change of 316L feedstock part mass, W, with both mould temperature and melt temperature. The top right box plots the means of part mass as a function of melt temperature, the bottom left box plots the means of part mass as a function of mould temperature.
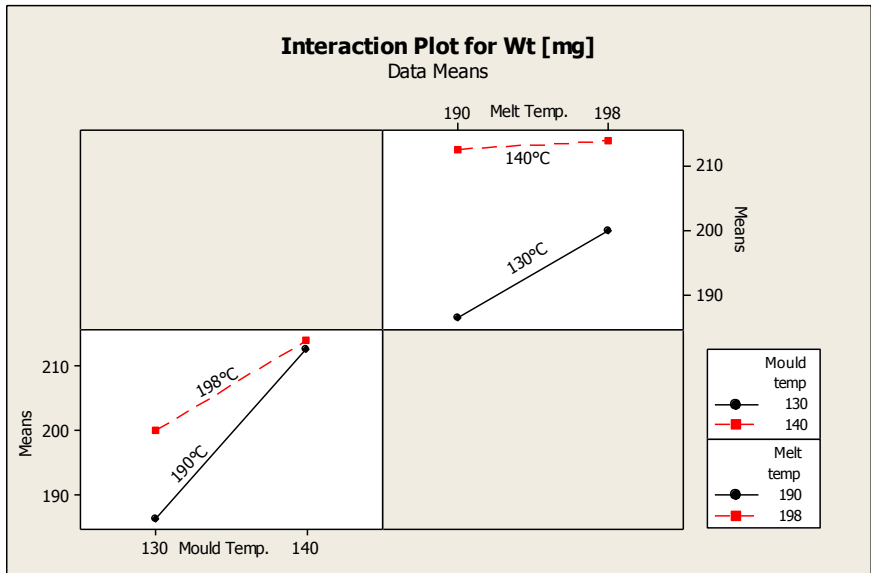
Figure 8-3. Interaction plot of 316L feedstock part mass between melt and mould temperature.

Considering melt temperature (top right box), the increase of part mass as we move from the low (190°C) to the high (198°C) temperature is larger when mould temperature is low (130°C) than when it is high (140°C), even if the value of part mass means with mould temperature equal to 140°C is greater with respect to 130°C and produce an increase too. Considering mould temperature (bottom left box), the increase of part mass moving from the low (130°C) to the high (140°C) temperature is larger when melt temperature is low (190°C) than when is high (198°C), even if the value of part mass means with melt temperature equal to 198°C is greater with respect to 190°C and produce an increase too.

8.2 Optimization step

Similarly to the procedure adopted in chapter 6 for POM, desirability functions were implemented for minimizing shrinkage and maximizing part mass. The individual functions for matching with these requirements were represented in Equation 2 and Equation 3 respectively.

Shrinkage minimisation and part mass maximisation requires upper and lower limits selected using the results reported in Table 8-1. As depicted in Figure 8-4 for optimization stage, shrinkage target S_T was set to 0.5% and the upper limit was set to 1.4%; mass target value was set to 217 mg and the low limit was set to 210 mg.
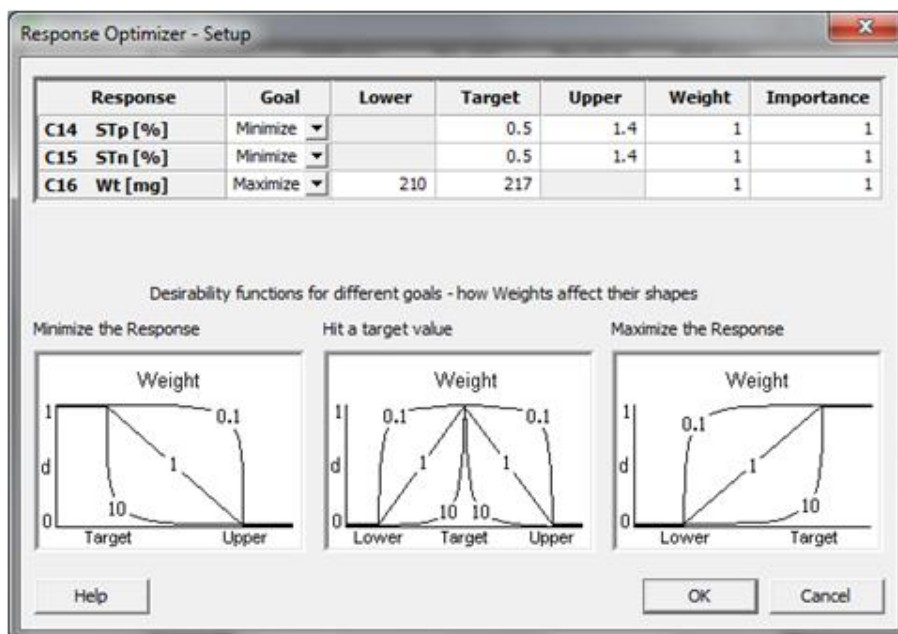
Figure 8-4. 316L feedstock response optimizer values.

Figure 8-5 reports the results of the optimization stage. Desirability value was equal to 1, and the optimized processing parameters combination reported in bracket.
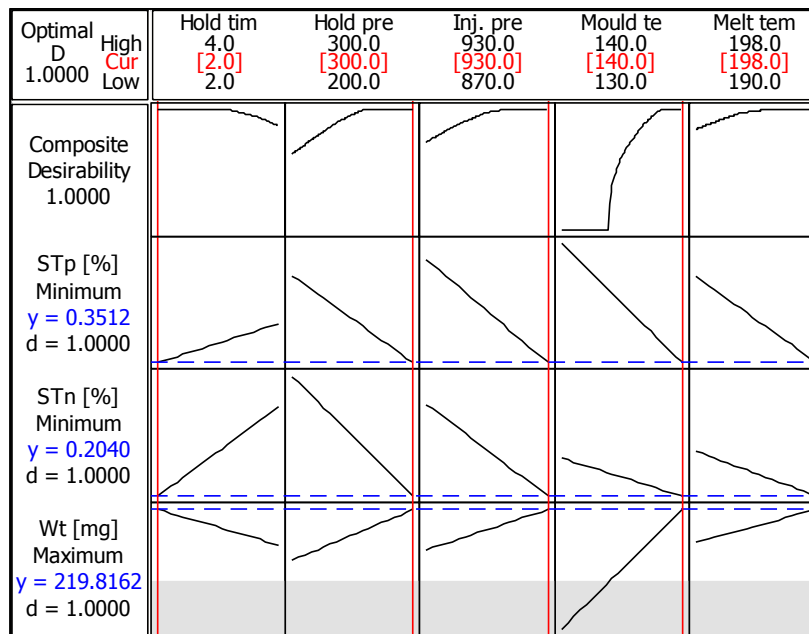
Figure 8-5. 316L feedstock optimization stage.

Table 8-3 summarises the critical factors observed for shrinkage and part mass.

316L feedstock critical factors		
Parallel to the flow	**Normal to the flow**	
S_T	None	Hold press-Injection press	↓
W	Mould temp, melt temp, their combination		↑

Table 8-3. 316L feedstock critical processing parameters. The arrows indicate whether a factor increasing causes an increase (↑) or a decrease (↓) in shrinkage or part mass.

The optimisation stage depicted in Figure 8-5 identified the optimum combination of parameters that minimized shrinkage and maximized 316L feedstock part mass. Table 8-4 reports 316L feedstock shrinkage and part mass values of specimens moulded with optimized parameters.

Hold t [s]	Hold P [bar]	Inj. P [bar]	Mould T [°C]	Melt T [°C]	S_{Tp} [%]	S_{Tn} [%]	W [mg]
2	300	930	140	198	0.590±0.004	0.283±0.002	211.79±0.65

Table 8-4. 316L feedstock optimized parameters with total shrinkage and part mass results.

The results reported in Table 8-4 can be compared with those reported in Table 8-2. Table 8-5 summarise the comparison.

316L feedstock		$S_{Tp\ Opt}$ [%] (0.59)	$S_{Tn\ Opt}$ [%] (0.28)	W_{Opt} [mg] (211.79)
$S_{Tp\ Av}$ [%]	(0.87)	-30%		
$S_{Tn\ Av}$ [%]	(0.59)		-53%	
W_{Av} [mg]	(203.26)			+4%
$S_{Tp\ Low}$ [%] (1st run)	(0.52)	+13%		
$S_{Tn\ Low}$ [%] (5th run)	(0.10)		+280%	
W_{High} [mg] (2nd run)	(215.37)			-2%

Table 8-5. Analysis of 316L feedstock optimization stage effect.

In Table 8-5, the actual average, low and optimised values of shrinkage and weight are given in parentheses, the optimised in the first row of data and the average and lower in the first column of data. The body of the table compares the optimised with the non-optimised values as a percentage change. The first set of three rows compares against average values from prior experiment. The second set of three rows compare against the best values (lowest shrinkage or highest mass) from prior experiment. A negative value in the table indicates a reduction in shrinkage or part mass.

Figure 8-6 reports the specimens mass as resulted from Table 8-1. Specimen number 17 was moulded using the combination of optimised processing parameters of Table 8-4. The part mass was expressed in milligrams.

163
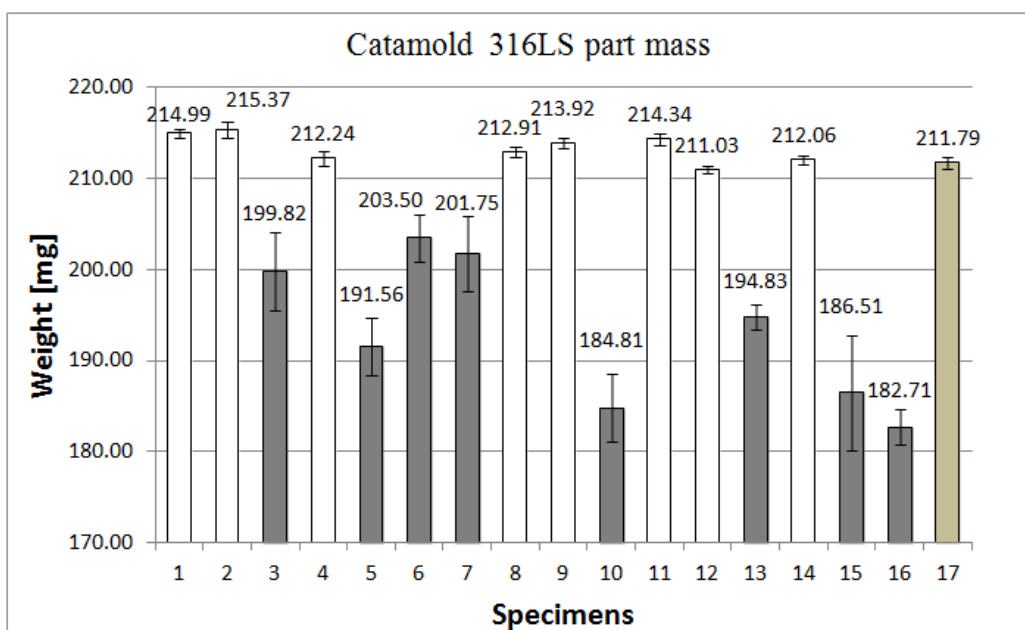
Figure 8-6. 316L feedstock part mass distribution.

The white bars represented in Figure 8-6 referred to specimens moulded with high mould temperature (140°C), while the grey bars referred to specimens moulded with low mould temperature (130°C). The 17th specimen was moulded with high mould temperature. Error bars are the standard deviation of five specimens examined.

8.3 Discussion

The numerical results reported in Table 8-1 confirmed the general shrinkage trend about a more balanced and overall lower shrinkage in amorphous polymers respect and semi-crystalline polymers (described in paragraph 7.4.2).

The critical factors that affect 316L feedstock total shrinkage and part mass were summarized in Table 8-3. The combination holding pressure-injection pressure was identified as critical factor for total shrinkage normal to the flow direction. The analysis of combined effect has shown as general trend that shrinkage was reduced with a combination high-high of values of injection pressure and hold pressure (Figure 7-10). Pomerleau et al. [74] confirmed this trend also: generally, an increase of holding pressure can reduce shrinkage in parallel to and normal to the flow direction. No critical parameters were found for total shrinkage in parallel to the flow direction.

A similar trend resulted by considering part mass results (Figure 8-2 and Figure 8-3), where the mould temperature, the melt temperature and their combination were identified as critical factors that affect part mass: by increasing these critical factors, leads to increase part mass. These experimental results were confirmed by the literature, that stated the influence of melt and mould temperature in terms of amount of material inside the cavity mould [85].

Table 8-4 indicates the 316L feedstock optimized parameter values that reduced shrinkage and maximized part mass. As noticed in chapter 6 about POM, also for 316L feedstock the optimized parameters were the maximum values investigated (except the holding time) reported in Table 7-1 without intermediate values, despite of the factors range investigated the entire mouldability region as depicted in Figure 4-26. This behaviour it is likely due to the similar trend of shrinkage and part mass. Indeed, the fulfillment of both requests (shrinkage minimization and part mass maximization) was

achieved by maximizing the processing parameters and this explain why the greater part of optimized parameters (except holding time) resulted to the maximum values.

Table 8-5 reports the effect of optimisation using multiple quality criteria. Comparing the numerical results after the optimisation with those before the optimisation (both average and low values), it was possible to evaluate that shrinkage in parallel to the flow direction was reduced respect the average (-30%) but lightly improved respect to the lowest value (+13%, first specimen). The optimized shrinkage in normal to the flow direction was reduced respect to the average value (-53%) but not respect to the lowest value (+280%, fifth specimen). The optimised part mass has shown a +4% change with respect to the average part mass and a -2% change with respect to the highest part mass value. The optimised values were the result of a compromise between shrinkage minimisation and part mass maximisation and Table 8-5 represent a good example. Considering the average values (total shrinkage and part mass), the optimized results shows the fulfillment to shrinkage minimization and part mass maximisation. Otherwise considering the lowest results, seems that the optimized parameters produced a worsening of final product both for shrinkage than for part mass, but it is necessary to consider all the results related to that combination of processing parameters and compare these results with optimized values. Hence the best S_{Tp} result of the 1st run (0.52%) have to be considered also with its S_{Tn} (0.57%), as well as the S_{Tn} best result for the 5th run (0.10%) have to be considered also with its part mass value (191.6 mg).

The 316L feedstock part mass analysis depicted in Figure 8-6 confirmed the critical influence of mould temperature: the relatively short white bars indicate mass values for specimens moulded low mould temperature (130°C). The longer grey bars refer to specimens moulded with high mould temperature (140°C). The 17th bar referred to part mass of the specimen moulded with optimised values. Although the 17th specimen did not show the highest value of mass, it exhibited a shrinkage that is more balanced in parallel to, and normal to, the flow direction (0.59% and 0.28% respectively) compared to shrinkages reported in Table 8-1.

8.4 Summary

Multiple quality criteria optimization was applied to 316L feedstock. Results confirmed, similarly to POM case study, that this methodology could efficiently reduce shrinkage and increase part mass simultaneously.

The comparison performed between results before and after optimization, confirmed that outcomes of statistical-based optimization represents a compromise between potentially contradicting process conditions.

Chapter 9 . Results: feedstock feature reproduction at the micro-scale.

This chapter investigated the behaviour of 316L feedstock for filling micro-features with different aspect ratio. The features consisted in micro-channels parallel to, and normal to, the flow direction. Statistical approach was adopted for determining the processing parameters that affect the feature reproduction of the micro-channel with a breadth of 600 μm in a perpendicular direction (z-axis) with respect to the flow direction (x-axis): these data were calculated by converting the height of the channel on feature reproduction value. Optical analysis of the 60μm feature was used for determining the connection between channel orientation and low mouldability limit.

9.1 Purpose of chapter

Objectives of the present chapter were to study the influence of feedstock processing parameters for filling a micro-feature in a direction perpendicular (z-axis) with respect to the injection flow (x-axis), and to collect information about the effect of texture orientation for filling channels with dimension close to the lower mouldability limit of the material injected. As noted below, both aspects were investigated in the literature for pure polymers but not for feedstock, and the results reported in this chapter may bridge this gap.

9.2 Theoretical aspects

Filling dynamic behaviour

No data are available in the literature about works that investigated the influence of processing parameters – in feedstock moulded parts – for the filling of micro-channels in a perpendicular direction (along the z-axis) with respect to the melt flow direction.

At date, Zhang et al. [186] published the only similar work present in the literature. The authors adopted a channel configurations similar to the design reported in Figure 9-1, and investigated five processing parameters (injection speed, hold pressure and time,

barrel and mould temperature) by implementing an half factorial matrix. With respect to the present chapter, Zhang et al. [186] considered a pure polymer (HDPE) instead of feedstock. The results have shown that replication quality increase by increasing the critical parameters holding pressure and mould temperature.
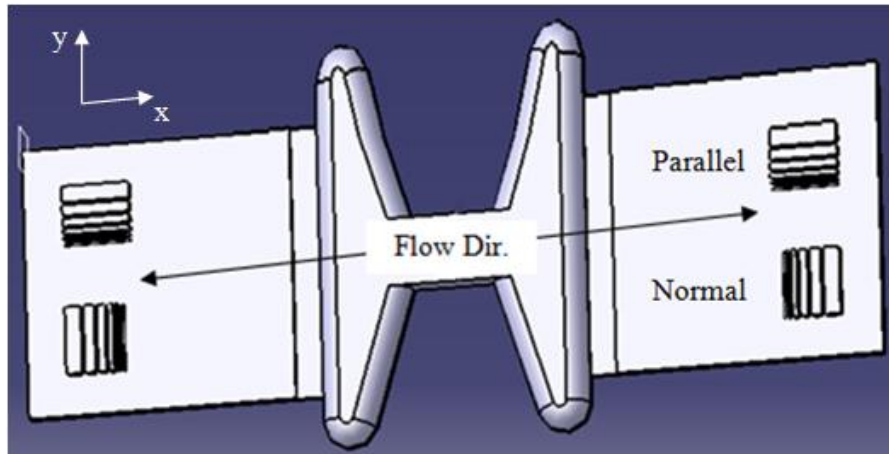
Figure 9-1. Micro-texture position.

Low mouldability limits and feature orientation

No data are available in the literature about the connection between feature orientations and lowest mouldability limit. On other words, there are no data for determining if the reproduction of the littlest micro-channel (with dimension equal to the low mouldability limit of feedstock) is affected by the channel orientation. By manufacturing a micro-channel of 60 μm and by orienting the channel parallel to and normal to the flow direction, it could be possible to determine this connection. Tests for manufacturing a channel with dimension lower that 60 μm were reported in the appendix A.

The dimension of 60 μm was chosen because according to Gonzales et al. [206], it is usual to assume that the smallest feature of a moulded part can be ten times larger than the mean particle diameter of powder. By considering that the mass median particle diameter (MMD) of 316L feedstock powder is D_{50}=4-5 μm, it is likely that the low mouldability limit is around 50μm. By considering the 316L feedstock, the assumption reported above was confirmed by Fu et al.[207], which successfully moulded micro-pillars with a diameter of 60μm.

Zhang et al. [186] demonstrated the influence of feature orientation (with geometry similar to Figure 9-1) in terms of feature reproduction: by moulding a pure polymer (HDPE), Zhang observed that parallel to the flow feature presented sharp edges and better-replicated profile with respect to normal oriented features. Yang et al. [208] reported similar conclusions by studying HDPE moulded parts: results have shown that normal to the flow features were partially filled with respect to parallel to the flow.

Hesitation effects

The micro-feature geometries adopted in this chapter could generate hesitation effects (Figure 9-2).
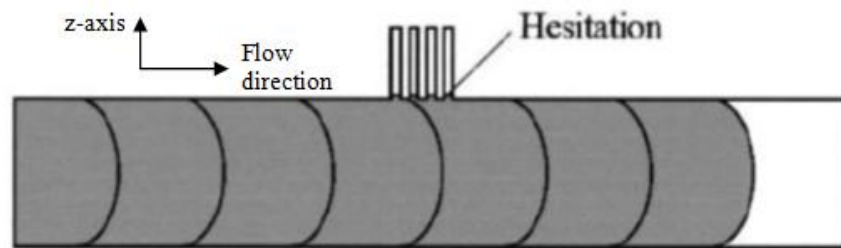
Figure 9-2. Hesitation-effect in high aspect ratio micro-cavities [209].

Indeed, this effect is common when an injection-moulded part contains different thicknesses [209] and as consequence, the flow moves preferentially into thick area [210]. The hesitation effect occur with A/R usually larger that 2. During injection process, when the flow front reaches the first thin wall section, if the pressure is insufficient for filling the thin section the melt continue along the flow direction. Melt that just entered the thin section, cools until the rest of cavity mould is filled. When the main cavity is completely filled, the injection pressure is fully available but the melt in the thin section has frozen and the section cannot be filled further. This phenomenon has to be considered because results can be affected by hesitation effect.

9.3 Results

Table 3-5 reports the processing parameters and their values investigated in this chapter. Table 9-1 reports the experimental data concern the feature with a breadth of 600 μm, measured both in parallel to than normal to the flow direction. In details are reported the combinations of processing parameters tested, the height of the feature expressed in μm

and the feature reproduction (FR) expressed as percentage with respect to the cavity micro-feature height. The absence of data (−) in Table 9-1 means that no features were reproduced. It was possible to measure only the 600 μm wide feature because the measurements were performed with a touch probe with a ball nose of 1 mm of diameter: the smaller channels (below a wide of 400 μm) requests different measurement technique (e.g. confocal microscopy).

Equation 5 [103] was used for determining the feature reproduction and concerns the height of the texture of 600 μm wide. The terms c_d is the cavity micro-feature height used as reference (300 ± 1 μm), whilst f_d is the average height of the feature filled by 316L feedstock.

Equation 5 $$FR = \left(1 - \left(\frac{c_d - f_d}{c_d} \right) \right) * 100$$

During each moulding run (16 runs, Table 9-1), five sample were selected after an uninterrupted number of cycles. The height of each 600 μm feature (in parallel to and normal to the flow direction) was measured in three points (see Figure 3-22), for 480 measurements in total.

Run	Melt temp [°C]	Mould temp [°C]	Hold press [bar]	Hold time [s]	Inj. speed [mm s^{-1}]	Paral height [μm]	Norm height [μm]	FR Paral [%]	FR Norm [%]
1	198	130	200	2	150	-	-	-	-
2	192	130	200	5	150	-	-	-	-
3	192	140	200	2	150	212	192	70.7	63.9
4	192	140	400	5	150	165	275	55.2	91.5
5	198	140	200	2	250	-	-	-	-
6	198	130	200	5	250	163	143	54.5	47.5
7	198	140	400	2	150	240	160	80.0	53.4
8	192	130	400	5	250	241	237	80.5	78.9
9	192	140	400	2	250	204	252	68.0	84.1
10	198	140	200	5	150	145	-	48.2	-
11	198	130	400	5	150	-	-	-	-
12	192	130	200	2	250	282	220	93.9	73.3
13	198	140	400	5	250	-	-	-	-

14	198	130	400	2	250	-	-	-	-
15	192	130	400	2	150	-	-	-	-
16	192	140	200	5	250	-	-	-	-

Table 9-1. Processing combination values, height and feature reproduction (FR) of μ-textures parallel to, and normal to, the flow direction.

9.4.1 Statistical results of micro-texture measurements

The statistical analysis investigated the feature reproduction RF. The studies were performed by using Minitab 16; Pareto chart, main effects and the interaction plots analyzed the results. Similarly to the previous 316L feedstock study (chapter 7), the alpha value adopted was 0.1.

The study of FR allowed determining the critical factors that affect the filling dynamic along the z-axis. The processing parameters were labelled as A (melt temperature), B (mould temperature), C (hold pressure), D (hold time) and E (injection speed). The combined influence of two of these parameters was described using two of the above letters.

The Pareto Chart depicted in Figure 9-3 represents the critical factors that affect FR for the μ-feature parallel to the flow direction: the interaction between injection speed and mould temperature is a critical factor.
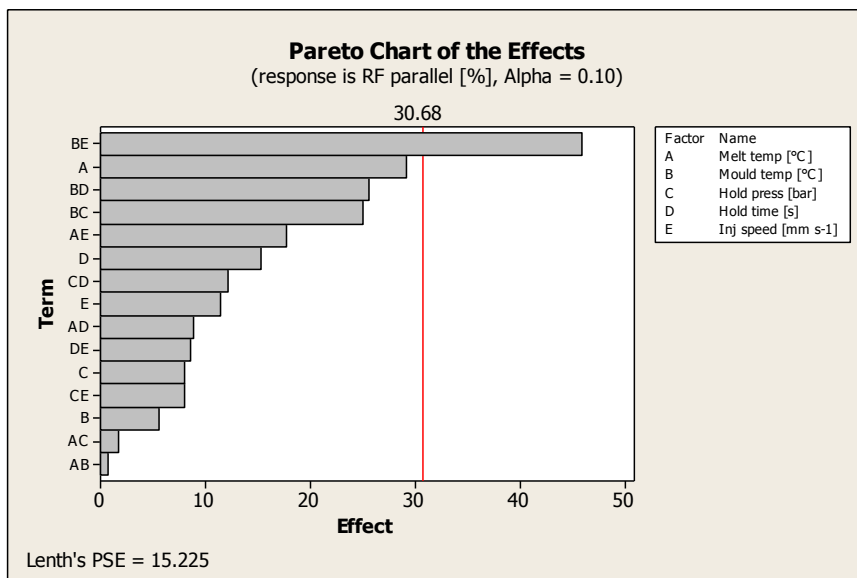
Figure 9-3. Pareto chart of FR 316L feedstock (parallel direction).

Figure 9-4 depicts the corresponding interaction plot between mould temperature and injection speed, labelled as BE in Figure 9-3. The top right box plots FR as a function of injection speed, the bottom left box plots FR as a function of mould temperature. By considering injection speed (top right) moving from the low (150 mm s^{-1}) to the high (250 mm s^{-1}) speed value, FR increase when mould temperature is low (130°C) and decrease when it is high (140°C). Considering the mould temperature (bottom left) moving from the low (130 °C) to the high (140°C) temperature, FR increase when injection speed is low (150 mm s^{-1}) and decrease when it is high (250 mm s^{-1}). As overall trend, FR was not easily predictable because of the antagonistic interaction, characterized by a cross combination of the factors (low-high or high-low).
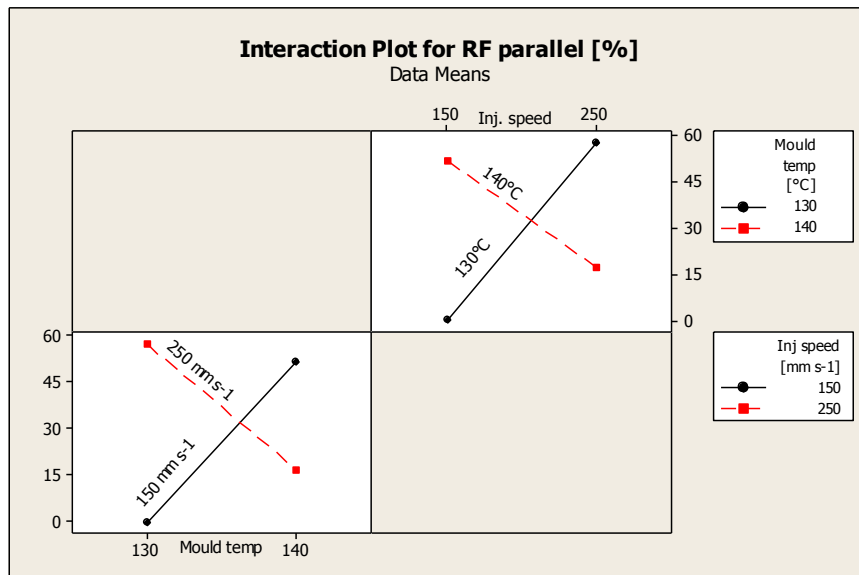
Figure 9-4. Interaction plot of FR 316L feedstock (parallel direction).

The Pareto Chart depicted in Figure 9-5 represent the critical factors that affect the FR of the μ-feature normal to the flow direction: the interaction between injection speed and mould temperature, and the melt temperature.
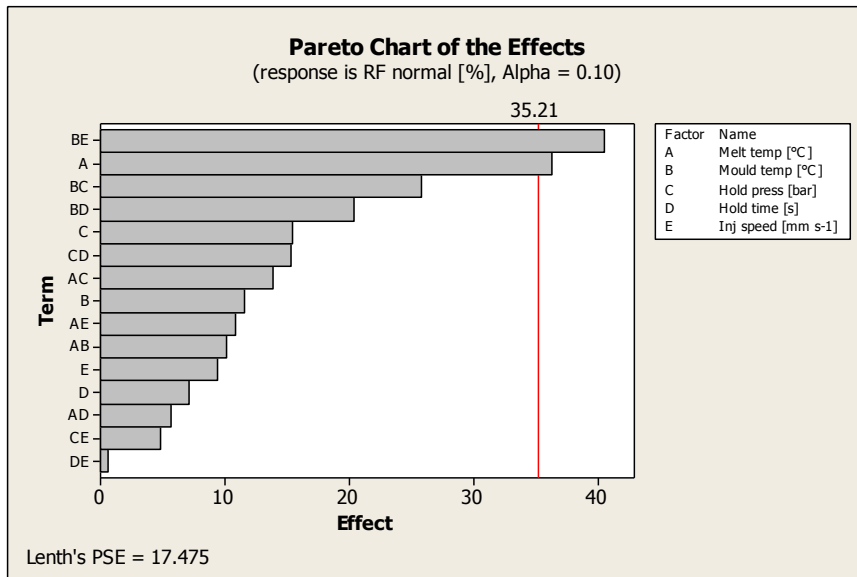
Figure 9-5. Pareto chart of RF 316L feedstock (normal direction).

Figure 9-6 and Figure 9-7 respectively depict the main effect plot of the melt temperature (labelled as A in Figure 9-5) and the interaction plot of the combined effect between injection speed and mould temperature (labelled as BE in Figure 9-5). According to Figure 9-6, RF decrease by increasing the melt temperature.
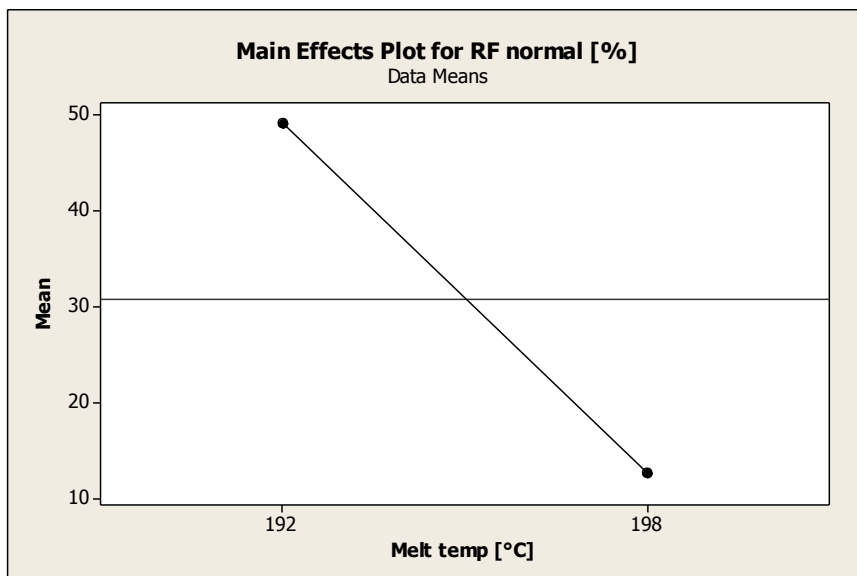
Figure 9-6. Main effect plot of FR 316L feedstock (normal direction).

In Figure 9-7, the top right box plots FR as a function of injection speed, the bottom left box plots FR as a function of mould temperature. These critical factors presented the

same interaction reported in Figure 9-4, and leads to the same results: FR trend was not easily predictable because of the cross combination of the factors.
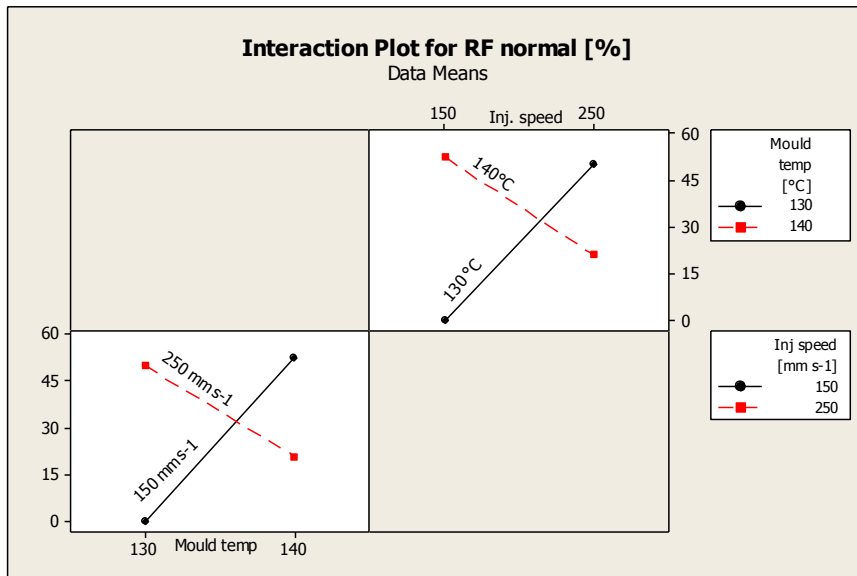
Figure 9-7. Interaction plot of FR 316L feedstock (normal direction).

9.4.2 Optical results

Figure 9-8 reports the optical analysis of the μ-features normal and parallel oriented. Each specimen was moulded with the processing combination reported in Table 9-1.
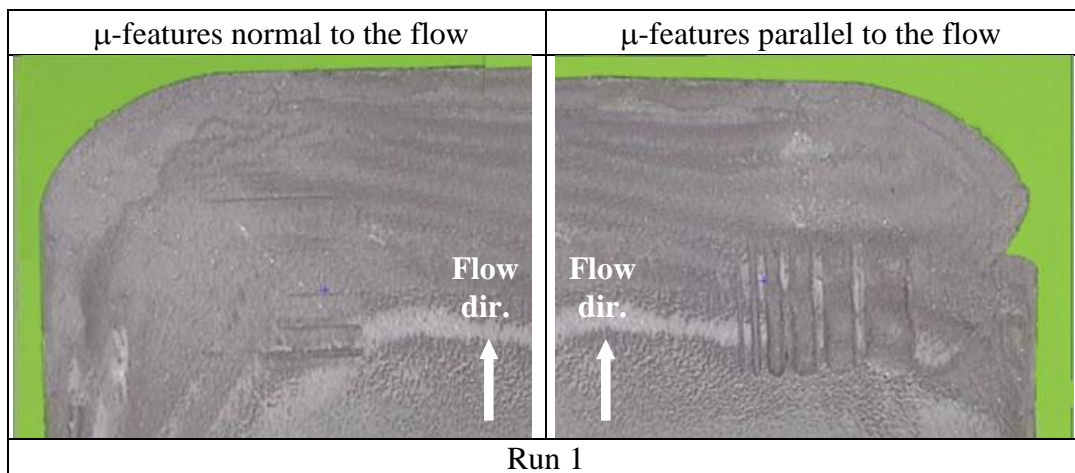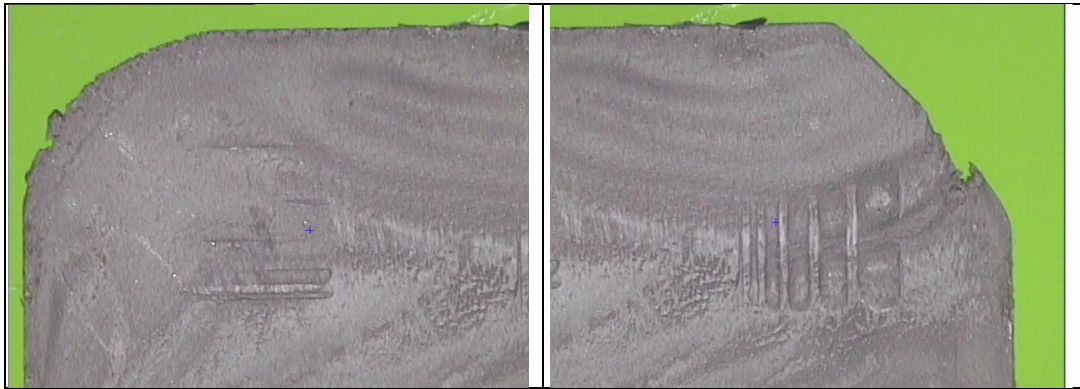
Run 2
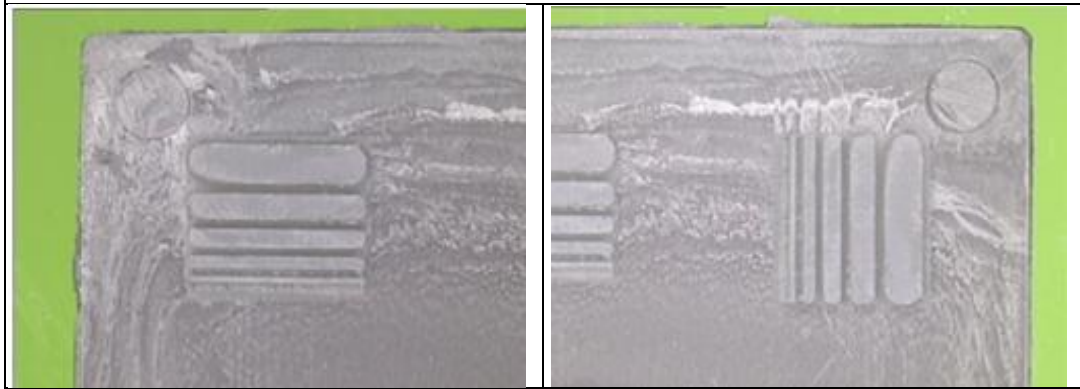
Run 3
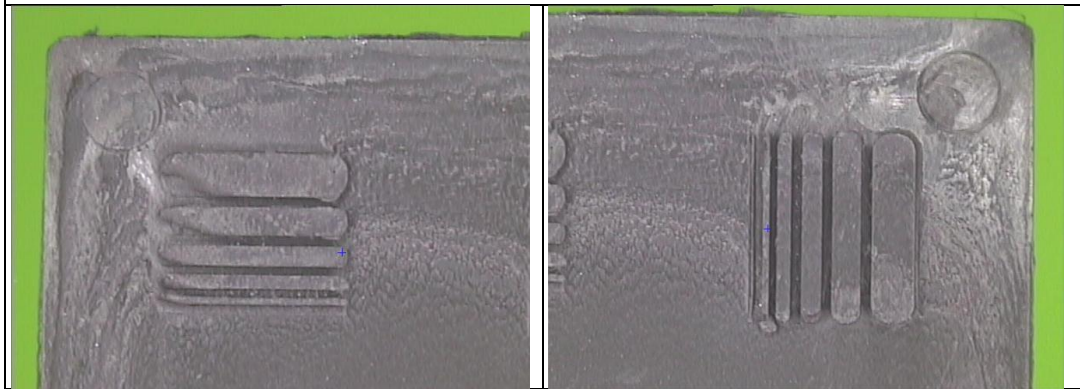
Run 4
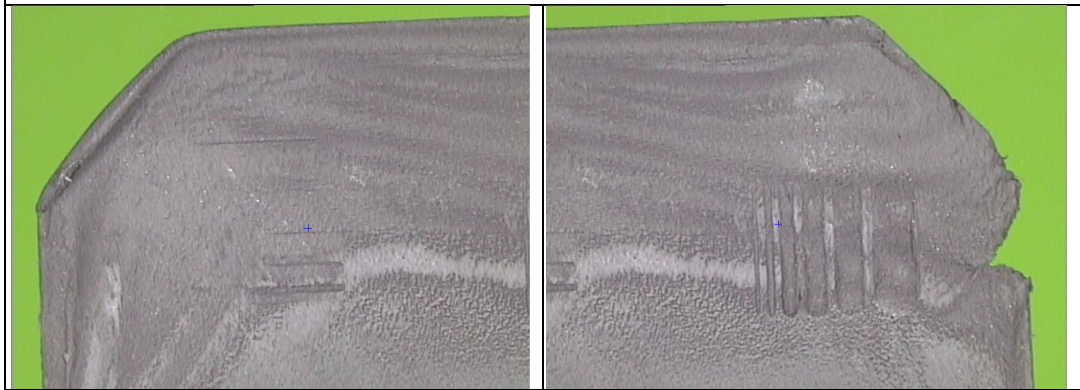
Run 5
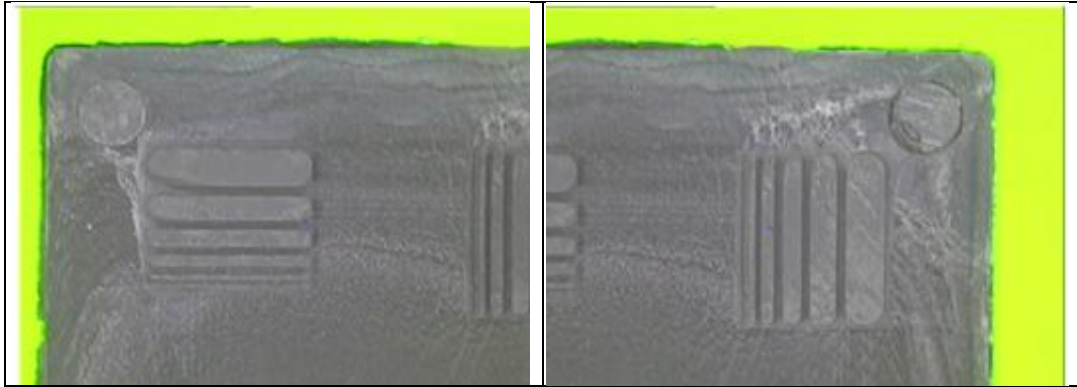
Run 6
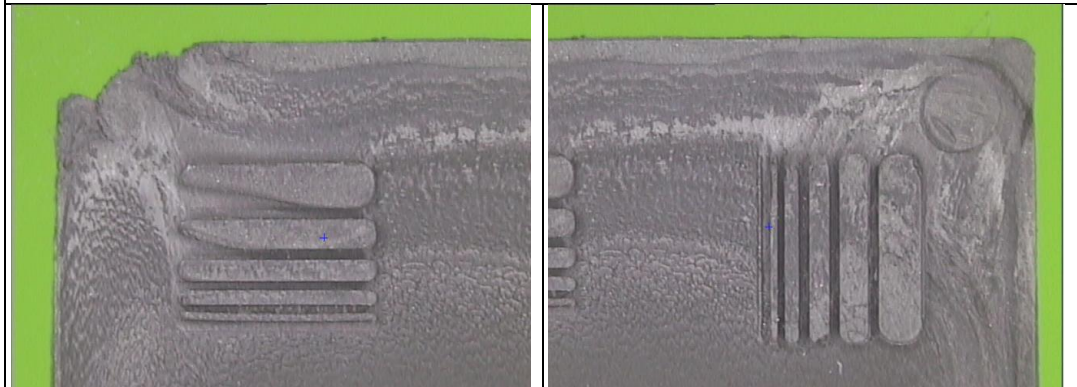
Run 7
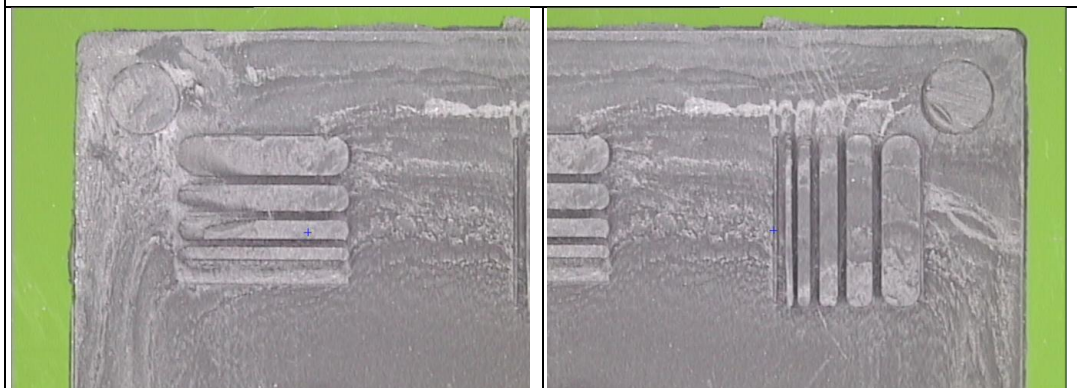
Run 8
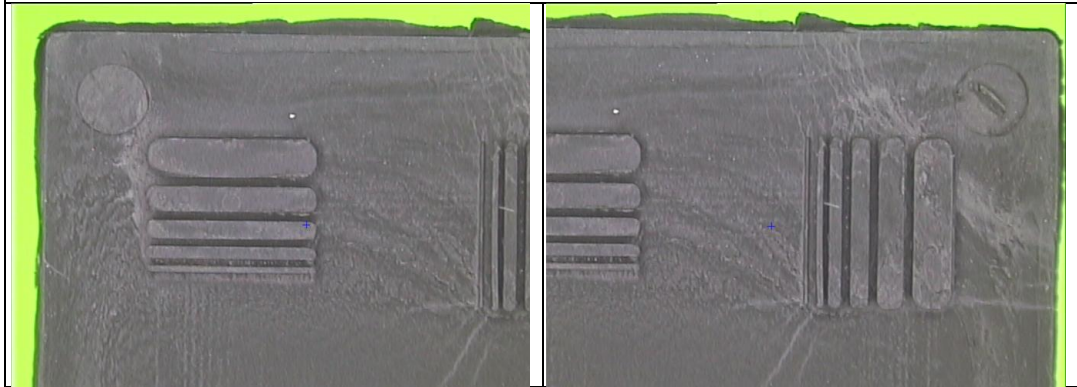
Run 9
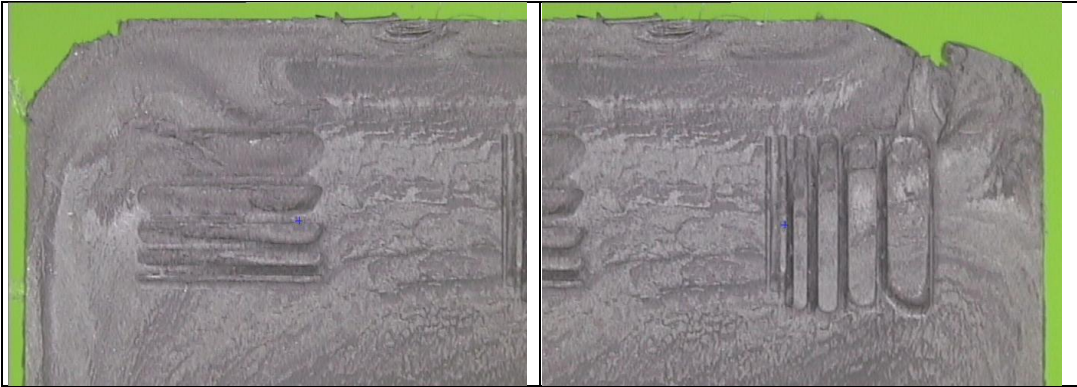
Run 10
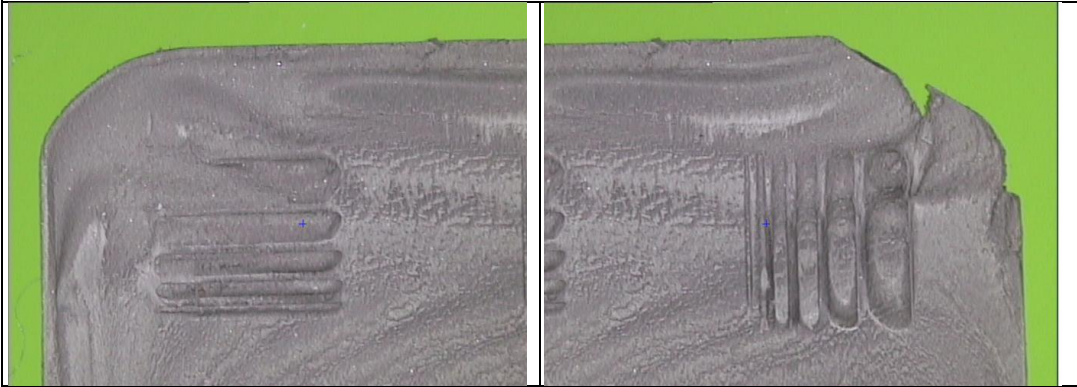
Run 11
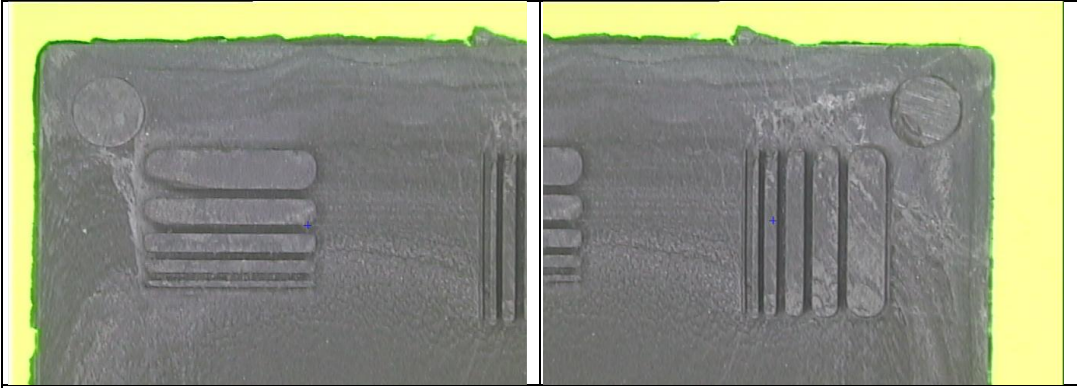
Run 12
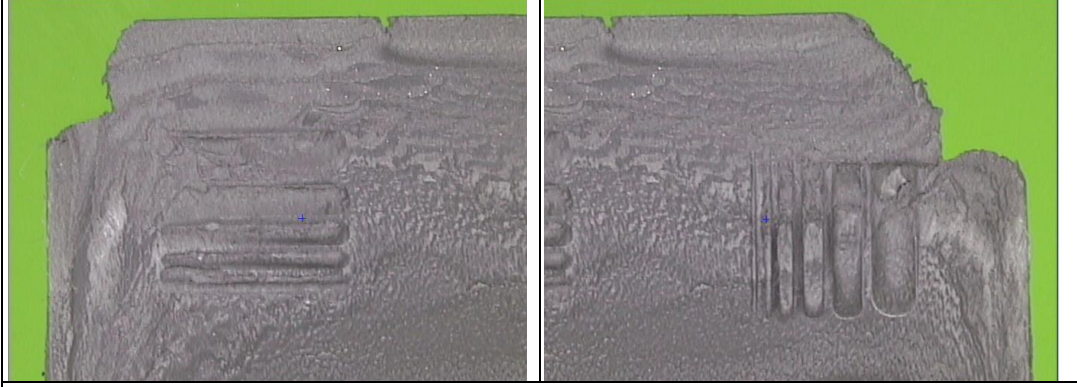
Run 13
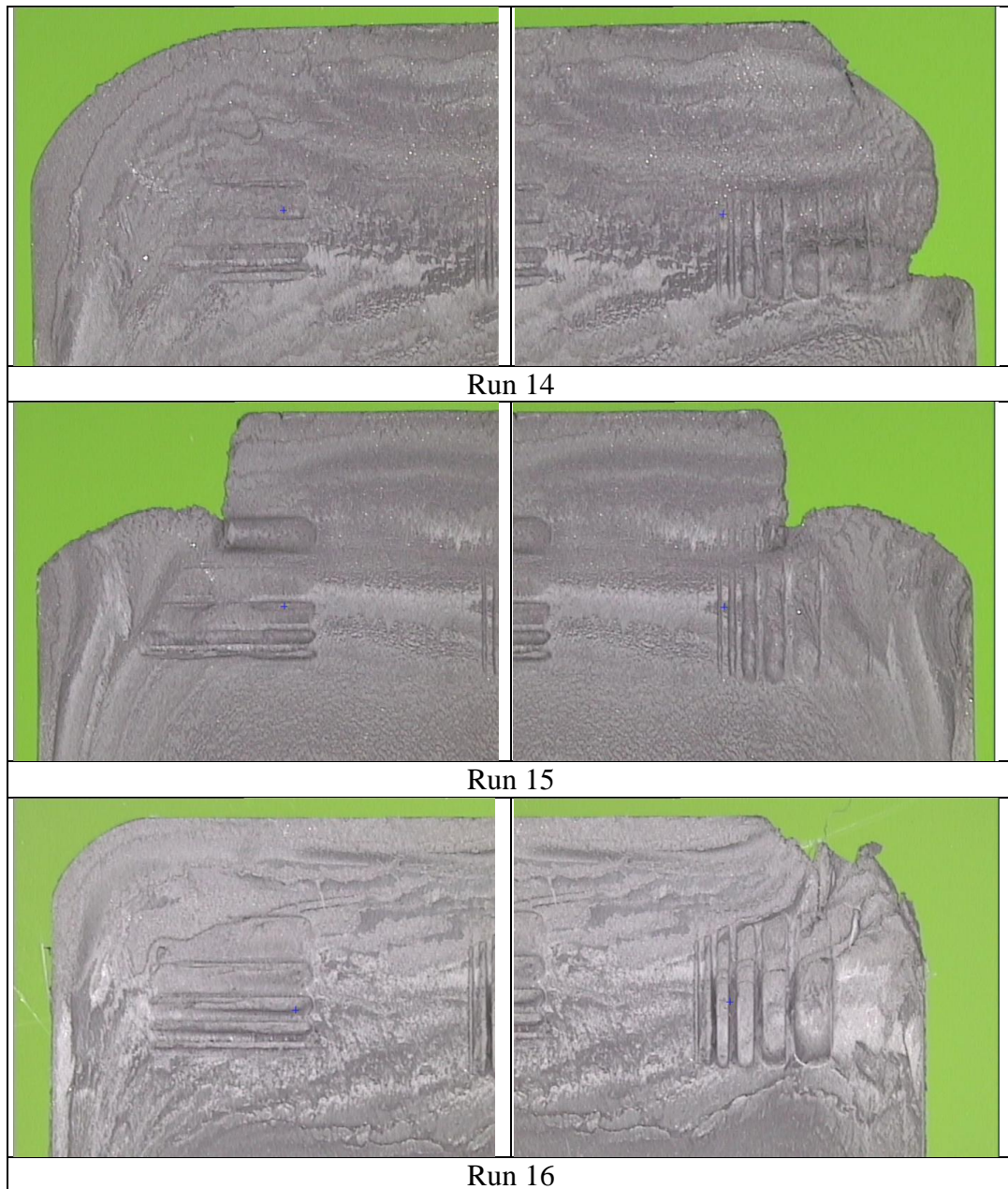
Figure 9-8. Optical analysis of µ-features parallel to (right) and normal (left) to the flow direction.

As resulted from Table 9-1, many processing combinations did not produce textures. However, Figure 9-8 confirm that the combination of processing parameters fully investigated the feedstock mouldability range because specimen shape varied from well moulded with flash (e.g. specimen 9) to partially unfilled (e.g. specimen 15).

9.4 Discussion

9.4.1 Discussion of statistical analysis

The combination between mould temperature and injection speed, resulted critical for RF. It is likely that the feature reproduction results are not affected by hesitation effects, because this effect occur in μ-features with A/R > 2 [209], and the 600 μm feature present an A/R = 0.5. Table 9-2 summarize the critical factors that affect FR of feedstock.

316L feedstock filling along z-axis		
FR Parallel	Mould temperature-inj. speed	-
FR Normal	Mould temperature-inj. speed	-
	Melt temperature	↓

Table 9-2. Critical factors that affect the FR of the 600 μm feature breadth, along z-axis. The arrow (↓) indicates the FR response after a factor increase, (-) indicates no clear trend.

The analysis of results reported in Table 9-2 evidences some analogies with Zhang et al. [186]. Zhang identified mould temperature and holding pressure as critical parameters for HDPE channel height, regardless the channel orientations. The 316L feedstock results evidenced the critical effect of the interaction between mould temperature and injection speed; features normal to the flow oriented was affected also by melt temperature. Even if for different materials, the studies seems to confirm that a temperature (mould temperature in both) and a pressure related parameters (hold pressure for [186] and injection speed in the present thesis) affects the feature reproduction. The importance of injection speed during the filling of micro-channels was demonstrated in a previous work of Zhang [211].

About the trends, the results of 316L feedstock is opposite with respect to HDPE investigated by Zhang et al. According to [186], an increasing of critical parameter leads to increase channel height, whilst according to results presented in the present thesis and reported in Table 9-2 feature reproduction of channel normal oriented was increase by decreasing the melt temperature. It was not possible to identify a clear trend for the interaction between mould temperature and injection speed.

9.4.2 Discussion about low mouldability limit and feature orientation

The optical results of the 60μm breadth feature were summarized in Table 9-3.

Specimen	60 μm Paral	60 μm Normal
1	-	-
2	-	-
3	-	-
4	Yes	-
5	-	-
6	Yes	-
7	Yes	-
8	Yes	-
9	Yes	-
10	Yes	-
11	P	-
12	Yes	-
13	P	-
14	-	-
15	P	-
16	P	-

Table 9-3. Optical investigation results for the feature of 60 μm. Yes indicate feature fully and P partially replicated.

Results of Table 9-3 evidenced the presence of a low mouldability limit equal to 60 μm, and the influence of features orientation. Indeed, only the micro-features parallel to the flow oriented were reproduced, whilst no normal oriented features are present.

The low mouldability value (60 μm) confirmed the assumption of Gonzales et al. [206], Fu et al.[207] and Zauner [212]: the smallest feature of a moulded part can be ten times larger than the mean particle diameter of powder, and 316L feedstock can reproduce features of 60 μm. Besides, similarly to Zhang et al. [186] and Yang et al. [208] results, features parallel to the flow presented better FR with respect to normal to the flow.

The absence of normal oriented features it is likely to be caused by an air entrapment phenomenon: most of the air inside the parallel oriented features can escape from the cavity during the filling process, opposite to the case of normal oriented features.
This phenomenon was observed also by Zhang et al. [186], which made further considerations about the gap δ between the melt flow profile and the cavity edge. By

adapting the model reported by [186] (laminar flow fully developed inside the cavity thickness, 350 μm, and a semi-circle melt front), it is possible to estimate δ. Figure 9-9 represent the advancing melt flow and the 60 μm feature profile.

By adopting the Equation 6, it is possible to estimate the gap: by assuming R=175 μm and w=60 μm, δ resulted equal to 10 μm.

Equation 6
$$\delta = R - \sqrt{R^2 - w^2}$$

It is likely that this value did not permit the complete air discharge from the feature, and the consequent lack of filling of features normal to the flow find an explanation in this phenomenon.
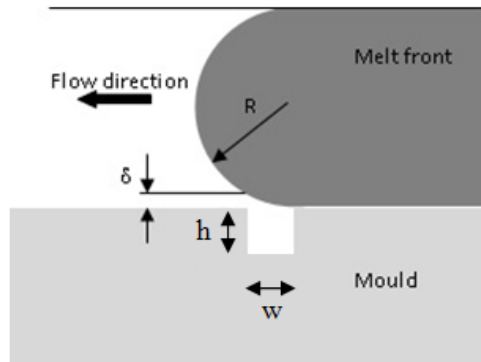
Figure 9-9. Scheme of advancing melting front. R is the radius of melt front; δ is the gap, h is the cavity deep and w the cavity width (both 60μm).

9.5 Summary

Micro-channels parallel to and normal to the flow direction, were manufactured for investigating the influence of processing parameters for filling features along the perpendicular direction (z-axis) with respect to the injection flow direction (x-axis). Moreover, micro-channels with a breadth of 60 μm (parallel to and normal to the flow direction) were optically investigated for determining if the orientation may affect the filling of channel with dimensions close to the lower mouldability limit.

Five factors were investigated: the injection speed, the holding pressure, the melt temperature, the mould temperature and the holding time. About the critical parameters that affect the filling along the z-axis, the interaction between mould temperature and injection speed affect the filling of parallel oriented features; whilst the interaction

between mould temperature and injection speed, and the single factor melt temperature, affect the filling of normal oriented features.

About the low mouldability limit, the value was identified around 60 µm: this result agreed with the general assumption to consider the average dimensions of smallest moulded feature around ten times larger than the MMD. Besides, it was observed that no features normal oriented were replicated; hence, the feature orientation can affect the filling of micro-channels. The absence of moulded channels oriented normal to the flow could be a consequence of entrapped air.

Chapter 10 . Discussion

The experimental results of single chapters were discussed previously. In this chapter, by starting from the thesis aim, the discussion was performed by analysing each single objective.

10.1 Thesis aim

The great numbers of aspects that may affect shrinkage are detectable by the literature review reported in chapter 2. Shrinkage can heavily affect the outcomes of moulded part, and scale effects did not permit to extrapolate directly the micro-scale results from macro-scale. By considering the importance that micro-moulding is assuming in these years and the number of defects that shrinkage can generate, the aim of the present thesis was to characterize the effects of shrinkage in micro-injection moulding.

10.2 Thesis objectives

Under the thesis aim, different objectives were identified. The objectives arise from the analysis of literature review gaps. More in details, the objectives were:

  i.   Set a standardised methodology suitable for the micro-scale (identified as research gap);

  ii. Statistically detect the critical processing parameters with the proposed methodology;

  iii. Characterize shrinkage in micro-injection moulding with the proposed methodology;

  iv. Identify and validate with a multiple quality criteria approach the combination of optimised processing parameters (identified as research gap);

v. To define the low mouldability limit of the feedstock and to determine the influence of feature orientation;

vi. To analyse the feedstock feature reproduction along the z-axis.

10.3 Discussion

The objectives listed in paragraph 10.2 were discussed in detail in the next paragraphs.

10.3.1 Standard methodology approach

The analysis of the literature review reported in chapter 2, permitted to identify a research gap in the absence of standardized methodology suitable to characterize moulding shrinkage at the micro-scale for injected moulded parts. Indeed, the material behaviour was affected by the scale and is not possible to extend the results obtained at the macro-scale in micro-scale. By starting from the more similar standard available for measuring shrinkage (ISO 294-3) a procedure suitable for the scale was proposed: the methodology implemented the entire standard except the dimensions adapted to the scale. The mould design was reduced of a factor of six: the micro-mould was manufactured and validated, and then specimens moulded. This methodology, as reported in the paragraph 10.2.2 and 10.2.3, established to be suitable for the micro-scale.

Moreover, the analysis of literature review has shown that shrinkage was affected not only by the scale but also by the geometry (paragraph 2.4.3.2 Design solutions at the micro-scale). Each author that investigated shrinkage has adopted the geometry considered most appropriate, but in such way, it was determined shrinkage connected to the particular geometry more than material behaviour. As result, shrinkage data available in the literature has to be considered within the geometry adopted. From this point of view, the standardized methodology proposed in this thesis can produce results "geometry free": this aspect demonstrated to be very useful in chapter 7, during the comparison between 316L feedstock and POM shrinkage.

10.3.2 Statistical detection of critical factors

Five processing parameters, chosen between the factors considered as critical by the literature review, were investigated. By exploring the mouldability region of tested

materials (POM and 316L feedstock), each parameter was identified with a range. By adopting a statistical approach (DoE), 16 combinations of processing values were arranged by an half fractional factorial matrix and results statistically processed.

The results were studied by using the Pareto chart, the main effects graph and the interaction plot. The Pareto chart is a bar chart that graphically ranks the criticity of factors from largest to smallest. By using this statistical tool the criticity of the factor (or combination of factors when the effect of a one factor depends on the level of the other factor) within the interval of confidence was determined. The main effects graph helps to visualize the effects of the critical factors identified by Pareto chart and to compare the relative strength of the effects. By considering the slope of the factor, it is possible to quantify the effect (the greater the slope of the line, the stronger the effect) and to draw a trend. When Pareto chart identify a combination of factors instead of a single factor as critical, the analysis was performed by using the interaction plot. The interaction plot draw a line for each factor: if the lines are parallel, then no interaction exists. Otherwise the greater the difference in slope between the lines, the higher the degree of interaction.

By processing the results with the statistical tools described above, it was possible to identify the critical parameters that affect shrinkage at the micro-scale.

The critical factors resulted from the statistical detection were confirmed by the literature results, by validating that the methodology adopted permitted to distinguish between parallel and normal shrinkage.

10.3.3 Shrinkage characterization

For determining POM and 316L feedstock shrinkage, was implemented all of ISO 294-4. This standard converts specimen measure in moulding (S_M), post-moulding (S_P) and total shrinkage (S_T) parallel to (p), and normal to (n), the flow direction.

After the statistical treatment of experimental data, were identified the following factors as critical (within the interval of confidence):

- POM, interval of confidence 95%: mould temperature for S_{Mp} and S_{Mn}; the combined effect between holding time and mould temperature for S_{Pn}; mould temperature, holding pressure, the combined effect between mould temperature

185

and holding pressure, melt temperature and the combined effect between melt temperature and mould temperature for S_{Tp}.

- 316L feedstock, interval of confidence 90%: mould temperature for S_{Pp} and the combined effect between holding pressure and injection pressure for S_{Tn}.

About the trends - except for POM S_{Mn} (that exhibited an increased response) and for POM S_{Pn} (undetermined trend) - shrinkages can be decreased by increasing the value of critical factor. The latter general trends were confirmed by Ong et al. [197] (that recommended high processing parameter values for reducing shrinkage) and by the literature review analysis: this evidenced that the approach followed in the present thesis is valid. However, the exceptions can be explained. Indeed, according to Table 2-9 results, the trend of mould temperature in the literature is not clearly identified and both the responses are present: by increasing this factor, shrinkage can increase or decrease. The trend of the critical combination that affect POM S_{Pn} cannot be clearly determined because of the antagonistic interaction between holding time and mould temperature: shrinkage can be decreased either by increasing holding time and decreasing mould temperature, than by decreasing holding time and increasing mould temperature. It is likely that the aliasing effects generated this situation, because the resolution of statistical model adopted (V) can confound the two terms interactions with the three terms interactions: for removing this aliasing, a full factorial model has to be adopted.

10.3.4 Multiple quality criteria optimization

Chapter 6 for POM and chapter 8 for 316L feedstock reports the optimization stage according to multiple quality criteria approach. The optimization implemented desirability functions that predict the factor combinations that fulfil the requests of shrinkage minimization and part mass maximization. This approach was considered to bridge another research gap because no works available in the literature considered these two aspects together. Moreover, few papers considered part mass as outcome because this factor is not a variable that can be easily controlled.

The optimized processing parameter values were experimentally validated and results have shown that:

- POM: shrinkage parallel to the flow decreased of 34% and shrinkage normal to the flow increased of 9.2% with respect to the shrinkage average values before the optimization; part mass increased of 3%.

- 316L feedstock: shrinkage parallel to the flow decreased of 30% and shrinkage normal to the flow decreased of 53% with respect to the shrinkage average values before the optimization; part mass increased of 4%.

The optimization results demonstrated that multiple quality criteria approach could efficiently fulfil both the requests. The lightly increment of POM normal to the flow shrinkage after optimization may be explained by considering that desirability functions represents a compromise between potentially-contradicting process conditions and effectiveness of results has to be always globally considered.

A consideration regarding the optimized parameter settings has to be made. As resulted from Table 6-4 for POM and Table 8-4 for 316L shrinkage, the optimized values resulted maximized, except injection pressure for POM, and holding time for 316L feedstock (both with their lower value). This result can be clarified by considering the trend of part mass and shrinkage critical factors: indeed, for both aspects, the accomplishment of requests (part mass maximization than shrinkage minimization) can be achieved only by maximizing the values of critical factors.

10.3.5 Feedstock low mouldability limit and orientation influence

The analysis of the feedstock low mouldability limit was achieved by optical analysis of the 60μm micro-feature manufactured in parallel to and normal to the flow direction. Results have shown that the feature parallel to the flow was reproduced 11 times above 16, whilst the feature normal to the flow was never filled. These outcomes permitted to establish the low mouldability limit value for the 316L feedstock (60 μm) and to prove the influence of texture orientation: both aspects were investigated in the literature and explained for pure polymers but not for feedstock, and the results reported in this chapter bridged this gap. The absence of features normal oriented could be due to the entrapped air that prevented the cavity filling of 60 μm feature with this particular orientation.

10.3.6 Feedstock feature reproduction along z-axis

Similarly to the low mouldability limit, data about the feature reproduction along a direction perpendicular (z-axis) to the flow direction (x-axis) was available only for pure polymer but not for feedstock: results reported in chapter 9 bridged this gap. The micro-mould was modified by manufacturing micro features with direction parallel to and normal to the flow. The height of the feature with a breadth of 600μm was converted in feature reproduction value (FR). The FR was statistically treated for determining the critical factors that influence the filling along the z-axis. Results has shown that, within the interval of confidence on 90%, the parallel oriented feature was critically affected by the combination between mould temperature and injection speed, whilst the normal oriented feature was critically affected by the combination between mould temperature and injection speed, and by the single factor melt temperature.

The only similar work present in the literature has investigated the filling behaviour of HDPE along the z-axis, and identified the mould temperature and the injection pressure as critical parameters. Compared to the prior work, results seem to confirm that a temperature (mould temperature) and a pressure related parameters (injection speed) affects replication quality. Differences may be caused by the different material investigated (a feedstock instead of pure polymer).

Chapter 11 . Conclusions

The conclusions were organized by using a scheme similar to the previous chapter. Besides, for each objective, it was highlighted the contribution to knowledge.

Even if not reported between the thesis objective, also the literature review on shrinkage can be considered a contribution, because not present elsewhere.

11.1 Standard methodology

The literature review stated that is not possible to extend shrinkage data from the macro to the micro-scale because the material behaviour is different between these two scales. Besides, the analysis of previous works shows that a tailored procedure was not jet suggested. For dealing with these problems, a micro-mould was manufactured by adapting the standard available at the macro-scale and a procedure for determining shrinkages in such scale was set. The specimen measurements were converted in shrinkage by following a standard and by adopting a protocol.

This approach demonstrated its correctness, because the results and their trend found confirmation in the literature: at the micro scale, temperature and pressure related parameters are the factors that greater affect shrinkage and their increase lead to reduce the dimensional variations of moulded parts.

As conclusion, it is possible to say that the proposed methodology successfully extended at the micro-scale the standard normally used for measuring shrinkage in conventional scale. This methodology allowed detecting with a standard the influence of processing parameters otherwise not directly deducible from conventional scale (evidences have shown the peculiar behaviour of material in such scale). The results have shown their reliability because confirmed the literature trend: generally, shrinkage was reduced by increasing the processing parameter values. Compared to the only prior work that adapted a conventional standard at the micro-scale (rectangular geometry), the proposed methodology (square geometry) provided more reliable results because designed for detecting normal to the flow shrinkage, and this can be considered an improvement of knowledge.

Moreover, the use of a standard permits to get over the limitations ordered by the geometry; indeed, the analysis of literature review has shown that shrinkage was affected not only by the scale but also this aspect. Each author that investigated shrinkage has adopted the geometry considered most appropriate, but in such way it was determined shrinkage connected to the particular geometry more than material behaviour. As result, shrinkages data available in the literature have to be considered within the geometry adopted. From this point of view, the standardized methodology proposed in this thesis can produce results "geometry free": this aspect demonstrated to be very useful during the comparison between 316L feedstock and POM shrinkage, but generally speaking can furnish objective information.

11.2 Statistical approach

Two possible statistical approaches were considered for dealing with shrinkage characterization: the DoE and the Taguchi methods. At the end of the analysis, the DoE demonstrated to be the most suitable technique for this research because of the initial "blind condition" and the impossibility to use the knowledge gained in previous works. According to the literature review, five processing parameters were considered as critical for micro-shrinkage: injection pressure, holding pressure, melt temperature, mould temperature and holding time. The five parameters were arranged according to the half-fractional factorial design; the injection speed replaces the injection pressure for studying the feedstock replication quality in Chapter 9.

The statistical methodology has drawn a path (screening, optimization, results) that allow identifying the critical parameters within an interval of confidence (95% for POM, 90% for 316L feedstock) that provide dependability to the results.

11.3 Shrinkage characterization

Once the standard methodology was set and the statistical approach has been decided, the characterization of shrinkage at the micro-scale can be pursued. The standard ISO 294-4 provide the guide for converting specimen dimensions in moulding, post moulding and total shrinkage parallel to, and normal to, the flow direction. The critical factors for POM and 316L feedstock, were summarized on Table 11-1.

316L feedstock	POM	
	Mould T	S_{Mp}
	Mould T	S_{Mn}
S_{Pp} Mould T		
	Hold t - mould T	S_{Pn}
	Mould T Hold P Mould T - hold P Melt T Mould T – melt T	S_{Tp}
S_{Tn} Hold P- Injection P		

Table 11-1. 316L feedstock and POM critical factors

Results show that temperature related parameters strongly affects pure polymer, whilst pressure related parameters seems to influence the feedstock. Concerning the percentage values, pure polymer total shrinkage is about five times more in parallel to the flow (5.089±1.658) and six times more in normal to the flow (3.026±0.266) with respect to feedstock (0.867±0.274 and 0.590±0.227 respectively). Moreover, the polymer total shrinkage in parallel to the flow direction is 68% greater than normal direction; for the feedstock, it is 47%. At last, the spherical steel powder is thought to influence shrinkage as it makes the feedstock more isotropic with respect to crystalline pure polymer.

Conclusion about the results highlight how is not negligible the possibility to discriminate, throughout the adoption of a standard, different type of shrinkages along different directions. This aspect can enrich the literature because fewer works discriminated between shrinkage directions, and no one reported the difference in terms of shrinkage after 1 hour (moulding shrinkage) and 24 hours (post-moulding and total shrinkage). Is desirable that the standardized approach at the micro-scale will be widely applied because it has been shown to provide detailed information on the shrinkage behavior, and this can improve the knowledge of this phenomenon at the micro-scale.

These results could be used for considering the outcomes from a pure speculative point of view: the reason of different number of critical parameters could be the consequence of thermal effects. This thesis has shown that 316L feedstock is affected by fewer temperature related factors with respect to POM. According to previous works, thermal conductivity of feedstock is 3.35 $Wm^{-1}°C^{-1}$ [213], whilst for POM is 0.36 $Wm^{-1}°C^{-1}$

[214; 215]. The consequence of the increased feedstock thermal conductivity is high heat dissipation during the injection moulding processing [213]. Because of the increased thermal conductivity, the feedstock moulded part cools quickly [12; 216] with respect to POM. According to this behaviour, it is reasonable to assume that the increased feedstock thermal conductivity could determine the lower influence of temperature parameters compared to the pure binder results. A more focused research should be performed on such direction, but the standardized methodology presented in this thesis suggested a trend that deserves further checks.

11.4 Multiple quality criteria optimization

The optimization of processing parameters follows the identification of critical factors. According to the literature review results, the optimization stage is a usual and widely adopted procedure for obtaining outcomes that fulfil with some specific request. Considering the standard methodology adopted (DoE), the use of desirability functions has demonstrated in other researches to suggest correct predictions of optimized parameters. However, optimization stages usually considered one request at time.

The novelties presented in the present thesis was the simultaneous request of two conditions (few time adopted), and the adoption of a parameter never used as outcome before. About the two conditions, it was requested both shrinkage minimization than part mass maximization. Moreover, the part mass is a difficult factor to consider in an experiment because not easily controllable (as processing parameters) and because can be affected by the same factors that influence shrinkage. Under these conditions, desirability functions were used as parameters for monitoring the fulfillment of optimization: to operate under desirability value equal to one means that the requests can be achieved.

The next validation step implemented the optimized values for moulding a specimen, and comparisons between average values before the optimization and specimen moulded with optimized parameters, confirmed that shrinkage was reduced and part mass was increased.

Table 11-2 reports the optimized parameters results.

	$S_{Tp\ opt}$ [%]	$S_{Tn\ opt}$ [%]	W [mg]
POM	3.352±0.001	3.298±0.004	49.42±0.08
316L feedstock	0.590±0.004	0.283±0.002	211.79±0.65

Table 11-2. Optimized parameters results.

Conclusions of multiple quality criteria optimization shows that desirability functions can be used for determining optimized parameters among different requests, and part mass can be proficiently adopted as experiment factor. Contribution to knowledge was to enhance the cases that this statistical function could analyse. This proposes that the next step could be to consider more than two requests to be optimized and see if the desirability functions can fulfil the new conditions: if not, it could be necessary to identify the function limits and offer a solution. This approach is more statistical oriented, but can be performed by using the micro-mould proposed in this thesis.

11.5 Low mouldability and feature orientation of feedstock.

The study of the orientation influence during replication of channels with dimensions close to the lower feedstock mouldability limit was performed by manufacturing micro-features parallel and normal oriented with respect to the melt flow. This aspect has been considered worthy of being studied because the only prior work investigated a pure polymer. Literature conclusions agreed that the smallest feature to be replicated could be ten times larger than the mean particle diameter of powder.

The results permitted to identify feedstock lower mouldability limit (60 μm) and evidenced that features normal to the flow oriented was never replicated (on the contrary, the features parallel to the flow were replicated 11 times above 16). This last result confirms the easier replicability of the features parallel to the flow oriented with respect the normal to the flow oriented already observed with pure polymers. It is likely that normal to the flow features were not replicated for an air entrapment phenomenon along this direction.

This section can be considered an improvement of knowledge from different point of view. Concerning the feedstock, two outcomes not previously achieved were established: the low mouldability value and the influence of features orientation in terms of replication. Besides, the influence of orientation for feedstock-moulded parts has to be carefully considered during design of micro-parts. As confirmed also by the

literature review, specimen design is an important aspect and the air entrapment can cause unexpected problems if not take into account.

The phenomenon of trapped air could be further investigated with the mould with micro-features designed in this thesis. Indeed, it could be possible to consider alternative techniques for dealing with the problems caused by the air inside the normal to the flow oriented features. The authors [207] removed the problem by vacuuming the mould, and similar solution could be reproduced in this case. According to the results reported by [207], this solution permits to increase the feature reproduction.

11.6 Feedstock feature reproduction

The micro-features were used for determining the factors that critically affect the feedstock feature reproduction: this aspect was considered worthy of being studied because the only prior work investigated a pure polymer. The height of the texture was compared with respect to the cavity mould deep, and data about the feature reproduction of micro-features parallel to and normal to the flow direction was obtained. The results were statistically studied, and it was possible to determine the critical factors that affect the filling dynamic along a perpendicular direction (z-axis) with respect to the flow direction (x-axis). In detail, the combined effect between mould temperature and injection speed was considered critical for the reproduction of features in parallel to the flow direction; whilst the combined effect between mould temperature and injection speed and the single factor melt temperature were considered critical for the replication of features normal to the flow oriented. Even if the only prior work investigated a pure polymer, the influence of temperature and pressure related parameters were confirmed.

This study contributed to improve the knowledge of critical parameters that affect the feedstock filling mechanisms along a direction (z-axis), an aspect few time considered.

Respecting the importance of temperature parameters (according to the results of chapter 9) for filling the micro-features along the z-axis, the micro-mould adopted in this thesis could be implemented by modifying the mould as a variotherm type, similarly to [207]. The variotherm approach permits to incorporate into a mould a rapid heating/cooling system, a vacuum unit, hot sprue and cavity pressure transducer [217] and to avoid the freezing of polymer melt when the flow is in contact with relatively

cold cavity wall: during the injection stage, the mould temperature is increased for achieving the complete cavity filling, then the mould temperature is reduced for a easy ejection. This approach demonstrated to increase the feature reproduction (especially for features with high aspect ratio), to remove the problem of air entrapment and to reduce the cycling time.

Chapter 12 . Future work

The different aspects raised during this thesis may be further studied.

- The reason of the specimens' expansion for post-moulding shrinkage (values with sign minus in Table 5-3 and Table 7-3) is actually not well established. This behaviour could be due to an over pressure of material (especially for metal powder in 316L feedstock) during the injection stage followed by a sort of relaxation after moulding. A more focused analysis of this phenomenon could be performed by positioning strain gages inside the mould (similarly to other works that investigated injection pressure inside the cavity mould during the injection) for connecting injection and holding pressure to material (polymer or feedstock) packing arrangement inside the specimen.

- The relationship between powder density and processing parameters is not properly known. The moulded parts could be analyzed with a NDT technique (X-ray tomography) for mapping the powder distribution and connect this aspect to processing parameters, then the procedure adopted in the present thesis could be used for optimizing the powder distribution. This aspect deserves to be optimized because it is known that a uniform powder distribution produce lower likelihood of cracking during debinding and sintering steps. The mapping of powder distribution could contribute to explain the specimens expansion observed during the post-moulding shrinkage as well.

- The fewer number of temperature related parameters for 316L feedstock compared to POM did not find explanation in the literature. It has known that the increased 316L feedstock thermal conductivity decreased the cooling time, but if this can affect also the critical parameters connected to the temperature and their number is actually unknown. The absence of experimental results and theoretical models that investigated this trend merit to be further studied by adding rheological and thermal characterizations to shrinkage investigation.

- There are no data about feedstock shrinkage at the micro-scale along the z-axis (perpendicularly to the flow direction). This problem could be approached by

196

designing a micro-mould with different aspect ratio features. However, on the contrary with respect to the design adopted in chapter 9, it is necessary that the features have to be filled by a uniform melt front along the z-axis because − similarly to the conditions assured by the standard design adopted in the present thesis − shrinkage standard requests these conditions. By filling this gap it could be possible to complete the knowledge of material behaviour in all the three directions (x, y and z-axes), and results used for making the modelling approach more reliable.

- The modelling aspect represents another field that has to be further investigated. As stated recently by [218], still there is a gap between simulation and experimental tests as result of simplifications and error of approximations. The first modelling programs (in the Eighties) [219] approached the problem by adapting macro results to micro scale. Nowadays this approach was improved by considering more complex aspects connected to the particular conditions of the micro scale as the different polymer behaviour with respect to the macro-scale, the slip wall phenomenon caused by the higher shear rate at the micro-scale, the risk of powder segregation in case of feedstock injected and the different thermal behaviour between feedstock and polymer [220]. For dealing with these aspects, modern modelling software (i.e. Sigmasoft 3D) considered also rheological data set for the scale (capillary rheometer). A more focused knowledge of micro-scale data should be used for creating dedicated software for μ-IM and μ-PIM modelling and the approach proposed in this thesis for determining shrinkage at the micro-scale can work in such sense.

A great number of researches investigated the modelling, and an exhaustive discussion about these studies is beyond the aims of this thesis. However for further details, works that investigated the modelling at the micro scale were published by [221] (the authors highlighted differences between experiments and numerical investigations likely due to the incorrect assumption of a model based on Newtonian fluid behaviour, not suitable for the scale) and by [222]. Concerning the conventional scale, it is possible to consider [223] (the authors suggested to adopt artificial intelligence system as neural network for enhancing

the modelling approach) and [224-228]. At last, an interesting approach for dealing with the problem of modelling was reported by [229] that adopted COMSOL 4.0 for the micro-scale flow simulation and MOLDFLOW MPI 6.2 for the macro-scale case. The authors proposed a multi-scale method: in a first step conventional methods were applied to the macro-scale flow then, in a second step, the result of the macro-scale flow was implemented by taking as an inlet the slip and surface tensions boundary conditions. This approach demonstrated its validity and could represent a valid solution for reducing the gap between simulation and experimental results.

- The standardized methodology was investigated by using DoE but not Taguchi methods. The robustness of the methodology proposed in the present thesis is actually unknown, and Taguchi could give relevant information in such direction.

References

[1]   Attia, U. M. and Alcock, J. R. (2011), "A review of micro-powder injection moulding as a microfabrication technique", *J. Micromech. Microeng.,* vol. 21, no. 4.

[2]   Sparrow, N. (1999), *The Microtechnology Revolution,* , EMDM (European Medical Device Manufacture): March/April 1999: Special Report on Microtechnology.

[3]   Gabriel, K. J. (ed.) (1995), *Engineering Microscopic Machines,* 150th Anniversary Issue, Scientific American: Technology in the 21st Century ed, .

[4]   Lippmann, J. M., Geiger, E. and Pisano, A. (2007), "Polymer investment molding: method for fabricating hollow, microscale parts", *Science Direct, Sensors and Actuators,* vol. A 134, pp. 2-10.

[5]   Buchenauer et al. (2009), "Microbioreactors with microfluidic control and a user-friendly connection to the actuator hardware", *Journal of Micromechanics and Microengineering,* vol. 19.

[6]   Jejurkan, E. and Mishra, D. (2009), "A review of recent patents on micro-combustion and applications", *Recent Paper of Engineering,* vol. 3, pp. 194-209.

[7]   Injection   moulding   process   ,   available   at: http://shodhganga.inflibnet.ac.in/bitstream/10603/3400/8/08_chapter%202.pdf (accessed June 2013).

[8]   Zhao, J., Mayes, R. H., Chen, G., Xie, H. and Chan, P. S. (2003), "Effects of Process Parameters on the Micro Molding Process", *Polymer Engineering and Science,* vol. 43, no. 9, pp. 1542-1554.

[9]   Forcada, M. L. and Mate, C. M. (1993), "The flow of thin viscous-liquid films on rotating-disk", *Colloid Interface Science,* vol. 169, pp. 218-225.

[10]   Eringen, A. C. and Okada, K. (1995), "A lubrication theory for fluids with microstructure", *Int. J. Eng.Sci.,* vol. 33, pp. 2297-2308.

[11]   Yao, D. and Kim, B. (2002), "Simulation of the filling process in micro channels for polymeric materials", *Journal of Micromechanics and Microengineering,* vol. 12, no. 5, pp. 604-610.

[12]   Atre, S. V., Park, S. J., Zauner, R. and German, R. M. (2007), "Process simulation of powder injection moulding: identification of significant parameters during mould filling phase", *Powder Metallurgy,* vol. 50, pp. 76-85.

[13]   Sotomayor, M. E., Várez, A. and Levenfeld, B. (2010), "Influence of powder particle size distribution on rheological properties of 316L powder injection moulding feedstocks", *Powder Technology,* vol. 200, no. 1-2, pp. 30-36.

[14]   González-Gutiérrez, J., Stringari, G. B. and Emri, I. *, Powder Injection Molding of Metal and Ceramic Parts*, available at: http://www.intechopen.com/books/some-critical-issues-for-injection-molding/powder-injection-molding-of-metal-and-ceramic-parts- (accessed May 2013).

[15]   BASF site *,   http://www.basf.com/group/corporate/en/* (accessed September 2012).

[16]   Anonymous *, Catamold processing instructions-BASF technical informations*, available   at: http://docsfiles.com/view.php?view=http://www.catamold.de/cm/internet/Catamold/en_GB/function/conversions:/publish/content/Microsite/Catamold/Technische_Informationen_/Verfahrensanweisungen/GeneralProcessingInstructions_Catamold_MIM.pdf&keyword=catamold ao f&count= (accessed 30 May 2013).

[17]   Fischer, J. M. (2003), "Handbook of molded part shrinkage and warpage-Determination of shrinkage", in Inc. Brent Beckley (ed.) , pp. 10.

[18]   Stan, D., Tulcan, A., Tulcan, L. and Iclanzan, T. (2008), "Influence factors on the dimensional accuracy of the plastic parts", *Materiale Plastice,* vol. 45, no. 1, pp. 119-124.

[19]   Liu, F., Zeng, S., Zhou, H. and Li, J. (2012), "A study on the distinguishing responses of shrinkage and warpage to processing conditions in injection molding", *Journal of Applied Polymer Science,* vol. 125, no. 1, pp. 731-744.

[20]   Wang, J., Xie, P., Yang, W. and Ding, Y. (2010), "Online pressure-volume-temperature measurements of polypropylene using a testing mold to simulate the injection-molding process", *Journal of Applied Polymer Science,* vol. 118, no. 1, pp. 200-208.

[21]   Wang, Y. *, PVT Properties of Polymers for Injection Molding (last access date 15 February 2013),* available at: http://cdn.intechopen.com/pdfs/33643/InTech-Pvt_properties_of_polymers_for_injection_molding.pdf.

[22]   Tan, H. -., Yu, Y. -., Xing, L. -., Zhao, L. -. and Sun, H. -. (2013), "Density and Shrinkage of Injection Molded Impact Polypropylene Copolymer/Coir Fiber Composites", *Polymer - Plastics Technology and Engineering,* vol. 52, no. 3, pp. 257-260.

[23]   Isayev, A. I., Kwon, K. and Kim, K. H. (2006), "Anisotropic shrinkage in injection molding of various polyesters", *Annual Technical Conference - ANTEC, Conference Proceedings,* Vol. 3, pp. 1190.

[24]   Coppola, S., Grizzuti, N. and Maffettone, P. L. (2001), "Microrheological modeling of flow-induced crystallization.", *Macromolecules,* vol. 34, pp. 5030–5036.

[25]   Chang, Y., Liu, C. S., Huang, S. T., Huang, C. -., Chen, M. -. and Yang, W. -. (2009), "Dynamic property of the frozen-layer and its effects on warpage in injection molded parts", *Annual Technical Conference - ANTEC, Conference Proceedings,* Vol. 5, pp. 2905.

[26]   Giroud, T. and Vincent, M. (2004), "Evaluation of residual stresses in short fiber reinforced thermoplastic molded parts", *Mecanique et Industries,* vol. 5, no. 4, pp. 481-487.

[27]   Shen, C., Kramschuster, A., Ermer, D. and Turng, L. -. (2006), "Study of shrinkage and warpage in microcellular co-injection molding", *International Polymer Processing,* vol. 21, no. 4, pp. 393-401.

[28]   Sepe, M. (2013), "Dimensional stability after molding - Part 2", *Plastics Technology,* vol. 59, no. 2, pp. 17-19.

[29]   De Santis, F., Pantani, R., Speranza, V. and Titomanlio, G. (2010), "Analysis of shrinkage development of a semicrystalline polymer during injection moulding", *Ind. Eng. Chem. Res.,* vol. 49, pp. 2469–2476.

[30]   Greene, C. D. and Heaney, D. F. (2004), "The PVT effect on final sintered MIM components", *Annual Technical Conference - ANTEC, Conference Proceedings,* Vol. 1, pp. 713.

[31]   Chang, T. C. and Faison, E. (May 2001), "A study of the effect of process conditionson the shrinkage of plastic parts in injection molding by the Taguchi method", *Polymer Engineering & Science,* vol. 41, no. 5, pp. 703-710.

[32]   Yang, S. Y., Huang, C. K., Lin, B. C. and Wei, W. C. J. (2006), "Kneading and molding of ceramic microparts by precision powder injection molding (PIM)", *Journal of Applied Polymer Science,* vol. 100, no. 2, pp. 892-899.

[33]   Huang, C. K. and Chiu, S. W. (2005), "Formability and accuracy of micropolymer compound with added nanomaterials in microinjection molding", *Journal of Applied Polymer Science,* vol. 98, no. 5, pp. 1865-1874.

[34]   Zhang, J., Huang, B., Li, Y. and Li, S. (2004), "Influence of microcrystalline wax on properties of MIM multi-component wax matrix binder", *Xiyou Jinshu Cailiao Yu Gongcheng/Rare Metal Materials and Engineering,* vol. 33, no. 10, pp. 1084-1088.

[35]   Sri Yulis M. Amin, Khairur Rijal Jamaludin and Norhamidi Muhamad (2009), "Rheological properties of SS316L MIM feedstock prepared with different particle sizes and powder loadings", *The Institution of Engineers, Malaysia,* vol. 71, no. 2.

[36]   Zauner, R., Binet, C., Heaney, D. F. and Piemme, J. (2004), "Variability of feedstock viscosity and its correlation with dimensional variability of green powder injection moulded components", *Powder Metallurgy,* vol. 47, no. 2, pp. 151-156.

[37]   Fanghui, L., Chao, G., Xian, W., Xinyuan, Q., Hong, L. and Jie, Z. (2012), "Morphological comparison of isotactic polypropylene parts prepared by micro-injection molding and conventional injection moulding", *Polym. Adv. Technol.,* , no. 23, pp. 686-694.

[38]   Jingsong, C., Hrymak, A. and Kamal, M. R. (2007), "Microstructural characteristics of micro-injection molded thermoplastics", *Annual Technical Conference - ANTEC, Conference Proceedings,* Vol. 4, pp. 1973.

[39]   Somani, R. H., Yang, L., Zhu, L. and Hsiao, B. S. (2005), "Flow-induced shish-kebab precursor structures in entangled polymer melts", *Polymer,* vol. 46, pp. 8587-8623.

[40]   Giboz, J., Copponnex, T. and Mélé, P. (2007), "Microinjection molding of thermoplastic polymers: A review", *Journal of Micromechanics and Microengineering,* vol. 17, no. 6, pp. R96-R109.

[41]   Chu, J., Kamal, M. R., Derdouri, S. and Hrymak, A. (2008), "Effects of processing conditions on mechanical properties and crystallinity of micro injection molded thermoplastics", *Technical Papers, Regional Technical Conference - Society of Plastics Engineers,* Vol. 4, pp. 2451.

[42]   Autronic Plastic, I. *, Glossary of plastic injection moulding*, available at: http://www.apisolution.com/images/glossary_plastic_injection_molding_engineering_manufacturing.pdf (accessed January 2013).

[43]   Azdast, T. and Behravesh, A. H. (2008), "An analytical study of constrained shrinkage of injection molded semi-crystalline plastic parts", *Polymer - Plastics Technology and Engineering,* vol. 47, no. 12, pp. 1265-1272.

[44]   Chen, C. -. A. and Chang, S. -. (2008), "Shrinkage analysis on convex shell by injection molding", *International Polymer Processing,* vol. 23, no. 1, pp. 65-71.

[45]   Mehat, N. M., Kamaruddin, S. and Othman, A. R. (2012), "A study of hybrid optimization of injection moulding process parameters for plastic gear", *Advanced Materials Research,* vol. 591-593, pp. 2135-2138.

[46]   Elleithy, R., Ali, I., Al-Haj Ali, M. and Al-Zahrani, S. M. (2011), "Different factors affecting the mechanical and thermo-mechanical properties of HDPE reinforced with micro-CaCO3", *Journal of Reinforced Plastics and Composites,* vol. 30, no. 9, pp. 769-780.

[47]   Xu, Y. -., Yang, W., Xie, B. -., Liu, Z. -. and Yang, M. -. (2009), "Effect of injection parameters and addition of nanoscale materials on the shrinkage of polypropylene copolymer", *Journal of Macromolecular Science, Part B: Physics,* vol. 48, no. 3, pp. 573-586.

[48]   Kramschuster, A., Cavitt, R., Ermer, D., Chen, Z. and Turng, L. S. *, Quantitative study of shrinkage and warpage behavior for microcellular and conventional injection molding*, available at: http://www.trexel.com/download/UWisconsinStudy.pdf (accessed 24 April 2013).

[49]   Othman, M.H., Shamsudin, S. and Hasan, S., (2012), *The effects of parameter settings on shrinkage and warpage in injection molding through cadmould 3D-F simulation and taguchi method*.

[50]   Jayanarayanan, K., Karthick, H. S., Suganya, V., Shivashankari, A. L. and Bhagawan, S. S. (2006), "Optimization of process parameters of an injection moulded gear using taguchi methodology", *Annual Technical Conference - ANTEC, Conference Proceedings,* Vol. 2, pp. 1088.

[51]   AlKaabneh, F. A., Barghash, M. and Mishael, I. (2012), "A combined analytical hierarchical process (AHP) and Taguchi experimental design (TED) for plastic injection molding process settings", *International Journal of Advanced Manufacturing Technology,* , pp. 1-16.

[52]   Oktem, H., Erzurumlu, T. and Uzman, I. (2007), "Application of Taguchi optimization technique in determining plastic injection molding process parameters for a thin-shell part", *Materials and Design,* vol. 28, no. 4, pp. 1271-1278.

[53]   Kramschuster, A., Cavitt, R., Ermer, D., Chen, Z. and Turng, L. -. (2005), "Warpage comparison between microcellular and conventional injection molding", *Annual Technical Conference - ANTEC, Conference Proceedings,* Vol. 2, pp. 151.

[54]   Kramschuster, A., Cavitt, R., Ermer, D., Chen, Z. B. and Turng, L. -. (2006), "Effect of processing conditions on shrinkage and warpage and morphology of injection moulded parts using microcellular injection moulding", *Plastics, Rubber and Composites,* vol. 35, no. 5, pp. 198-209.

[55]   Yadav, A. J., Dravid, S. V. and Rajput, V. D. (2012), "Taguchi technique in optimization of injection molding process parameters for manufacturing plastic parts", *Proceeding of the NCNTE-2012,* Feb 24-25 2012, .

[56]   Rezavand, S. A. M. and Behravesh, A. H. (2007), "An experimental investigation on dimensional stability of injected wax patterns of gas turbine blades", *Journal of Materials Processing Technology,* vol. 182, pp. 580–587.

[57]   Luo, T. G., Qu, X. H., Qin, M. L. and Ouyang, M. L. (2009), "Dimension precision of metal injection molded pure tungsten", *International Journal of Refractory Metals and Hard Materials,* vol. 27, no. 3, pp. 615-620.

[58]   Green, J.   *,   Shrinkage   -   Chapter   8*,   available   at: http://www.csuchico.edu/~jpgreene/m243/m243_ch08/m243_ch08.ppt   (accessed June 2013).

[59] Bryce, D. M. , *Injection moulding stages*, available at: http://www.plastictroubleshooter.com/ThePlasticTroubleshooter/molding_process.htm (accessed June 2013).

[60] Wu, C. -. and Huang, Y. -. (2007), "The influence of cavity deformation on the shrinkage and warpage of an injection-molded part", *International Journal of Advanced Manufacturing Technology,* vol. 32, no. 11-12, pp. 1144-1154.

[61] Jin, J., Yu, H. Y. and Lv, S. (2009), "Optimization of plastic injection molding process parameters for thin-wall plastics injection molding", *Advanced Materials Research,* vol. 69-70, pp. 525-529.

[62] Chiang, K. -. and Chang, F. -. (2006), "Application of grey-fuzzy logic on the optimal process design of an injection-molded part with a thin shell feature", *International Communications in Heat and Mass Transfer,* vol. 33, no. 1, pp. 94-101.

[63] Alam, M. M. and Kumar, D. (2013), "Reducing shrinkage in plastic injection moulding using Taguchi method in Tata magic head light", *International Journal Of Science and research,* vol. 2, no. 2, pp. 107-110.

[64] Pontes, A. J. and Pouzada, A. S. (2004), "Ejection force in tubular injection moldings. Part I: Effect of processing conditions", *Polymer Engineering and Science,* vol. 44, no. 5, pp. 891-897.

[65] Passilla, J. and Zupancic, K. (2005), "Warpage study on two-shot injection molding", *Annual Technical Conference - ANTEC, Conference Proceedings,* Vol. 10, pp. 93.

[66] Koppi, K. A., Barger, M. A., Chang, D. and Shields, C. (2007), "In-mold part shrinkage rate measurement", *Annual Technical Conference - ANTEC, Conference Proceedings,* Vol. 1, pp. 561.

[67]   Pontes, A. J., Oliveira, M. J. and Pouzada, A. S. (2004), "The effect of holding pressure on the shrinkage and birefringence of injection moulded polypropylene plates", *Materials Science Forum,* vol. 455-456, pp. 814-817.

[68]   Trejo, M., Villablanca, V., Sánchez, J. J., Morales, R. A., Villarroel, S. and Gordillo, A. (2008), "Use of linear relationships and simulation to assess the effect of the injection parameters on the dimensions of polypropylene test specimens", *Technical Papers, Regional Technical Conference - Society of Plastics Engineers,* Vol. 1, pp. 445.

[69]   Altan, M. (2010), "Reducing shrinkage in injection moldings via the Taguchi, ANOVA and neural network methods", *Materials and Design,* vol. 31, no. 1, pp. 599-604.

[70]   Othman, M. H., Hasan, S., Muhammad, W. N. A. W. and Zakaria, Z. (2013), "Optimising injection moulding parameter setting in processing polypropylene-clay composites through Taguchi method", *Applied Mechanics and Materials,* vol. 271, no. PART 1, pp. 272-276.

[71]   Kusić, D., Kek, T., Slabe, J. M., Svečko, R. and Grum, J. (2013), "The impact of process parameters on test specimen deviations and their correlation with AE signals captured during the injection moulding cycle", *Polymer Testing,* vol. 32, no. 3, pp. 583-593.

[72]   Tseng, W. J. (1998), "Statistical analysis of process parameters influencing dimensional control in ceramic injection molding", *Journal of Materials Processing Technology,* vol. 79, no. 1-3, pp. 242-250.

[73]   Chen, R. -., Ho, C. -. and Fan, H. -. (2004), "Shrinkage properties of ceramic injection moulding part with a step-contracted cross-section in the filling direction", *Ceramics International,* vol. 30, no. 6, pp. 991-996.

[74]   Pomerleau, J. and Sanschagrin, B. (2006), "Injection molding shrinkage of PP: Experimental progress", *Polymer Engineering and Science,* vol. 46, no. 9, pp. 1275-1283.

[75]   Liao, S. J., Chang, D. Y., Chen, H. J., Tsou, L. S., Ho, J. R., Yau, H. T. and Hsieh, W. H. (2004), "Optimal process conditions of shrinkage and warpage of thin-wall parts", *Polymer Engineering & Science,* vol. 44, no. 5, pp. 917-928.

[76]   Chih, C. C., Pao, L. S. and Yan, C. L. (2009), "Analysis and modeling of effective parameters for dimension shrinkage variation of injection molded part with thin shell feature using response surface methodology", *Int J Adv Manuf Technol,* vol. 45, pp. 1087-1095.

[77]   Sepe, M. (2013), "Dimensional stability after molding: Part 1", *Plastics Technology,* vol. 59, no. 1, pp. 13-14.

[78]   Fernandes, C., Pontes, A. J., Viana, J. C. and Gaspar-Cunha, A. (2010), "Using multiobjective evolutionary algorithms in the optimization of operating conditions of polymer injection molding", *Polymer Engineering and Science,* vol. 50, no. 8, pp. 1667-1678.

[79]   Pontes, A. J. and Pouzada, A. S. (2006), "Predicting shrinkage in semi-crystalline injection mouldings - The influence of pressure", *Materials Science Forum,* vol. 514-516, no. PART 2, pp. 1501-1505.

[80]   Mulyana, R., Daniel, T., Min, Y., Castro, J. M. and Lee, L. J. (2010), "The use of water containing TPO/activated carbon in injection molding", *Annual Technical Conference - ANTEC, Conference Proceedings,* Vol. 2, pp. 1339.

[81]   Zhang, Z. and Jiang, B. (2007), "Optimal process design of shrinkage and sink marks in injection molding", *Journal Wuhan University of Technology, Materials Science Edition,* vol. 22, no. 3, pp. 404-407.

[82]   Dangayach, G. S. and Kumar, D. (2012), "Reduction in defect rate by Taguchi method in plastic injection molded components", *Advanced Materials Research,* vol. 488-489, pp. 269-273.

[83] Huang, M. -. and Hsu, H. -. (2011), "Influence of injection moulding and sintering parameters on properties of 316L MIM compact", *Powder Metallurgy,* vol. 54, no. 3, pp. 299-307.

[84] Ozek, C. and Celik, Y. H. (2012), "Calculating Molding Parameters in Plastic Injection Molds with ANN and Developing Software", *Materials and Manufacturing Processes,* vol. 27, pp. 160-168.

[85] Guan, W. -. and Huang, H. -. (2011), "Effect of backward melt flow on injection-compression molded part thickness distribution", *Annual Technical Conference - ANTEC, Conference Proceedings,* Vol. 2, pp. 1523.

[86] Lenz, J., Enneti, R. K., Park, S. and Atre, S. V. (2013), "Powder Injection Molding Process Design For UAV Engine Components Using Nanoscale Silicon Nitride Powders", *Ceramics International,* , no. article in press.

[87] Gutowski, T. , *Injection moulding*, available at: http://web.mit.edu/2.810/www/lecture/Injection_Molding.pdf (accessed June 2013).

[88] Yoshihara, N. (2008), "Molding shrinkage and warpage for reinforced poly(ethylene terephthalate)", *Journal of Polymer Engineering,* vol. 28, no. 6-7, pp. 449-465.

[89] Rudolph, N., Kühnert, I. and Ehrenstein, G. W. (2009), "Compression induced solidification (CIS) - A novel injection molding strategy for high precision parts", *Annual Technical Conference - ANTEC, Conference Proceedings,* Vol. 4, pp. 2087.

[90] Zhang, H., Li, M. and Yang, L. (2011), "Optimization of packing pressure curve in injection molding based on numerical simulation", *Advanced Materials Research,* vol. 221, pp. 522-527.

[91] Subramanian, N. R., Tingyu, L. and Seng, Y. A. (2005), "Optimizing warpage analysis for an optical housing", *Mechatronics,* vol. 15, no. 1, pp. 111-127.

[92]   Huang, H. -., Yang, C. and Li, K. (2009), "Effects of process parameters on shrinkage uniformity and birefringence of injection-compression molded parts", *ASME International Mechanical Engineering Congress and Exposition, Proceedings,* Vol. 15, pp. 193.

[93]   Chang, Y., Huang, S. T., Huang, S. -., Chen, S. -., Huang, C. -., Chen, M. C. and Yang, V. (2009), "Warpage management using three dimensional thickness control method in injection molding", *Annual Technical Conference - ANTEC, Conference Proceedings,* Vol. 4, pp. 2429.

[94]   Hussin, R., Mohd Saad, R., Hussin, R. and Mohd Dawi, M. (2012), "An optimization of plastic injection molding parameters using Taguchi optimization method", *Asian Transaction of Engineering - ATE ISSN: 2221-4267,* vol. 2, no. 5.

[95]   Huang, H. -., Li, K. and Li, S. (2008), "Effects of processing parameters on shrinkage uniformity of injection-compression molded part", *Technical Papers, Regional Technical Conference - Society of Plastics Engineers,* Vol. 1, pp. 400.

[96]   Huang, H. -., Li, K. and Li, S. (2009), "Injection-compression molded part shrinkage uniformity comparison between emicrystalline and amorphous plastics", *Polymer - Plastics Technology and Engineering,* vol. 48, no. 1, pp. 64-68.

[97]   Chen, C. -., Su, P. -. and Lin, Y. -. (2009), "Analysis and modeling of effective parameters for dimension shrinkage variation of injection molded part with thin shell feature using response surface methodology", *International Journal of Advanced Manufacturing Technology,* vol. 45, no. 11-12, pp. 1087-1095.

[98]   Rajalingam, S., Bono, A. and Sulaiman, J. *, Determining optimal moulding process parameters by two level factorial design with center point*, available at: http://www.sljol.info/index.php/SLJAStats/article/view/4968 (accessed 24 April 2013).

[99]   Prashantha, K., Soulestin, J., Lacrampe, M. F., Lafranche, E., Krawczak, P., Dupin, G. and Claes, M. (2009), "Taguchi analysis of shrinkage and warpage of

injection-moulded polypropylene/multiwall carbon nanotubes nanocomposites", *eXpress Polymer Letters,* vol. 3, no. 10, pp. 630-638.

[100] Liang, J. -., Qi, W., Li, Y. and Liu, C. -. (2008), "Microcellular injection molding process for car instrument panel", *Gaofenzi Cailiao Kexue Yu Gongcheng/Polymeric Materials Science and Engineering,* vol. 24, no. 3, pp. 113-117.

[101] Hwang, S. -., Hsu, P. P. and Chiang, C. -. (2007), "Shrinkage study of textile roller molded by the microcellular injection process", *Annual Technical Conference - ANTEC, Conference Proceedings,* Vol. 2, pp. 737.

[102] Liu, Y., Song, M. C., Wang, M. J. and Zhang, C. Z. (2009), "Quality defects and analysis of the microfluidic chip injection molding", *Materials Science Forum,* vol. 628 629, pp. 417-422.

[103] Xie, L., Shen, L. and Jiang, B. *, Modelling and simulation for micro-injection molding process*, available at: http://cdn.intechopen.com/pdfs/16394/InTech-Modelling_and_simulation_for_micro_injection_molding_process.pdf (accessed July 2013).

[104] Thakur, V. and Angstadt, D. C. (2007), "Influence of temperature on micro-feature replication at ambient pressure in micro-molding", *Annual Technical Conference - ANTEC, Conference Proceedings,* Vol. 5, pp. 2936.

[105] Ong, N. S., Zhang, H. and Woo, W. H. (2006), "Plastic Injection Molding of High-Aspect Ratio Micro-Rods", *Materials and Manufacturing Processes,* vol. 21, no. 8, pp. 824-831.

[106] Huang, C. K. and Chiu, S. W. (2005), "Formability and accuracy of micropolymer compound with added nanomaterials in microinjection molding", *Journal of Applied Polymer Science,* vol. 98, no. 5, pp. 1865-1874.

[107]   Lee, J. L., Ho, C. H., Lin, Y. and Shen, Y. K. (2010), "Fabrication and detection for the skeletons of micro aerial vehicle using precision injection molding", *Key Engineering Materials,* vol. 443, pp. 75-80.

[108]   Wang, J. and Yang, W. (2011), "Numerical simulation of shrinkage in the microinjection molding of multi-microparts produced in one mold", *Advanced Materials Research,* vol. 221, pp. 649-656.

[109]   Wen, J. and Wen, P. (2005), "Simulation and optimization of aspheric plastic lens injection molding", *Journal Wuhan University of Technology, Materials Science Edition,* vol. 20, no. 2, pp. 86-89.

[110]   Shen, Y. K. and Wu, W. Y. (423-431, 2002), "An analysis of the three-dimensional micro injection moulding", *Int. Comm. Heat Mass Transfer,* vol. 29, no. 3, pp. 423-431.

[111]   B. Shaa, S. Dimova, C. Griffithsa and M.S. Packianather (2007), "Investigation of micro-injection moulding: Factors affecting the replication quality", *Journal of Materials Processing Technology,* vol. 12, pp. 284-296.

[112]   Chen, C. -., Chen, S. -., Liao, W. -., Chien, R. -. and Lin, S. -. (2010), "Micro injection molding of a micro-fluidic platform", *International Communications in Heat and Mass Transfer,* vol. 37, no. 9, pp. 1290-1294.

[113]   Berger, G. R., Gruber, D. P., Friesenbichler, W., Teichert, C. and Burgsteiner, M. (2011), "Replication of stochastic and geometric micro structures - Aspects of visual appearance", *International Polymer Processing,* vol. 26, no. 3, pp. 313-322.

[114]   Fu, G., Loh, N. H., Tor, S. B., Murakoshi, Y. and Maeda, R. (2004), "Replication of metal microstructures by micro powder injection molding", *Materials & Design,* vol. 25, no. 8, pp. 729-733.

[115]   Rean-Der Chien (2006), "Micromolding of biochip devices designed with microchannels", *Sensors and Actuators A: Physical,* vol. 128, no. 2, pp. 238-247.

[116] Angelov, A. K. and Coulter, J. P. (2008), "The Development and Characterization of Polymer Microinjection Molded Gratings", *Polymer Engineering and Science,* , pp. 2169-2177.

[117] Chen, C. -., Lin Su, P., Chiou, C. -. and Chiang, K. -. (2011), "Experimental Investigation of Designed Parameters on Dimension Shrinkage of Injection Molded Thin-Wall Part by Integrated Response Surface Methodology and Genetic Algorithm: A Case Study", *Materials and Manufacturing Processes,* vol. 26, pp. 534-540.

[118] Beck, M., Piotter, V., Ruprecht, R. and Haußelt, J. (2006), "Dimensional tolerances of micro precision parts made by ceramic injection moulding", in Wolfgang Menz A2Stefan Dimov and Bertrand FillonA2 Wolfgang Menz,Stefan Dimov and Bertrand Fillon (eds.) *4M 2006 - Second International Conference on Multi-Material Micro Manufacture,* Elsevier, Oxford, pp. 135-138.

[119] Annicchiarico, D., Attia, U. M. and Alcock, J. R. (2013), "A methodology for shrinkage measurements in micro-injection moulding", *Polym.Test.,* vol. 32, pp. 769-777.

[120] Thakur, V., Mosaddegh, P. and Angstadt, D. C. (2007), "Micro-feature replication via polymer molding at ambient pressure", *Proceedings of the ASME International Manufacturing Science and Engineering Conference 2007, MSEC2007,* pp. 171.

[121] Tay, B. Y., Liu, L., Loh, N. H., Tor, S. B., Murakoshi, Y. and Maeda, R. (2005), "Injection molding of 3D microstructures by μpIM", *Microsystem Technologies,* vol. 11, no. 2-3, pp. 210-213.

[122] Shaw, H. M. and Edirisinghe, M. J. (1995), "Shrinkage and Particle Packing during Removal of Organic Vehicle from Ceramic Injection Mouldings", *Journal of the European Ceramic Society,* vol. 15, pp. 109-116.

[123]   Nian, S. C. and Yang, S. Y. (2005), "Molding of thin sheets using impact micro-injection molding", *International Polymer Processing,* vol. 20, no. 4, pp. 441-448.

[124]   Surace, R., Trotta, G., Bellantone, V. and Fassi, I. *, The micro injection moulding process for polymeric components manufacturing*, available at: http://cdn.intechopen.com/pdfs/34671/InTech-The_micro_injection_moulding_process_for_polymeric_components_manufacturing.pdf (accessed 08/02/2013).

[125]   Plastic Engineering Company *, PLENCO processing guide*, available at: http://www.plenco.com/plenco_processing_guide/Sect%204%20Injection%20Molding.pdf (accessed June 2013).

[126]   Lee, B. -., Hwang, C. J., Kim, D. S. and Kwon, T. H. (2008), "Replication quality of flow-through microfilters in microfluidic lab-on-a-chip for blood typing by microinjection molding", *Journal of Manufacturing Science and Engineering, Transactions of the ASME,* vol. 130, no. 2.

[127]   Amaranan, S. and Manonukul, A. (2009), "Aspect ratio of green MIM parts on shrinkage during sintering", *The Minerals, Metals and Materials Society - 3rd International Conference on Processing Materials for Properties 2008, PMP III,* Vol. 2, pp. 880.

[128]   Kabanemi, K. K., Vaillancourt, H., Wang, H. and Salloum, G. (1998), "Residual stresses, shrinkage, and warpage of complex injection molded products: Numerical simulation and experimental validation", *Polymer Engineering & Science,* vol. 38, no. 1, pp. 21-37.

[129]   Song, M., Jing, X. and Zhao, D. (2006), "Experimental research on injection molding shrinkage characteristics of plastic parts", *Zhongguo Jixie Gongcheng/China Mechanical Engineering,* vol. 17, no. SUPPL., pp. 180-182.

[130]   Othman, M. H., Hassan, S., Ibrahim, S. Z. and Li, L. (2013), "The Effects of Mould Design on Shrinkage and Warpage of Polypropylene Integral hinges", *3rd*

International Conference on Trends in Mechanical and Industrial Engineering (ICTMIE 2013), January 8-9, 2013, Kuala Lumpur (Malaysia), .

[131]   Chen, S. -., Chang, Y., Hsu, P. -., Huang, S. -., Chang, Y. -. and Huang, C. -. (2011), "Simulation on the part warpage and photoelastic stress when molding discontinuous-thickness-variation parts combined with differential mold cooling", *Annual Technical Conference - ANTEC, Conference Proceedings,* Vol. 2, pp. 1740.

[132]   Park, H. -. and Dang, X. -. (2010), "Optimization of conformal cooling channels with array of baffles for plastic injection mold"*, International Journal of Precision Engineering and Manufacturing,* vol. 11, no. 6, pp. 879-890.

[133]   Harris, R. A., Newlyn, H. A., Hague, R. J. M. and Dickens, P. M. (2003), "Part shrinkage anomilies from stereolithography injection mould tooling", *International Journal of Machine Tools and Manufacture,* vol. 43, no. 9, pp. 879-887.

[134]   Vasco, J. C., Selada, A., Neves, T. and Pouzada, A. S. (2010)*, A study on the mouldability of POM micro details in moulding blocks using micro manufacturing technologies*,   available   at: http://repositorium.sdum.uminho.pt/bitstream/1822/20365/1/Vasco%20JC%202010.pdf (accessed June 2013).

[135]   Erzurumlu, T. and Ozcelik, B. (2006), "Minimization of warpage and sink index in injection-molded thermoplastic parts using Taguchi optimization method", *Materials and Design,* vol. 27, no. 10, pp. 853-861.

[136]   Anonymous *, Center for Nanoscale Science and technology - Fluctuations and Nanoscale Control*, available at: http://www.nist.gov/cnst/nrg/nano_control.cfm (accessed Aug 2013).

[137]   Sari-Sarraf, H., Hequet, E., Abidi, N., Dai, Y. and Chan, H. Y. (2002), "Automatic measurement of fabric shrinkage", *American Association of Textile Chemists and Colorists Review,* vol. 2, no. 10, pp. 20-23.

[138]   Fano, V., Ortalli, I., Pizzi, S. and Bonanini, M. (1997), "Polymerization shrinkage of microfilled composites determined by laser beam scanning", *Biomaterials,* vol. 18, no. 6, pp. 467-470.

[139]   Marinel, S. and Savary, E. (2009), "In situ measurement of the shrinkage during microwave sintering", *Journal of Materials Processing Technology,* vol. 209, no. 10, pp. 4784-4788.

[140]   Régnier, G. and Trotignon, J. P. (1993), "Local orthotropic shrinkage determination in injected moulded polymer plates", *Polymer Testing,* vol. 12, no. 5, pp. 383-392.

[141]   C K Huang (2007), "Polymeric nanofeatures of 100 nm using injection moulding for replication", *Journal of Micromechanics and Microengineering,* vol. 17, no. 8, pp. 1518-1526.

[142]   Chen, T. C., Yin, W. Q. and Ifju, P. G. (2010), "Shrinkage Measurement in Concrete Materials using Cure Reference Method", *Experimental Mechanics,* vol. 50, no. 7, pp. 999-1012.

[143]   Neubauer, C. M., Bergstrom, T. B., Sujata, Y. X., Garboczi, E. J. and Jennings, H. M. (1997), "Drying shrinkage of cement paste as measured in an environmental scanning electron microscope and comparison with microstructural models", *Journal of Material Science,* vol. 32, no. 24, pp. 6415-6427.

[144]   Kotani Masahiro, Arao Yoshihiko, Koyanagi Jun, Kawada Hiroyuki, Hatta Hiroshi and Ishida Yuichi (2007), "Quantitative evaluation of curing shrinkage in polymeric matrix composites", 16TH ICCM, International Conference on Composite Materials, .

[145]   Reddy, B. R., Xu, Y., Ravi, K., Gray, D. and Pattillo, P. D. (2009), "Cement-shrinkage measurement in oilwell cementing - A comparative study of laboratory methods and procedures", *SPE Drilling and Completion,* vol. 24, no. 1, pp. 104-114.

[146]   Takuji Higashioji and Bharat Bhushan (2002), "Creep and Shrinkage Behavior of Improved Ultrathin Polymeric Films", *Journal of Applied Polymer Science,* vol. 84, no. 8, pp. 1477-1498.

[147]   Revilla-Díaz, R., Sánchez-Valdés, S., López-Campos, F., Medellín-Rodríguez, F. J. and López-Ouintanilla, M. L. (2007), "Comparative characterization of PP nano- and microcomposites by In-mold shrinkage measurements and structural characteristics", *Macromolecular Materials and Engineering,* vol. 292, no. 6, pp. 762-768.

[148]   Darshil U. Shah and Peter J. Schubel (2010), "Evaluation of cure shrinkage measurement techniques for thermosetting resins", *Polymer Testing,* vol. 29, no. 6, pp. 629-639.

[149]   Kleverlaan, C. J. and Feilzer, A. J. (2005), "Polymerization shrinkage and contraction stress of dental resin composites", *Dental Materials,* vol. 21, no. 12, pp. 1150-1157.

[150]   Matsui, K., Tanaka, K., Yamakawa, T., Uehara, M., Enomoto, N. and Hojo, J. (2007), "Sintering kinetics at isothermal shrinkage: II, effect of Y2O3 concentration on the initial sintering stage of fine zirconia powder", *Journal of the American Ceramic Society,* vol. 90, no. 2, pp. 443-447.

[151]   ASTM, American Society for Testing and Materials, *ASTM D955-89 Standard test method of measuring shrinkage from mold dimensions of thermoplastics*.

[152]   BS EN ISO 294-4 : 2003, (2003), *BS EN ISO 294-4:2003 "Plastic - Injection moulding of test specimens of thermoplastic materials - Part 4:Determination of moulding shrinkage*.

[153]   BS EN ISO 294-3 : 2003, (2003), *BS EN ISO 294-3 : 2003 - Plastics - Injection moulding of test specimens of thermoplastic materials - Part 3: Small plates*.

[154]   Saechtling, H. (2006), "Handbook of plastic material. Physical test for polymer characterization. Longitudinal and transversal shrinkage.", in "Tecniche Nuove Edizioni" (ed.) , pp. 61.

[155]   Davis J.R. (2004), "Tensile Testing of Plastic Test", in ASM International (ed.) .

[156]   Uniplast , *UNIPLAST "Italian Society of Unification for Plastic Material"*, available at: http://www.uniplast.info/ (accessed May 2011).

[157]   Chang, T. C. and Faison, E. (2001), "Shrinkage behaviour and optimization of injection molded parts studied by the Taguchi Method", *Polymer Engineering and Science,* vol. 41, no. 5.

[158]   Maghsoodloo, S., Ozdemir, G., Jordan, J. and Huang, C. H. *, Strengths and Limitations of Taguchi's Contributions to Quality, Manufacturing, and Process Engineering*, available at: www.researchgate.net/...Strengths_and_limitations_of_Taguchi's.../... (accessed April 2013).

[159]   Bianchi, L. A. , *Design of Experiments*, available at: http://users.dma.unipi.it/~flandoli/noteDOE.pdf (accessed March 2013).

[160]   Cesarone, J. , *DOE or Taguchi?*, available at: http://engineeringsolutions.homestead.com/taguchi_article3.html (accessed March 2013).

[161]   Statistical Handbook site , *Statistical Handbook on line*, available at: http://www.itl.nist.gov/div898/handbook/pri/section5/pri5322.htm Last Access January 2013 (accessed January 2013).

[162]   Minitab Web Page , *http://www.minitab.com/en-US/products/minitab/default.aspx?WT.srch=1&WT.mc_id=SE004815* (accessed Novembre 2012).

[163]   Anderson, M. J. and Kraber, S. L. *, KEYS TO SUCCESSFUL DESIGNED EXPERIMENTS*, available at: http://www.isixsigma.com/offsite.asp?A=Fr&Url=http://www.statease.com/pubs/doe-keys.pdf4/7/2008 (accessed April 2013).

[164]   Anthony, J. (2003), *Design of Experiments for Engineers and Scientists,* Butterworth-Heinemann ed, Elsevier Science & Technology Books, Oxford.

[165]   Jialing, W. and Pengfei, W. (2005), "The Simulation and Optimization of Aspheric Plastic Lens Injection Molding", *Journal of Wuhan University of Technology - Mater. Sci. Ed.,* vol. 20, no. 2, pp. 86-89.

[166]   Anonymous *, Shrinkage and warpage*, available at: http://www.dc.engr.scu.edu/cmdoc/dg_doc/develop/process/physics/b3500001.htm (accessed Sept 2013).

[167]   Zhao, J., Chen, G., Chan, P. S. and Debowski, M. *, Investigation of Interactions of Polymer Material, Mould Design and Process Condition in the Micro Moulding Process*, available at: http://citeseerx.ist.psu.edu/viewdoc/download?doi=10.1.1.2.3291&rep=rep1&type=pdf (accessed September 2013).

[168]   Samanta, S. K., Chattopadhyay, H. and Godkhindi, M. M. (2011), "Thermo-physical characterization of binder and feedstock for single and multiphase flow of PIM 316L feedstock", *Journal of Materials Processing Technology,* vol. 211, pp. 2114-2122.

[169]   Supriadi, S., Baek, E. R., Choi, C. J. and Lee, B. T. (2007), "Binder system for STS 316 nanopowder feedstocks in micro-metal injection molding", *Journal of Materials Processing Technology,* vol. 187-188, pp. 270-273.

[170]   Seokyoung, A., Seong, J. P., Shiwoo, L., Sundar, V. A. and Randall, M. G. (2009), "Effect of powders and binders on material properties and molding parameters in iron and stainless steel powder injection molding process", *Powder Technology,* vol. 193, pp. 162-169.

[171]   Quinard, C., Barriere, T. and Gelin, J. C. (2009), "Development and property identification of 316L stainless steel feedstock for PIM and mPIM", *Powder Technology,* vol. 190, pp. 123-128.

[172]   Titomanlio, G., Brucato, V. and Kamal, M. R. (1987), "Mechanism of Cooling Stresses Build-Up in Injection Molding of Thermoplastic Polymers", *Int. Polym. Process.,* vol. 1, pp. 55–59.

[173]   Jansen, K. M. B., Van Dijk, D. J. and Husselman, M. H. (1998), "Effect of processing conditions on shrinkage in injection moulding", *Polym. Eng. Sci.,* , no. 38, pp. 838–846.

[174]   Mat web site , available at: http://www.matweb.com/ (accessed June 2012).

[175]   Carazzolo, G. and Mammi, M. (2003), "Crystal structure of a new form of polyoxymethylene", *Journal of Polymer Science Part A: General Papers,* vol. 1, no. 3, pp. 965-983.

[176]   Kongkhlang, T., Tashiro, K., Kotaki, M. and Chirachanchai, S. (2008), "Electrospinning as a new technique to control the crystal morphology and molecular orientation of polyoxymethylene nanofibers", *J. Am. Chem. Soc.,* vol. 130, pp. 15460-15466.

[177]   Tashiro, K., Kamae, T., Asanaga, H. and Oikawa, T. (2004), "Structural analysis of polyoxymethylene whisker single crystal by the electron diffraction method", *Macromolecules,* vol. 37, pp. 826-830.

[178]   Kumaraswamy, G., Surve, N. S., Mathew, R., Rana, A., Jha, S. K., Bulakh, N. N., Nisal, A. A., Ajithkumar, T. G. and Rajamohanan, P. R. (2012), "Lamellar Melting, Not Crystal Motion, Results in Softening of Polyoxymethylene on Heating", *Macromolecules,* vol. 45, pp. 5967−5978.

[179]   Kongkhlang, T., Kotaki, M., Kousaka, Y., Umemura, T., Nakaya, D. and Chirachanchai, S. (2008), "Electrospun Polyoxymethylene: Spinning Conditions

and Its Consequent Nanoporous Nanofiber", *Macromolecules,* vol. 41, pp. 4746 4752.

[180]   *,   MMD   definition*,   available   at: http://www.ispe.org/glossary?term=Mass+Median+Particle+Diameter+(MMD) (accessed June 2013).

[181]   Karatas, C., Sozen, A., Arcaklioglu, E. and Erguney, S. (2008), "Investigation of mouldability for feedstocks used powder injection moulding", *Materials and Design,* vol. 29, pp. 1713-1724.

[182]   Su, Y. C., Shah, J. and Lin, L. (2004), "Implementation and analysis of polymeric microstructure replication by micro injection molding", *J. Micromech. Microeng.,* vol. 14, pp. 415–422.

[183]   *, Battenfeld Web site*, available at: http://www.wittmann-group.co.uk/product-Micropower_5___15t-120.htm (accessed May 2012).

[184]   TESA   Visio   web   site   ,   available   at: http://www.tesabs.co.uk/multimedia/docs/2010/08/P_2010_EN_TESA-VISIO.pdf (accessed April 2011).

[185]   Launsby, R. G. and Lahey, J. P. (1998), "Experimental Design for Injection Molding", in Launsby Consulting (ed.) .

[186]   Zhang, N., Chu, J. S., Byrne, C. J., Browne, D. J. and Gilchrist, M. D. (2012), "Replication of micro/nano-scale features by micro injection molding with a bulk metallic glass mold insert", *J. Micromech. Microeng.,* vol. 22, pp. 13 pp.

[187]   Park, S. H., Lee, I. W., Moon, S. N., Yoo, Y. -. and Cho, Y. H. (2011), "Injection molding micro patterns with high aspect ratio using a polymeric flexible stamper", *eXPRESS Polymer Letters,* vol. 5, no. 11, pp. 950-958.

[188]   Rosato, D. V., Rosato, D. V. and Rosato, M. G. (eds.) (2000), *Injection moulding handbook,* 3rd Ed. ed, Kluwer Academic Publishers, Norwell, Massachusetts.

[189]   Lenth, R. V. *, Lenth's method for the analysis of unreplicated experiments*, available at: http://www.wiley.com/legacy/wileychi/eqr/docs/sample_1.pdf (accessed December 2012).

[190]   Ghi Ho Tae and Eun Soo Choi *, Time Dependent Behavior of Polymer Concrete Using Unsaturated Polyester Resin*, available at: http://www.intechopen.com/download/get/type/pdfs/id/39409 (accessed March 2014).

[191]   Bociaga, E. and Jaruga, T. (2007), "Experimental investigation of polymer flow in injection moulding", *Archives of Material Science and Engineering,* vol. 38, no. 3, pp. 165-172.

[192]   C-MOLD (ed.) (1998), *C-MOLD Design Guide. A Resource for Plastics Engineers,* 3rd Edition ed, , Ithaca, New York, USA.

[193]   Thornagel, M. (October 2009), " MIM-simulation: A virtual study on phase separation ", *Proceedings of EURO PM 2009,* Vol. 2, Copenhagen, European Powder Metallurgy Association, pp. 135-140.

[194]   Image J , available at: http://www.imagej.en.softonic.com/ (accessed March 2011).

[195]   *, Injection Moulding GE Mini Guide*, available at: http://gaetanmabille.free.fr/process/Engineering%20Thermoplastics%20Injection%20Molding%20Processing%20Guide%20-%20GE%20plastics.pdf (accessed June 2013).

[196]   Reading, M., Price, D. M. and Orliac, H. (2001), "Measurement of Crystallinity in Polymers Using Modulated Temperature Differential Scanning Calorimetry", *ASTM Special Technical Publication,* vol. 1402, pp. 17-32.

[197]   Ong, N. S. and Koh, Y. H. (2005), "Experimental investigation into micro injection molding of plastic parts", *Mater Manuf Process,* vol. 20, pp. 245-253.

[198]   Attia, M. and Alcock, J. R. (2010), "Optimising process conditions for multiple quality criteria in micro-injection moulding", *The International Journal of Advanced Manufacturing Technology,* vol. 50, no. 5-8, pp. 533-542.

[199]   Velarde, D. A. and Yeagley, M. J. (2000), "Linear shrinkage differences in plastic injection molded parts", *Plastic Engineering,* vol. 56, no. 12.

[200]   Huang, M. S. and Hsu, H. C. (2009), "Effect of backbone polymer on properties of 316L stainless steel MIM compact", *Journal of Material Science,* vol. 209, pp. 5527-5535.

[201]   Heunisch, A., Dellert, A. and Roosen, A. (2010), "Effect of powder, binder and process parameters on anisotropic shrinkage in tape cast ceramic products", *Journal of the European Ceramic Society,* vol. 30, pp. 3397–3406.

[202]   Antony, J. (2003), *Design of experiments for engineers and scientists,* Butterworth-Heinemann, Oxford.

[203]   Nor, N. H. M., Muhamadb, N., Ismail, M. H., Jamaludinc, K. R., Ahmadd, S. and Ibrahimd, M. H. I. (2009), "FLOW BEHAVIOUR TO DETERMINE THE DEFECTS OF GREEN PART IN METAL INJECTION MOULDING", *International Journal of Mechanical and Materials Engineering,* vol. 4, no. 1, pp. 70-75.

[204]   Zhao, J., Lu, X., Lin, M., Chen, G., Liu, S. and Yong, M. S. (2006), "Effects of rheological properties of polymer blends on micro mold filling behavior", *Materials Research Innovations,* vol. 10, no. 4, pp. 111-112.

[205]   Annicchiarico, D., Attia, U. M. and Alcock, J. R. (2013), "Part mass and shrinkage in micro injection moulding: Statistical based optimisation using multiple quality criteria", *Polymer Testing,* vol. 32, no. 6, pp. 1079-1087.

[206]   González-Gutiérrez, J., Stringari, G. B. and Emri, I. , *Powder Injection Molding of Metal and Ceramic Parts*, available at: http://cdn.intechopen.com/pdfs/33645/InTech-Powder_injection_molding_of_metal_and_ceramic_parts.pdf (accessed May 2013).

[207]   Fu, G., Loh, N. H., Tor, S. B., Tay, B. Y., Murakoshi, Y. and Maeda, R. (2005), "Injection molding, debinding and sintering of 316L stainless steel microstructures", *Appl. Phys. A,* vol. 81, pp. 495-500.

[208]   Yang, C., Huang, H. -., Castro, J. and Yi, A. , *High-aspect-ratio microfeature injection moulding*, available at: http://www.4spepro.org/view.php?article=003610-2011-05-11 (accessed June 2013).

[209]   Yao, D. and Kim, B. (2002), "Injection molding high aspect ratio micro features", *J Inject Molding Technol,* vol. 6, no. 1, pp. 11-17.

[210]   Shaharuddin, S., Salit, M. and Zainudin, E. (2006), "A review of the effect of moulding parameters on the performance of polymeric composite injection moulding", *Turkish J. Eng. Env. Sci.,* vol. 30, pp. 23-34.

[211]   Zhang, N. C. J. and Gilchrist, M. D. (2011), "Micro injection molding: characterization of cavity filling process", *Proceeding of SPE Annual Technical Conference,* , pp. 2085-91.

[212]   Zauner, R. (2006), "Micro powder injection moulding", *Microelectronic Engineering,* vol. 83, pp. 1442–1444.

[213]   Kowalsky, L., Kuszczyk, J. and Katgerman, L. (1999), "Thermal conductivity of metal powder-polymer feedstock for powder injection moulding", *Journal of Material Science,* vol. 34, no. 1, pp. 1-5.

[214]   Zhao, X. and Ye, L. (2009), "Thermal conductive polyoxymethylene/graphite composites", *Journal of Applied Polymer Science,* vol. 111, no. 2, pp. 759-767.

[215]   Anonymous , *Engineering polymers database*, available at: http://www.matbase.com/material-categories/natural-and-synthetic-polymers/engineering-polymers/material-properties-of-polyoxymethylene-homopolymer-pom-h.html (accessed June 2013).

[216]   Ahn, S., Park, S. J., Lee, S., Atre, S. V. and German, R. M. (2009), "Effect of powders and binders on material properties and molding parameters in iron and stainless steel powder injection molding process", *Powder Technology,* vol. 193, no. 2, pp. 162-169.

[217]   Fu, G., Loh, N. H., Tor, S. B., Tay, B. Y., Murakoshi, Y. and Maeda, R. (2005), "A variotherm mold for micro metal injection molding", *Microsystem Technologies,* vol. 11, pp. 1267-1271.

[218]   Dang, X. -. (2014), "General frameworks for optimization of plastic injection molding process parameters", *Simulation Modelling Practice and Theory,* vol. 41, pp. 15–27.

[219]   Kennedy, P. K. *, Practical and Scientific Aspects of Injection Molding Simulation*, available at: http://alexandria.tue.nl/extra2/200810899.pdf (accessed March 2014).

[220]   Anonymous (May/June 2013), "3D moulding simulation – the 'whole process' approach", *Metal Powder Report,* vol. 68, no. 3, pp. 30-32.

[221]   Gava, A. and Lucchetta, G. (2012), "On the performance of a viscoelastic constitutive model for micro injection moulding simulations", *eXPRESS Polymer Letters,* vol. 6, no. 5, pp. 417–426.

[222]   Hakimian, E. and Sulong, A. B. (2012), "Analysis of warpage and shrinkage properties of injection-molded micro gears polymer composites using numerical simulations assisted by the Taguchi method", *Materials and Design,* vol. 42, pp. 62-71.

225

[223]   Galantucci, L. M. and Spina, R. (2003), "Evaluation of filling conditions of injection moulding by integrating numerical simulations and experimental tests", *Journal of Materials Processing Technology,* vol. 141, pp. 266-275.

[224]   Jauregui-Becker, J. M., Tosello, G., J.A.M. van Houten, F. and Hansen, H. N. (2013), "Performance evaluation of a software engineering tool for automated design of cooling systems in injection moulding;", *Procedia CIRP 7,* , pp. 270-275.

[225]   Khor, C. Y., Ariff, Z. M., Che Ani, F., Mujeebu, M. A., Abdullah, M. K., Abdullah, M. Z. and Joseph, M. A. (2010), "Three-dimensional numerical and experimental investigations on polymer rheology in meso-scale injection molding", *International Communications in Heat and Mass Transfer,* vol. 37, pp. 131-139.

[226]   Ahn, S., Chung, S. -., Park, S. J. and German, R. M. (2010), "Metals Process Simulation; Volume 22B", in Furrer, D. U. and Semiatin, S. L. (eds.) *Modeling and Simulation of Metal Powder Injection Molding; ASM Handbook,* , pp. 343-357.

[227]   Lenz, J., Enneti, R. K., Park, S. J. and Atre, S. V. (2014), "Powder injection molding process design for UAV engine components using nanoscale silicon nitride powders", *Ceramics International,* vol. 40, pp. 893–900.

[228]   Zhou, H., Yan, B. and Zhang, Y. (2008), "3D filling simulation of injection molding based on the PG method", *Journal of materials processing technology,* vol. 204, pp. 475–480.

[229]   Choi, S. -. and Kim, S. K. (2011), "Multi-scale filling simulation of micro-injection molding process ", *Journal of Mechanical Science and Technology,* vol. 25, no. 1, pp. 117-124.

Appendix A – PCM technique

In this appendix were reported the tests performed for trying to realize a micro-feature with breadth lower that 60μm. The only technique present in Cranfield was the photochemical machining (PCM). A brief technique description was reported. Two metallic materials were chosen (steel and aluminium): the resulted micro-channel dimensions were measured by optical confocal microscopy.

A.1 PCM technique

The PCM is the process of fabricating sheet metal components using a combination of photo-resists and etchants to corrosively machine a selected area. A photo-resist is a light-sensitive material, usually mounted on a polymer film. It is used to form a patterned coating on the substrate.

The metal sheet is thoroughly cleaned and the resist coated onto the sheet by various methods including lamination, dipping or spinning. A phototool (a black and transparent image) is located in contact with the resist-coated metal sheet and a vacuum is draw to assure maximum contact between the two. The application of UV light through the transparent regions of the phototool causes the resist to become insoluble in a developer in the subsequent developing stage (if it a negative working resist) or soluble (if it is a positive working resist). A developing stage then takes place (by spraying or immersion) and the soluble areas are removed to leave a "stencil" on the sheet metal surface. In the case of a negative working resist (as used in this work), the regions protected from UV under the black areas of the phototool remain chemically unchanged and develop out to leave regions of bare metal. The "transparent" areas undergo polymerization and these remain to protect the surface, see Figure A-0-1.

Then the metal is ready to be etched in an etching machine (or by immersion etching). During etching, the etchant is able to attack unprotected metal zones in an advanced corrosion process. The etchant is typically an aqueous solution of acid, frequently ferric chloride that is heated and directed under pressure to both sides of the plate. After

neutralizing and rinsing, the remaining resist is removed and the sheet of parts is cleaned and dried.
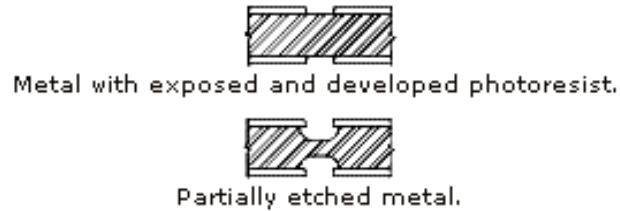
Figure A-0-1. Only the un-protected areas will be etched.

A.2 Channel manufacturing and results

Tests were performed for studying the feasibility to realise channels smaller than 60 μm by using two different metals both used as mould materials: aluminium and steel. A picture of the manufactured channels using an aluminium disc was reported in Figure A-0-2: only this metal was depicted because the steel disc was identical.
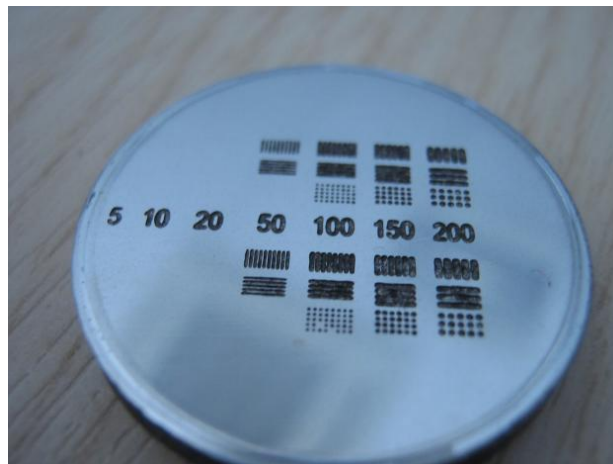
Figure A-0-2. The patterns manufactured by PCM using an aluminium disc. The numbers represents the line dimensions in microns.

Figure A-0-3 and Figure A-0-4 depicts the results of channel profile respectively for the steel and aluminium.
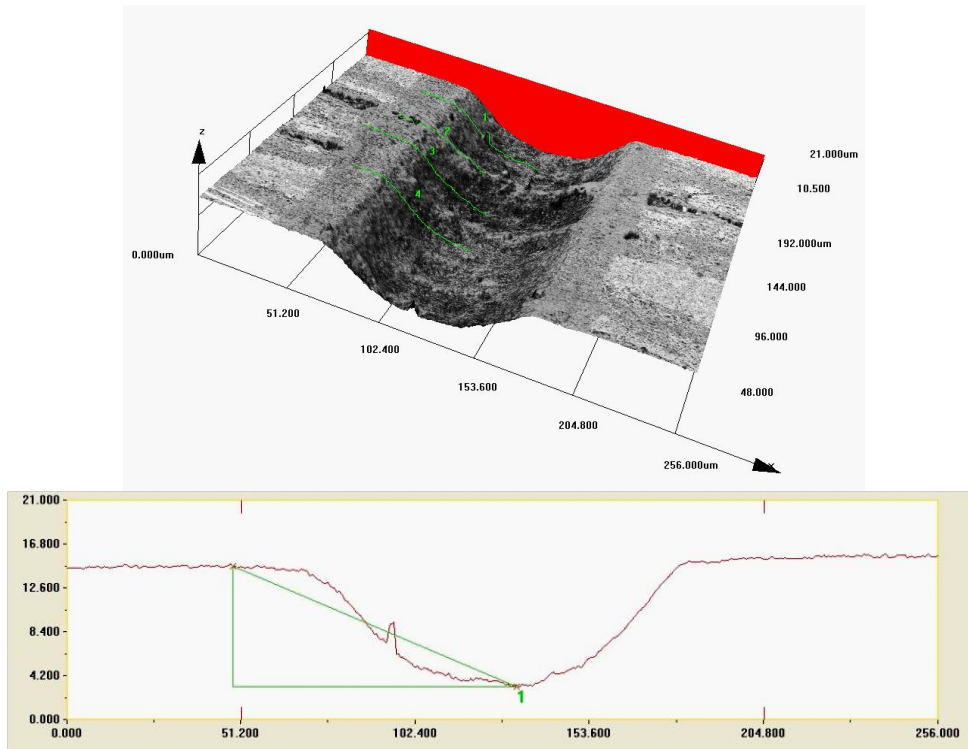
Figure A-0-3. Steel channel profile.
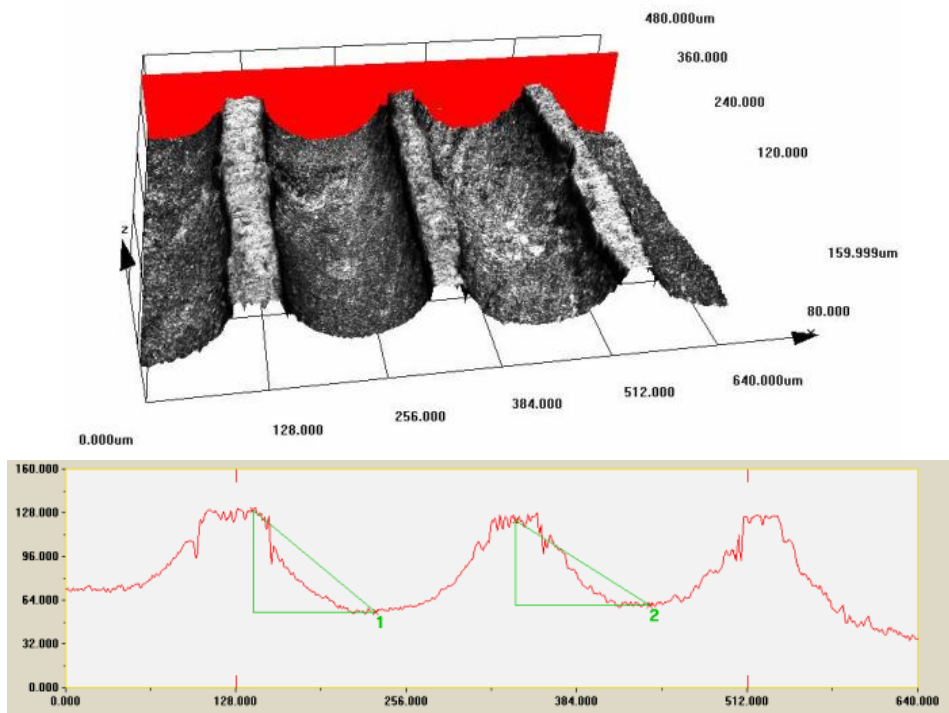
Figure A-0-4. Aluminium channel profile.

The profiles were measured by using a confocal microscope. Despite of the minimum channels seems to have dimensions around 50 μm (Figure A-0-2), optical measurement shown the contrary. The channel height shown values suitable for the purposes to realize channels with dimensions smaller than 60 μm, but the width was too big. Table A-0-1 reports the average dimensions of these channels. As it is possible to see, neither steel nor aluminium permitted to realize a channel with width lower than 60 μm.

	Steel	Aluminium
Height channel [μm]	13	67
Distance channel [μm]	115	165

Table A-0-1. Average of the channel dimensions.

Moreover, PCM technique was not a precise technique in terms of dimensional control: a greater precision can be realized with different materials as silica that shows an highly directional structure.

Appendix B. Mould design

This appendix reports the micro-mould and pin designs.

B.1 Mould design

This section reports the details of mould design. Figure B-0-1 and Figure B-0-2 reported the mould design, Figure B-0-3 depicted the pin positioning, Figure B-0-4concern the mould dimensions, Figure B-0-5 the mould back side, Figure B-0-6 is about a mould section and evidenced the ejection pins inside the blind holes, Figure B-0-7 and Figure B-0-8 are about the micro-feature design. All the dimensions were expressed in millimetres; the tolerance was ± 1μm.
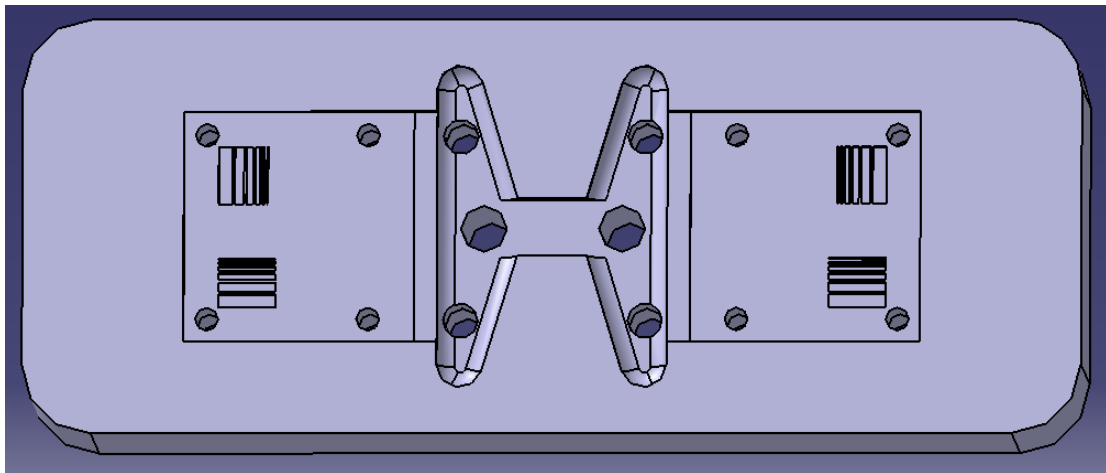
Figure B-0-1. Micro-mould.
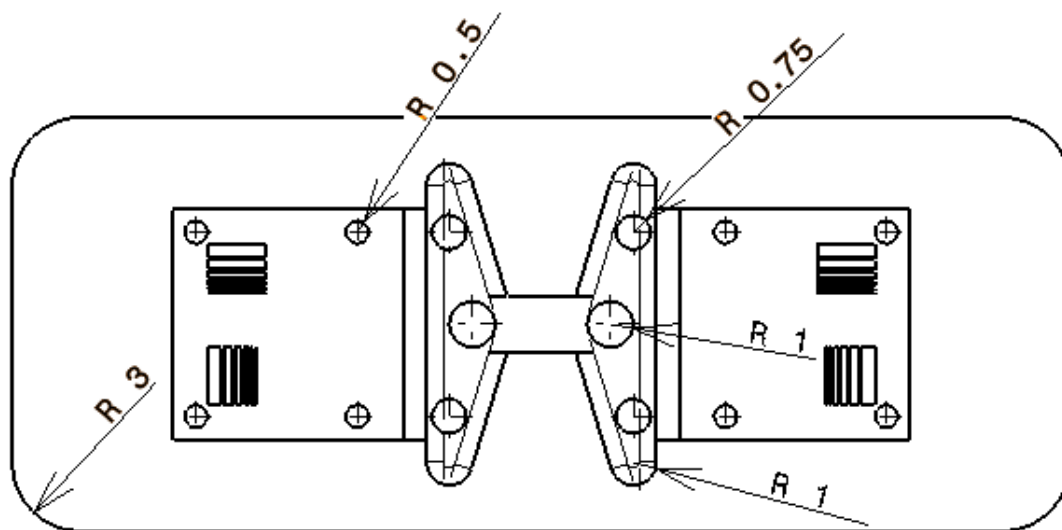
Figure B-0-2. Mould plate with pin diameters.
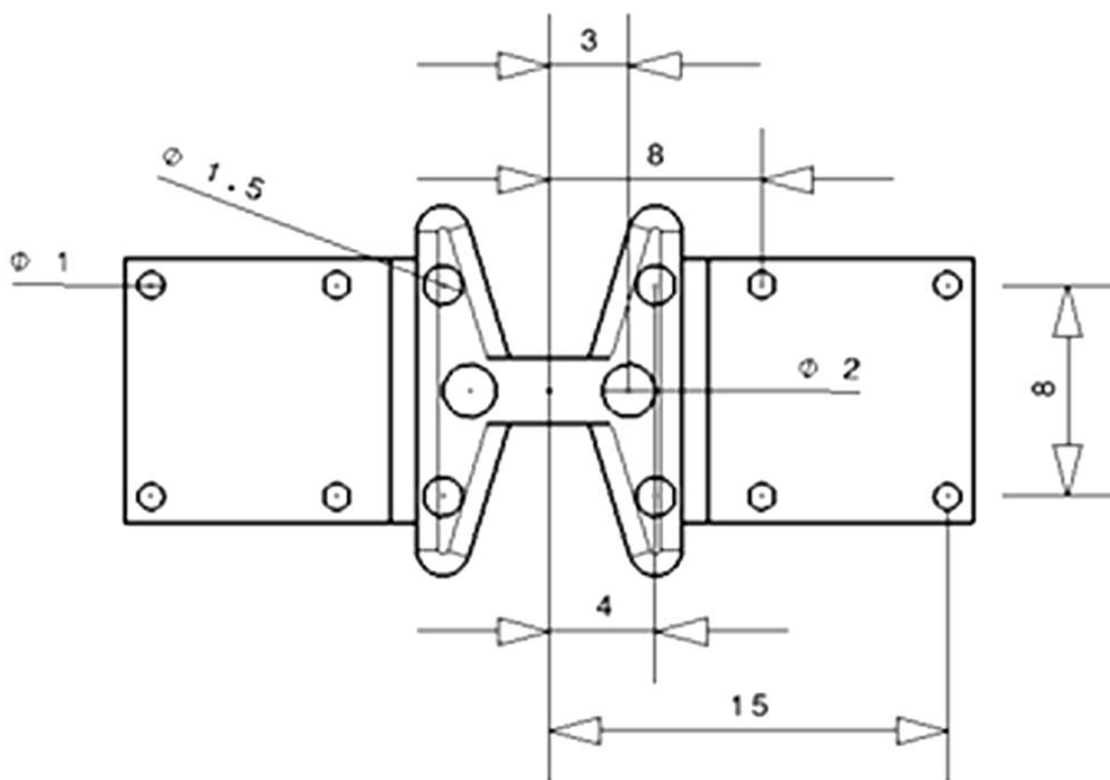
Figure B-0-3. Micro-mould pin positioning.

Figure B-0-4. Micro-mould dimensions.
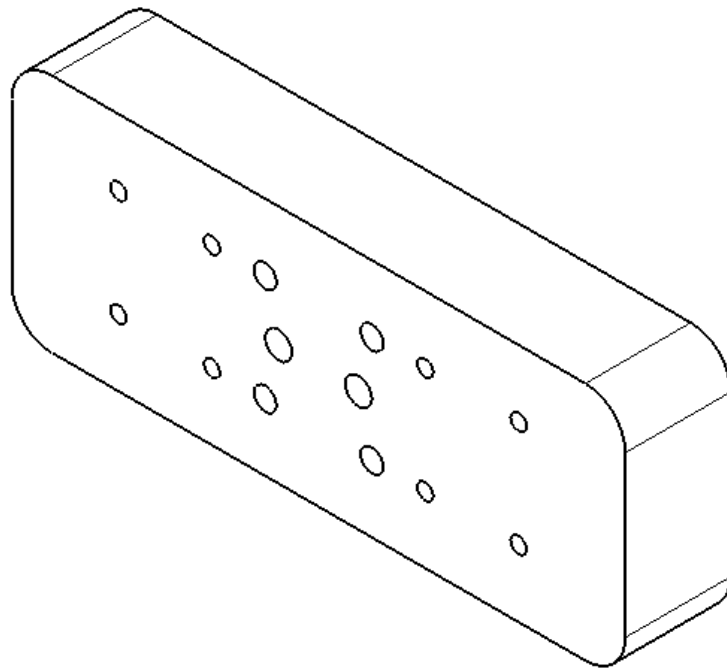
Figure B-0-5. Micro mould backside, with ejection pins holes.
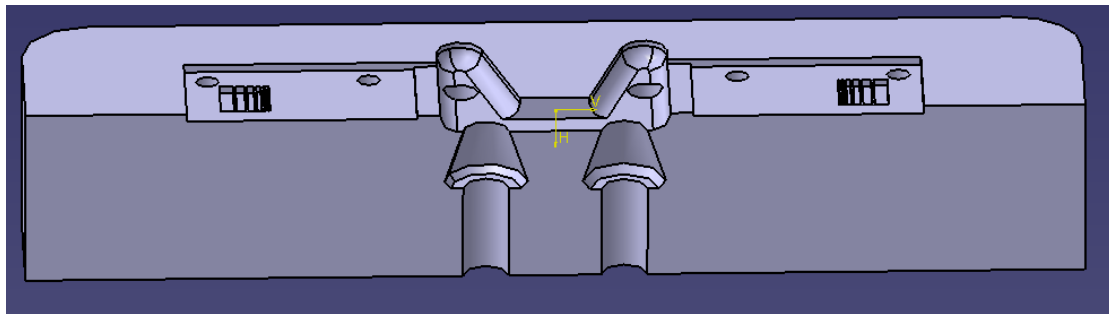
Figure B-0-6. Mould section. In evidence, the blind holes modified.
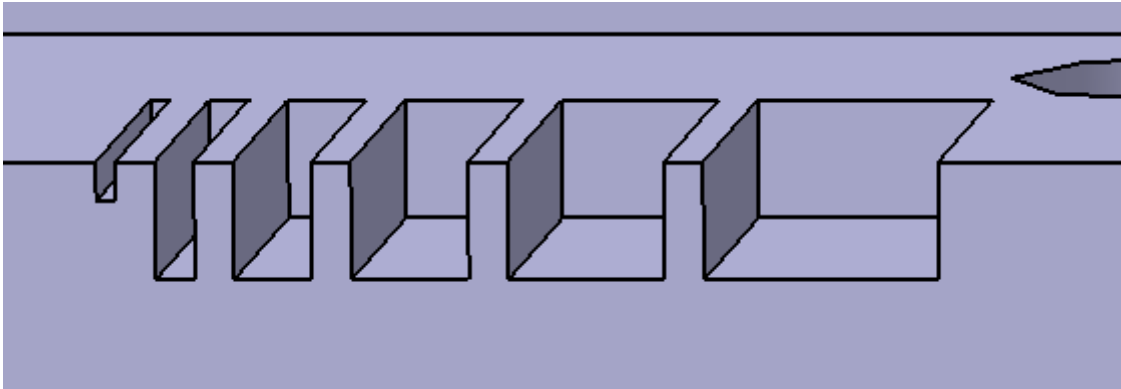
Figure B-0-7. Micro-features section.
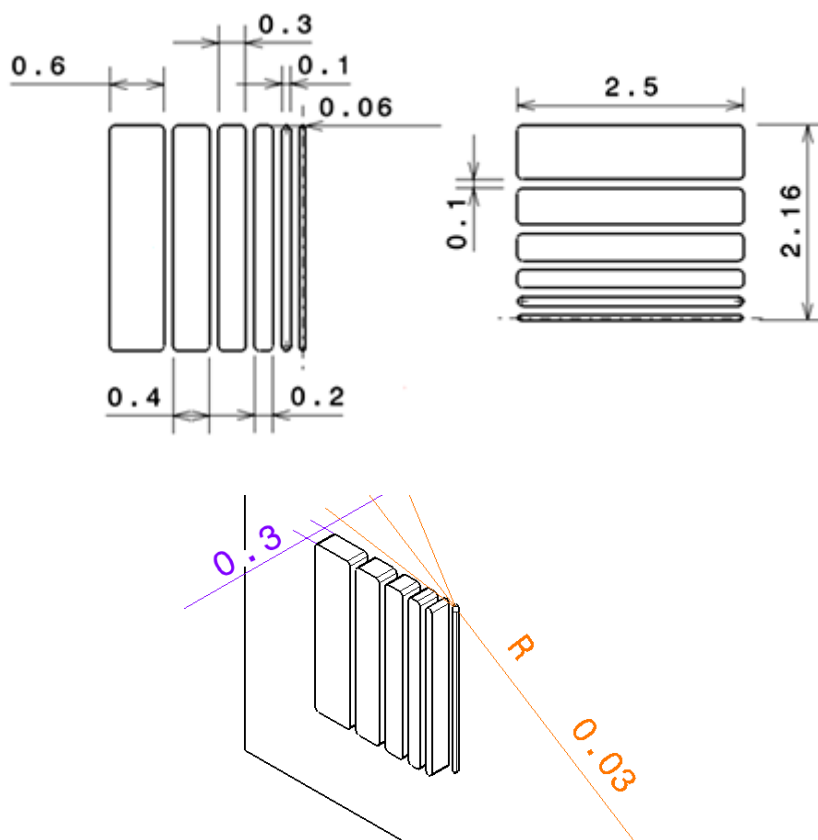
Figure B-0-8. Micro-features details.

B.2 Ejection pins

Figure B-0-9 depicts the back mould plate. This plate is located behind the micro mould, and can contain the 14 pins used for ejecting the specimen in the micro-mould:

- 2 pins with a diameter of 2 mm located in the runner (Figure B-0-10, Figure B-0-11, Figure B-0-12, Figure B-0-13, Figure B-0-14);

- 4 pins with a diameter of 1.5 mm located in the triangular gate (Figure B-0-15, Figure B-0-16, Figure B-0-17, Figure B-0-18, Figure B-0-19);

- 8 pins with a diameter of 1mm located in the square mould cavity (Figure B-0-20, Figure B-0-21, Figure B-0-22, Figure B-0-23, Figure B-0-24).

All the dimensions were expressed in millimetres; the tolerance was ± 1μm.
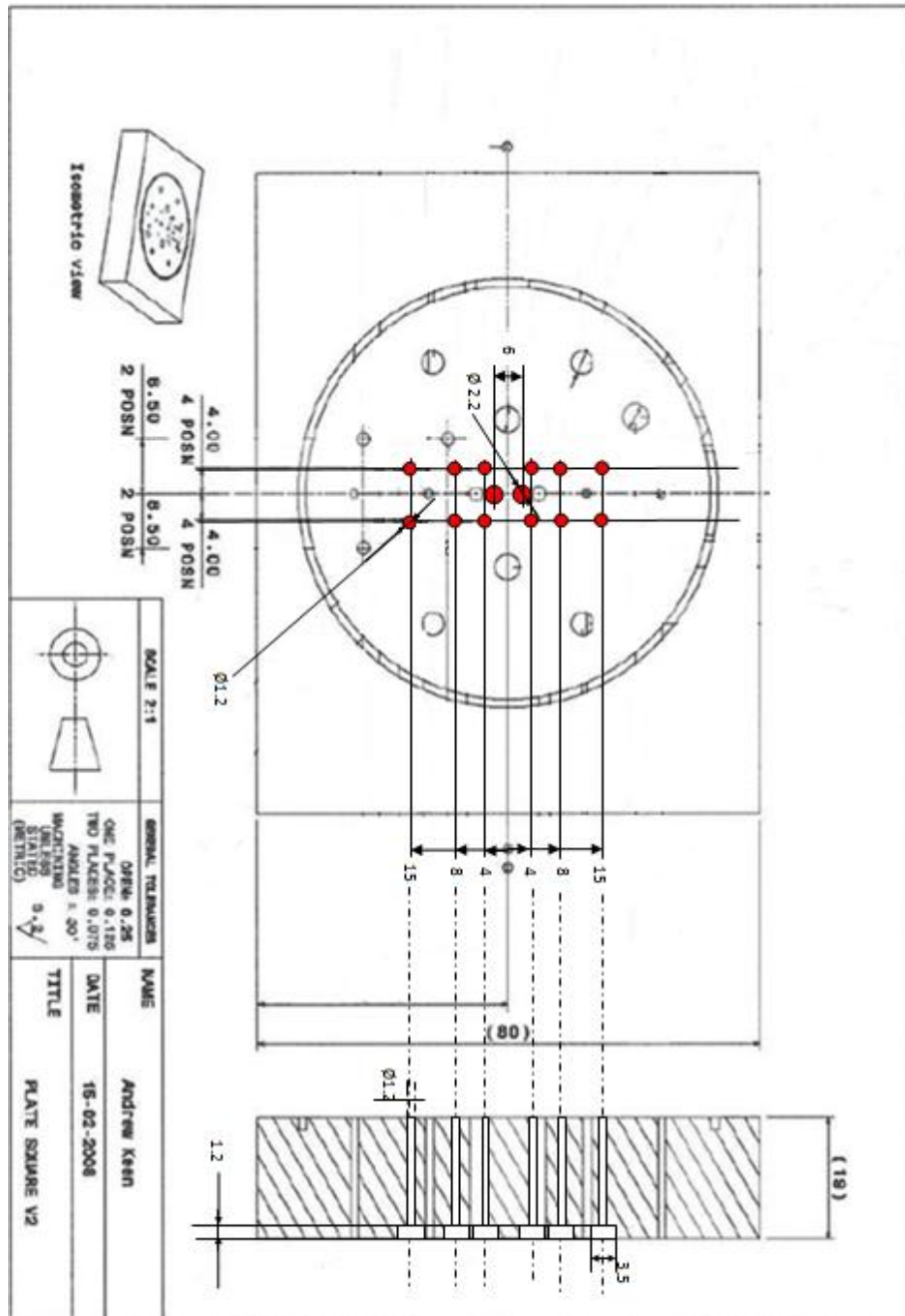
Figure B-0-9. Back mould plate design.

227
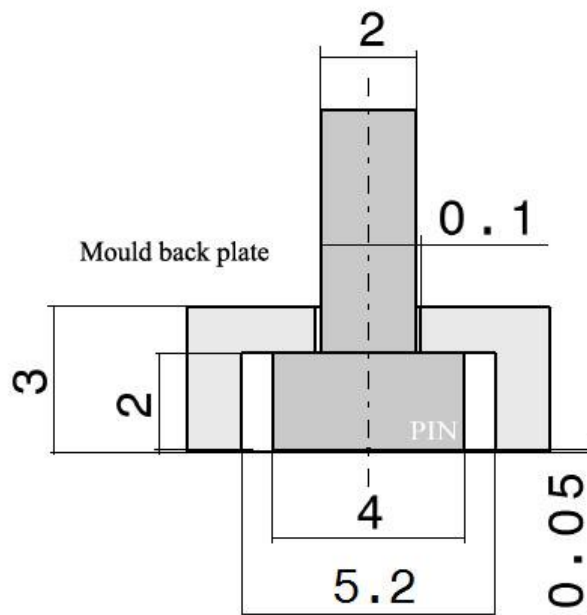
Figure B-0-10. Design pinhead ϕ 2.
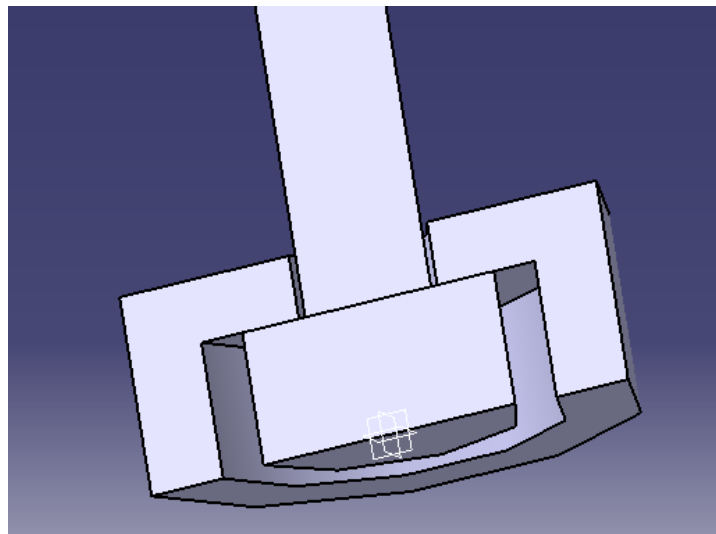
Figure B-0-11. Isometric view of head pin ϕ2.
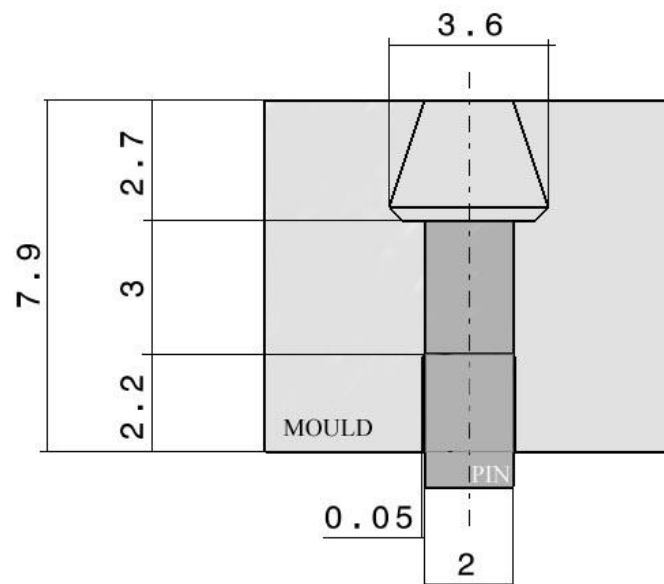
Figure B-0-12. Design pin ϕ 2 mould side.
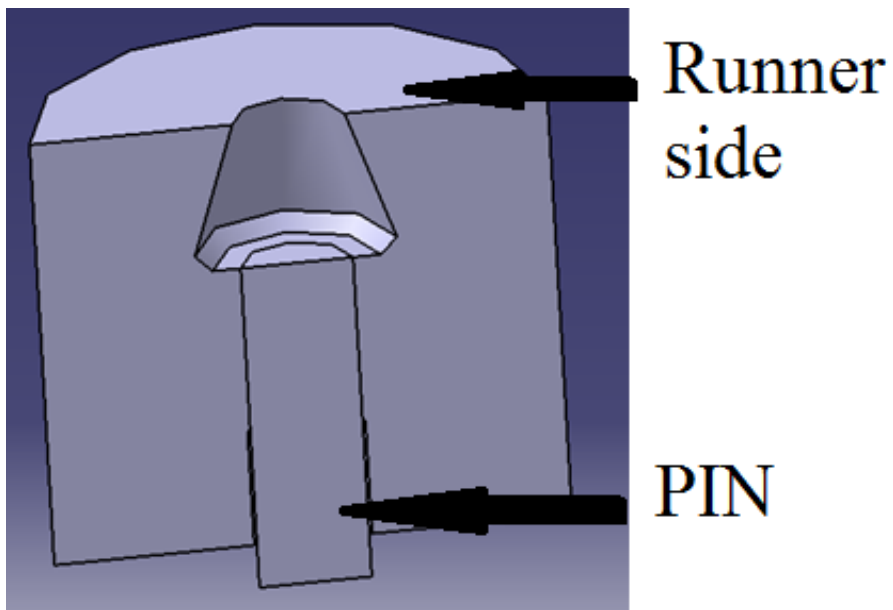
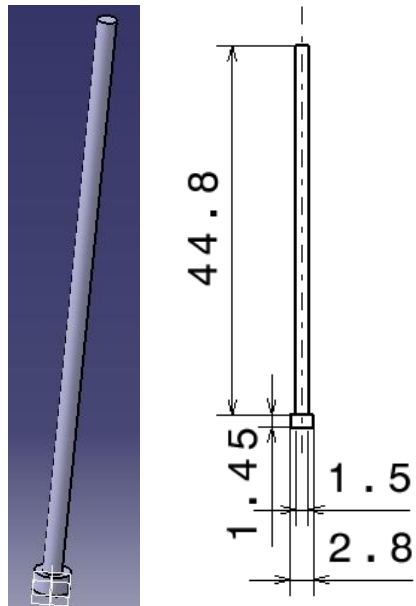**Figure B-0-13.** Isometric view pin ϕ2 mould side.

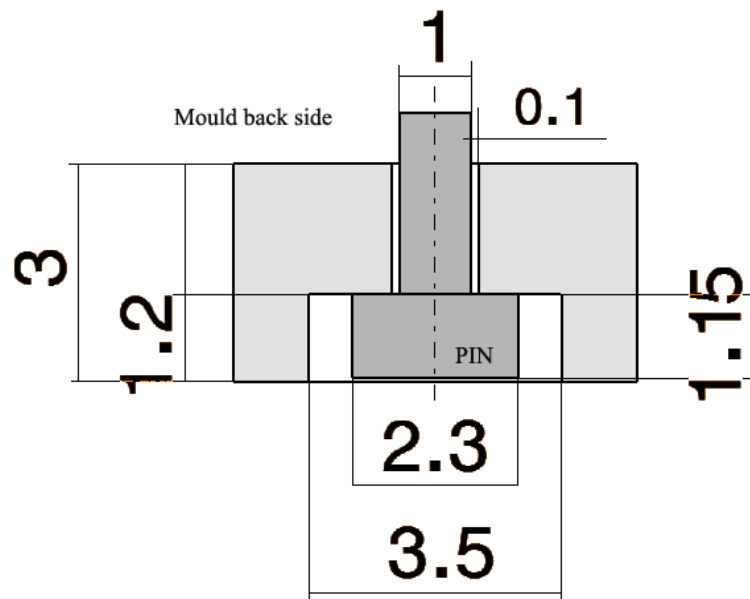**Figure B-0-14.** Pin ϕ2.

Mould back side

PIN
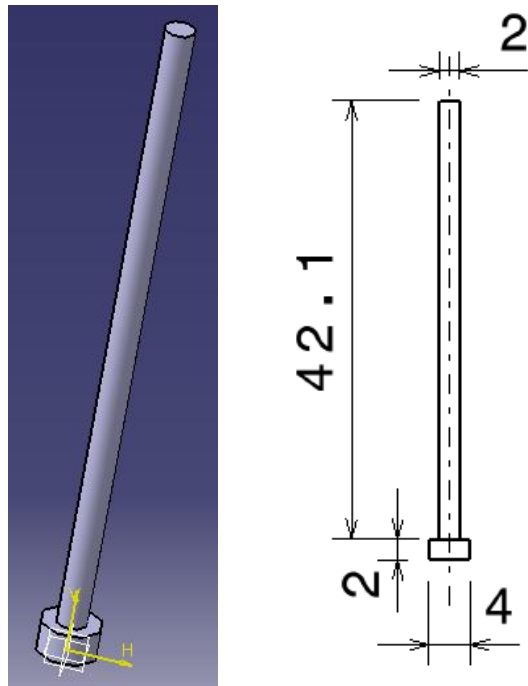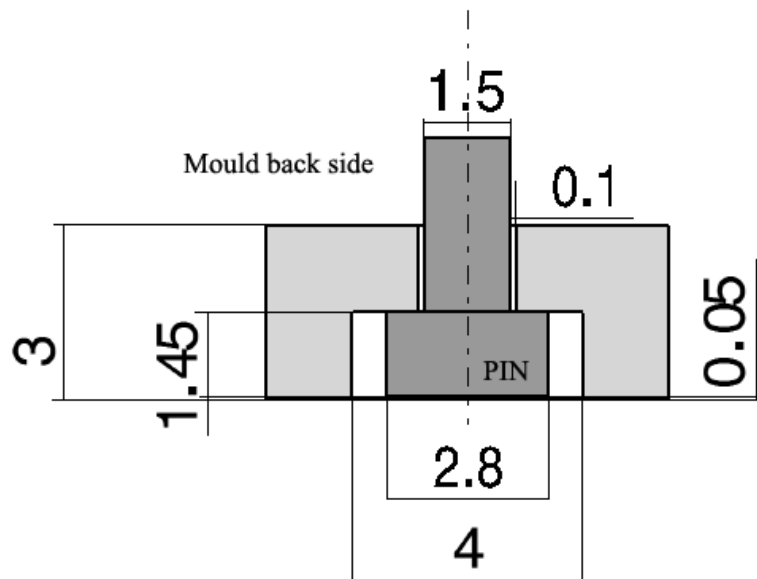
Figure B-0-15. Design head pin ϕ 1.5.
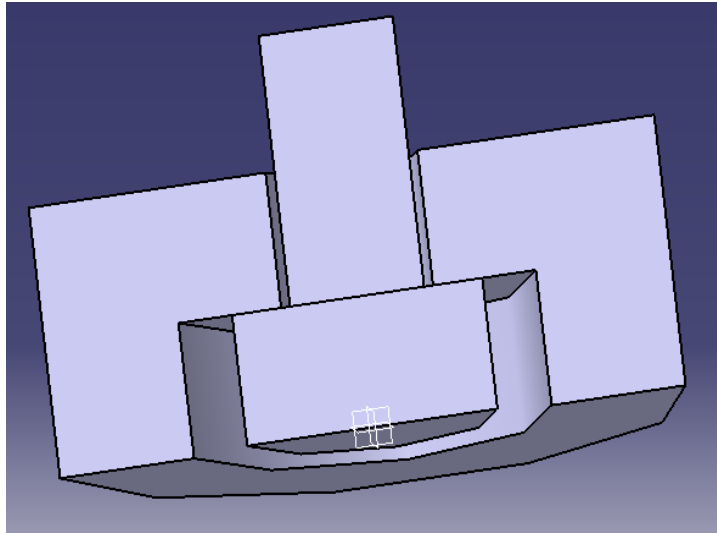
Figure B-0-16. Isometric view head pin ϕ1.5.
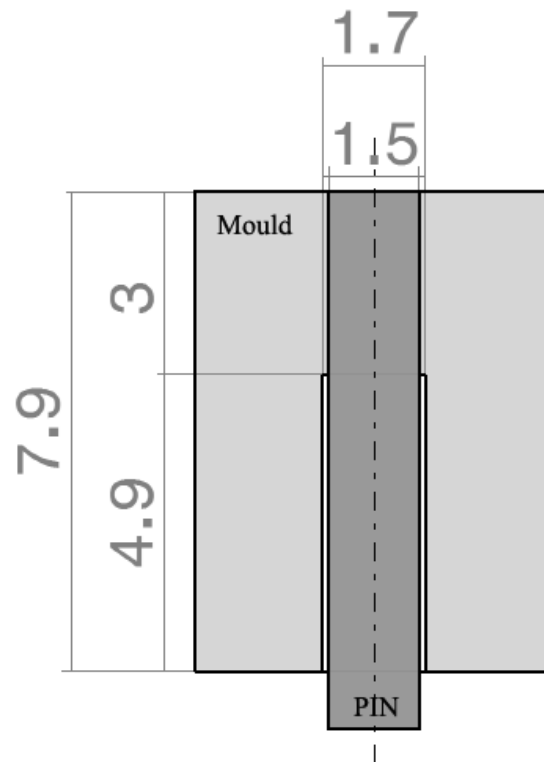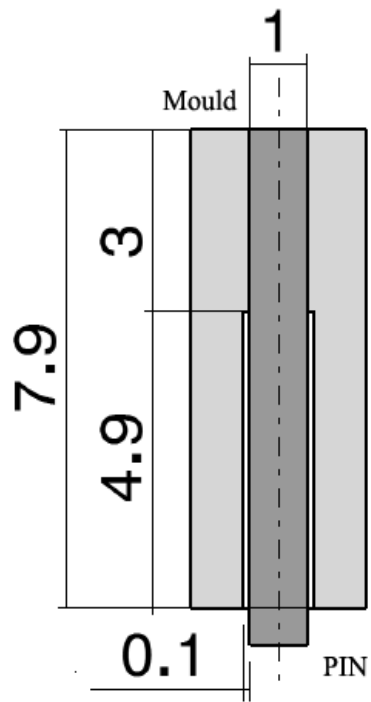

Figure B-0-17. Design pin ϕ 1.5 mould side.
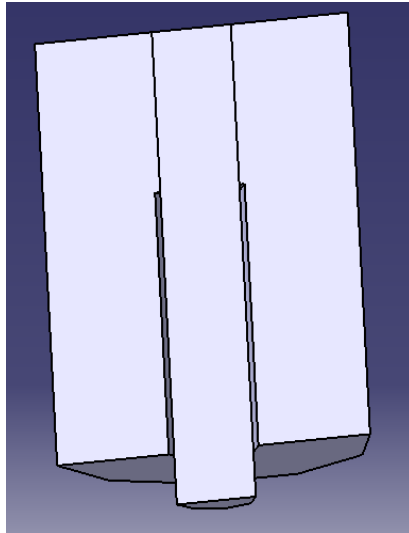
Figure B-0-18. Isometric view pin ϕ1.5 mould side.

Figure B-0-19. Pin ϕ 1.5

Figure B-0-20. Design head pin ϕ 1.
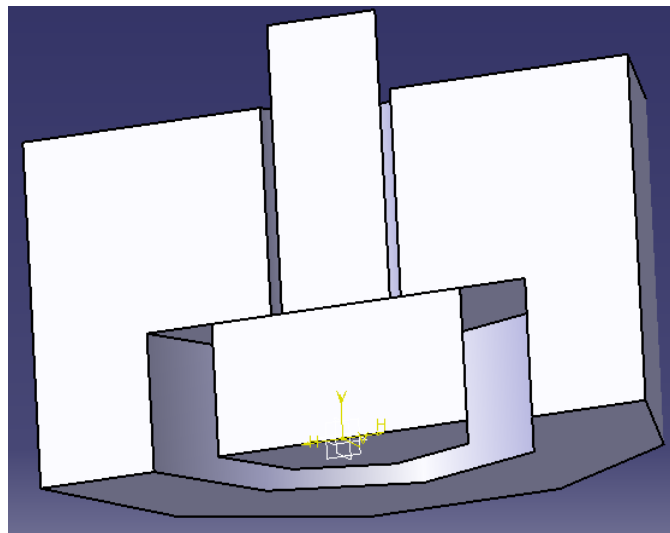
Figure B-0-21. Isometric view head pin ϕ1.

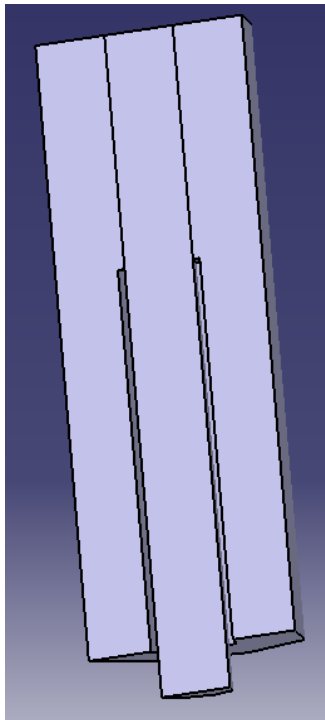**Figure B-0-22.** Design pin ϕ 1 mould side.
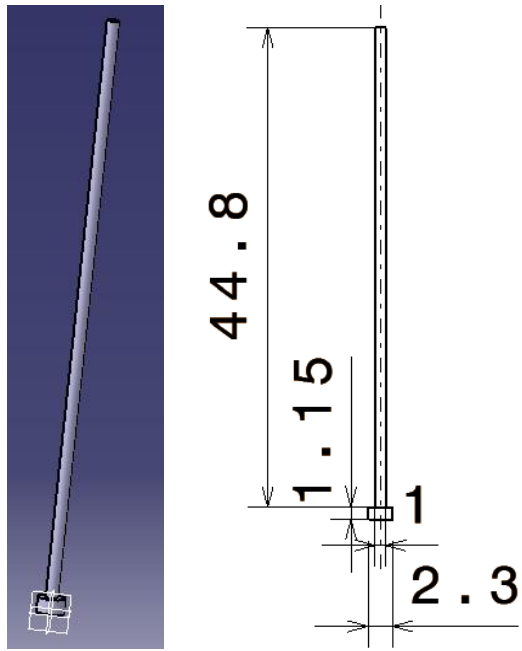

Figure B-0-23. Isometric view pin ϕ1 mould side.

Figure B-0-24. Pin φ 1